ZfK-382

Technical University Dresden
Section of Physics

Proceedings of the VIIIth International Symposium on the Interaction of Fast Neutrons with Nuclei – Nuclear Reaction Mechanisms –

November 13–17, 1978 in Gaussig (GDR)

Eds. R. Reif
S. Sassonov

January 1979

Postanschrift: Akademie der Wissenschaften der DDR
Zentralinstitut für Kernforschung Rossendorf
8051 Dresden
Postfach 19 Deutsche Demokratische Republik

Diese Publikation wurde in der Abteilung Literatur und Information des Zentralinstitutes für Kernforschung hergestellt

III-12-12 / 83 79

AKADEMIE DER WISSENSCHAFTEN DER DDR

ZENTRALINSTITUT FÜR KERNFORSCHUNG
ROSSENDORF BEI DRESDEN

ZfK - 382

Proceedings
of the VIIIth International Symposium on the Interaction of Fast Neutrons with Nuclei
- Selected Topics in Nuclear Reaction Mechanisms -

organized by
the Technical University of Dresden
November 13-17, 1978 in Gaussig (GDR)

edited by
R. Reif and S. Sassonov

January 1979

Organizing Committee

R. Reif
S. Sassonov
H. Ludwig

Technical University Dresden
Section of Physics
Nuclear Physics Group

PREFACE

This report contains the contributions presented at the "VIII-th International Symposium on the Interaction of Fast Neutrons with Nuclei" organized by the Nuclear Physics Group of the Technical University Dresden.

150 JAHRE TU 1828 - 1978

The Symposium was devoted to current problems in experimental and theoretical investigations of nuclear reaction mechanism, covering a broad range of aspects. Extending the scope of topics discussed during the preceding meetings in Gaussig, also experimental and theoretical investigations of heavy ion reactions as well as selected problems in nuclear physics at medium energies have been included in the scientific program containing

- heavy ion reactions, especially deep inelastic collisions
- general statistical aspects of nuclear reactions
- experimental and theoretical investigations of nucleon induced reactions at lower energies
- direct reactions, preequilibrium models.

We would like to thank all participants, especially our lecturers, for their active work during the sessions and all subsequent informal discussions. Further we want to thank the International Department of the Technical University Dresden for the valuable support in organizing this Symposium. A special thanks is due to the staff of the rest home in Gaussig. Moreover, we would like to thank the Central Institute for Nuclear Research of the Academy of Science of GDR for making possible the publication of this report. We are much indebted to H. Ludwig, R. Krause, R. Prengel, and B. Krause for technical assistance in preparing this Proceedings.

The Symposium has been devoted to the 150-th anniversary of the foundation of the Technical University Dresden.

R. Reif
S. Sassonov

CONTENTS

LIST OF PARTICIPANTS

S. Adel Fowzy	TU Dresden
W. Andrejtscheff	Institute of Nuclear Research and Nuclear Energy, Sofia
B. Apagyi	Technical University Budapest
R. Arlt	TU Dresden
H.W. Barz	ZfK Rossendorf
B. Basarragtscha	TU Dresden
Z.T. Bödy	Kossuth University, Debrecen
V.M. Bychkov	PEI Obninsk
L.P. Csernai	Central Research Institute for Physics, Budapest
V.N. Dushin	Radiuminstitut Leningrad
M. Gmitro	JINR Dubna
I. Hamamoto	NORDITA, Copenhagen
H. Helfer	TU Dresden
E. Hentschel	ZfK Rossendorf
D. Hermsdorf	TU Dresden
M. Jaskoła	Institute of Nuclear Research, Warsaw
M. Josch	TU Dresden
D. Kluge	JINR Dubna
Koltypin	Kurtschatov-Institut Moskau
B. Kühn	ZfK Rossendorf
S. Landowne	Universität München
G. Lovtschikova	PEI Obninsk
P. Mädler	TU Dresden
V. Manochin	PEI Obninsk
H. Märten	TU Dresden
A. Meister	JINR Dubna
L. Münchow	ZfK Rossendorf
G. Musiol	TU Dresden
C. Ngo	CEN Saclay
W. Nörenberg	GSI Darmstadt
G. Ortlepp	TU Dresden
G. Pausch	TU Dresden
A. Pfitzner	ZfK Rossendorf
L.B. Pikelner	JINR Dubna
R. Reif	TU Dresden
H. Reinhard	JINR Dubna
U. Richter	TU Dresden
I. Rotter	ZfK Rossendorf
K. Rusek	Institute of Nuclear Research, Warsaw
S. Sassonoff	TU Dresden
G. Saupe	TU Dresden
D. Schmidt	TU Dresden
R. Schmidt	JINR Dubna
H. Schulz	ZfK Rossendorf
T. Schweitzer	TU Dresden
D. Seeliger	TU Dresden

K. Seidel	JINR Dubna
B.V. Shuravlov	PEI Obninsk
H. Sodan	ZfK Rossendorf
T. Streil	TU Dresden
A. Strzalkowski	Jagellonian University, Cracow
J. Szabo	Kossuth University, Debrecen
J. Teichert	TU Dresden
R. Teichner	TU Dresden
S. Tesch	ZfK Rossendorf
Thanh	TU Dresden
D. Trautmann	Institut für Theoretische Physik der Universität Basel
A. Truvanov	PEI Obninsk
H. Tschammer	TU Dresden
R. Tschammer	TU Dresden
J. Turkiewicz	Institute of Nuclear Research, Warsaw
S. Unholzer	TU Dresden
V.V. Volkov	JINR Dubna
H. Vonach	Institut für Radiumforschung und Kernphysik Wien
P.E. Vorotnikov	Kurtschatov-Institut Moskau
W. Wagner	TU Dresden
H.J. Wiebicke	ZfK Rossendorf
R. Wolf	TU Dresden
R. Wünsch	ZfK Rossendorf
J. Zimanyi	Central Research Institute for Physics, Budapest
G. Zschornack	JINR Dubna

SOME REGULARITIES OF THE EVOLUTION AND DISINTEGRATION OF THE DOUBLE NUCLEAR SYSTEM FORMED IN DEEP INELASTIC COLLISIONS OF COMPLEX NUCLEI

V.V.Volkov

Laboratory of Nuclear Reactions, Joint Institute for Nuclear Research, Dubna, USSR

The systems Ag+^{40}Ar (285 MeV) and Au+^{11}B (86 MeV) have been used to study deep inelastic transfer (DIT) reactions. It has been established that the nuclear structure of the light fragment influences the cross section of its production. The heavy fragments from DIT have been shown to undergo a large dynamical deformation. It is found that the Q_{gg}-systematics describe cross sections of different DIT channels in reactions with ^{40}Ar and heavier ions.

1. Introduction

Studies of the interactions of heavy ions with nuclei have led to the discovery of the new type of nuclear reactions — deep inelastic transfers, which proceed via the formation of a double nuclear system (DNS). The latest reviews on the DIT are contained in refs.[1-4]. The present paper deals with some regularities of the evolution and decay of the DNS, which have been established from experimental data obtained at the JINR Laboratory of Nuclear Reactions.

2. The shell effects in DIT

The excitation energy of the DNS formed in DIT amounts to several tens of MeV. The nuclei incorporated in the DNS interact with each other strongly. It may seem that under such conditions the shell structure of the nuclei can hardly influence the DNS evolution. However, experiment shows that the structure of the nuclei, especially that of light fragments, has its imprint on the DNS evolution.

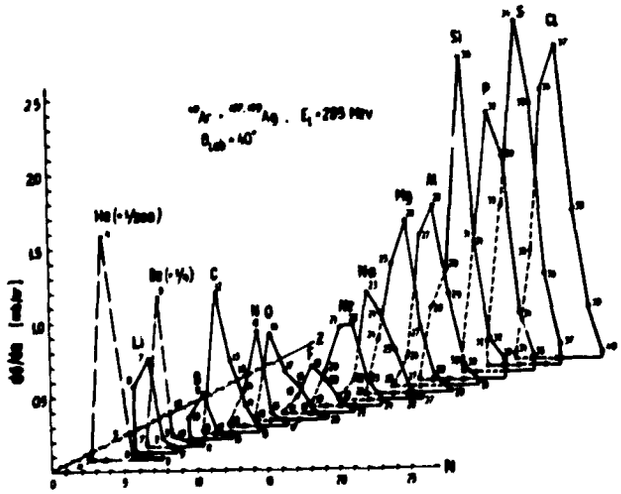

Fig. 1
Differential cross sections $(d\sigma/d\Omega)_{40°}$ for the production of isotopes of $2 \leq Z \leq 17$ in the reaction Ag+^{40}Ar (285 MeV), θ_L=40°.

Fig. 1 shows the differential cross sections $(d\sigma/d\Omega)_{40°}$ of the production of various isotopes of elements from Cl to He in the reaction Ag+^{40}Ar (285 MeV). The cross sections for the production of ^{8}Be and helium isotopes have been obtained by extrapolation according to the Q_{gg}-systematics. The cross sections of isotopes with maximum yields decrease initially as Z decreases. Following fluorine, however, the opposite tendency is observed. A pronounced growth of the cross section is observed for nuclei with closed shells and subshells such as:

^{16}O, ^{15}N, ^{12}C and ^{4}He as well as for ^{8}Be. For ^{4}He, the cross section reaches ~ 300 mb, that is two orders of magnitude larger than the cross section of any other recorded channel of transfer reactions. The cross sections for the production of isotopes of elements from helium to fluorine in the reaction Ag+^{11}B (86 MeV) are shown in fig. 2. In this reaction the yields of the isotopes ^{3}He, ^{4}He and ^{6}He were measured experimentally. It is noteworthy that the production cross sections for helium isotopes obey the Q_{gg}-systematics like those of other elements (see fig. 11). This indicates that the main contributor to the production of helium isotopes are DIT reactions. Here again the channel of DNS decay involving the ^{4}He emission sharply dominates over the rest of the multinucleon transfer reactions. Fig.3 elucidates the possible interpretation of the observed features of DIT for the reaction Ag+^{40}Ar (285 MeV). Apparently the DNS evolves in stages, from shell to shell, with delays in the configurations of tightly bound nuclei.

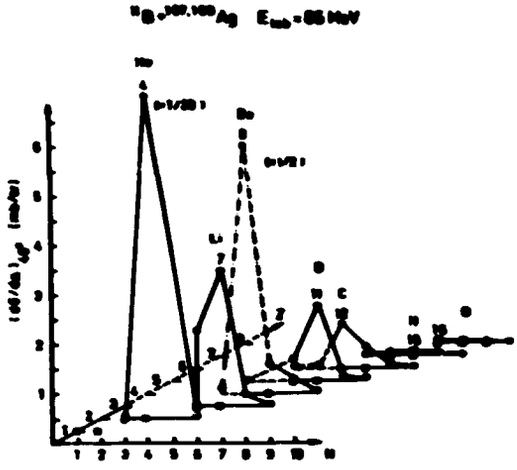

Fig. 2

Differential cross sections $(d\sigma/d\Omega)_{40°}$ for the production of isotopes of $2 \leq Z \leq 9$ in the reaction Ag+^{11}B (86 MeV) $\theta = 40°$.

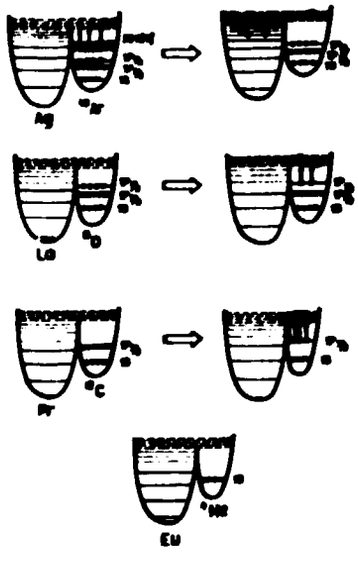

Fig. 3

Illustration of the effect of the shell structure.

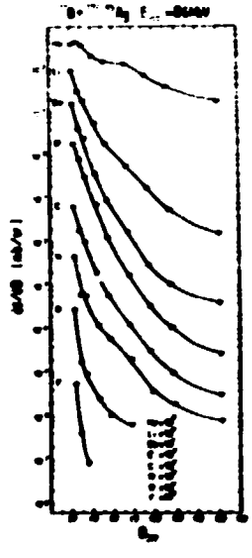

Fig. 4

Angular distributions of transfer reaction products in the reaction Ag+^{11}B (86 MeV).

A further evolution of the DNS requires the breaking of a nucleon pair in the light nucleus by transferring nucleons to the exchange zone[1]. However, this requires a concentration of a considerable amount of energy in the light nucleus. The coupling energies in ^{12}C, ^{8}Be and ^{4}He are equal to 9.6, 16.6 and 19.8 MeV,

respectively. The delay of the DNS evolution in configurations with tightly bound nuclei may manifest itself in a larger isotropy of the angular distribution (fig. 4). The α-cluster configuration of the DNS deserves special attention. Apparently the tightly bound α-particle may long be in close contact with a highly excited nucleus, without being destroyed.

3. Dynamical deformation of the DNS

One of the aspects of the DNS evolution is conversion of the angular momentum of the collision into the spins of the nuclei and dynamical deformation of the system. In the case of fully damped tang[illegible]l velocity the DNS is a system of two sticking nuclei, which rotates a[illegible]hole. The total kinetic energy (TKE) of the fragments is, in this case, de[illegible]ined by the sum of the exit Coulomb and centrifugal barriers, and by the systems deformation. The calculation of the dynamical deformation of the heavy fragment as a function of the number of the transferred nucleons has been done for the reaction Ag+^{40}Ar (285 MeV). The spectra of the TKE for the isotopes of elements from O to Mg is shown in fig. 5.

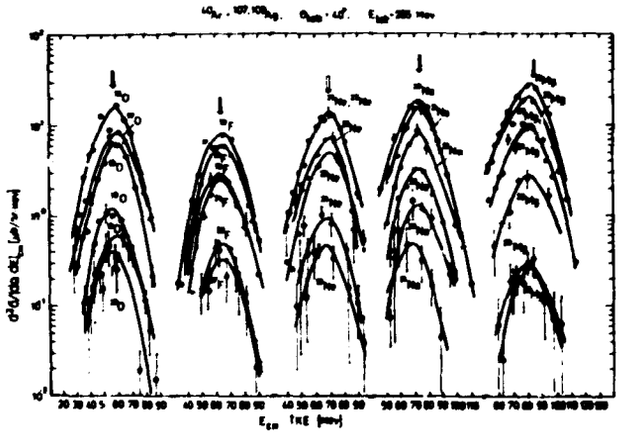

Fig. 5
Energy spectra $d^2\sigma/d\varepsilon d\Omega$ of isotopes of $8 \leq Z \leq 12$ for the reaction Ag+^{40}Ar (285 MeV) measured at θ=40°. The arrows show exit Coulomb barriers.

Fig. 6
Calculated data for the dynamical deformation of heavy fragments from the reaction Ag+^{40}Ar (285 MeV): Z_3 and Z_4 are the atomic numbers of the light and heavy fragments, I_3 and I_4 are their spins, respectively. Experimental data (open circles) from ref. 5) are also used.

The TKE for the isotopes of other elements have also a similar shape. The calculation has been performed for the maximum TKE values and for the isotopes with

the largest production cross sections. To simplify the calculation the shape of the light fragment was assumed to be spherical, and the heavy fragment a prolate rotational ellipsoid. The moments of inertia of the fragments were assumed to be rigid-body ones, and the total angular momentum of the DNS equal to $110\hbar$. The calculated deformation of the heavy fragment (the ratio of the large to the small semiaxis) is shown in fig. 6.

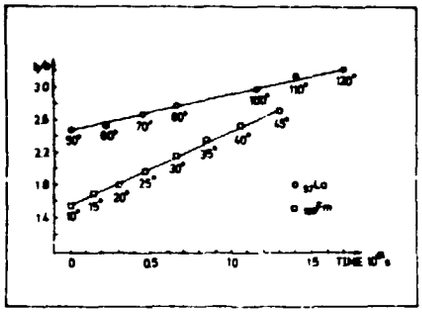

Fig. 7
Dynamical deformation of DIT heavy fragments as a function of the DNS lifetime. The increase of the DNS moment of inertia with time is taken into account.

Fig. 7 shows the increase of dynamical deformation of the La and Fm nuclei in the reactions Ag+^{40}Ar $\longrightarrow$ La+O (285 MeV) and Th+^{40}Ar $\longrightarrow$ Fm+O (379 MeV). The deformation was calculated from the TKE of oxygen nuclei, the energy spectra of which were measured at several angles in refs.[5,6].

4. Regularities of the DNS decay

In DIT a great variety of reaction products are formed, including tens and even hundreds of various isotopes. Whatever causes the disintegration of the DNS into one or another reaction channel? In ref.[7] the so-called Q_{gg}-systematics have been established for the cross sections of isotopic production in multinucleon transfer reactions. As an example, the Q_{gg}-systematics for the reaction Th+^{22}Ne (174 MeV) are shown in fig. 8 [1]. In fig. 9 one can see the Q_{gg}-

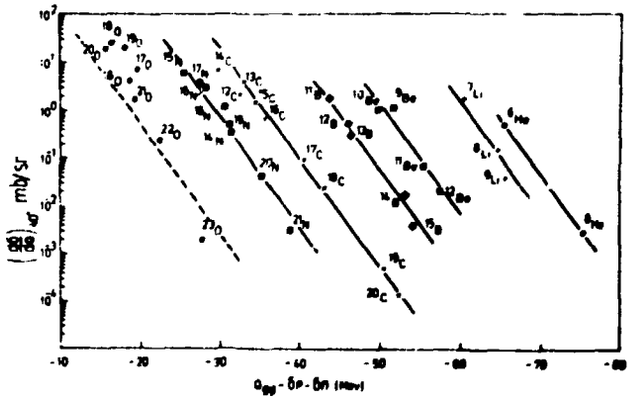

Fig. 8
The Q_{gg}-systematics of the production cross sections for the O N, C, B, Be, Li, He isotopes for the reaction ^{232}Th +^{22}Ne (174 MeV).

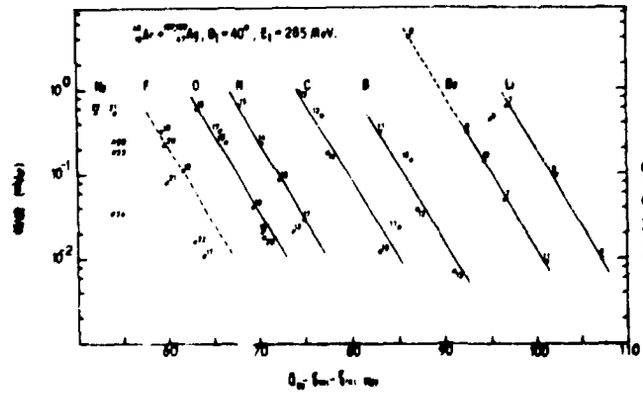

Fig. 9
The Q_{gg}-systematics of the production cross sections for the isotopes of $3 \leq Z \leq 10$ for the reaction Ag+^{40}Ar (285 MeV).

systematics of cross sections for the production of isotopes of elements from lithium to fluorine in the reactions Ag+^{40}Ar (285 MeV). One can see that up to the oxygen isotopes the Q_{gg}-systematics are fulfilled satisfactorily. For the heavier elements the sequential nuclear processes such as the evaporation of nucleons and α-particles violate the Q_{gg}-systematics. The validity of the Q_{gg}-systematics for the still heavier ions (^{86}Kr, ^{136}Xe) has been checked against the data of ref.[9], in which by using radiochemical methods the cross sections for the production of gold isotopes with masses 190-199 were measured in the bombardment of ^{181}Ta with ^{40}Ar ions (290 MeV), ^{86}Kr ions (550 MeV) and ^{136}Xe ions (850 MeV). The yield of these same isotopes were calculated under the assumption that they are produced due to multinucleon transfer reactions followed by neutron evaporation (fig. 10)[10].

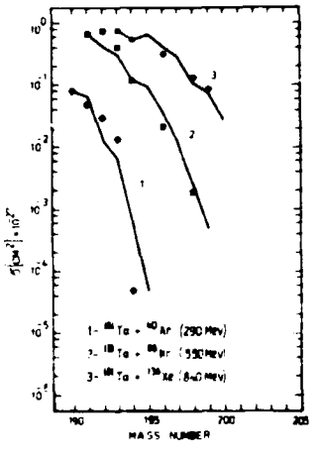

Fig. 10

Comparison of the calculated (solid curves) and experimental (points) data on the yield of the gold isotopes in the bombardment of ^{181}Ta with the ^{40}Ar ions at 290 MeV, with the ^{86}Kr ions at 550 MeV, with the ^{136}Xe ions at 840 MeV. The calculated data are normalized to the experimental yield of the isotope with minimum A.

The yield of primary products was calculated according to the Q_{gg}-systematics, whereas neutron evaporation was calculated using the Jackson model. Fig. 11 shows the Q_{gg}-systematics of isotopic production cross sections for the reaction Ag+^{11}B (86 MeV), which cover the isotopes produced as a result of both the stripping and pick-up of protons by the ^{11}B projectile. Thus the Q_{gg}-systematics describe the cross section of the production of isotopes in DIT reactions for any target-projectile combination, being one of the general regularities of the DNS decay.

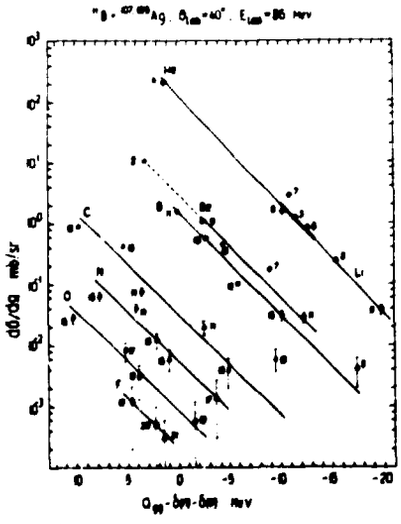

Fig. 11

The Q_{gg}-systematics of the production cross section for the isotopes of $2 \leqslant Z \leqslant 9$ for the reaction Ag+^{11}B (86 MeV). The measurements are done at the emission angle $\theta = 40°$.

The results presented in this paper have been obtained by a Laboratory of Nuclear Reactions group including A.G.Artukh, G.F.Gridnev, A.N.Mezentsev, V.L. Mikheev, A.Popescu, D.G.Popescu, and V.V.Volkov. The author expresses his gratitude to Academician G.N.Flerov fo his stimulating interest in and support of

the DIT studies. Thanks are also due to Mrs. L.Pashkevich for translating the paper into English.

References

1. V.V.Volkov, Physics Reports 44 (1978) 93.
2. M.Lefort and Ch.Ngô, Ann.Phys. 3, 5 (1978).
3. W.V.Schröder and J.R.Huizenga, Ann.Rev.Nucl.Sci. 27, 465 (1977).
4. R.Bock, Proceedings of the International Conference on Nuclear Structure, Tokyo, September 5-10, 1977. Suppl. to the J.Phys.Soc. Japan, 44, 730 (1978).
5. L.G.Moretto and R.Schmitt, J. de Phys. 37 (1976) C5-109.
6. A.G.Artukh, G.F.Gridnev, V.L.Mikheev, V.V.Volkov and J.Wilczynski, Nucl.Phys. A215 (1973) 91.
7. A.G.Artukh, V.V.Avdeichikov, G.F.Gridnev, V.L.Mikheev, V.V.Volkov and J.Wilczynsky, Nucl.Phys. A168, 321 (1971).
8. J.C.Jacmart, P.Colombani, H.Doubre, N.Frascaria, N.Poffe, M.Riou, J.C.Roynette, C.Stephan, Nucl.Phys. A242, 175 (1975).
9. Yu.Ts.Oganessian, Yu.E.Penionzhkevich, Nguyen Thak An, D.M.Nadkarni, K.A.Gavrilov, Kim De En, M.Russonnois, Yad. Phys. 18, 734 (1973).
10. E.A.Cherepanov, Li Gen Su, A.N.Mezentsev, V.V.Volkov, Preprint JINR E7-11364, Dubna, 1978.

DEEP INELASTIC REACTIONS : A PROBE FOR LARGE SCALE COLLECTIVE MOTION STUDIES.

C. Ngô
DPhN/MP, CEN Saclay, BP n° 2, 91190 Gif-sur-Yvette, France.

Abstract

We review the properties of slow collective modes in deep inelastic reactions. The assumption of statistical equilibrium among the intrinsic degrees, on which are based all the theories for deep inelastic reactions, is justified in the light of a neutron multiplicity experiment on the 400 MeV Cu+Au system. We discuss a recent experiment devoted to the study of a fast collective mode (charge equilibration) wich probably indicates that quantal fluctuations are dominant for this degree of freedom.

Since a few years experiments in heavy ion physics are devoted to deep inelastic reactions [1]. The huge interest in this domain comes mainly to the observation of collective phenomena. This is not without similarities with the fission process : In both cases large scale collective motion is the proeminent feature of the reaction. The rather large number of nucleons which are involved in such processes allows to study the interactions between two large pieces of nuclear matter. As compared to compound nucleus formation where all the nucleons are involved, much shorter contact times ranging between 10^{-22} and 10^{-20}s can be obtained. This allows to study relaxation phenomena [2] and studies of deep inelastic reactions are of great interest in the understanding of the evolution of microsystems out of equilibrium. In the experiments not all the parameters necessary to determine completely the system are measured. A consequence of this loss of information is the appearance of irreversible processes.
The deep inelastic process is binary in the sense that two main products are observed in the exit channel. Therefore most of the studies are concerning the properties of the light fragment. We always look at the experimental data with some kind of model in mind. To which extend this model is valid can only be checked by further experiments. We would like to present here our present understanding of the deep inelastic phenomena even if for some particular cases the experimental situation is not so clear.
It is usually admitted in deep inelastic reactions that one can divide the system into slow and fast degrees with respect to the time. The slow degrees are of collective nature and they are related either directly or indirectly to measured quantities. One can study their relaxation to equilibrium. The other degrees which are fast are assumed to relaxe very quickly to equilibrium. They are usually referred to as intrinsic degrees and are related to single particle motion. In addition there also exist fast collective modes which play the same role as the intrinsic degrees as far as the slow collective modes are concerned but which have a great interest in their own. Therefore during the course of the deep inelastic process it usually assumed that, except at the very beginning of the reaction, the intrinsic degrees are in statistical equilibrium.
In part 1 we shall briefly describe the main properties of these slow collective modes. In part 2 the assumption of statistical equilibrium of the intrinsic degrees will be discussed in the light of an experiment recently done on neutron multiplicities [3]. Finally part 3 will deal with a fast collective degree which we have recently studied at GSI [4].

1. Slow collective modes.

The most striking feature of deep inelastic reactions is the large energy loss observed in relative motion. The correlation between the total kinetic energy of the fragments and the deflection

angle is of particular interest because this later parameter is connected to the interaction time. Examples are shown in fig. 1 for the 280 MeV Ar + Ni system studied by Galin et al. 5). For the plot corresponding to Z = 19 which only corresponds to one charge transfer a large amount of cross section is observed in the region corresponding to the grazing angle ($\simeq$ 30°) and for an energy close to the initial energy This region corresponds to quasi elastic reactions. Another area can be seen at low energy, extending over a wide angular range. It corresponds to completely energy relaxed products because for these, the memory of the initial energy has been completely lost. Between these two regions, there is a continuous evolution between them due to incompletely energy relaxed products. When the mass transfer increases, the quasi elastic area gradually disappears as well as incompletely energy relaxed region and there only remains the completely energy relaxed component. We see that we are faced with two collective modes. One connected to the energy loss in relative motion and the other connected to mass asymmetry. From fig. 1 we can draw the inference that the energy transfer is a faster process than the mass asymmetry degree of freedom because as soon as a small number of nucleons have been transferred, only the completely energy relaxed component remains.

The energy loss occurs because there is a coupling between relative motion and other modes. By looking at the desexcitation of the products one knows that each fragment has a lot of intrinsic excitation energy. Because of phase space considerations the energy flow will go from relative motion to the intrinsic degrees due to such a coupling. In the bombarding energy range used to study deep inelastic reactions it is most likely that this coupling is mainly governed by single particle fields or using a classical concept that one has to deal with one body dissipation [ ]. This means that the elementary excitations are of 1 particle - 1 hole type.

Relative motion is not only coupled to the intrinsic motion but also to other slow collective modes. For instance it is coupled to surfaces vibrations. Indeed the composite system formed during the reaction separates into two highly deformed fragments. The evidence for that can be found in the mean total kinetic energy of the completely energy relaxed fragments. For instance the Ni+Ag system has been studied at two different bombarding energies 365 and 443 MeV. In both cases the mean total kinetic energy of the completely energy relaxed products (quasifission) is [illegible] MeV whereas the interaction barrier in the entrance channel (which corresponds to two spherical nuclei) is [illegible] MeV. Therefore at scission the two fragments are highly deformed. After separation the vibrations which are in turn coupled to the intrinsic degrees will be damped into intrinsic excitation energy. This excitation of surface vibrations has two inferences : it decreases the total kinetic energy of the fragments and increases their contact time.

Rotations are also excited during the deep inelastic process, this means in a classical picture that the fragments will spin after the interaction. The angular momentum transfer to the fragments can be measured by looking at their γ multiplicity. It appears that the relaxation time connected to angular momentum transfer is intermediate between the one connected to the energy damping and the one connected to mass assymetry.

As far as mass asymmetry is concerned it seems that the Q value corresponding to mass transfer is completely converted into intrinsic excitation energy. Mass transfer is closely related to the energy dissipation in relative motion in the sense that it may be viewved as the excitation of one particle in one nucleus and one hole in the other whereas the energy loss in relative motion may be viewed as 1 particle 1 hole excitation in the same nucleus.

The preceeding results concerning slow collective degrees suggest that they can be interpreted using statistical assumptions. It is assumed that during the evolution of the system the intrinsic degrees are in a state of statistical equilibrium. The transfer of energy from relative motion to intrinsic degrees is described in analogy to the physics of liquids and solids : A friction force proportional to the collective velocity is inserted into classical equations of

motion[7]. The classical limit is justified because the De Broglie wave length is much smaller than the typical dimensions of the system. However because there is dissipation, there are also statistical fluctuations (fluctuation-dissipation theorem) which are indeed observed experimentally. Microscopic theories [8] have been derived to describe both dissipation and statistical fluctuations. Applied to the computation of experimental quantities they give a good understanding of the deep inelastic phenomena. In fig. 2 is shown such a model applied to the Ar + Ni case of fig. 1 [9]. We see that the overall pattern of the plots is well reproduced.

2. Neutron multiplicities measurements : a justification of statistical assumptions.

The models which have been developped to describe deep inelastic reactions assume a statistical equilibrium for the intrinsic degrees of the fragments. If it is so, one of the consequence will be that the excitation energy is shared between the two fragments in proportion to their mass. In the very first stage of the reaction this assumption is certainly not valid and preequilibrium particles might be emitted. Therefore one has to know with which probability this effect may occur and to which amount of the total energy loss it corresponds.
A deep inelastic reaction can be imagined to proceed in the following way : when the two ions begin to touch, preequilibrium particles may be emitted, then the reaction proceeds in a statistical way. During the separation of the composite system in two fragments, particles may be emitted before or after they are fully accelerated. Finally γ rays will be emitted in the last stage of the desexcitation. Therefore to know how the excitation energy is shared between the fragments one has to know how many particles and γ rays are emitted by each of them and which amount of kinetic energy they carry away.
It is difficult for technical reasons to measure all kind of emitted particles in coincidence with the fragments. By choosing a heavy target and projectile at not too high bombarding energy above the interaction barrier one can favor the evaporation of neutrons compared to the evaporation of charged particles. We tried recently to measure the neutron multiplicity of each fragment on the 400 MeV Kr + Au system[3]. We measured the kinetic energy as well as the mass of the fragments at two different angles. The neutrons were detected and their velocity measured at several selected angles in and out of the reaction plane. Particular care has been taken to minimize neutron absorption and background by using the minimum of material as possible. In neutron experiments the problem is to know the efficiency of the neutron detectors. We solved it by measuring dynamically the efficiency by means of a ^{252}Cf source which was present during the whole experiment[10].
The main conclusion of the analysis is that within the experimental errors ($\sim$ 10 %) all the neutrons are emitted by fully accelerated fragments. Therefore if a preequilibrium neutron component would exist, its multiplicity is smaller than 1-2. It is interesting to look at the ratio of the neutron multiplicities ν_H/ν_L for the heavy and light fragment as a function of the mass ratio of the products. If the excitation is shared in proportion to the mass of the fragments (uniform temperature in the composite system) the experimental points should be on the bissector line and this is the case to a good approximation. The evolution of the ratio ν_H/ν_L as a function of the mass ratio of the fragments corresponds to the study of ν_H/ν_L along the mass asymmetry coordinate which is one of the slowest mode observed in deep inelastic reactions. A similar study of the ratio ν_H/ν_L as a function of the energy loss for the fixed initial asymmetry indicates that a constant value is very soon reached which mean that a statistical equilibrium is very rapidly reached even for small interaction time ($\sim 10^{-22}$s). Finally the total multiplicity $\nu_T = \nu_L + \nu_H$ as a function of the excitation energy indicates that in the mean, about 11 MeV, are needed for emitting a neutron over the whole range studied excitation energies. Furthermore

one observes that all the excitation energy is removed by neutrons for this particular system except about 15 MeV which are removed by γ rays emission. These results precise and confirm what has been observed by other authors[11] : that a statistical equilibrium of the intrinsic degrees is very soon reached during the course of the deep inelastic reaction.

3. Study of a fast collective mode : quantal fluctuations ?

Only little is known about the approach phase of deep inelastic reactions. Gatty et al.[10] have shown that the charge equilibration mode is much faster than the energy damping. It consists in the following : the ratio between the number of neutrons and the number of protons is generally different for the projectile and the target. For deep inelastic fragments this ratio is neither related to the one of the projectile nor to the one of the target but is a property of the composite system. This mode can be studied by fixing the mass asymmetry of the system and looking at its atomic number distribution. The most probable atomic number $\langle Z \rangle$ of a deep inelastic fragment is the one which minimize the potential energy of the composite system. Because the mode is very fast, it is difficult to study its relaxation to equilibrium. Furthermore because it is the secondary products which are detected, information about the primary products is sometimes difficult to obtain. More information is contained in the second moment of the atomic number distribution for fixed mass asymmetry. Indeed this quantity is less sensitive than the mean value to the evaporation of particles as one can check by a Monte-Carlo calculation for instance. For fixed mass asymmetry the potential energy of the composite system is parabolic if it is expanded around the liquid drop model. Therefore one may try to describe this mode by an harmonic oscillator. This oscillator has to be considered in a bath at temperature T which corresponds to the intrinsic degrees. Assuming the bath to be described by a Markovian operator, then $\sigma^2_{ZZ} = \langle Z^2 \rangle - \langle Z \rangle^2 = \frac{1}{m\omega^2}\left(\frac{\hbar\omega}{2} + \hbar\omega/(\exp(\frac{\hbar\omega}{T})-1)\right)$ where m is the inertia associated to this mode and $\hbar\omega$ the phonon energy of the oscillator. In the case where $\hbar\omega \ll T$: $\sigma_{ZZ} = \frac{T}{m\omega^2}$ which is independent of the temperature. This means that we observe only zero point motion with the fluctuations are of quantal type. When $\hbar\omega \gg T$: $\sigma_{ZZ} = \frac{T}{m\omega^2}$. This is characteristic of statistical fluctuations and the FWHM of the atomic number distribution at equilibrium should change as a function of the energy loss.

For the 400 MeV $^{86}Kr + ^{197}Au$ system we have measured the mass, the atomic number and the kinetic energy of the fragments at several detection angles[4]. This experiment was done at GSI. In fig. 3 are plotted for several masses the FWHM of the corresponding Z distribution as a function of the total kinetic energy of the fragments (elastic scattering corresponds to 220 MeV). We observe that the FWHM reaches very soon a plateau when the energy loss increases. It is due to the relaxation of the charge equilibration mode. For no mass transfer (A = 86) this plateau is reached when the energy loss is about 50 MeV which means that this mode is much faster than the energy transfer (completely energy relaxed products correspond to an energy loss of about 100 MeV). The existence of a plateau seems to indicate that at equilibrium σ_{ZZ} is independent of the temperature of the intrinsic system. This indicates either that one has statistical fluctuations but that the product $m\omega^2$ is large compared to the temperature range studied here or that one has to deal with quantal fluctuations and that it is the zero point motion of this mode which is observed. As the charge equilibration mode is closely related to the isovector dipole giant resonance, this could be expected.

The results presented in part 2 and 3 are due to the authors of ref.[5] and [4] and I would like to express them my gratitude to let me use the results prior to publication.

References

[1] For a review see for instance M. Lefort and C. Ngô, Annals of Physics Paris 3 (1978) 5.
[2] W. Nörenberg, Phys. Lett. 52B (1974) 289.
[3] B. Tamain, R. Chechik, H. Fuchs, F. Hanappe, M. Morjean, J. Peter, M. Dakowsky, B. Lucas, C. Mazur, C. Ngô, M. Ribrag and C. Signarbieux to be published.
[4] M. Berlanger, A. Gobbi, F. Hanappe, U. Lynen, C. Ngô, A. Olmi, H. Sann, H. Stelzer, H. Richel and M.F. Rivet, to be published.
[5] J. Galin, B. Gatty, D. Guerreau, M. Lefort, X. Tarrago, R. Babinet, B. Cauvin, J. Girard and H. Nifenecker, Nucl. Phys. A278 (1976) 347.
[6] D. Gross, Nucl. Phys. A240 (1975) 472.
W.J. Swiatecki, International School-Seminar on reactions of heavy ions with nuclei and synthesis of new elements, Dubna, USSR (1975) report LBL-4296 (1975).
[7] W.J. Swiatecki, J. de Phys. 33 (1972) 45.
W.J. Swiatecki and S. Bjornholm, Phys. Lett. Rep. 4C (1972) 326.
P.J. Siemens, Trieste publications 371 (PUB/386 paper IAEA-SMR-14/8 vol. I.
[8] H. Hofmann and P.J. Siemens, Nucl. Phys. A257 (1976) 165 and Nucl. Phys. A275 (1977) 464.
D. Agassi, C.M. Ko and H.A. Weidenmüller, Ann. Phys. 107 (1977) 140.
[9] M. Berlanger, P. Grangé, H. Hofmann, G. Ngô and J. Richert. Z. Phys. A286 (1978) 207.
[10] B. Lucas and C. Signarbieux, private communication.
[11] J. Peter, M. Berlanger, C. Ngô, B. Tamain, B. Lucas, C. Mazur, M. Ribrag and C. Signarbieux Z. Phys. A283 (1977) 413.
Y. Eyal, A. Gavron, I. Tserruya, Z. Fraenkel, Y. Eisen, S. Wald, R. Bass, G. Gould, K. Kreyling, R. Renfordt, K. Stelzer, R. Zitsmann, A. Gobbi, U. Lynen, H. Stelzer, I. Rode and R. Bock, Phys. Rev. Lett. 41 (1978) 625.
[12] B. Gatty, D. Guerreau, M. Lefort, J. Pouthas, X. Tarrago, J. Galin, B. Gauvin, J. Girard and H. Nifenecker, Z. Phys. A273 (1975) 65 and Nucl. Phys. A253 (1975) 511.

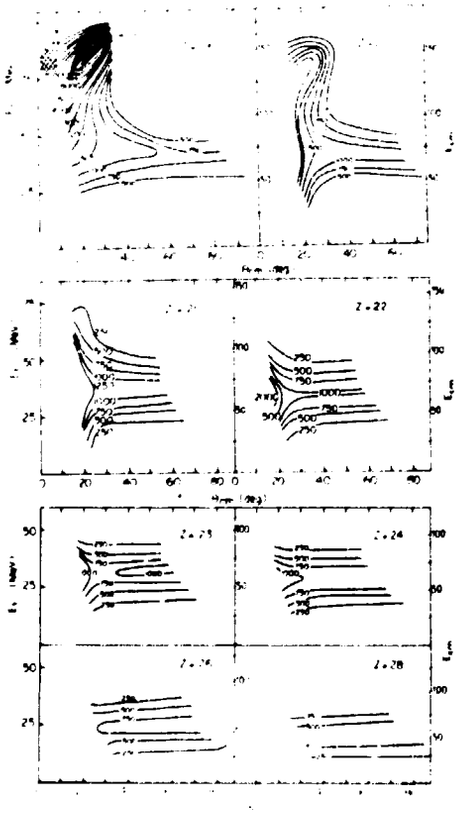

Fig. 1 - Contour plot of $d^2\sigma/dE_1d\theta_1$ (mb/MeV/rad/a.u.) in the energy angle (E_1-θ_1) plane for different atomic numbers Z for the 290 MeV ^{40}Ar+^{208}Pb system. The left hand side scale corresponds to the kinetic energy E_1 of the detected product and the right hand side scale to the total kinetic energy E_{tot} of both products - Results from ref.[5].

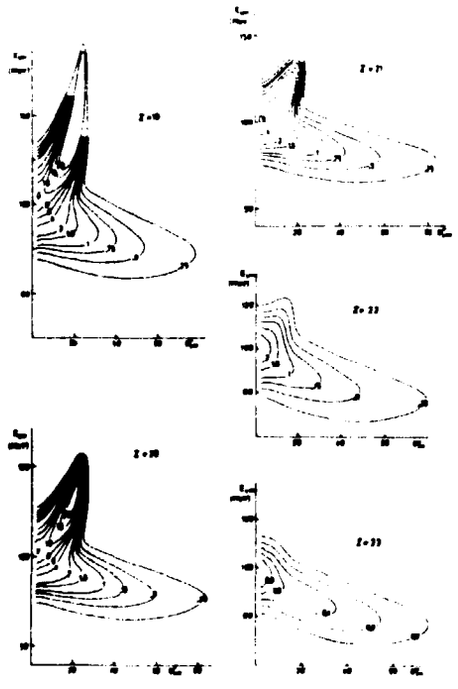

Fig. 2. Calculated contour plots for the light fragment [illegible] corresponding [illegible] the plots of fig. 1 - Results from ref.[5].

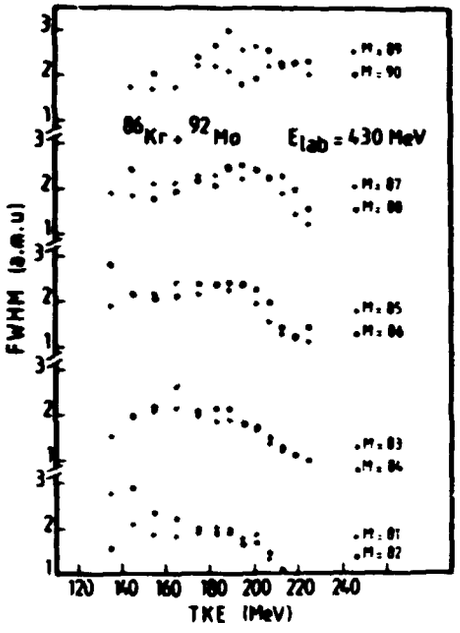

Fig. 3 - FWHM of the atomic number distribution for different fixed masses as a function of the center of mass total kinetic energy (TKE) Results from ref.[4].

MANIFESTATION OF SHELL EFFECTS IN THE INTERACTION OF HEAVY NUCLEI WITH IONS OF A > 40

R. Kalpakchieva, V.G. Kartavenko, Yu.Ts. Oganessian, Yu.E. Penionzhkevich

Laboratory of Nuclear Reactions, Joint Institute for Nuclear Research, Dubna, USSR - 101000 Moscow

H. Sodan

Zentralinstitut für Kernforschung Rossendorf, DDR - 8051 Dresden

The results of experiments to study the mass distributions of products formed as a result of fission of the system $^{40}Ar + ^{243}Am$ at low excitation energy are presented. The mass distributions are also calculated on the basis of the diffusion model. A conclusion is made for a possible asymmetric mode of decay of the heavy system studied.

Shell effects are known to play a significant role in the fission of actinide nuclei having excitation energy $E^{*} \lesssim 30 - 40$ MeV. They manifest themselves in various characteristics of the process, such as the mass distributions, the fragment kinetic energies, the number of neutrons emitted by the fragments, etc. The asymmetric mass distributions of the fission fragments of all studied nuclei from uranium [1] to $^{252}102$ (ref.[2]) and $^{265}105$ (ref.[3]) and also the symmetric mass distributions for spontaneous fission of the heavier fermium isotopes ^{258}Fm (ref.[4]) and ^{259}Fm (ref.[5]) are interpreted as being due to shell effects.

Until recently the characteristics of low energy fission have been studied for the nuclei formed in light-particle-induced reactions or for spontaneous fission. Heavy ion reactions allow in principle the production of heavy compound nuclei of $Z > 100$ with excitation energy sometimes as low as 18 - 25 MeV and small angular momentum, i.e. weakly excited heavy nuclei which are, in general, difficult to produce in the ground state. It seemed interesting to see whether and how shell effects would manifest themselves in reactions of this kind. At such low energies in heavy-ion-induced reactions, as it was shown for the first time in ref. [6], shell effects were well pronounced (as in the case of the low energy fission of practically all actinides) and it could be assumed, in analogy with the actinides, that the characteristics of low-energy induced and spontaneous fission of one and the same nucleus did not differ significantly.

Further, it is particularly interesting to investigate nuclei with $Z \geq 110$, as an enhanced nuclear stability is theoretically predicted in the region of the magic numbers Z=114 and N=184. These nuclei, owing to their shell structure, are expected to have a high fission barrier ($B_f \sim 5$-10 MeV).

We used the angular correlation method [7] to study the products of the reaction $^{40}Ar + ^{243}Am$ at four bombarding energies - 300, 240, 222, and 214 MeV of heavier systems. This method allowed us to kinematically separate the products of reactions occuring with a full momentum transfer from the bombarding ion. The contour diagrams of the total kinetic energy of reaction products as a function of mass are shown in fig. 1. In the distributions shown two groups of products can be distinguished: one group (A) centered around the projectile and target masses, and another, wider distribution (C, B) covering the intermediate-mass region from about 60 to about 220 a.m.u. one which we are interested in. It can be seen that at $E^{*} > 100$ MeV the mass distribution is a Gaussian with its maximum in the region of $A_f = (A_i + A_t)/2 \approx 140$, and dispersion ΔA_f[FWHM]= 100, which can be expected for the fission of a highly excited compound nucleus. As the projectile energy decreases, the mass distribution becomes asymmetric with the most probable heavy product mass lying in the region of A_f = 200-210 a.m.u. It should be noted that a similar behaviour of the mass distribution for the reaction $^{238}U + ^{48}Ca$ has been observed by H.-J. Sann et al. [8]. Fig. 2 shows the angular distributions for different mass regions in the reaction $^{40}Ar + ^{243}Am$ at a bombarding energy of 222 MeV. It can be seen that the angular distribution for the region (C, B) has an anisotropy different from that of the

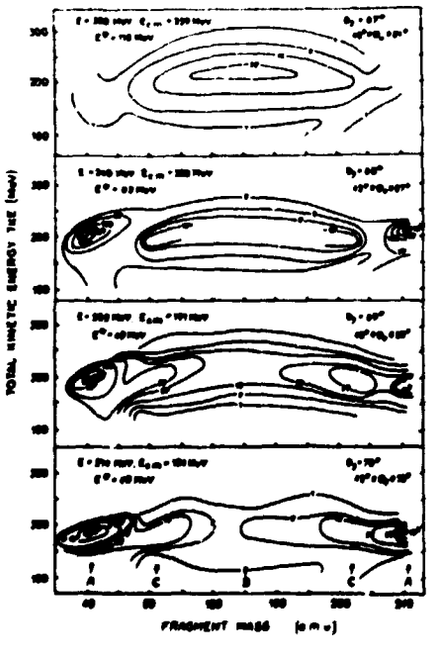

Fig. 1
Total c.m. kinetic energy vs fragment mass contour diagrams for the system $^{40}Ar + ^{243}Am$ at four different values of bombarding energy.

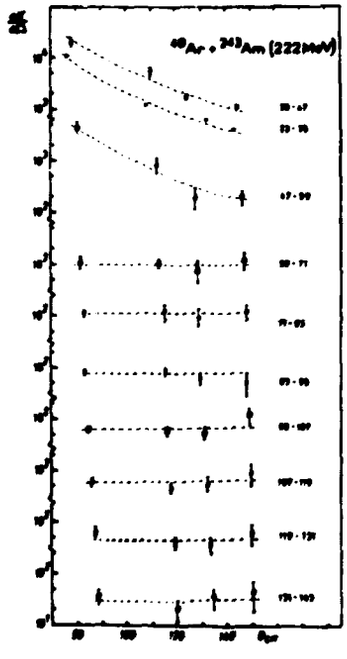

Fig. 2
Angular distributions of reaction products from different mass regions. The dashed lines are drawn to guide the eye.

region (A). The angular distribution of products of masses in the range $60 < A_f < 220$ is isotropic. One can draw the conclusion that the products of the regions (A) and (C, B) have been formed in different processes.

Two assumptions can be made concerning the origin of the maximum in the yield of products with masses A = 200 - 210. The first one is connected with the possible mechanism of deep inelastic reactions leading to the production of nuclei separated from the target by 20-40 mass units. These nuclei may have an excitation energy estimated, with the help of the experimentally obtained values of TKE, to be 40 - 80 MeV for the case, where the system excitation energy is ~40 MeV. Thus these nuclei can themselves fission and will therefore no more satisfy the condition of two-body events' detection and this in turn will lead to an artificial decrease of the detected yield of nuclei from uranium to lead. The fission probability W_f for these heavy nuclei can be calculated using the relation

$$W_f = 1 - \Pi \frac{\Gamma_{ni} + \Gamma_p}{\Gamma_{ni} + \Gamma_p + \Gamma_f}$$

The quantities Γ_n and Γ_p are calculated on the basis of the principle of detailed balancing. The fission width Γ_f is calculated using the Bohr-Wheeler formula. The parameters a_n, a_f, and r_o, contained in the expressions for Γ_n, Γ_p, and Γ_f are chosen by comparison with experimental data [9]. However, as it can be seen from fig. 3, the probability W_f of such a process is very low. Therefore the observed asymmetry in the mass distribution cannot be explained in this way.

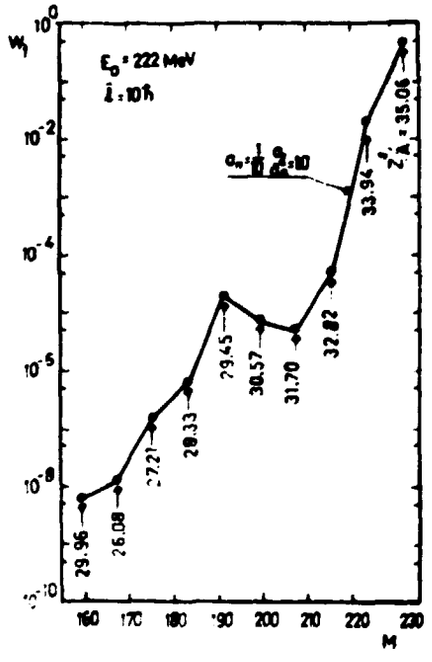

Fig. 3
Calculated fission probabilities of the heavy nuclei produced in the reaction $^{40}Ar+^{243}Am$, as a function of mass

The second assumption is connected with the existence of a shell structure in the composite system $^{283}113$ at $E^* < 50$ MeV. Traditionally the role of shell effects is analysed by calculations of the cross sections of reaction products on the basis of different models. To do this, the evolution of the formed complex system along the mass or charge asymmetry coordinate is usually studied. For this purpose we have used a somewhat version [10] of the diffusion model developed by Moretto [11], modelling the system's relaxation in the space of asymmetry coordinates (the atomic number Z of one of the fragments) by means of a stochastic process obeying the Master equation

$$dW_Z(t)/dt = \sum_{Z'} \left[\Lambda_{ZZ'} W_{Z'}(t) - \Lambda_{Z'Z} W_Z(t) \right]$$

where $W_Z(t)$ is the probability to find the system at a moment t in an asymmetry configuration Z. The transition probabi-

lities $\Lambda_{ZZ'}$ between configurations Z' and Z are connected with the potential energy of the system V_Z, which includes the binding energy of the system, the Coulomb interaction of the subsystems and the rotational energy.

In order to estimate the influence of the system's shell structure on the diffusion process, in calculating V_Z a shell correction $\delta E = \delta E(T=0) + \delta E(T \neq 0)$ (T is the temperature of the system) was added to the liquid-drop component of the binding energy. Here, the corrections for the ground state, $\delta E(T=0)$, were the experimentally known values (or their extrapolations) taken from the nuclear mass tables [12], where the correction for the heated nucleus, $\delta E(T \neq 0)$, was calculated by means of Strutinsky's technique taking into account the nuclear temperature, as described in ref. [13]. Fig. 4 presents the dependence of the potential energy V_Z of the system $^{283}113$ on the asymmetry parameter Z for three different values of the nuclear temperature, viz. T=0, 1, and 2 MeV (or excitation energies E^*=0, 40, and 120 MeV, respectively). It can be seen that

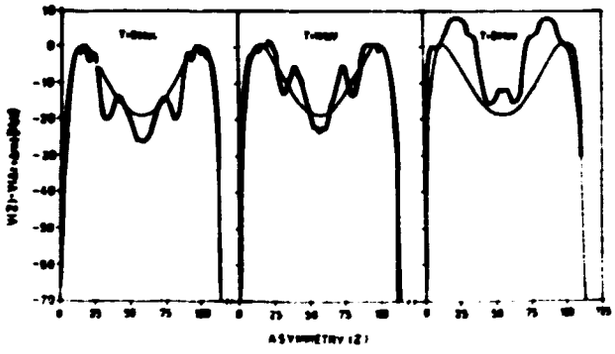

Fig. 4
Potential energy V_Z of the system $^{283}113$ as a function of the asymmetry parameter Z for three values of the nuclear temperature T=0, 1 and 2 MeV. The thick and thin curves show the results obtained taking and without taking the shell effects into account, respectively.

at T=0 and 1 MeV the studied system has two well pronounced minima in the potential energy corresponding to the region of the magic number Z=82 and to the complementary fragment with Z ~ 30. There is also a relative minimum corresponding to symmetric fission of the system, which may be somewhat enhanced because of its closeness to the shell Z=50. As the excitation energy increases (beginning from values of T ~ 1.2 MeV), the minima at Z ~ 30, 82 begin quickly to wash out and at T > 1.4 MeV almost fully vanish. The presence of minima in the potential energy naturally leads to maxima in the probability distribution function W(Z) and, consequently, to an increase in the cross sections of producing elements of Z ~ 30, 50-60, and 82. In principle, the noted dependence of the potential energy on the excitation energy adequately reflects the presented experimental data for the reaction $^{40}Ar + ^{243}Am$. In fig. 5, the distributions W(Z) for three values of the diffusion time ($t=10^{-21}$, 10^{-20} and 10^{-19} sec) are presented for T=1 MeV (E^*=40 MeV). It is seen that a better agreement with the experimental data can be obtained at greater diffusion times ($t > 10^{-19}$ sec). At such great times a nuclear system is close to statistical equilibrium [11, 14].

The authors would like to thank Professor G.N. Flerov for his constant support of the present investigations. Thanks are also due to E. Cherepanov for carrying out the calculations of the fission probabilities of heavy nuclei.

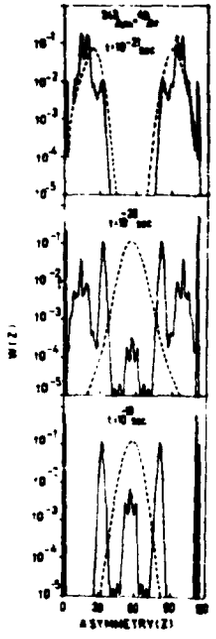

Fig. 5
Calculated probability distributions W(Z) for three values of the diffusion time $t=10^{-21}$, 10^{-20} and 10^{-19} sec in the case of T=1 MeV. The full and dashed curves show the results obtained taking and without taking the shell effects into account, respectively.

References

1. R. Vandenbosch, J.R. Huizenga, Nuclear Fission (Academic Press, New York, 1973)
2. C.E. Bemis et al., Phys. Rev. C15 (1977) 705
3. C.E. Bemis et al., Phys. Rev. Lett. 39 (1977) 1246
4. D.C. Hoffman et al., Los Alamos Scientific Laboratory Report LA-UR-77-2901 (1977)
5. D.C. Hoffman et al., Proc. 3rd Int. Conf. on Nuclei far from Stability, Cargèse, Corsica, 1976, p. 558
6. R. Kalpakchieva, Yu.Ts. Oganessian, Yu.E. Penionzhkevich, H. Sodan, B.A. Gvozdev, Phys. Lett. 69B (1977) 287
7. H. Sodan et al., Communication JINR P7-10671, Dubna 1977
8. H.-J. Sann et al., Proc. Int. Workshop on gross properties of nuclei and nuclear excitations VI, Austria, 1978, p. 106
9. V.S. Barashenkov et al., Preprint JINR P7-7165, Dubna 1973
10. V.G. Kartavenko, Proc. of 16th Winter School, Bielsko-Biala, Poland, 1978, p. 221
11. L.G. Moretto and R. Schmitt, Journal de Phys., C5 no. 11, 37, 109 (1976) and references therein
12. Atomic Data and Nuclear Data Tables, 17, 1976
13. A.V. Ignatyuk et al., Communication JINR P4-11597, Dubna, 1978
14. V.N. Bugrov et al., Preprint JINR P7-11032, Dubna 1977

SEMICLASSICAL TRANSPORT THEORY OF DISSIPATIVE HEAVY-ION COLLISIONS

W. Nörenberg
Gesellschaft für Schwerionenforschung[x)], Darmstadt and Max-Planck-Institut für Kernphysik, Heidelberg

The derivation of a transport equation within the semiclassical reaction theory is presented. The limits of weak and strong coupling are discussed in relation to characteristic times involved in the process.

1. Introduction

The initial stage of dissipative heavy-ion collisions is characterized by the mutual approach of the nuclei in their ground states. From our knowledge about grazing collisions we expect that this first stage of the process is dominated by the excitation of collective degrees of freedom, for example of surface vibrations and giant vibrations. After times of order 10^{-21}s also non-collective states should become important. The critical value of 10^{-21}s is associated with the equilibration time which is obtained in precompound reactions[1)]. At this later stage of the collision the complexity of the wave function suggests to take advantage of statistical properties of the system. Within a semiclassical description the use of randomness for the interaction matrix elements between excited states of the nuclei has led to a transport theory for dissipative collisions[2)]. This treatment within a non-perturbative theory has shown that the coupling between excited states of the nuclei is too strong for a perturbative approach. Instead, a strong-coupling limit has been formulated which gives a master equation in the Markoff approximation. The transition probabilities have been expressed completely by averages over coupling matrix elements. Within the Fokker-Planck approximation of the master equation, transport coefficients for mass transfer, energy loss and angular momentum dissipation have been evaluated and compared with experimental results[3-9)]. The theory has been generalized to include explicitly the relative motion[10,11)]. The statistical approach of Weidenmüller and coworkers start out from a formulation of precompound reactions[12)]. After a study within a perturbative approach[13)] (van Hove limit), the theory has been generalized to the strong-coupling limit and has been applied to various reactions[14-16)].

The purpose of this contribution is to discuss the ingrediences and features of a non-perturbative transport theory. The aim is to give, in the course of the derivation of the transport equation, a clear understanding of the characteristic times of the process (interaction or collision time, correlation time, lifetime or decay time of propagators which corresponds to the mean free path, memory time, relaxation time, recurrence time). Inequalities between these characteristic times define the different limits and approximations which have been discussed in the literature (ordinary perturbation limit, van Hove limit, strong-coupling limit, Markoff approximation).

2. Semiclassical scattering theory

For simplicity of presentation we choose a description within the semiclassical scattering theory[17,18)] and neglect modifications due to non-orthogonality and antisymmetrization. We assume that the trajectory $\vec{r}(t)$ for the relative motion of the colliding nuclei is known such

[x)] On leave from the Institut für Theoretische Physik der Universität Heidelberg

that we are left with the Schrödinger equation

$$i\hbar \frac{\partial}{\partial t} \mid \psi(t) > = H(t) \mid \psi(t) > \tag{2.1}$$

for the time-dependent Hamiltonian

$$H(t) = H_o(\xi) + V(\xi, \vec{r}(t)) \tag{2.2}$$

where $H_o(\xi)$ denotes the sum of the intrinsic Hamiltonians of the separated nuclei. The interaction $V(\xi,r(t))$ is the sum of Coulomb and nuclear interaction between the nuclei.

Introducing the channel wave functions $\phi_i(\xi)$ as the eigenfunctions of $H_o(\xi)$ with energies ε_i, we expand the solution $|\psi(t)>$ of the Schrödinger equation (2.1) in terms of the ϕ_i's as

$$|\psi(t)> = \sum_i a_i(t)|\phi_i> \tag{2.3}$$

with the occupation amplitudes $a_i(t)$. Inserting (2.3) in (2.1) yields with the assumed orthogonality of the channel wave functions $|\phi_i>$, the set of coupled equations

$$i\hbar \frac{da_j}{dt} = \sum_i [\varepsilon_j \delta_{ji} + V_{ji}(t)] a_i(t) \tag{2.4}$$

with $V_{ji}(t) \equiv <\phi_j|V(t)|\phi_i>$. The following description generalizes the derivation of the semi-classical transport equation given earlier[2)] to the weak-coupling limits (van Hove limit and first-order perturbation limit).

For the density matrix

$$\rho_{ji}(t) \equiv a_j(t) a_i^*(t) \tag{2.5}$$

we obtain from (2.4) the von Neumann or Liouville equation

$$i\hbar \frac{d}{dt} \rho_{ji}(t) = [V(t),\rho(t)]_{ji} \equiv \sum_{l,k} L_{ji,lk}(t) \rho_{lk}(t) \tag{2.6}$$

where the Liouville operator is defined by

$$L_{ji,lk}(t) = [\varepsilon_j \delta_{jl} + V_{jl}(t)]\delta_{ik} - [\varepsilon_k \delta_{ki} + V_{ki}(t)]\delta_{jl} \ . \tag{2.7}$$

The introduction of the Liouville operator simplifies the formal solution of (2.6) significantly. All algebraic expressions for $L_{ji,lk}$ and ρ_{ji} can be considered to be the same as for square matrices and vectors if the double subscript ji is regarded as a simple index (superspace).

3. Coarse-grained generalized master equation

Since we are not interested in the detailed knowledge of the system, we define averages over intrinsic states (channels i) by dividing (coarse graining) the total channel space $\mathcal{K}$ into subsets $\mathcal{K}_\mu$. Each subset μ contains all channels with approximately the same values for some macroscopic variables like the total excitation energy E^* and the mass-asymmetry given by the mass A_1 of one of the fragments.

The aim is now to transform the Liouville equation (2.6) into an equation for the macroscopic occupation probabilities

$$f_\mu(t) \equiv \sum_{m \in \mathcal{K}_\mu} \rho_{mm}(t) \tag{3.1}$$

of a subset μ. The knowledge of these quantities allows to calculate the differential cross-section for populating states in the subset μ by

$$\frac{d\sigma_\mu}{d\Omega} = f_\mu^\Omega \frac{d\sigma}{d\Omega}_{cl} \tag{3.2}$$

where $(d\sigma/d\Omega)_{cl}$ denotes the classical cross-section and f_μ^Ω denotes the asymptotic value $f_\mu(t\to\infty)$ for the trajectory leading to the scattering angle Ω. If more than one trajectory lead to the same scattering angle, the r.h.s. of (3.2) has to be replaced by a sum over the corresponding contributions.

In transforming the Liouville equation (2.6) into an equation for the macroscopic occupation probabilities $f_\mu(t)$ we make use of the elegant superspace notation. Simply speaking this means to regard the double index ij as a vector component in the superspace. The basis vectors in the superspace, denoted by $|ij)$, are orthogonal and normalized, $(ij|lk) = \delta_{il}\delta_{jk}$. Thus in the superspace notation, the Liouville equation (2.6) is written as

$$i\hbar \frac{d}{dt}|\rho(t)) = L(t)|\rho(t)) \tag{3.3}$$

which is similar in form to the Schrödinger equation in Hilbert space.

According to the coarse-graining procedure described above, we introduce the coarse-graining operators

$$C_\mu \equiv d_\mu^{-1} \sum_{m,m'\in\mathcal{K}_\mu} |mm)(m'm'| \tag{3.4}$$

where d_μ denotes the dimension of $\mathcal{K}_\mu$, i.e., the number of channels contained in the subset $\mathcal{K}_\mu$. The application of C_μ is a projection on and an averaging over the diagonal elements in the subset μ. We project the Liouville equation (3.3) on $C=\sum_\mu C_\mu$ and $Q=1-C$ and obtain two coupled equations for $C|\rho(t))$ and $Q|\rho(t))$. Eliminating the non-relevant part ("correlations") $Q|\rho(t))$ we find the generalized master equation

$$\frac{\partial}{\partial t}f_\mu(t) = I_\mu(t,t_o)+\sum_\mu \int_o^{t-t_o} d\tau K_{\mu\nu}(t,\tau)d_\mu f_\nu(t-\tau) \tag{3.5}$$

with

$$I_\mu(t,t_o) = \frac{1}{i\hbar}\sum_{m\in\mathcal{K}_\mu} (mm|L_1(t)G(t,t_o)Q|\rho(t_o)), \tag{3.6}$$

$$K_{\mu\nu}(t,\tau) = \left(\frac{1}{i\hbar}\right)^2 \frac{1}{d_\mu d_\nu}\sum_{m\in\mathcal{K}_\mu}\sum_{n\in\mathcal{K}_\nu} (mm|L_1(t)G(t,t-\tau)L_1(t-\tau)|nn) \tag{3.7}$$

Here we have used $CLC=0$ and we have divided the Liouville operator into two parts, $L=L_o+L_1$ where $(n\in\mathcal{K}_\nu, m\in\mathcal{K}_\mu)$

$$(L_o)_{nm,lk} \equiv \delta_{nl}\delta_{mk}(\varepsilon_n+U_\nu(t)-\varepsilon_m-U_\mu(t)) \tag{3.8}$$

is diagonal. The mean potential energy $U_\mu(t)$ is defined by

$$U_\mu(t) \equiv \frac{1}{d_\mu}\sum_{m\in\mathcal{K}_\mu} V_{mm}(t) . \tag{3.9}$$

The propagator (time-evolution operator) for the intermediate states in Q-space is given by the integral equation

$$G(t,t_o) = 1+\frac{1}{i\hbar}\int_{t_o}^{t} dt' QL(t')QG(t',t_o) . \tag{3.10}$$

The generalized master equation (3.5) is an exact transformation of the Liouville equation (2.6) to relevant macroscopic quantities. It conserves the total probability

$$\frac{\partial}{\partial t}\sum_\mu f_\mu(t) = 0 . \tag{3.11}$$

The first term on the r.h.s. of (3.5) given by (3.6) describes the contribution from the initial correlations $Q|\rho(t_o))$. These initial correlations propagate in Q-space from t_o to t and then contribute via the coupling $L_1(t)$ to the relevant part of the density matrix. The second term on the r.h.s. of (3.5) describes the coupling between different subsets. In analogy to the Boltzmann equation it is referred to as the collision term. According to (3.7) the coupling $L_1(t-\tau)$ leads from the C-space into the Q-space. This amplitude propagates from $t-\tau$ to t and then contributes via the coupling $L_1(t)$ to the relevant part of the density matrix. The collision term consists of gain terms ($\nu\neq\mu$) which correspond to transitions from all subsets $\nu\neq\mu$ to the subset μ, and another term $\nu=\mu$ which describes the loss from the subset μ. The kernel $K_{\mu\nu}(t,\tau)$ is non-local in time. The change of the macroscopic occupation probabilities at time t depends on all earlier times $t-\tau>t_o$. Because of this property, the kernel and its characteristic decay time are referred to as the memory kernel and the memory time $\tau_{mem}^{\nu\mu}$, respectively.

4. Random coupling and transport equations for weak and strong coupling

The formal and exact transformation of the Schrödinger equation (2.4) into the generalized master equation (3.5) would be worthless if the macroscopic variables μ have not been chosen in a way which allows for subsequent approximations, e.g., for the introduction of randomness of the coupling matrix elements. Therefore, the definition of the macroscopic variables is the most crucial problem in deriving useful transport equations. So far, no systematic method is known for making this choice or even for deciding wether any proposed choice is correct[19]. Only the application of the resulting transport equations to specific physical problems and comparison with experimental results can tell us wether the choice of macroscopic variables is reasonable or not. In the following we assume that we have found a set of macroscopic variables such that the assumption of randomness for the coupling matrix elements is justified. This allows to evaluate easily the mean values defined by (3.6) and (3.7).

We consider the memory kernel $K_{\mu\nu}(t,\tau)$ as defined by (3.7). For sufficiently small times τ, the main contribution to $K_{\mu\nu}$ is due to the diagonal elements $G_{nm,nm}(t,t-\tau)$ of the intermediate propagator. For finite times τ, random properties of the coupling matrix elements favour the contributions from the diagonal elements of the propagator. For large τ diagonal and non-diagonal elements become small because the amplitudes are spread over all possible states. Since the density of states is large and the coupling matrix elements couple only to a relatively small class of all these states, the total contribution to $K_{\mu\nu}$ becomes negligible for large τ. For a further evaluation of $K_{\mu\nu}$ we approximate the propagators $G_{nm,nm}$ by their mean value $G_{\nu\mu}$ for $n\in\mathcal{R}_\nu$ and $m\in\mathcal{R}_\mu$, and hence,

$$K_{\mu\nu}(t,\tau)\approx\frac{1}{\hbar^2}\langle v_{mn}(t)v_{nm}(t-\tau)\rangle_{\nu\mu}G_{\nu\mu}(t,t-\tau)+\text{c.c.} \qquad (4.1)$$

where we have introduced the traceless coupling matrix elements

$$v_{nj}(t)\equiv V_{nj}(t)-\delta_{nj}U_\nu(t)\ . \qquad (4.2)$$

The approximation (4.1) should be well satisfied if collective states can be neglected. Only for collective states we expect a time dependence of the propagator which is significantly different from the mean behaviour. Similarly, we obtain for the initial-correlation term (3.6)

$$I_\mu(t,t_o)\approx\frac{1}{i\hbar}\sum_\nu d_\mu d_\nu\langle v_{mn}(t)\rho_{nm}(t_o)\rangle_{\nu\mu}G_{\nu\mu}(t,t_o)+\text{c.c.} \qquad (4.3)$$

with $n\neq m$. This term vanishes if the non-diagonal density matrix elements are initially randomly distributed and uncorrelated with the coupling matrix elements. In the following we neglect the initial-correlation term.

For a further evaluation of the memory kernel (4.1) we have to study the time dependences of the mean autocorrelation function $\langle v_{mn}(t)v_{nm}(t-\tau)\rangle_{\nu\mu}$ and the mean propagator $G_{\nu\mu}(t,t-\tau)$. We distinguish the two limits of weak and strong coupling by the relation between the (auto-)correlation time $\tau_{cor}^{\nu\mu}$ of the autocorrelation function and the lifetime $\tau_{dec}^{\nu\mu}$ of the propagator. The weak-coupling limit is defined by

$$\tau_{cor}^{\nu\mu} \ll \tau_{dec}^{\nu\mu} \quad , \tag{4.4}$$

the strong-coupling limit by

$$\tau_{cor}^{\nu\mu} \gg \tau_{dec}^{\nu\mu} \quad . \tag{4.5}$$

Since the decay of the propagator is due to the coupling between different channels, the weak coupling limit corresponds to the neglect of the coupling L_1 in the intermediate propagator. Thus we obtain with (3.8) for the memory kernel (4.1) in the weak-coupling limit

$$K_{\mu\nu}^{(W)}(t,\tau)=\frac{1}{\hbar^2}\langle v_{mn}(t)v_{nm}(t-\tau)\rangle_{\nu\mu}\exp\left[-\frac{i}{\hbar}\int_{t-\tau}^{t} dt'(E_\nu(t')-E_\mu(t'))\right]+c.c. \tag{4.6}$$

where we have introduced the mean local energies $E_\nu(t) \equiv \langle\varepsilon_n\rangle_\nu + U_\nu(t)$ of the channel states within the subset ν. If the coupling between different channels is very weak, the nuclei remain essentially in their ground states. This is the limit of ordinary perturbation theory. Integration of (3.5) over t and τ yields the familiar result

$$f_\mu(t\to\infty) = \left(\frac{2\pi}{\hbar}\right)^2 d_\mu \langle|\tilde{v}_{mo}\left(\frac{\varepsilon_\mu-\varepsilon_o}{\hbar}\right)|^2\rangle_\mu \tag{4.7}$$

where $\varepsilon_\mu \equiv \langle\varepsilon_n\rangle_\nu$ and $\tilde{v}_{mn}(\omega)$ denotes the Fourier transform of $v_{mn}(t)$. In deriving (4.7) the difference between the mean potentials U_o, U_μ has been neglected which is consistent in the first-order perturbation limit. This limit is justified if the relaxation times τ_{rel}^{μ} of the probabilities $f_\mu(t)$ are large compared to the collision time

$$\tau_{col} \ll \tau_{rel}^{\mu} \tag{4.8}$$

In all other cases of the weak-coupling limit (4.4) where the relaxation times become comparable or even smaller than the collision time, we speak of the van Hove limit. Thus in contrast to first-order perturbation, multistep processes are considered in this limit. We note that $\tau_{dec}^{\nu\mu} \ll \tau_{rel}^{\nu}, \tau_{rel}^{\mu}$ whenever the introduced macroscopic variable μ is reasonable, i.e., if the macroscopic variable corresponds to the slow modes of the process. This condition is the consequence of the assumed local equilibrium (randomness) within the subsets μ. Combining all this with (4.4) we find the inequalities

$$\tau_{mem}^{\nu\mu} \equiv \tau_{cor}^{\nu\mu} \ll \tau_{dec}^{\nu\mu} \ll \tau_{rel}^{\nu}, \tau_{rel}^{\mu} \lesssim \tau_{col} \tag{4.9}$$

for the van Hove limit. In this limit the correlation time is by far the smallest characteristic time of the process. According to (4.9) we can neglect the time dependence of the occupation probabilities during time intervals of order $\tau_{cor}^{\nu\mu}$. This justifies the Markoff approximation for (3.5) which yields the master equation

$$\frac{d}{dt} f_\mu(t) = \sum_{\nu\neq\mu} w_{\mu\nu}(t)\left[d_\mu f_\nu(t)-d_\nu f_\mu(t)\right] \tag{4.10}$$

with the transition probabilities

$$w_{\mu\nu}(t) \equiv \int_0^\infty d\tau K_{\mu\nu}(t,\tau)\propto\langle|\tilde{v}_{mn}\left(\frac{E_\mu(t)-E_\nu(t)}{\hbar}\right)|^2\rangle_{\mu\nu} \ . \tag{4.11}$$

In contrast to (4.7) where the energy is conserved for the asymptotic region, we have here energy conservation (approximately within $\hbar/\tau_{rel}^{\nu}$, $\hbar/\tau_{rel}^{\mu}$) for the local energies.

If the strength of the coupling between the channels increases, the decay time of the propagator decreases. We speak of the strong-coupling limit if the decay time of the propagator is the smallest characteristic time in the process and in particular if (4.5) is satisfied. In order to evaluate the transition probabilities in the master equation (4.10) for strong coupling, we have to know the explicit form of the propagator (3.10). For simplicity we assume that the coupling matrix elements are different from zero only for energy differences $|E_\mu(t)-E_\nu(t)| \ll \hbar/\tau^{\nu\mu}_{dec}$. Then we can approximate L by L_1 in (3.10). Because of the inequality (4.5) we can replace $L_1(t')$ by $L_1(t_o)$ in (3.10) and find

$$G(t,t_o) \approx \exp\left[\frac{1}{i\hbar} L_1(t_o)(t-t_o)\right] \tag{4.12}$$

in the strong-coupling limit. Assuming Gaussian distributions of L_1 within the subsets we obtain

$$G_{\mu\nu}(t,t-\tau) = \exp\left[-\frac{1}{2}(\tau/\tau^{\mu\nu}_{dec})^2\right] \tag{4.13}$$

with the decay time

$$\tau^{\mu\nu}_{dec} = \hbar\left[\langle|v(t)|^2\rangle_\mu + \langle|v(t)|^2\rangle_\nu\right]^{-1/2} , \tag{4.14}$$

and hence for the memory kernel

$$K^{(s)}_{\mu\nu}(t,\tau) = \frac{2}{\hbar^2}\langle|v_{mn}(t)|^2\rangle_{\mu\nu} \exp\left[-\frac{1}{2}\left(\frac{\tau}{\tau^{\mu\nu}_{dec}}\right)^2\right] . \tag{4.15}$$

This is the same result derived earlier [2] with a somewhat different notation for the decay time. Since

$$\tau^{\mu\nu}_{mem} \equiv \tau^{\mu\nu}_{dec} \ll \tau^{\mu\nu}_{cor}, \tau^{\mu}_{rel}, \tau^{\nu}_{rel} \lesssim \tau_{col} \tag{4.16}$$

we can perform the τ-integration in (3.5) and obtain the master equation (4.10) with the transition probabilities

$$w_{\mu\nu}(t) = \sqrt{2\pi}\,\hbar^{-2}\langle|v_{mn}(t)|^2\rangle_{\mu\nu}\,\tau^{\mu\nu}_{dec} . \tag{4.17}$$

It is important to realize that (4.17) is not restricted to on-shell transitions like (4.11). This is due to the small value for $\tau^{\mu\nu}_{dec}$ in the strong-coupling limit. Of course, the resulting off-shell probabilities are not allowed to survive in the asymptotic region. When the nuclei start to separate, the memory time begins to increase and tend to infinity asymptotically. Thus, the Markoff approximation is not applicable for the last stage of the process. In order to retain the simplicity of the master equation, the coupling matrix elements $v_{mn}(t)$ have been replaced in [2] by effective interactions which are restricted to on-shell transitions only.

5. Concluding remarks

We have described the derivation of transport equations for dissipative heavy-ion collisions. Starting from the time-reversal Liouville equation we have obtained time-irreversible transport equations by the neglect of the initial correlations and the dissipative nature of the collision terms, which is introduced by the random properties of the coupling matrix elements. The validity of the transport equation is limited to the range of times $\tau^{\nu\mu}_{mem} \ll t-t_o \ll \tau_{rec}$. The lower limit is imposed by the neglect of the initial correlations and by the Markoff approximation. The upper limit is due to the finite density d of intrinsic states. The system can come close to the initial state after a time of the order of Poincaré's recurrence time $\tau_{rec} = 2\pi\hbar d$. Already for small excitation energies this recurrence time is large compared to interaction times of heavy-ion collisions.

In ref.[11] the relative motion has been treated explicitely in the semiclassical approximation. In a consecutive moment expansion with respect to the relative coordinate and momentum of the resulting transport equation one recovers the master equation (4.10) and obtains the classical equations of relative motion for the mean values and equations for the variances.

One of the basic problems in the derivation of transport equations is the adequate choice of basis states. At present we are trying to find a basis which allows for the treatment of further collective variables and at the same time leads to the weak-coupling limit (van Hove limit).

References

1) M. Blann, Nucl. Phys. A 213, 570 (1973)
2) W. Nörenberg, Z. Physik A 274, 241 (1975) and 276, 84 (1976)
3) S. Ayik, B. Schürmann and W. Nörenberg, Z. Physik A 277, 299 and 279, 145 (1976)
4) W. Nörenberg, Proc. of the European Conference on Nuclear Physics with Heavy Ions, Caen 1976, J. de Physique 37, C5-141 (1976)
5) G. Wolschin, Fizika 9 Suppl. 3, 513 (1977) and Nukleonika 22, 1165 (1977)
6) B. Schürmann, W. Nörenberg and M. Simbel, Z. Physik A 286, 263 (1978)
7) S. Ayik, G. Wolschin and W. Nörenberg, Z. Physik A 286, 271 (1978)
8) G. Wolschin and W. Nörenberg, Z. Physik A 284, 209 (1978)
9) G. Wolschin and W. Nörenberg, Phys. Rev. Lett. 41, 691 (1978)
10) S. Ayik, Phys. Lett. 63 B, 22 (1976)
11) S. Ayik and W. Nörenberg, Z. Physik A (in press)
12) D. Agassi, H.A. Weidenmüller and G. Mantzouranis, Phys. Lett. C 22, 145 (1975)
13) C.M. Ko, H.J. Pirner and H.A. Weidenmüller, Phys. Lett. 62 B, 248 (1976)
14) D. Agassi, C.M. Ko and H.A. Weidenmüller, Ann. Phys. (N.Y.) 107, 140 (1977) and in press; Phys. Lett. 73 B, 284 (1978); Phys. Rev. C (in press)
15) C.M. Ko, D. Agassi and H.A. Weidenmüller, Ann. Phys. (in press)
16) H.A. Weidenmüller, Proceedings of the International Conference on Nuclear Structure, Tokyo, 1977, Suppl. J. Phys. Soc. Japan 44, 701 (1978) and Proceedings of the NATO Advanced Studies Institute on Theoretical Methods in Medium Energy and Heavy-Ion Physics, Madison, Wisconsin, 1978 (in press)
17) R.A. Broglia and A. Winther, Phys. Lett. C 4, 153 (1972)
18) W. Nörenberg and H.A. Weidenmüller, Introduction to the Theory of Heavy-Ion Collisions, Lecture Notes in Physics, vol. 51 (Springer Verlag, Berlin-Heidelberg-New York, 1976)
19) N.G. van Kampen, Phys. Lett. C 24, 171 (1976)

MASS TRANSPORT AND RELATIVE MOTION IN DEEP INELASTIC HEAVY ION COLLISIONS

R. Schmidt +)
Joint Institute of Nuclear Research Dubna, USSR

Abstract

We investigate the mass transport combined with a dynamical statistical treatment of the relative motion in deep inelastic heavy ion collisions. The deformation of the fragments is taken into account implicitly. We calculate multidifferential cross sections of deep inelastic reaction products and compare it with experiment. Remaining discrepancies between theory and experiment in the $^{238}U + ^{238}U$ reaction are discussed.

1. Introduction

Deep inelastic heavy-ion collisions (DIC) are mainly characterized by two processes, strong energy damping in the relative motion and a large amount of mass (charge) transfer between projectile and target.

Whereas the energy damping of the initial kinetic energy appears within a short approach phase in the relative motion the mass diffusion takes place mainly during the time evolution of the "double nuclear system" /1/ which is formed in such type of reactions.

This circumstance has lead to the development of some statistical diffusion models /2, 3/ for heavy-ion collisions which look only at the time dependence of the mass asymmetry of the double nuclear system by means of Master- or Fokker-Planck equations. On the other hand, the strong energy damping in the relative motion has often been treated in solutions of dynamical Newton-type equations including frictional terms. The coupling of the classical trajectory of the relative motion to the intrinsic degrees of freedom can be taken into account /4/. This leads to a statistical treatment of the relative motion, too /5, 6/.

It is the purpose of this paper to combine an investigation of the mass transport /3/ with a dynamical statistical treatment of the relative motion /6/. Special attention is given to the influence of the dynamical deformation of the double nuclear system on the interaction times of DIC. We calculate single, double and triple differential cross sections of DI-products and compare it with experiment. Discrepancies between theory and experiment in the $^{238}U + ^{238}U$ reaction are discussed.

+) On leave from TU Dresden, Sektion Physik, DDR - 8027 Dresden

2. The model

We investigate DIC by means of a dynamical coupling of the classical trajectory of the relative motion to the mass transfer between projectile and target. Both the relative motion and the mass transfer are treated statistically however we provide that relative motion and mass transfer are statistically uncorrelated. Then the total distribution function is a product

$$F(t) = d_1(R, \Theta, P_R, P_\Theta, \langle Z_1 \rangle, t) \cdot d_2(Z_1, t) \tag{1}$$

where d_1 is the distribution function for the degrees of freedom of the relative motion R, Θ, P_R, P_Θ (polar coordinates and corresponding conjugate momenta) and d_2 represents the distribution function for the mass asymmetry degree of freedom (measured at the projectile like charge number Z_1). Eq. (1) we expect to be fulfilled since experimentally the ratio of width to mean value of the element distribution is found to be small. The coupling between relative motion and nucleon diffusion is taken into account through the mean value $\langle Z_1 \rangle$ in d_1 and the time t.

For the calculation of the distribution function d_1 we use a model /6/ which has been applied earlier to study mass integrated angular distributions of DI-fragments. This model is based on the theory of Hofmann and Siemens /4/ who derived in linear response theory a Fokker-Planck equation for the distribution function d_1 in the phase space of the collective degrees of freedom. Its Gaussian type solution is determined completely by the first (mean values) and second moments (statistical fluctuations) of the collective coordinates R, Θ and their conjugate momenta P_R, P_Θ. The equations of motion for the first moments are Newton-type equations including frictional terms. For the corresponding equations of the second moments a coupled set of first order differential equations can be derived /5, 6/. Here a time dependent temperature appears which is calculated with the internal excitation energy produced by friction. In the equation of the first moments we take into account the deformation of the fragments by modifying the nuclear interaction in the exit channel /6/. The deformation energy has a drastic influence on the calculated exit channel kinetic energy. It has been shown that the consideration of the deformation also improves the agreement between theoretical and experimental energy and mass integrated angular distributions of DI-fragments /7/. In this paper we are interested in element distributions too, and in view of the fact that the nucleon diffusion is strong correlated with the mean interaction time we shall study the influence of the dynamical deformation on the calculated interaction times.

We describe the time dependence of the distribution function for the charge assymmetry degree of freedom d_2 (see eq. (1)) by the Fokker-Planck equation

$$\frac{\partial d_2(t)}{\partial t} = -\frac{\partial}{\partial Z_1}\left[V_Z(E^*)d_2\right] + \frac{\partial^2}{\partial Z_1^2}\left[D_Z(E^*)d_2\right] \tag{2}$$

Here the relative motion enters via time variable t. For the drift coefficient V_Z and diffusion coefficient D_Z analytical expression have been derived by Nörenberg et al. /2/ within a microscopic model. In these expressions the relative motion enters via the mean excitation energy E^* produced by friction. Since for low excitation energies the statistical theory /2/ is not applicable (in particular the drift coefficient diverges for vanishing excitation energy) we introduce a form factor for the transport coefficients which is not included in the theory /2/. This form factor effects a linear decay of the transport coefficients for excitation energies smaller than 3o MeV /8/.

The solution $d_2(Z_1,t)$ of eq. (2) is a Gaussian with time dependent mean values $\langle Z_1 \rangle (t)$ and variances $\sigma_Z^2(t)$ /3/.

With the solutions d_1 and d_2 we obtain from the total distribution function F(t) (eq.(1)) multidifferential cross sections as

$$\frac{d^3\sigma}{d\Theta dE dZ_1} = \frac{2\pi}{k}\left(\frac{\mu}{2E}\right)^{1/2} \int_{\ell_{cr}}^{\ell_{max}} d\ell \cdot \ell \cdot d_2(t=\tau_{int}) \int dR\, dP_\Theta\, d_1(t\to\infty) \qquad (3)$$

where Θ represents the deflection angle, E the final kinetic energy and Z_1 the charge number of the DI-fragment. In eq. (3), k is the wave number of the relative motion, l_{cr} is the critical angular momentum as calculated dynamically, and l_{max} is the maximum value of l that contributes. Other cross sections are derived by integrating over the corresponding variables.

3. Results

Calculated interaction times as function of the initial relative angular momentum $\tau_{int}(l)$ are displayed in fig. 1. As it is seen, the deformation enhances the mean interaction times, but only by up to 30%. The interaction time for U+U is larger than for Xe+Sn in the high-l region due to the large amount of inertia, but smaller in the low-l regime since here the Coulomb repulsion is the dominating effect. The interaction times for Xe+Sn show an exponential behaviour near the critical angular momentum below which fusion occurs.

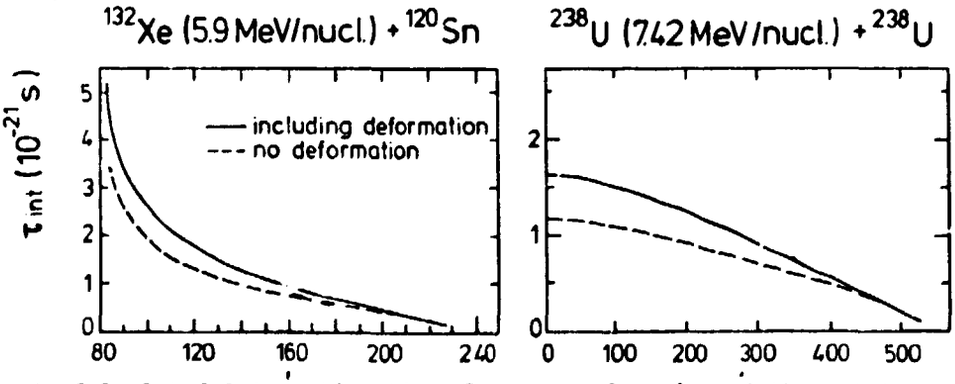

Fig. 1 Calculated interaction time τ_{int} as a function of the initial relative angular momentum l for the reaction Xe+Sn and U+U. Solid and dashed lines represent calculations with and without the consideration of the deformation energy, respectively. The indicated bombarding energies refer to all figures.

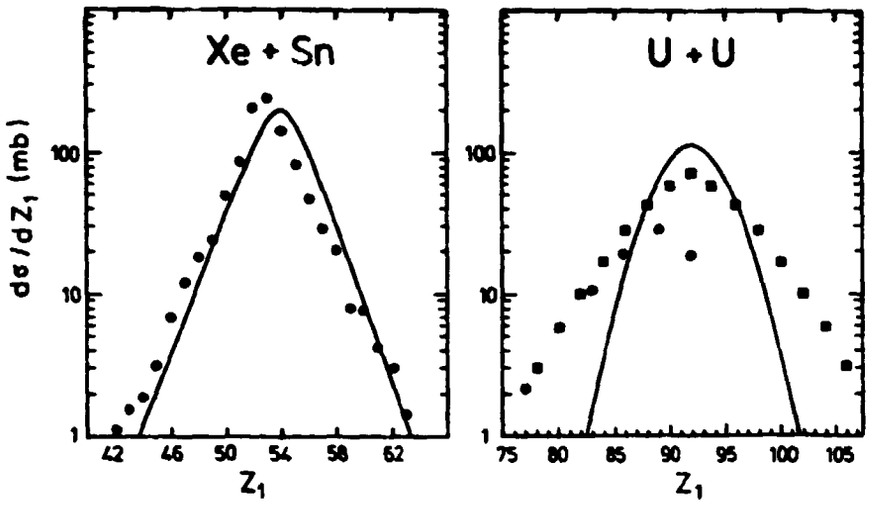

Fig. 2 Theoretical element distributions for the reactions from fig. 1 compared with experimental data (circles) /9/, /10/. In the U+U case the calculation has to compare with the primary element distribution (squares) as reconstructed /10/ from the data.

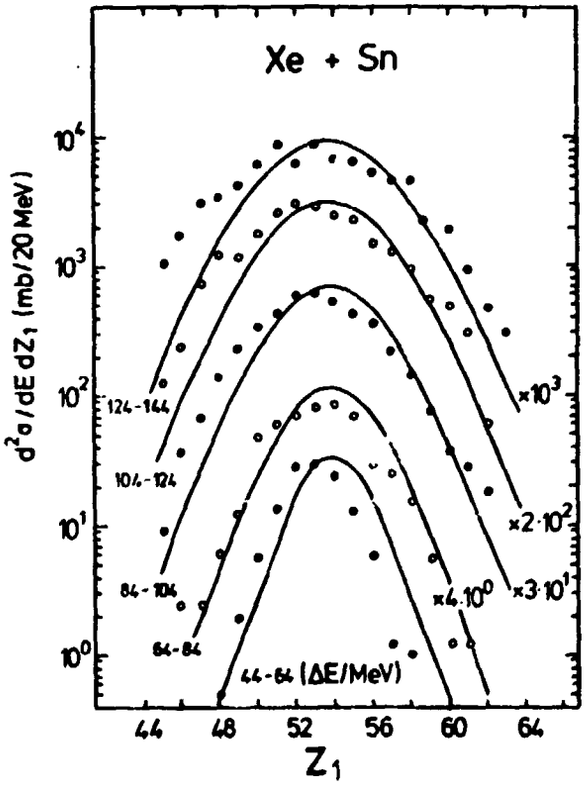

Fig. 3

Calculated double differential cross section $d^2\sigma/dZ_1 dE$ for Xe+Sn in comparison with the data /9/. The energyloss bins are indicated on the left. The normalization numbers on the right refer to both data and experiment.

With the mean interaction times from fig. 1 and the excitation energy dependent transport coefficients we calculate energy and angle integrated element distributions and compare it with the experimental data (fig. 2). Good agreement is found for Xe+Sn. For U+U the theoretical element distribution $d\sigma/dZ_1$ comes out to be too narrow by comparing with the experimental points for the reconstructed primary element distribution /10/. Particulary

the increase in the mean interaction time due to the deformation is by far not sufficient to explain this discrepancies as it was expected in /3/. In a schematic calculation /8/ we found that the effect of the closed Pb-shell on the diffusion process leads to a broadening of the element distribution and thus explains part of this discrepancy. It must be also realized that the extraction of the experimental points /10/ for the primary element distribution in the U+U case involves considerable uncertainties.

In fig. 3 we represent double differential cross sections $d^2\sigma/dZ_1dE$ for five cuts of the total kinetic energy loss in the Xe+Sn reaction. The increasing spread of the experimental element distribution with increasing energy loss ΔE as well as the absolute magnitude of the cross section is well reproduced by the model.

Finally, we have calculated triple differential cross sections $d^3\sigma/d\theta_{c.m}dE_f dZ_1$ for fragments Z_1 = 92, 86 and 80 in the U+U reaction (fig. 4). Here the calculation can only be expected to reproduce the correct trend, not the absolute magnitude of the triple-differential cross section because the experimental integrated element distribution $d\sigma/dZ_1$ is not reproduced (see fig. 2). The strong Coulomb repulsion in the U+U system leads to a backward-angle scattering for large energy loss. For elements around U a large amount of cross

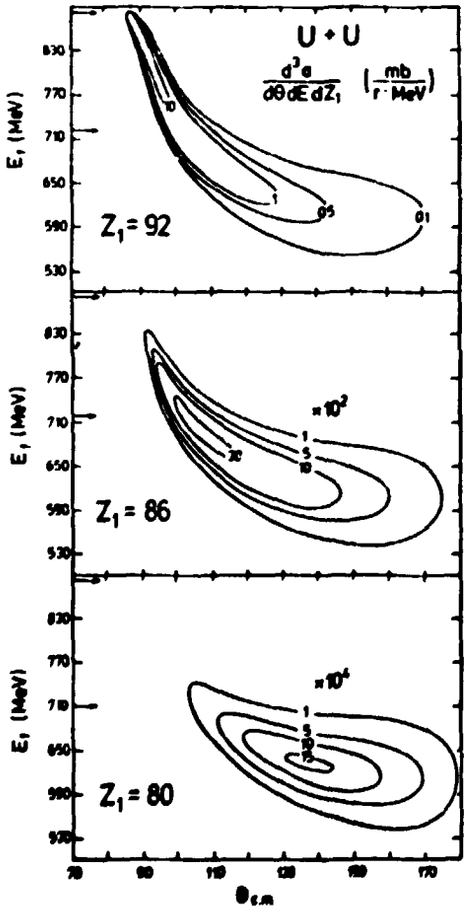

Fig. 4

Calculated correlation between mean fragment energy E_f, scattering angle $\theta_{c.m.}$ and charge number Z_1 of the outgoing fragments with Z_1 = 92, 86 and 80 in the U+U collision. The upper and the lower arrows indicate the initial kinetic energy and the Coulomb energy at the interaction radius calculated for spheres, respectively.

section is expected in the region corresponding to the grazing angle ($\approx 86^{\circ}$) and for kinetic energy close to the initial energy. With increasing transferred nucleons the distribution shifts towards larger angle and lower energies. In addition the width of the energy and angle distributions increase with increasing amount of nucleon transfer. Elements with charge numbers sufficiently far from that of the projectile one we expect at energies well below the Coulomb energy for spheres.

A large part of the results presented in this paper was obtained together with V.D. Toneev and G. Wolschin. I would like to express them my gratitude for the collaboration. I am grateful to V.V. Volkov for stimulating discussions.

References

/1/ V.V. Volkov, Physics Report 44 (1978) 93

/2/ W. Nörenberg, J. Phys. C5, 37 (1976) 141;
S. Ayik, B. Schürmann and W. Nörenberg, Z. Physik A277 (1976) 299 and A279 (1976) 145

/3/ G. Wolschin, Nukleonika 22 (1977) 1165 and Fizika 9 (1977) 513

/4/ H. Hofmann and P.J. Siemens, Nucl. Phys. A275 (1977) 464

/5/ H. Hofmann and C. Ngo, Phys. Lett. 65B (1976) 97;
C. Ngo and H. Hofmann, Z. Physik A282 (1977) 83

/6/ R. Schmidt and V.D. Toneev, Nukleonika 23 (1978) 83

/7/ R. Schmidt, V.D. Toneev and R. Reif, TU preprint 05-11-77, Dresden (1977) and submitted to Phys. Lett.

/8/ R. Schmidt, V.D. Toneev and G. Wolschin, Nucl. Phys. A, in print

/9/ H. Sann, A. Olmi, Y. Civelekoglu, D. Pelte, U. Lynen, H. Stelzer, A. Gobbi, Y. Eyal, W. Kohl, R. Renfordt, P. Rode, G. Rudolf, D. Schwalm and R. Bock, International Meeting on Heavy-Ion Collisions, Oak Ridge National Laboratory, Pikeville 1977

/10/ K.D. Hildenbrand, H. Freiesleben, F. Pühlhofer, W.F.W. Schneider, R. Bock, D.v.Harrach and H.J. Specht, Phys. Rev. Lett. 39 (1977) 1065

THE NUCLEAR FRICTION PROBLEM

L. Münchow, A. Pfitzner, H. Schulz
Zentralinstitut für Kernforschung Rossendorf, DDR - 8051 Dresden

A microscopic description of friction in heavy-ion collisions is given on the basis of a generalized master equation. The possible origin of dissipation is demonstrated by a simple model.

1. Outline of the problem

In deep-inelastic heavy-ion collisions a large amount of energy is transferred from the relative motion to the intrinsic degrees of freedom. Because practically all channels are open a usual coupled-channel-calculation is too difficult. One way to overcome this difficulty is to approximate the relative motion by a classical equation of motion with a dissipative force which accounts for the energy loss. Because all the underlying microscopic equations are symmetrical with respect to time reversal the first question is how the dissipation comes into play.

Denoting the many intrinsic degrees by $\{x\}$ and the variable for the relative distance of the two ions by $\{q\}$ we derive an equation of motion for the expectation value $\overline{q(t)} = \mathrm{tr}\, W(x,q,t)q$, W being the density operator of the system. Dissipative forces in this equation must have their origin in additional conditions which have to be imposed on the Liouville equation for $W(x,q,t)$. The Hamiltonion of the system is

$$H = H_0 + V(x,q),\quad H_0 = H_{in}(x) + H_c(q),\quad H_c(q) = \frac{p^2}{2\mu} + U(q)\,, \tag{1}$$

and the corresponding equations of motion are

$$i\dot{W}(x,q,t) = LW(x,q,t) \qquad i\dot{W}_0 = L_0 W_0 \qquad L = [H,\,] \tag{2a}$$

$$\mu\ddot{\bar{q}} = -\overline{\frac{\partial U}{\partial q}} - \bar{F} \qquad F \equiv \partial V/\partial q \qquad \bar{F} = \mathrm{tr}\, W(t) F. \tag{2b}$$

Before the collision begins the two nuclei are well separated, and $W(x,q,t)$ can be factorized:

$$\lim_{t\to-\infty} W(x,q,t) = W_0(x,q,t) \qquad W_0(x,q,t) = B_0(x)\,\rho_0(q,t)\,. \tag{3}$$

$B_0(x)$ is the density operator for the intrinsic degrees of the two ions and $\rho_0(q,t)$ the density operator for free relative motion. As the nuclei approach the interaction V comes into play. This may be simulated replacing V by $e^{\varepsilon t}V$. In scattering theory we have to take $\lim(\varepsilon\to 0^+)$ at the end of the calculation. This means an adiabatic switching on of the interaction in the remote past. Taking over the formal solution from scattering theory we may write [1]

$$W(t) = \lim_{\varepsilon\to 0^+} W_\varepsilon(t) \qquad W_\varepsilon(t) = W_0(t) - i\int_{-\infty}^{0} d\tau\, e^{iL\tau}\left[e^{\varepsilon\tau}V,\, W_0(t+\tau)\right]. \tag{4}$$

This expression is used by Gross to obtain from $\bar{F} = \lim_{\varepsilon \to 0} \mathrm{tr} W_t P$ a frictional force in the classical equation of motion[2]. This procedure is doubtfull because (i) dissipation in heavy-ion collisions cannot be produced by an adiabatic switching on in the remote past, but takes place only during contact of the two finite systems (e.g. in a time interval $0 \leq t \leq t_{coll}$), and (ii) dissipation has to do with energy sharing among many degrees of freedom during relaxation of the internal system.

2. A model for relaxation

Before considering the internal system we separate the relevant part for relative motion by a projection operator P used in the Zwanzig-formalism[3]:

$$PW(x,q,t) = B(x)\,\varrho(q,t) \qquad \varrho(q,t) = \mathrm{tr}_B W(x,q,t) \qquad P \equiv B(x)\,\mathrm{tr}_B$$
$$\mathrm{tr}_B \equiv \sum_n \langle n| \cdots |n\rangle \qquad H_{in}|n\rangle = \varepsilon_n |n\rangle \qquad \mathrm{tr}_B B(x) = 1. \tag{5}$$

PW is just that part of W which has to satisfy the scattering boundary condition (3):

$$\lim_{t\to-\infty} W(t) = \lim_{t\to-\infty} PW(t) = B_0(x)\,\varrho_0(q,t) \qquad B_0(x) = |0\rangle\langle 0| \,, \tag{3a}$$

where $|0\rangle$ denotes the ground state of the internal system. Now we imagine qualitatively the following first stages of the collision:

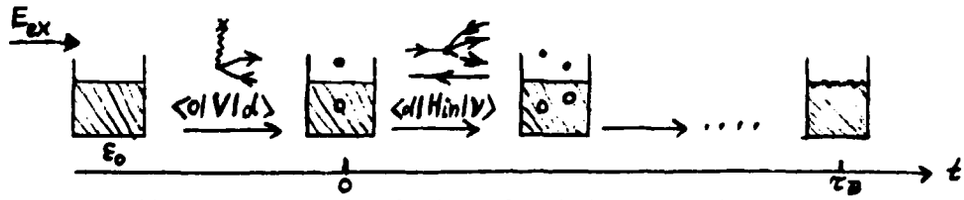

Fig. 1: Excitation energy E_{ex} is transfered from relative motion to the 0p-0h-state $|0\rangle$ forming a 1p - 1h - state $|d\rangle$, which "decays" into the complex states $|\gamma\rangle$ via the internal interaction contained in H_{in}

This picture implies the doorway-concept: The relative motion couples to the intrinsic degrees of freedom only via the doorway-states $|d\rangle$. In agreement with our approach we subdivide the remaining part of W(t) according to $(1-P)W(t) \equiv QW(t) = Q_0W(t) + Q_1W(t)$, where $\{Q_0\}$ represents the subspace of 1p-1h-states $|d\rangle$ and $\{Q_1\}$ the more complex np-nh-states with $n > 1$. This way we have the following conditions for the $\{Q\}$ -space:

$$(1)\ \ t<0:\ \ QW(t) = 0;\ \ (2)\ \ t = 0:\ \ Q_1W(0) = 0;\ \ (3)\ \ t \geq \tau_B:\ \ Q_0W(t) \approx 0 \tag{6}$$

The refinement of the $\{Q\}$ -space by subdivision into $\{Q_0\}$ and $\{Q_1\}$ is the new aspect which makes the dissipation mechanism more explicite.

If one could find a time-development operator T(t,0) in the $\{Q_0\}$ -space the third condition could be written as

$$T(t,0)Q_0W(0) \approx 0 \text{ for } t > \tau_B. \tag{6a}$$

The central question is then how to approximate T(t,0) in a proper way in order to satisfy condition (6a).

3. A generalized master equation for the relative motion

Applying the projection operators P, Q_0 and Q_1 to the Liouville equation (2a) yields a coupled system of equations for PW, Q_0W and Q_1W:

$$(i\frac{\partial}{\partial t} - PL)PW = PLQ_0W \qquad (i\frac{\partial}{\partial t} - Q_0L)Q_0W = Q_0LPW + Q_0LQ_1W \tag{7}$$

$$(i\frac{\partial}{\partial t} - Q_1L)Q_1W = Q_1LQ_0W \qquad \text{doorway concept: } PLQ_1 = Q_1LP = 0.$$

Elimination of Q_1W in the second equation and taking into account the initial condition $Q_1W(0) = 0$ provides

$$(i\frac{\partial}{\partial t} - Q_0L_{eff}(t))Q_0W = Q_0LPW \qquad Q_0L_{eff}(t)Q_0W(t) = Q_0LQ_0W(t) - i\int_0^t dt' Q_0Le^{-iQ_1Lt'}Q_1LQ_0W(t-t'). \tag{8}$$

The memory effect contained in $Q_0W(t-t')$ can be formally extracted by $Q_0W(t-t') = e^{i\mathcal{L}t'}Q_0W(t)$, where $\mathcal{L}$ describes the complete time-development in the $\{Q_0\}$ -space. We assume in the following that the energy transfer back to the relative motion is negligeble during t_{coll}. Therefore we may $\mathcal{L}$ approximate by the operator which describes time-development in $\{Q_0\}$ without coupling to $\{P\}$. This way we get a closed functional equation for $\mathcal{L}$, which may be "solved" by iteration:

$$\mathcal{L} \approx Q_0L - i\int_0^t dt' Q_0Le^{-iQ_1Lt'}Q_1LQ_0e^{i\mathcal{L}t'}. \tag{9}$$

There are, however, no arguments to treat the coupling Q_1LQ_0 as a perturbation. Therefore we keep the full $\mathcal{L}$ in $L_{eff}(t)$. With respect to V, however, we shall restrict ourselves to second order in the final equation for PW(t) and therefore we drop it completely in $L_{eff}(t)$:

$$Q_0L_{eff}(t) \approx Q_0L_0 - i\int_0^t dt' Q_0L_{in}e^{-iQ_1L_0t'}Q_1L_{in}Q_0e^{i\mathcal{L}t'}, \qquad L_{in} = [H_{in}, \cdot] \tag{10}$$

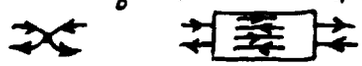

The first term contains the coupling between different 1p-1h-states, the second term represents the coupling of the doorway states via the more complex states $|v\rangle$.

To arrive at the final equation for $\varrho(q,t)$ we assume as usual the diagonal elements of V to be already included in H_c and therefore $tr_B\, V = 0$. From the definition of P in (5) we easily deduce $PLP = L_cP$, $Q_0L_cP = 0$ and $Q_0LP = Q_0L_VP$, with $L_c\,.. = [H_c, ..]$ and $L_V\,.. = [V, ..]$. Inserting the solution $Q_0W(t)$ of equ. (8) into the first equation of (7), we obtain the generalized master equation

$$(i\frac{\partial}{\partial t} - L_c)\varrho(q,t) = I(t) - i\int_0^t d\tau\, K(t,\tau)\varrho(t-\tau), \tag{11}$$

with

$$I(t) = tr_B\, l_V \exp[-iQ_0 \int_0^t dt' L_{eff}(t')]\, Q_0 W(0)$$

$$K(t,\tau) = tr_B\, L_V \exp[-iQ_0 \int_{t-\tau}^t dt' L_{eff}(t')]\, Q_0 L_V B_0$$

This basic equation for $\rho(q,t)$ has the same structure as the equation for an open system coupled to a "heat bath"[3]. It has still time reversal symmetry. The time-development operator T(t,0) which must satisfy condition (6a) is seen to be just $\exp[-iQ_0 \int_0^t dt' L_{eff}(t')]$. If it would be possible, for instance, to extract from it a factor $\exp[-\eta t]$ with $\eta = 1/\tau_B$, condition (6a) would be fulfilled automatically, but time reversal symmetry would then be destroyed.

4. A simple estimate for dissipation

After the initial state $|d\rangle$ (see fig. 1) has been formed we may forget how it was created and imagine it to be the first step in the formation of a compound nucleus during the scattering of an incident particle with energy $E = E_{ex} + \varepsilon_0(A) - \varepsilon_0(A-1)$ on a 1h-target. In the spirit of Feshbach's Unified Theory of Nuclear Reactions the 1p-1h-states then form the "open-channel-subspace"[4]. The corresponding component of the total wave function is the solution of a Schrödinger equation with the effective Hamiltonian

$$\mathcal{H}_{dd}(E) = H_{dd} - H_{d\nu} \frac{1}{H_{\nu\nu} - E} H_{\nu d} \qquad H_{dd} = \sum_{dd'} |d\rangle\langle d| H_{in} |d'\rangle\langle d'| . \tag{12}$$

The E-dependent part contains the coupling via the more complex states $|\nu\rangle$ and should therefore correspond to the stationary analogon of the time-dependent part of $L_{eff}(t)$ in equ. (10). Because the excitation energy E_{ex} is not sharp and the levels ε_ν lie very dense around E it seems to be appropriate to average over an interval ΔE around E. Doing this with a Lorentzean weighting function we arrive at

$$\overline{\mathcal{H}_{dd}(E)}^{\Delta E} = \mathcal{H}(E+iI) = H_{dd} - \Delta_{dd} - \frac{i}{2}\Gamma_{dd} , \qquad I = \frac{2\Delta E}{\pi} \tag{13}$$

with the shift and width operators Δ_{dd} and Γ_{dd}, respectively. We now imagine the real part of (13) to be already diagonalized leading to shifted 1p-1h-energies $\bar{\varepsilon}_d$ and the operator Γ_{dd} to have only diagonal elements. Then we obtain

$$\overline{\mathcal{H}_{dd}(E)}^{\Delta E} \approx \sum_d (\bar{\varepsilon}_d - \frac{i}{2}\Gamma_d^{\downarrow}) |d\rangle\langle d| \tag{14}$$

The damping width $\Gamma_d^{\downarrow}$ may me be roughly approximated by an average value independent of the special state $|d\rangle$[5]:

$$\Gamma_d^{\downarrow} = I \sum_\nu \frac{|H_{d\nu}|^2}{(\varepsilon_\nu - E)^2 + I^2/4} \approx \frac{4}{I} \sum_\nu |H_{d\nu}|^2 \approx \frac{2\pi}{D} \overline{v^2} \tag{15}$$

Here $\overline{v^2}$ is an average of $|H_{d\nu}|^2$ and D the mean distance of levels ε_ν inside ΔE.

Having this in mind we may write

$$\exp[-iQ_0\int_0^t dt' L_{eff}(t')] \approx \exp[-i(\bar{L}_0 - i\eta)t] \qquad \bar{L}_0 = [H_c + \bar{H}_{in}, \quad]$$
$$\bar{H}_{in} = \varepsilon_0 |0\rangle\langle 0| + \sum_d \bar{\varepsilon}_d |d\rangle\langle d| \qquad \eta \equiv 1/\tau_B = 2\pi\bar{v}^2/D. \tag{16}$$

It is obvious now that I(t) and $K(t,\tau)$ in (11) are proportional to $e^{-\eta t}$ and $e^{-\eta\tau}$, respectively, and therefore time reversal symmetry is violated. As a consequence $\bar{q}(t) = \mathrm{tr}_c\, \varrho(t) q$ follows an irreversible equation of motion. The result for η is rather plausible: the relaxation time $\tau_B \propto D/\bar{v}^2$ decreases with increasing level density and coupling of the 1p-1h-states to the more complex states. We may distinguish two cases:

1) $\tau_B \gtrsim t_{coll}$: The equation for $\bar{q}(t)$ becomes very complicated. May be it is more convenient to introduce for these long-living (coherent) excitations collective variables α, say, and include them in the subspace $\{P\}$. This would lead to a density operator $\varrho(q,\alpha,t)$ and, consequently, to coupled equations for $\bar{q}(t)$ and $\bar{\alpha}(t)$.

2) $\tau_B \ll t_{coll}$: The internal degrees relax very quickly to "near equilibrium". We may imagine the process to proceed by successive steps during t_{coll}:

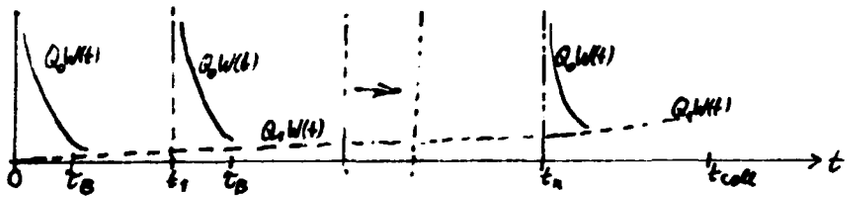

Fig. 2: Internal and relative motion are governed by different time-scales: $\tau_B \ll t_{coll}$. Each step at the times t_n should start with slightly modified initial conditions.

In the following we consider only times $t > \tau_B$. Then we may drop I(t) in equ. (11) and extend the integration $\int d\tau$ to $+\infty$, because the integral kernel K (τ) is essential only for $\tau < \tau_B$. For the solutions we keep the same symbol $\varrho(q,t)$. Eqs. (11) reduces to

$$(i\frac{\partial}{\partial t} - L_c)\varrho(q,t) = -i\int_0^\infty d\tau\, K(\tau)\,\varrho(t-\tau)$$
$$K(t,\tau) \approx K(\tau) = \mathrm{tr}_B\, L_V e^{-i(\bar{L}_0 - i\eta)\tau} Q_0 L_V B_0 . \tag{17}$$

One may ask if case 2) is realistic. The following values are considered as characteristic for heavy-ion collisions [6]:
10^{-22} sec $\leq t_{coll} \leq 10^{-20}$ sec, life time for a single particle excitation $\tau_{sp} \approx 10^{-22}$ sec. With $\tau_B \approx \tau_{sp}$ we may expect situations where $\tau_B \ll t_{coll}$ is well satisfied.

5. Classical equation of motion

The advantage to perform an expectation value with the relevant part $\varrho(q,t)$ instead of the complete density operator W(x,q,t) is obvious. With cyclic permutation under the trace tr = $\mathrm{tr}_c \mathrm{tr}_B$ and because of $[V(x,q),q] = 0$ we obtain

instead of (2b)

$$\dot{\bar{q}} = tr_c\, \dot{\varrho}(t) q = \frac{1}{\mu} tr_c\, \varrho(t) p \qquad p = \frac{1}{i}\partial/\partial q \tag{18}$$

$$\mu \ddot{\bar{q}} = tr_c\, \dot{\varrho}(t) p = - tr_c\, \varrho(t) \frac{\partial U}{\partial q} - \frac{1}{i}\int_0^\infty dt' e^{-\eta t'} tr_c\, tr_B\, B_0 \varrho(t-t') [F^I(t'), V] \ ,$$

with $F^I(t') = \exp[i\bar{H}_0 t'] F \exp[-i\bar{H}_0 t']$ and $\bar{H}_0 = H_c + \bar{H}_{int}$. It resembles only formally the corresponding equation in [2] because our physical background is different. At least at the beginning of the collision we have $B_0 = |0\rangle\langle 0|$ and therefor $tr_B B_0 \ldots = \langle 0| \ldots |0\rangle$. The memory contained in $\varrho(t-t')$ is essential only back to times $t-\tau_B$. For this small interval it seems justified to put $\varrho(t-t') \approx \exp[iL_c t'] \varrho(t)$. In accordance with our model we have $\langle 0 | d\rangle = 0$. Introducing the operators $\hat{\omega}^\pm \equiv \bar{H}_{int} - \varepsilon_0 \pm i\eta$ we write the integral in (18) in compact form:

$$\int_0^\infty dt' \ldots = tr_c\, \varrho(t) \langle 0| \mathcal{J} |0\rangle \qquad \mathcal{J} = F\mathcal{J}^{(-)} - \mathcal{J}^{(+)} F$$

$$\mathcal{J}^{(-)} = \frac{1}{2\mu i}\int_0^\infty dt' e^{-i\hat{\omega}^- t'} X_1(t') \qquad \mathcal{J}^{(+)} = \frac{1}{2\mu i}\int_0^\infty dt' X_1(t') e^{i\hat{\omega}^+ t'} \tag{19}$$

The time dependence of the operator $X_1(t')$ is governed by H_c only: $X_1(t') = 2\mu i \cdot \exp[-iL_c t'] V$. Expression (19) is suited to extract systematically conservative and dissipative contributions by succesive partial integration. Doing so we obtain finally

$$\langle 0|\mathcal{J}|0\rangle = \frac{1}{2\mu}\sum_{\ell=1}^{N} \langle 0| F \frac{(-1)^\ell}{(\hat{\omega}^-)^\ell} X_\ell(0) - X_\ell(0) \frac{1}{(\hat{\omega}^+)^\ell} F |0\rangle - \langle 0| \mathcal{J}_N |0\rangle \ , \tag{20}$$

where the rest integral takes the form

$$\mathcal{J}_N = \frac{1}{2\mu i}\int_0^\infty dt' \left\{ F \frac{e^{-i\hat{\omega}^- t'}}{(\hat{\omega}^-)^N} X_{N+1}(t') - (-1)^N X_{N+1}(t') \frac{e^{i\hat{\omega}^+ t'}}{(\hat{\omega}^+)^N} F \right\} \ , \tag{21}$$

and the operators $X_1(0)$ follow the recurrence relations

$$X_\ell(0) = [H_c ; X_{\ell-1}(0)] \qquad X_1(0) = 2\mu i V \ ; \qquad X_N(t') = e^{-iL_c t'} X_N(0) \ . \tag{22}$$

It is remarkable that the time development operator of relative motion $\exp[-iL_c t']$ is removed from the sum and shifted to the rest integral. We shall restrict ourselves to the first three terms in (20) which correspond to the Taylor expansion in powers of t' up to t'^2 in linear response theory [7,8].

In the following we assume that average values like $tr_c\, \varrho(t)(F_{od} V_{do} - V_{od} F_{do})$ vanish. This is satisfied, e.g. by the more restrictive assumption that the matrix elements of V and its derivatives are real [7]. Using the formal relations

$$\frac{1}{\hat{\omega}^\pm} = \frac{P}{\hat{\omega}} \mp i\pi\delta(\hat{\omega}) \qquad \frac{P}{\hat{\omega}} = \frac{\hat{\omega}}{\hat{\omega}^2 + \eta^2} \qquad \pi\cdot\delta(\hat{\omega}) = \frac{\eta}{\hat{\omega}^2 + \eta^2} \tag{23}$$

we can express the terms in (20) by the "derivatives" of the operators $\frac{P}{\hat{\omega}}$ and $\pi\cdot\delta(\hat{\omega})$ with respect to $\hat{\omega}$. As an example we give the contributions to equation (18) from the first two terms in (20):

$$\ell=1: \quad \mathrm{tr}_c\, \varrho(t) \frac{\partial}{\partial q} \langle 0|V \frac{\rho}{\omega} V|0\rangle \tag{24}$$

$$\ell=2: \quad \frac{1}{\mu}\mathrm{tr}_c\, \varrho(t)\left\{\pi\langle 0|F\delta_1 F p + pF\delta_1 F|0\rangle - i\langle 0|[F\rho_1 F, p]|0\rangle - \frac{1}{2}\frac{\partial}{\partial q}\langle 0|F\rho_1 F|0\rangle\right\} \tag{25}$$

$$\delta_1 \equiv \partial\delta(\hat{\omega})/\partial\hat{\omega} \qquad \rho_1 \equiv \partial\frac{\rho}{\omega}/\partial\hat{\omega}\,.$$

It is obvious that (24) and the third term of (25) are purely conservative. To get an ordinary friction force we have to extract $\overline{p(t)}$ from the p-dependent terms. For this purpose we must make assumptions about $\varrho(q,t)$. Taking into account $V(x,q)$ only up to second order we may approximate $\varrho(q,t)$ by $\varrho_0(q,t) = |\Psi(q,t)\rangle\langle\Psi(q,t)|$, where $\Psi(q,t)$ represents a wave packet. To have a practicable expression we approximate this packet by an ansatz footing on the structure of a free-motion-packet:

$$\Psi(q,t) \approx \left(\frac{\gamma^2}{\pi}\right)^{1/4} e^{-i\bar{E}t}\, e^{i\bar{p}\cdot q}\, e^{-\frac{\gamma^2}{2}(q-\bar{q})^2}\,. \tag{26}$$

$\bar{E}$ means center-of-mass energy of the packet and γ^2 characterizes its width: $\gamma^2 = 1/2\,\overline{\Delta q^2} = 2\,\overline{\Delta p^2}$ = const (spreading is neglected). From (26) we easily find $p|\Psi(q,t)\rangle \approx [\bar{p}(t) + i\gamma^2(q-\overline{q(t)})]\,|\Psi(q,t)\rangle$ and a corresponding expression for $p^2|\Psi(t)\rangle$.

To apply the Ehrenfest Theorem γ^2 has to satisfy the two conditions (i) $\gamma^2 \ll \mu^2\dot{\bar{q}}^2$ and (ii) $\gamma^2 \gg \frac{1}{a_0^2}$, where a_0 is a characteristic distance over which the nuclear potential changes essentially. For strong energy loss of the relative motion (i) may be violated as times goes by. We therefore keep the corresponding fluctuation term with $\overline{\Delta p^2}$ in the final equation:

$$\mu\ddot{\bar{q}} = -\frac{\partial U_{eff}(\bar{q})}{\partial\bar{q}} - c(t)\dot{\bar{q}} - \left(\frac{d}{dt}\frac{\partial}{\partial\dot{\bar{q}}} + \frac{\partial}{\partial\bar{q}}\right)\frac{m(\bar{q})}{2}\dot{\bar{q}}^2 - \frac{1}{2}\frac{\partial m(\bar{q})}{\partial\bar{q}}\cdot\frac{\overline{\Delta p^2}}{\mu^2}\,, \tag{27}$$

with $m(\bar{q}) = \langle 0|F\rho_2 F|0\rangle$ and the effective potential $U_{eff}(\bar{q}) = U - \tilde{U}$, where

$$\tilde{U}(\bar{q}) = \langle 0|V\frac{\rho}{\omega}V|0\rangle - \frac{1}{2\mu}\langle 0|F\rho_1 F|0\rangle - \frac{3}{8}\frac{1}{\mu^2}\langle 0|F'\rho_2 F'|0\rangle + \frac{1}{8}\frac{1}{\mu^2}\frac{\partial^2}{\partial\bar{q}^2}m(\bar{q})\,. \tag{28}$$

The friction coefficient becomes

$$c(t) = -2\pi\langle\Psi(t),0|\dot{F}\delta_1 F + \frac{1}{2\mu}F'\delta_2 F' - \frac{1}{4\mu}\frac{\partial^2}{\partial q^2}(\dot{F}\delta_2 F)|0,\Psi(t)\rangle\,. \tag{29}$$

Because all derivatives of the operator $\delta(\hat{\omega})$ are $\propto \eta = 1/\tau_B$, we find explicitely that friction increases with decreasing relaxation time. Apart from the quantum mechanical fluctuation term $\propto \overline{\Delta p^2}$ equation (27) has exactly the same structure as in linear response theory, and $m(\bar{q})$ corresponds to the inertial tensor in the three-dimensional case [7]. But U_{eff} and $c(t)$ are different from the results of linear response theory and resemble them only for heavy masses and smooth potentials.

The energy-balance following from (27) is slightly modified by the fluctuation term:

$$\frac{d}{dt}\left[\frac{m_{eff}}{2}\dot{\bar{q}}^2 + U_{eff}(\bar{q})\right] = -c(t)\dot{\bar{q}}^2 - \frac{d}{dt}\frac{m(\bar{q})}{2}\frac{\overline{\Delta p^2}}{\mu^2}\,, \qquad m_{eff}(\bar{q}) = \mu + m(\bar{q})\,. \tag{30}$$

If the fluctuation term is not small it makes no more sense to speak of a mass m_{eff} which moves in an average potential U_{eff}. It is evident that other dissipation mechanisms than ordinary friction come into play if we consider in (20) also terms with $\ell > 3$. We obtain, for instance, a contribution proportional to $\langle 0|F\delta_3 F^* + F^*\delta_3 F|0\rangle \dot{\bar{q}}^3$, and via $\dot{\bar{q}}\,\partial^2 U/\partial\bar{q}^2 \sim \mu\dot{\bar{q}}$ something like "radiation damping".

One concluding remark should be made. If we keep only the first term in equ. (29) we get a friction coefficient of similar form as in linear response theory [7,8]:

$$C(t) \approx -2\pi\langle\Psi(t),0|F\,\partial\delta(\hat{\omega})/\partial\hat{\omega}\,F|0,\Psi(t)\rangle = 4\pi\eta\sum_d \langle\Psi(t)||F_{0d}|^2|\Psi(t)\rangle \frac{\bar{\omega}_{d0}}{(\bar{\omega}_{d0}^2+\eta^2)^2} \qquad (31)$$

with $\bar{\omega}_{d0} \equiv \bar{\varepsilon}_d - \varepsilon_0$. The intermediate sum is not performed over the complicated eigenstates $|n\rangle$, but according to our model over the doorway states only. Because $\eta \to 0$ is strongly forbidden, c(t) never vanishes inspite of the energy gap $\bar{\omega}_{d0} > 0$. If we follow the concept of linear response theory from the beginning assuming a separable potential $V(x,q) \approx V(x,\bar{q}) \approx A(\bar{q})\cdot F(x)$ we find as usual the friction coefficient to be proportional to the first moment $\int_0^\infty dt'\, t'\, \chi_\eta(t')$, however with a damped "response function" $\chi_\eta(t) = \exp[-\eta t]\langle 0|\cdot F e^{-i\hat{\omega}t} - e^{i\hat{\omega}t} F|0\rangle$. If the damping factor is missing an additional smoothing procedure is necessary to make c(t) different from zero [8]. It is obvious that such artificial procedures are avoided in our formalism.

References

[1] N. Zubarev, Fortschr. Phys. 20 (1972) 471, 485

[2] D. H. E. Gross, Nucl. Phys. A 240 (1975) 472

[3] F. Haake in Springer Tracts in Modern Physics 66 (1973)

[4] H. Feshbach, Ann. Phys. 19 (1962) 287

[5] A. Pfitzner in ZfK-185 (1969)

[6] D. H. E. Gross, H. Kalinowski, Phys. Rep. 45, No. 3 (1978) 175

[7] H. Hofmann, P. J. Siemens, Nucl. Phys. A 257 (1976) 165

[8] P. J. Johannson, P. J. Siemens, A. S. Jensen, H. Hofmann, Nucl. Phys. A 288 (1977) 152

SOME ASPECTS OF THE STATISTICAL DESCRIPTION OF NUCLEAR REACTIONS

P. Mädler and R. Reif
Technische Universität Dresden, Sektion Physik, DDR - 8027 Dresden

The theoretical treatment of deeply inelastic heavy ion collisions assumes different relaxation times for different collective and intrinsic degrees of freedom. From experimental data one can conclude that the intrinsic degrees of freedom are rather fast modes. Therefore, they are assumed generally to be in a statistical equilibrium if one looks for the dynamics of the deeply inelastic process (see the contributions of W. Mörenberg and C. Ngo, p. 24 and 13 , respectively).

Using a time-dependent density matrix formalism nucleon induced precompound reactions are considered in order to study the relaxation of the intrinsic degrees of freedom. We start from the non-equilibrium statistical operator

$$\rho(t) = \frac{1}{Q}\exp\left\{-\sum_m \left[F_m(t)P_m + \int_{-\infty}^{0} dt' e^{\varepsilon t'}\left[F_m(t+t')\,\dot{P}_m(t') + \frac{d}{dt}F_m(t+t')\,P_m(t')\right]\right]\right\} \qquad (1)$$

which can be constructed with an arbitrary chosen set of observables $\{P_m\}$ and the thermodynamic conjugated parameters $\{F_m(t)\}$. In the limit $\varepsilon \to +0$ this operator obeys the quantum-statistical Liouville equation and represents retarded solutions [1]. In eq. (1) geometry dependent effects have been neglected already. For a first application of this concept to relaxation phenomena in nuclear reactions the Fermi gas model have been used with a hydrodynamic description of the relaxing system. The compound system as it is created after a few scattering events between the projectile and the target nucleons is divided into subsystems, composed of particles occupying single particle states in different energy ranges. Then the transition to the equilibrium stage is viewed as a relaxation process between these subsystems. Furthermore, all subsystems are assumed to be in a quasi-equilibrium characterized by a Fermi distribution with time-dependent parameters.

The compound system is described by the Hamiltonian

$$H = \sum_i H_i + \sum_{\substack{jk \\ \ell m}} \langle m\ell | v | jk \rangle\, a_m^+ a_\ell^+ a_k a_j \qquad (2)$$

The matrix elements $\langle m\ell|v|jk\rangle$ have been derived from parametrized free nucleon-nucleon cross sections [2]. The following set of observables has been chosen: $\{H_i, N_i, \vec{P}_i\}$ (H_i - total energy, N_i - particle number, $\vec{P}_i$ - total momentum of subsystem i). The conjugated parameters $\{F_m(t)\}$ are connected with the inverse temperature $\beta_i(t)$, the chemical potential $\mu_i(t)$ and the mean particle velocity $\vec{v}_i(t)$ in subsystem i, respectively using eqs. (1) and (2) the mean fluxes $\langle P_m \rangle = \lim_{\varepsilon \to +0} \mathrm{Tr}\,(\rho(t)\,\dot{P}_m)$ between the subsystems have been calculated. Connecting these quantities with the time derivatives of the parameters $F_m(t)$ one ends up with a coupled system of strongly non-linear differential equations determining the time evolution of thermodynamic parameters $\{F_m(t)\}$ or,

equivalently, of the mean values $\langle P_m \rangle$ [3]:

$$\sum_i F_i(t) \int_{-\infty}^{0} dt' e^{\varepsilon t'} \langle \dot{P}_m, \dot{P}_i(t') \rangle = -\sum_i \dot{F}_i(t) \langle P_m, P_i \rangle \qquad (3)$$

Here the bracket $\langle \ldots, \ldots \rangle$ denotes quantum-statistical correlation functions. In order to derive eq. (3) the time derivative $\dot{P}_m$ in eq. (1) has been neglected compared with the time dependence of the operators $P_m(t)$ in the Heisenberg representation. Moreover, the operator $\varrho(t)$ was linearized with respect to the interaction which was assumed to be small. The integrals in eq. (3) representing the kinetic coefficients have been evaluated using Wick's theorem. For numerical calculations these coefficients were computed for the equilibrium stage, but in the correlation functions $\langle P_m, P_i \rangle$ on the right hand side of eq. (3) the non-linear dependence from $\{P_m(t)\}$ have been taken into account. Furthermore, using the principle of detailled balance and the inverse cross sections given in ref. [5], in eq. (3) fluxes have been added in order to describe the depletion of the nucleus. This procedure gives the possibility to calculate the differential cross sections $\partial^3\sigma / d\varepsilon d\Omega$ (in a. u.).

To start the numerical integration of eq. (3) the distribution of the two nucleons after the first collision of the projectile in nuclear matter has been estimated following ref. [7]. Fermi distributions with the same first and second moment as the distributions derived in this way are used to fix the initial conditions. A comparison of both distributions shows that it is quite sufficient for excitation energies of about 20 MeV to subdevide the compound system in two subsystems only, with particles above and below the Fermi level, respectively. For higher energies the number of subsystems should be larger in order to approximate the initial distributions by Fermi distributions.

The numerical solution of eq. (3) shows that these is a fast stage of the relaxation process (about $5 \cdot 10^{-21}$ sec) and a slow one ($3 \cdot 10^{-21}$ sec for ^{93}Nb+n at E_n = 14.1 MeV). Therefore, in order to estimate the dependence of relaxation times on excitation energy E^* and mass number A it is sufficient to calculate the correlation functions for the equilibrium stage. In a wide range of E^* and A the kinetic coefficients are proportional to E^* and nearly independent of A but $\langle P_m, P_i \rangle \sim \sqrt{E^* A}$. Thus, for the relaxation time τ follows $\tau \sim \sqrt{\frac{A}{E^*}}$. From the numerical solution of eq. (3) one can draw the conclusion, that because of the strong coupling of the equations there is no remarkable difference in the relaxation times for energy, momentum and particle number. As an example, in fig. 1 it is shown that the predicted angular distribution of 14 MeV neutrons inelastically scattered from ^{93}Nb is in good agreement with experimental data as well as with theoretical results obtained by Yrie et al. [6] with an extension of the exciton model suggested by direct reaction theories.

After equilibration one can follow the decay of the compound nucleus by integrating eq. (3) formally until the residual nucleus has an excitation energy U below the neutron threshold. Interpretating the number of emitted neutrons $\langle A_3 \rangle = A_3(t)$ as an ensemble average mean neutron decay widths Γ_n, $\Gamma_n = \hbar \dot{A}_3(t) \equiv \Gamma_n(U)$, have been estimated. The index 3 refers to particles leaving the compound nucleus. These values correspond to the expression for the decay width,

which can be calculated from the total decay probability extracted from the Weisskopf expression in the Fermi gas model: $\Gamma_n(U) \sim e^{-\mathrm{const}\sqrt{\frac{A}{U}}\,B_n}$ (B_n - neutron binding energy).

References

[1] D.N. Zubarev, Dokl. Akad. Nauk USSR 140 (1961) 92;
D.N. Zubarev, Neravnovesnaja statistitsheskaja termodinamika, Moskva 1971

[2] N. Metropolis et al., Phys. Rev. 110 (1958) 185

[3] P. Mädler, R. Reif, G. Röpke, H.-E. Zschau, Phys. Letters 61B (1976) 427;
P. Mädler, R. Reif, to be published

[4] J. Dostrovsky, Z. Fraenkel, G. Friedlander, Phys. Rev. 116 (1959) 683

[5] M.L. Goldberger, Phys. Rev. 74 (1948) 1269

[6] Y. Yrie et al., J. Phys. Soc. Japan 39 (1975) 537;
Y. Yrie et al., Phys. Letters 62B (1976) 9

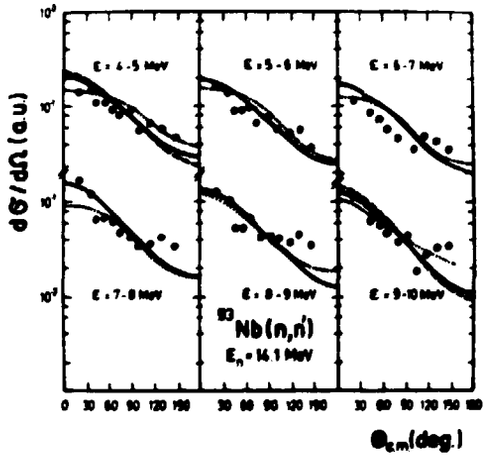

Fig. 1
Reaction ^{93}Nb(n,n'), E_n = 14 MeV. Comparison of calculated angular distributions with experimental data [6] and with theoretical predictions from an extended exciton model [6] (dotted lines). Solid lines: without precompound decay. Dashed lines: with precompound decay.

HEAVY-ION REACTIONS IN THE LIGHT OF TDHF§)

I.Hamamoto
NORDITA, Blegdamsvej 17, Copenhagen, Denmark

Abstract

By solving the time-dependent Hartree (TDH) equation in a one-dimensional model, I am going to discuss the following three subjects : By taking a single united system, 1) the damping of collective motions, 2) the ultimate state of TDH (related to the particle-evapolation spectra). By taking asymmetric collisions, 3) the particle-number transfer and the fluctuations in particle-number transfer.

The possibility of using the TDHF approximation to study significant features of heavy-ion collisions has been especially emphasized by the MIT group[1], and elaborate TDHF calculations with so-called realistic interactions and with full 3-dimensional geometry have been performed by several groups. However, we study a model[2], which is highly simplified but which we expect has sufficient structure for studying what can be reasonably studied by TDHF, what is the limitation of the TDHF model, what is the role of the normal modes in the time-development of the system, and so on.

It is known that there is no many-body bound-state in the one-dimensional model of Fermions interacting with a δ-function interaction. Thus, our model is one-dimension, but we choose an exponential form for the two-body interaction. The parameters of the model are chosen, so that the form of the Hartree potential is similar to that of the nuclear system. Each single-particle level is doubly degenerate. The system has the parity as a good quantum number. For the discussion of the subjects 1) and 2), I shall take the case of the excitation with positive-parity.

We have tried various ways of exciting the system at t=0, such as stretching the Hartree solution by a certain amount, or imposing a velocity-field, or random excitations of the system, or choosing initial conditions that correspond to a given amplitude of one of RPA modes. In addition, we have studied various ways of analyzing the time-dependent wave-functions such as the observation of the excitation energy, the distribution of the excitation energy over the bound RPA modes, the rate of particle-emission, the projection of the wave function onto the Hartree states. And if the system comes to a quasi-stationary oscillation, we project the TDH wave-functions onto RPA modes. Then, we Fourier-analyze the projected amplitudes of RPA modes, from which we study the anharmonicity and coupling of RPA modes.

In all cases, the excitation energy of the system is eventually taken away by particle-emission, and the ultimate state of the system is a static Hartree solution with fewer particles.

Now, as an example, let me take the system of 10 particles. There are 3 bound RPA modes with positive parity, of which the quantum-energies are 16, 39 and 44 in our energy unit. Fig.1 shows the two quantities which are considered to be a measure of the collective motion, for the case in which at t=0 the amplitude of the 10 % of respective RPA modes is added to the Hartree solution, and then as a function of time the system is developed according to the TDH equation. Note that the excitation energy is 0.16, 0.39 and 0.44, respectively,

---

§) This work was done together with B.R.Mottelson.

in our energy unit.

1) The damping of collective motions

Fig.2 shows the system's length for the case in which the Hartree solution of the 10-particles system is stretched by 10 % at t=0, and then the system develops as a function of time according to the TDH equation. The excitation energy of this example is 6.7, which is considerably smaller than the quantum energy of the lowest RPA mode. One sees that a damping of the collective stretching motion occurs clearly at the initial stage, but the damping is strongly dependent on the amplitude (or velocity) of the collective motion. Namely, after the amplitude is reduced by a factor 2~3 the damping becomes much smaller, and we are unable to observe any further reduction in collective motion. The energy which was removed from the collective motion is found to appear eventually as emitted particles. That is, the wave functions of the system develop tails extended far outside of the nucleus, and the tail describes a flux of particles running away to infinity. (In the numerical calculation we add to the self-consistent interaction in the TDH equation an imaginary potential far outside of the system, so that the particles once coming out from the system are absorbed and never come back to the system.) Around t=10~20, about half of the excitation energy has been taken away by emitted particles, while the rest remains in the bound RPA modes. The period of the oscillation, seen in fig.2, is in fact the period of the lowest RPA mode. Damping is certainly going on also for the small-amplitude oscillation around t=10~20, since we observe the particle-flux which is continuously outgoing. However, it takes too much time to follow this very moderate damping.

In fig.3 the kinetic energy of collective current of the same system as in fig.2 is drawn. Around t~0, almost all the excitation energy appears as kinetic energy of collective current, twice during each period. We can see that the damping of the kinetic energy of collective current is more or less the same as that of the system's length oscillation.

For comparison, in fig.4 we show the system's length as a function of time, for the case where at t=0 the Hartree solution is stretched by 30 % . The excitation energy is 39. Also in this case, the basic period of oscillation seen in the figure is the period of the lowest RPA mode.

2) The ultimate state of TDH

We examine what is the ultimate state of TDH, if we prevent particles from being emitted. Our expectation is : The TDH system is essentially a classical coupled field with an infinite number of degree of freedom. Therefore, the system follows eventually the "law of equi-partition of energy" which is a characteristic feature of classical statistical mechanics though not of quantum statistical mechanics. (In practice, the number of degree of freedom is finite, since we solve the TDH equation by taking a discrete space-mesh and thus the effective number of degree of freedom of the field is (particle-number) times (number of mesh-points). Anyhow the number of degree of freedom is very large.) That means, in TDH system the temperature distribution will never be obtained. Namely, we will not have evaporation of particles with a given temperature, but rather the ejection of particles whose velocities are directly related to the wall coupling mechanism and the separation energy.

Let me show the result of numerical calculation. At t=0 the Hartree solution

of the system was stretched by 30 %. Instead of adding an absorptive potential, we put an infinite wall at the place twice the nuclear size, so that the particles never leave the system and, thus, the energy of this system remains constant for ever. Fig.5 shows the quantity $\ln((1-f_n)/f_n)$ for the energies of the n-th Hartree single-particle states with positive-parity, where f_n is defined as $f_n = \sum_{\nu:\text{occ}} |\langle \phi_n^H | \psi_\nu \rangle|^2$ by using the TDH wave-functions ψ_ν and the n-th Hartree single-particle wave-functions ϕ_n^H. Namely, f_n is the occupation probabilities of the n-th Hartree single-particle state. Dots express the points at the very beginning, while cross-points are for $t \sim 70$. (Note that the time period of the lowest-lying positive-parity RPA mode is ~ 0.40) The single-particle states with positive energy are discrete due to the finite number of mesh points taken in the numerical calculations. Note that if we have the Fermi-distribution of excitations $f_i = (1+\exp((\epsilon_i - \lambda)\beta))^{-1}$ we get $\ln((1-f_i)/f_i) = (\epsilon_i - \lambda)\beta$, while if the system approaches "the equi-partition of energy", f_i becomes proportional to $(\epsilon_i - \lambda)^{-1}$ for $\epsilon_i - \lambda > 0$, and $(1-f_i)$ becomes proportional to $(\lambda - \epsilon_i)^{-1}$ for $\epsilon_i - \lambda < 0$.

From fig.5 we see that : The points expressed by dots shows almost the Fermi-distribution of excitations, while as the system evolves as time, we see that the distribution starts to show the feature of the classical system mentioned above.

3) Asymmetric collisions

Now, as the last subjects, I leave the problem of a single united system, and talk about the asymmetric collisions by using the same one-dimensional TDH model, considering the fact that almost all the "realistic" 3-dimensional TDHF calculations have been done for the symmetric collisions such as $^{16}O+^{16}O$ or $^{40}Ca+^{40}Ca$, mainly due to the limitation of the computation time.

Since we have only an attractive interaction, the system fuses in a collision with a very small incident velocity. As the incident velocity increases, an appreciable amount of particles (in general, not an integer number of particles) starts to come out from the fused system, and thus the final state becomes a binary system, besides a very small amount of particles which are ejected from respective excited vibrating system. As the incident velocity increases further, the distribution of the particle-number in the final binary system becomes closer to the initial distribution. Finally, for the incident velocity larger than a critical value, the incident two systems just go through each other, as far as the number of the particles in the final states is concerned. Here we talk about the number of the particles in the final states almost immediately after the final scission, since the excitation energy in the final states is eventually taken away by particle-ejection, and thus the number of the particles in the final binary system becomes smaller if we wait longer.

In figs.6.1 and 6.2 we see typical density-distributions during the collision of the (6+8) system, which show how the two (6- and 8-particles) incident systems penetrate each other. It is useful to define the moment of "the first scission", at which the two incident systems have passed through each other, as far as the number of particles is concerned. We have observed the presence of the moment of "the first scission" for all values of incident energies, namely even for the case in which the final state is a fused system. Indeed, the characteristic feature of different final systems appears at the time after

"the first scission".

In fig.7 as an example we take the (6+8) collision-system and show the amount of the particles (ΔN_{TDH}), which are transfered from the 6-particles system to the 8-particles system, as a function of the incident energy in the centre of mass system. (Other asymmetric collisions show very similar qualitative features.) We see that for the incident energy per particle, $E_{cm,inc}/A$, smaller than about 3 the systems fuse while for $E_{cm,inc}/A$ larger than about 6.5 the incident two systems just go through. The value 6.5 is less than 1/3 of the Fermi-energy of the 6-particles system and is almost equal to 1/4 of the Fermi-energy of the 8-particles system. For the value of $E_{cm,inc}/A = 4.5 \sim 5.5$ a complicated situation happens sometimes and the final state is not always binary.

In fig.7 we show also the fluctuations in particle-number transfer defined by $(\Delta N_{fl})^2 \equiv \langle \Psi | (\hat{n}_R)^2 | \Psi \rangle - \langle \Psi | \hat{n}_R | \Psi \rangle^2$ where $\hat{n}_R$ is the particle-number operator defined in the right half-space. It is seen that the fluctuations in the particle-number transfer ΔN_{fl} varies surprisingly little over the range of $E_{cm,inc}$ investigated here and remains as an appreciable value even after the final transfered particle-number (ΔN_{TDH}) becomes zero. (The maximum value of ΔN_{fl} given[3] by the restriction of the TDH model is 1.8 in the present case.)

At least in this one-dimensional TDH calculation, the net transfered particles ΔN_{TDH} cannot be a measure of the amount of the energy transfered from the relative motion to intrinsic excitations. And the quantity ΔN_{fl} does not seem to be a measure of the transfered energy either. The smallness of the present ΔN_{TDH} might have a connection with the absence of Coulomb potential and with the smallness of the difference between the chemical potentials of the two incident systems.

References

1) e.g., P.Bonche, S.E.Koonin and J.W.Negele, Phys.Rev.C13(1976)1226
A.K.Kerman, Proc.Int.Conf.Nuclear Structure, p.711, Tokyo, 1977
J.W.Negele, Lecture at the NATO-NSF Summer School, Madison, Wisconsin, June, 1978
2) A report of this calculation was made : I.Hamamoto and B.R.Mottelson, Proc. Int.Conf.Nuclear Structure, p.368, Tokyo. 1977
3) C.H.Dasso, T.Dossing and H.C.Pauli, preprint

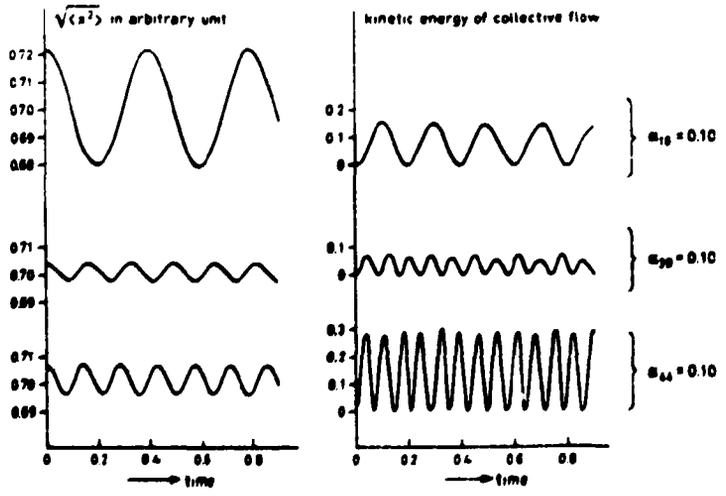

Fig.1

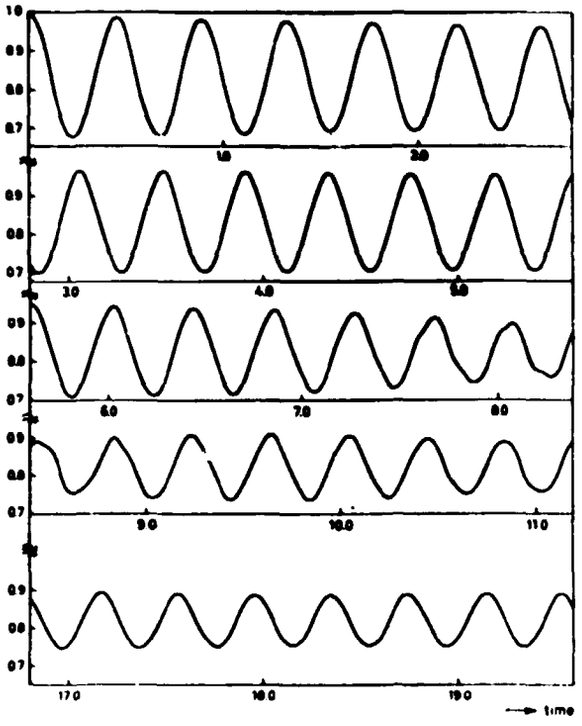

Fig.2 The system's length defined by

$$\left(\int_0^\infty \rho\, dx\right)^2 \Big/ \int_0^\infty \rho^2\, dx$$

as a function of time. At t=0 the Hartree solution of the system is stretched by 10 %

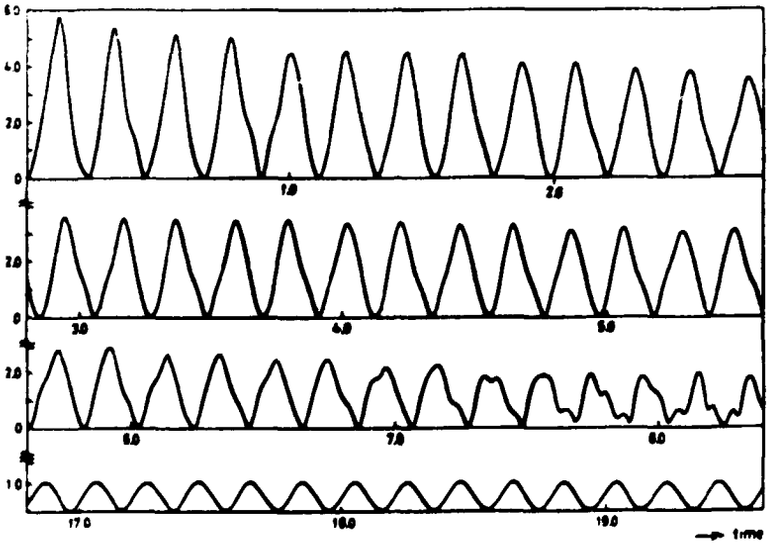

Fig.3 The kinetic energy of collective current defined by

$$T_{coll} \equiv \frac{1}{2}\int \frac{j^2}{\rho}\, dx \qquad \text{where} \qquad j \equiv \frac{\hbar}{m}\, \mathrm{Im}\left(\sum_{\nu;occ} \psi_\nu^* \frac{\partial \psi_\nu}{\partial x}\right)$$

as a function of time, for the same system as shown in fig.1.

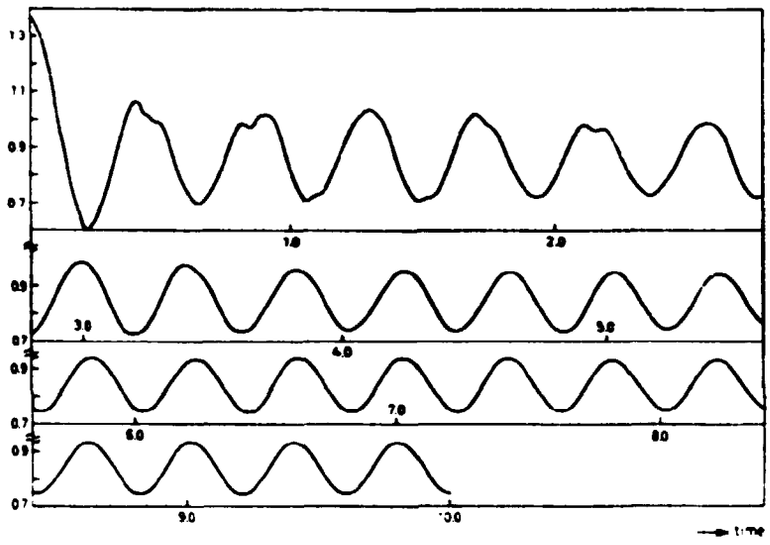

Fig.4 The system's length as a function of time. At t=0 the Hartree solution of the system is stretched by 30 % .

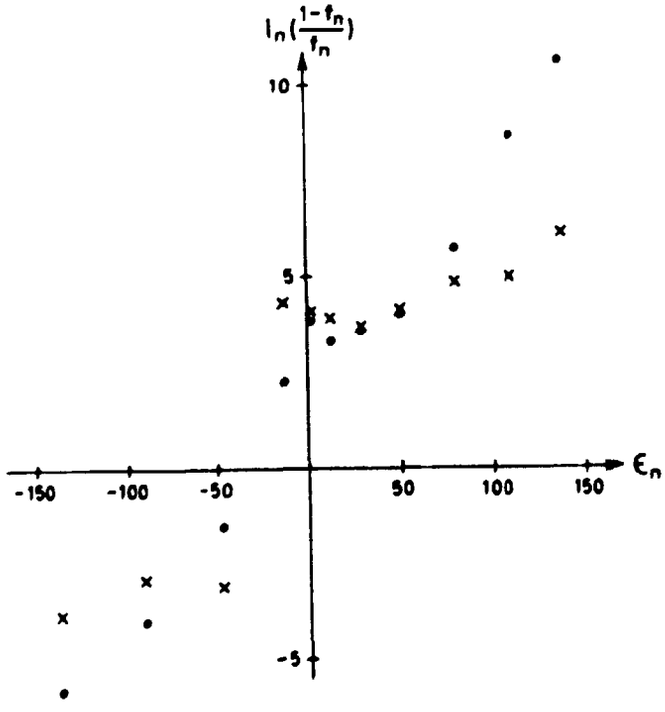

Fig.5 The occupation probabilities, f_n , of the n-th Hartree single-particle state as a function of the Hartree single-particle energy ϵ_n . Dots express the points at the very beginning, while cross-points are for t ~70.

Density-distribution of the [6 + 8] system
with $(E_{inc,cm}/A) = 4.29$

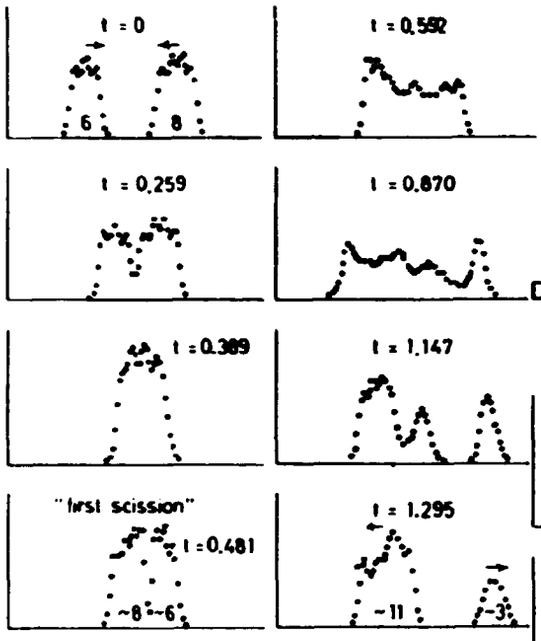

Fig.6.1 An example of asymmetric collisions

Fig.6.2 An example of asymmetric collisions.

Density-distribution of the [6 + 8] system
with $(E_{inc,cm}/A) = 9.94$

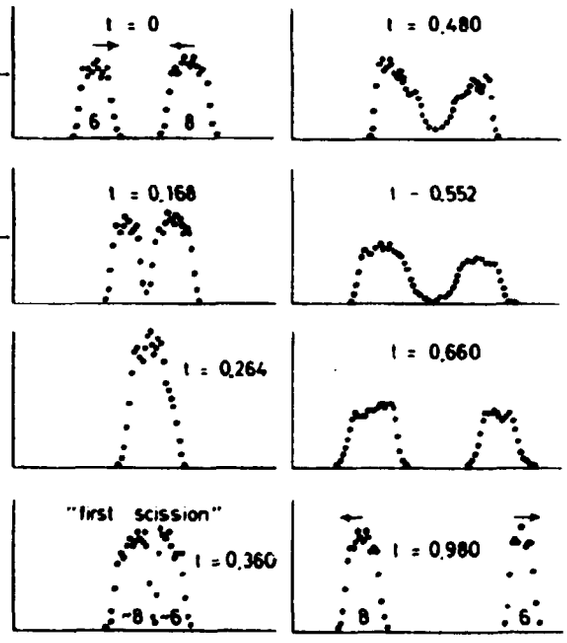

[6 + 8] collision-system

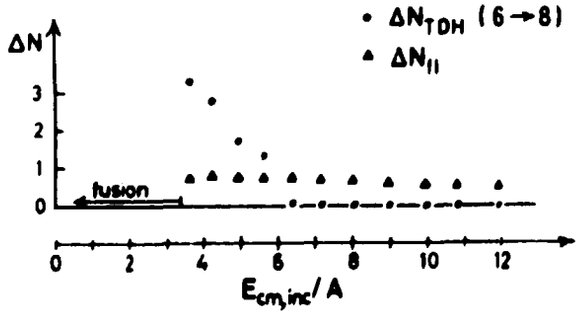

Fig.7 The amount of the net transfered particles, ΔN_{TDH}, and the fluctuations in particle-number transfer, ΔN_{fl}, as a function of the incident energy in the centre of mass system.

SCATTERINGS AND REACTIONS OF LIGHT HEAVY IONS

A. Strzałkowski
Institute of Physics, Jagellonian University and Institute of Nuclear Physics, Cracow, Poland

The interaction of light heavy ions with nuclei is discussed using alpha particle and ^{9}Be ion as two extreme examples of strong and weak bound projectiles.

In order to match as well as possible this review to its title alpha particle was selected as the first example. With its very tightly bound four nucleons it can be even considered an extreme example. To discuss also some peculiarities connected with weaker binding, the ^{9}Be ion was chosen as the second case. The neutron binding energy in ^{9}Be is so low /1.67 MeV/ that even its first excited state is not bound with respect to neutron emission.

The entrance channel phenomena are commonly described by the potential model with the complex optical model interaction. The question arises to what extent such description is physically reliable and unique for heavier projectiles. The fact that the interaction potential is derived from confrontation of the model predictions with experimental elastic scattering data leads to the well known ambiguities: the scattering cross section is determined by the asymptotic behaviour of the wave function at large distances, which can be matched to different internal wave functions for different potentials. The situation is even worse for heavy ions where the strong Coulomb interaction keeps the interacting particles at larger distances during collision.

Several attempts have been made to avoid this ambiguity by using some additional information to fix the values of parameters of the optical model potential, as e.g. deriving the real part of the potential from the effective nucleon- nucleon interaction and density distributions of the colliding nuclei in the microscopic models applying some folding procedure, 1/, 2/. For interaction of alpha particles with nuclei the most important conclusion from such models was that the form-factor of the potential differs definitely from the commonly assumed Woods-Saxon shape. As it follows from the microscopic models and was proved in many phenomenological analyses this form-factor can be well approximated by the n power of the Woods-Saxon expression with n = 2, 3/, 4/, or n = 2.65, 5/.

The most serious drawback of microscopic approaches using folding procedures is the neglect of antisymmetrization. Although in some recent studies, 6/, taking into account one nucleon exchange as the dominant part of the exchange amplitude, the main effects of antisymmetruzation were investigated and learned at least qualitatively, the complexity of such calculations forces us to use partly a phenomenological approach in determining the depth of the potential. The real progress was achived by D. Goldberg, 7/, who has shown that it is possible to fix unambiguously the parameters of the optical model potential for alpha particles from analysis of the elastic scattering data at sufficiently high energy, that the nuclear rainbow effect clearly appears, and for angles sufficiently large, that the great part of the nearly exponential fall-off of cross section is covered,

Fig. 1. It was shown recently, 8/, that such an analysis could be extended consequently to the region of lowe: energies using energy independent /Woods-Saxon/^{2} form-factor, Fig.2.

Unfortunately the situation is not so favourable for heavier ions. It was shown e.g., 9/, that the microscopic potential with density dependent nucleon-nucleon interaction and exchange effects included, leads to determination of the alpha particle-^{40}Ca potential at 104 MeV, while for ^{6}Li at 156 MeV some additional normalization of the potential depth is necessary. It is suggested that this behaviour is connected with the much weaker binding of ^{6}Li and importance of coupling with some break-up channels.

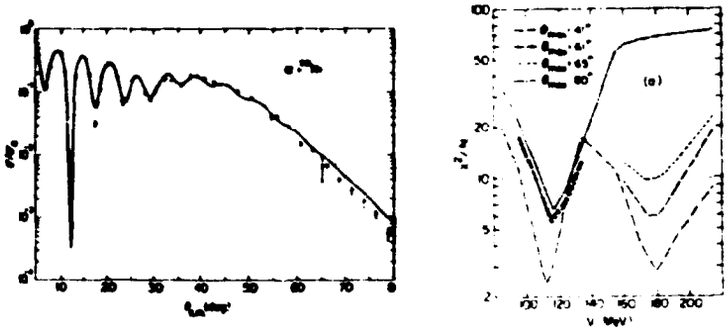

Fig. 1.

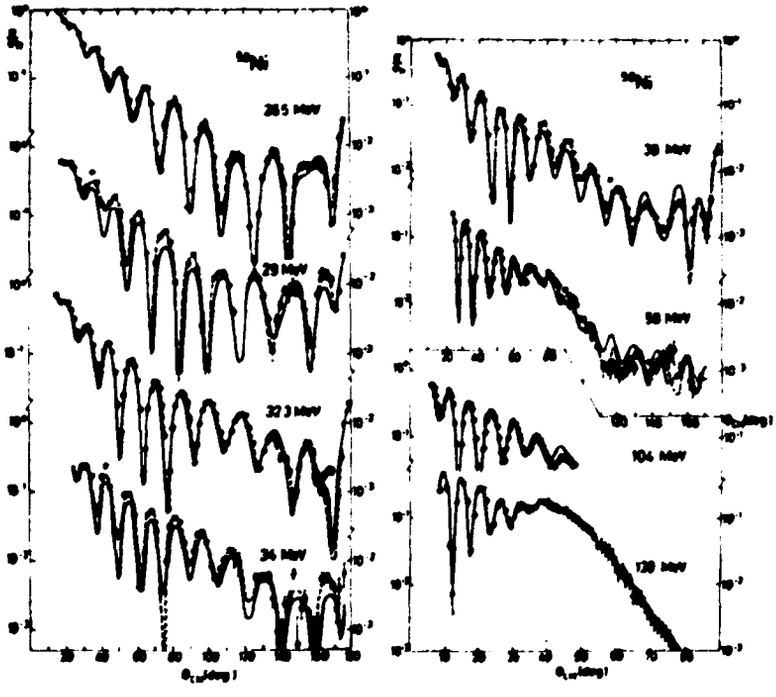

Fig. 2.

The low binding energy of the projectile leads to some interesting features of the scattering also in the region of lower energy where scattering could be well described by the simple Fresnel diffraction formula, 10/. This is especially distinctly visible for interaction of particlularly weakly bound ^{9}Be ions with ^{28}Si nuclei on the so called Wegner plot, Fig. 3, in which the ratio of the measured scattering cross section to the Rutherford one is presented in function of the classical distance of closest approach. While for some strongly bound projectiles like ^{16}O we obtain a sudden, almost exponential drop of cross section below some distance due to the absorption, for ^{9}Be ions two such absorption regions could be distinctly observed corresponding to the direct reaction

processes and to the more strong absorption due to the total fusion, respectively, 12/

The localization of the direct processes following from this picture could be confronted with the results concerning the dominating direct transfer process, i.e. $^{28}Si/^{9}Be, ^{8}Be/$ reaction, 13/. The angular distributions for this reaction have a typical bell shape, and from their maxima the value of the distance of closest approach could be calculated, at which the transfer process takes place according to the semiclassical model. From the measured angular distributions we obtain the value of d_0=2.3 fm in good agreement with the distance at which the weak absorption due to direct reactions sets in in the Wegner plot.

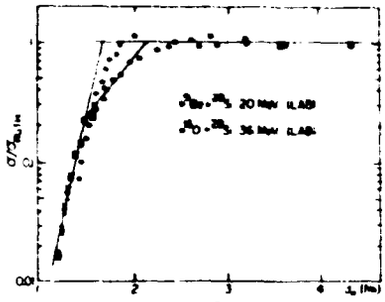

Fig. 3.

The total reaction and fusion cross sections show also some singularity connected with low binding energy of the projectile. For 20 MeV ^{9}Be ions interacting with ^{28}Si nuclei the total reaction cross section determined from the optical model analysis of the elastic scattering data, 14/, is equal σ_R = 1120 mb, and is much smaller than the fusion cross section estimated from light particle emission to be σ_{fu} = 735 mb, 12/. On the other hand the total reaction cross section determined according to the well known prescription from the quarter point of the angular distribution has a value $\sigma_{1/4}$ = 650 mb rather closer to the fusion cross section. Introducing corrections taking into account the further term in $\theta_{1/4}$ and smooth cut-off as suggested by W. Frahn, 15/, we obtain corrected value $\sigma_{1/4}^{corr}$ = 930 mb. It leaves still some discrepancy which is even larger at lower energies. This behaviour could be an indication that the strong absorption region, to which $\theta_{1/4}$ belongs, corresponds to the fusion process.

Discussing the interaction of light heavy ions it is impossible not to mention the so called anomalous large angle scattering /ALAS/ which in last few years attracted attention of many physicists. This effect - most distinctly appearing in scattering of alpha particles on ^{40} Ca nuclei - consists in considerable increase of the scattering cross section at extreme backard angles. It shows a remarkable isotope effect, beeing present for ^{40}Ca but not for ^{44}Ca nuclei, as well as a energy dependence, disappearing for energies above ca 50 MeV, Fig. 4. In the very extended studies performed recently, 16/, 17/, it was shown that the ALAS effect is connected essentially with considerably diminished absorption at lower energies for interaction with ^{40}Ca as compared with ^{44}Ca or other nuclei, Fig. 5, 18/. How such diminished absorption can lead to the observed increase of cross section at backward angles, could be understood on

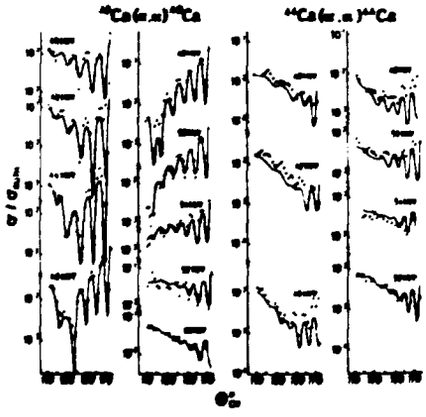

Fig. 4.

basis of a semiclassical model, 19/. In the semiclassical approximation scattering amplitude can be split in two parts: one corresponding to the reflexion at the external turning point in the potential and the second arising essentially from the reflexion at the internal turning point.

As the latter, responsible for the cross section at back-ward angles, is influenced mainly by the absorption, the decrease of absorption will result in the increase of cross section at backward angles, Fig. 6. It was also shown, 20/, that ALAS effect is strongly correlated with the energy levels density and the Q-values for the leading absorption process /α ,n/, which determine roughly the absorptive part of the potential.

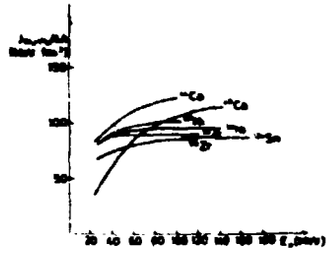

Fig. 5.

Although for alpha particles ALAS effects could be adequately described by the proper potential model, there exist also some other mechanisms capable to give account to the increase of cross section for scattering of heavy ions at large angles. One of such processes is the elastic transfer, 21/, well illustrated on Fig. 7 for the scattering of ^{9}Be on ^{12}C nuclei, 22/. As the Compound nucleus contribution /dotted line/ to the optical model one /dashed line/ is not sufficient to explain the rise of the cross section at backward angles, the elastic transfer of ^{3}He cluster was included in the DWBA approximation /dash-dotted line/. Such analysis involves the information about cluster states in the interacting nuclei i.e. about

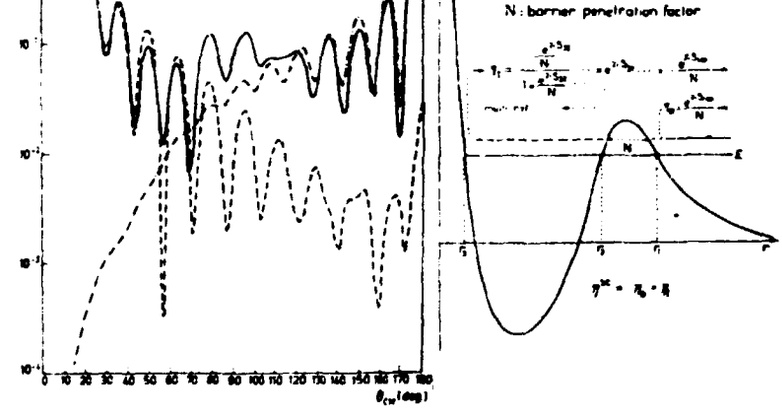

Fig. 6.

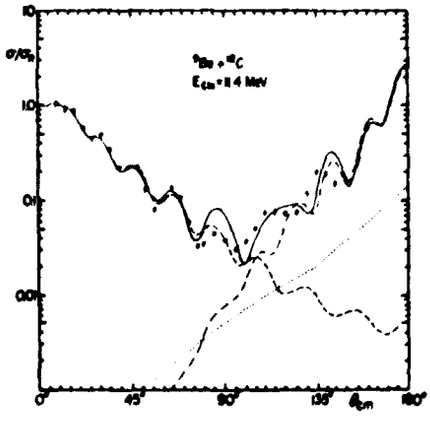

Fig. 7.

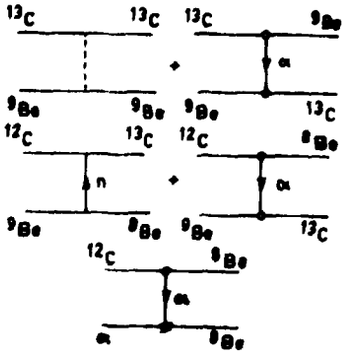

Fig. 8.

the cluster binding potential as well as about the cluster spectroscopic factors. Such information concerning the vertex of the elastic transfer graphs, Fig. 8, could occur also in vertexes of graphs for some other reactions. So e.g. the

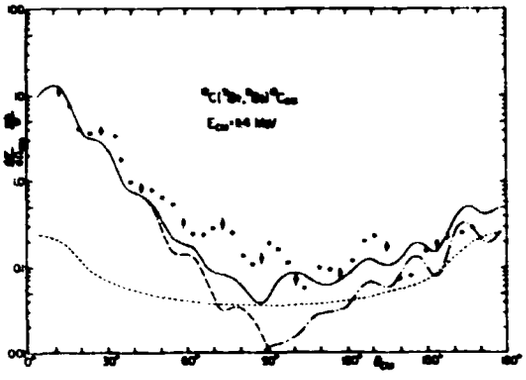

Fig. 9.

backward increase of cross section for the ^{12}C /^{9}Be,^{8}Be/ reaction, 23/, Fig. 9, could be succesfully explained as contribution from the alpha particle transfer reaction /line B/ using the same cluster parameters as in the elastic transfer contribution in the ^{9}Be + ^{13}C scattering. The ^{9}Be + ^{12}C system discussed here is very interesting also from some other point of view. For the nuclear system involving ^{12}C as one member the problem of resonances is one of the very long standing but still controversial problems of heavy ions physics. According to the well established criteria such resonances could be observed if the level density of the compound nucleus is low and the number of open channels small. This conditions are rather well fulfilled for the ^{9}Be + ^{12}C system, which since some time was considered a good candidate for observation of such resonances. Recently, 24/, 25/, quite strong energy dependence was observed for some reaction channels of this system, especially well visible for the /^{9}Be,^{8}Be/ reaction at backward angles. However the lack of correlation between structures observed in the excitation curves for different reaction channels and limitation of the observed phenomena to the extreme backward angular region only do not allow to draw a definite conclusion which of the three possible mechanisms: resonances, fluctuations or interference of some multistep direct reaction processes, is responsible for the observed phenomena.

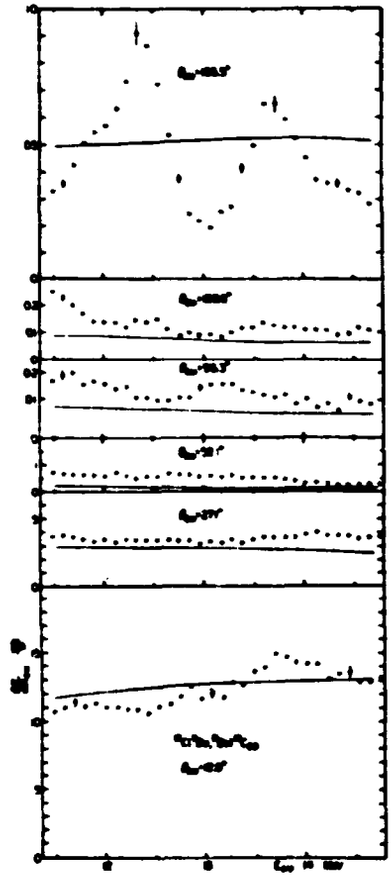

Fig. 10.

References

1/ A. Budzanowski, A. Dudek, K. Grotowski and A. Strzałkowski, Phys.Lett. 32B /1970/ 431,

A. Budzanowski, A. Dudek, K. Grotowski, Z. Majka and A. Strzałkowski, Particles and Nuclei 6 /1974/ 97,

2/ Workshop on Microscopic Optical Potentials, Hamburg /1978/.

3/ A. Budzanowski, K. Grotowski, M. Grzywacz and A. Strzałkowski, Inst. of Nucl. Phys., Cracow, Progr. Rep. 1 /1972/ 9,

4/ D.A. Goldberg, Phys. Lett. 55B /1975/ 59,

5/ F. Michel and R. Vanderpoorten, Phys. Rev. C16 /1977/ 142,

6/ Z. Majka, A. Budzanowski, K. Grotowski and A. Strzałkowski, Phys. Rev. C18 /1978/ 114,

7/ D.A. Goldberg and S.M. Smith, Phys. Rev. Lett. 29 /1972/ 500,
D.A. Goldberg, S.M. Smith and G.F. Burdzik, Phys. Rev. C10 /1974/ 1362,

8/ A. Budzanowski, H. Dąbrowski, L. Freindl, K. Grotowski, S. Micek, R. Płaneta, A. Strzałkowski, M. Bosman, P. Leleux, P. Macq, J.P. Meulders and C. Pirart, Phys. Rev. C17 /1978/ 951,

9/ Z. Majka, H.J. Gils and H. Rebel, Z. Phys. A288 /1978/ 139,

10/ W. Frahn, Nucl. Phys. 75 /1966/ 577,
W. Frahn, Ann.Phys.(N.Y.) 72 /1972/ 524,

11/ H.E. Wegner, R.M. Eisberg and G. Igo, Phys. Rev. 99 /1955/ 826,

12/ L. Jarczyk, J. Okołowicz, A. Strzałkowski, H. Witała, W. Zipper, J. Lang, R. Müller, E. Ungricht and J. Unternährer, Phys. Rev. C17 /1978/ 2106,

13/ J.Lang, R. Müller, J. Unternährer, L. Jarczyk, B. Kamys and A. Strzałkowski, Phys. Rev. C16 /1977/ 1448,

14/ R. Balzer, M. Hugi, B. Kamys, J. Lang, R. Müller, E. Ungricht, J. Unternährer, L. Jarczyk and A. Strzałkowski, Nucl. Phys. A293 /1977/ 518,

15/ W. Frahn, private comm.,

16/ Louvain-Zagreb-Mons-Cracow-Munich Collaboration, IPC-N-7801 1978,
T. Delbar, G. Gregoire, G. Paić, R. Ceuleneer, F. Michel, R. Vanderpoorten, A. Budzanowski, H. Dąbrowski, L. Freindl, K. Grotowski, S. Micek, R. Płaneta, A. Strzałkowski and K. Eberhard, Phys. Rev /in print/,

17/ H.P. Gubler, U. Kiebele, H.O. Meyer, G.R. Plattner and I. Sick, Phys. Lett. 74B /1978/ 202,

18/ K. Grotowski, IV EPS Nucl. Phys. Div. Conf.: Physics of Medium-Light Nuclei, Florence /1977/,

19/ D.M. Brink and N. Takigawa, Nucl. Phys. A279 /1977/ 159,
N. Takigawa and S.Y. Lee, Nucl. Phys. A292 /1977/ 173,

20/ J.S. Eck, W.J. Thompson, K.A. Eberhard, J. Schiele and W. Trombik, Nucl. Phys. A255 /1975/ 157,

21/ W. Von Oertzen and H.G. Bohlen, Phys. Rep. 19C /1975/ 1,

22/ L. Jarczyk, J. Okołowicz, A. Strzałkowski, K. Bodek, M. Hugi, J. Lang, R. Müller and E. Ungricht, to be publ.

23/ L. Jarczyk, B. Kamys, A. Strzałkowski, M. Hugi, J. Lang, R. Müller and E. Ungricht, J. Phys. G: Nucl. Phys. /in print/,

24/ J.F. Mateja, A.D. Frowley, A. Roy, J.R. Hurd and N.R. Fletcher, private comm.

25/ K. Bodek, J. Lang, R. Müller, E. Ungricht, L. Jarczyk, B. Kamys and A. Strzałkowski, to be publ.

ON MULTIPAIR TRANSFER BETWEEN SUPERFLUID NUCLEI

S. Landowne

Sektion Physik, Universität München, D-8046 Garching, Federal Republic of Germany

1. Introduction

A fascinating conjecture was raised some time ago by Goldanski and Larkin[1] about the possibility of observing a nuclear Josephson effect during the collision of two superfluid nuclei. Several theoretical papers have subsequently investigated this problem. (For a list of references, see ref.[2]) Because of technical difficulties - and in order to try to isolate the most essential features - the older works have relied on a number of simplifying or ad hoc assumptions. First of all, the reaction dynamics were considered below the Coulomb barrier in order to apply the semi-classical coupled channel formalism. This simplifies the dynamics but severely hinders the possibility of forming a good contact between the nuclei. Secondly, the nuclear structure problem of how to accurately calculate two-particle transfer form factors for heavy ion reactions was not solved. This is crucial in order to know the absolute strength of the pair transfer coupling. Because of recent progress in both areas, we have tried to reassess the question of multipair transfer between superfluid nuclei[2].

2. Reaction problem - the CCWKB approximation

When dealing with the collision of heavy systems at energies above the Coulomb barrier, we require a generalization of the semi-classical coupled channel formalism. This will be referred to as the coupled channel WKB (CCWKB) approximation. The CCWKB gives a set of coupled first order differential equations for the reaction amplitudes C_β which have the form[3]

$$\frac{d}{dr} C_\beta(r) = \sum_\alpha V_{\beta\alpha}(r) \frac{\exp(i[\phi_\beta(r) - \phi_\alpha(r)])}{\sqrt{k_\beta(r)\, k_\alpha(r)}} C_\alpha(r) \tag{1}$$

where ϕ_β is the radial action integral,

$$\phi_\beta(r) = \int_{r_\beta^0}^{r} dr'\, k_\beta(r') \tag{2}$$

and k_β is the local wave number,

$$k_\beta(r) = \frac{2\mu_\beta}{\hbar} \sqrt{1 - U_\beta(r)/E_\beta} \tag{3}$$

within the effective potential U_β. The turning point r_β^0 is defined by $k_\beta(r_\beta^0) = 0$. Finally, $V_{\beta\alpha}$ is the coupling between channels.

Eqs. (1) are integrated along a path which starts at large R and returns again to R, having encircled the turning points of the various channels. The initial values, $C_\beta(R) = \delta_{\beta,0}$, express the condition that

there are incoming waves only in the entrance channel. The final values give the WKB approximation to the S-matrix elements for the outgoing waves. Cross sections are obtained by summing the S-matrix elements in the usual way.

Eqs. (1) reduce to the semi-classical form if the transferred quantities (mass, energy, etc.) are small. One introduces an average wave number, k(r), and expands the phase difference to leading order in the transferred quantities. Then defining a time element, dt = dr/k(r), one recovers the classical trajectory picture.

In many cases the semi-classical form is adequate. There are, however, a few points to observe for reactions above the barrier which are not immediately clear from a trajectory viewpoint. Consider a wave incident upon the Coulomb barrier at an energy above it. Part of the wave is transmitted past the barrier and is absorbed from quasi-elastic channels while part is reflected at the barrier, corresponding to grazing collisions. The absorbed part corresponds to a classical motion with a turning point at very small distances. The "reflection above the barrier" is described by turning points which are near to the barrier position but lie off the real axis in the lower half of the complex r-plane[3]. These turning points are used to determine the integration path. In so doing, we eliminate contributions from distances inside the barrier and thus take into account the bulk of the absorption. Surface absorption can be added by imaginary parts of the effective potentials

3. Structure problem - two particle transfer form factors

Details of the two particle form factor problem for heavy ions can be found in ref.[4]. Here we will sketch the main points. The position coordinates for a reaction A(a,b)B where a = b + 2 are indicated in fig. 1. Since we consider the projectile and target to be superfluid, we express the wave functions of a and B in terms of correlated pairs of particles outside of superconducting cores. Thus,

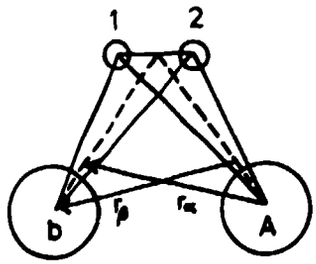

Fig. 1 Two particle transfer coordinates

$$\Psi_a = \sum_\nu (UV)_\nu \, \Psi_\nu(\vec{r}_{1b}, \vec{r}_{2b}) \, \Psi_b \quad (4)$$

and similarly for Ψ_B where U,V are the usual BCS occupation amplitudes. The two particle reaction is assumed to be governed by the potentials V_1, V_2 which bind the two particles to the cores. Thus (in post representation) the coupling interaction takes the form

$$V_{\beta\alpha}(r_\beta) = \sum_{\nu\nu'} (UV)_\nu (UV)^*_{\nu'} \int d^3\hat{r}_\beta \, d^3\vec{r}_{1A} \, d^3\vec{r}_{2A} \, Y^*_{\ell\beta}(\hat{r}_\beta) \, \Psi^*_{\nu'}(\vec{r}_{1A}, \vec{r}_{2A}) [V_1(r_{1b}) + V_2(r_{2b})] \, Y_{\ell\alpha}(\hat{r}_2) \, \Psi_\nu(\vec{r}_{1b}, \vec{r}_{2b}) \quad (5)$$

where the Y_ℓ are spherical wave functions for the angular realtive motions. Compared to uncorrelated pair transfer, this expression is super-enhanced by the factor[4)]

$$f \sim \sum_{\nu\nu'} (UV)_\nu (UV)_{\nu'} \approx [2\Delta/G]^2 \sim 50 \qquad (6)$$

The integrations in eq. (5) have been done explicitly. First the two particle functions are expressed in terms of relative and center of mass coordinates. The directions of the relative coordinate are trivially integrable while one numerical integration is required for the relative separation. Then eq. (5) reduces to the form of a one particle transfer where the one particle is located at the center of mass R_{12} of particles 1 and 2. An elegant procedure[4)] is to transform to a coordinate system defined by the triangle b - R_{12} - A. Exploiting the symmetry that the interaction depends only on the shape of the triangle, the orientation of the triangle can be integrated, trivially. This leaves a two dimensional numerical over the shape of the triangle.

Note that (5) depends on the center of mass coordinate r_β in the exit partition. To apply (1) we require a common radial coordinate r in each partition. Introducing a scaling parameter S_β, we can Taylor expand (5) about a point $S_\beta r$. The first term is used in eq. (1). Proper choice of S_β insures this is the main contribution[4)]. Thus we make a small approximation to longitudinal recoil. Transverse recoil is included in full. The main limitation of eq. (5) is the neglect of the successive transfer mechanism. Also for the two particle wave functions, we follow the usual method of binding the particles at half the reparation energy to simulate effects of continuum states.

4. The collision of Sn + Sn

We have considered the case of ^{122}Sn bombarding ^{120}Sn at an energy E_{LAB} = 630 MeV[2)]. We allowed for the stripping and pick-up of up to three neutron pairs leading to ground states. Thus we have a system of seven coupled channels indicated schematically in fig. 2.

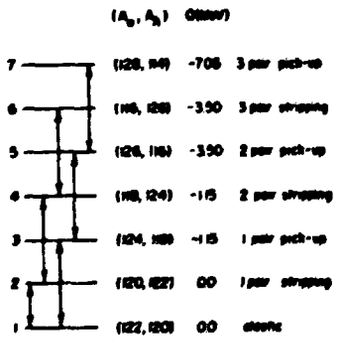

Fig. 2 Coupling scheme for multipair transfer

The coupling between channels is given by the form factor of eq. (5). It was calculated for the case of ^{122}Sn (^{120}Sn, ^{122}Sn) ^{120}Sn, allowing the two particles to move in eleven j-shells around the fermi level ($1h_{9/2}$). The same form factor was used for all couplings in keeping with the general pairing picture that the even Sn isotopes are a pairing rotational band based on the same intrinsic superfluid system.

If one furthermore neglects energy and mass transfer in eqs. (1), the resulting equations can be solved analytically with the result (see fig. 2),

$$
\begin{aligned}
c_1 &= \tfrac{1}{2}\,(\cosh\lambda_+ c + \cosh\lambda_- c) \\
c_2 = c_3 &= \tfrac{1}{4}\,(\lambda_+ \sinh\lambda_+ c + \lambda_- \sinh\lambda_- c) \\
c_4 = c_5 &= \tfrac{E}{\lambda_+}\,(\cosh\lambda_+ c - \cosh\lambda_- c) \\
c_6 = c_7 &= \tfrac{1}{4}\,(\lambda_- \sinh\lambda_+ c - \lambda_+ \sinh\lambda_- c)
\end{aligned}
\tag{7}
$$

where $\lambda_\pm = (2\mu E)^{1/2}$ while

$$c = \int dr\, V(r)/k(r) \tag{8}$$

is the first order amplitude for one-pair transfer. Expanding eqs. (7) to leading order gives

$$c_1 = 1;\quad c_3 = c;\quad c_5 = c^2/2;\quad c_7 = c^3/6 \tag{9}$$

For a given reaction one expects peak cross sections of

$$\sigma_i(\theta_g) \cong |c_i(\ell_g)|^2 \quad \sigma_{elastic}(\theta_g) \tag{10}$$

where θ_g is the grazing angle and ℓ_g is the grazing partial wave. Thus the above equations give simple relations between the transfer cross sections.

The crucial question is whether the enhancement due to the pairing correlations is sufficient to produce large probabilities for multipair transfer. Fig. 3 shows the result of the structure calculation. The curve labelled "superfluid-superfluid" is the fully correlated form factor. The other curves result from switching off the pairing correlations in the projectile and also in the projectile and target (treating ^{122}Sn as two independent particles in the $1h_{9/2}$ shell). This shows the expected enhancement (eq. (6)) of the two particle form factor due to the pairing interaction.

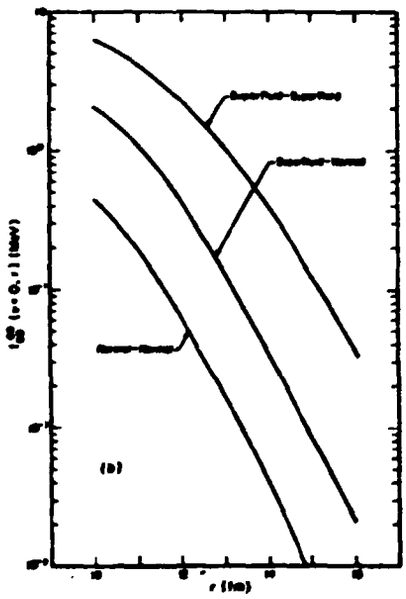

Fig. 3 Form factor for ^{120}Sn(^{122}Sn, ^{120}Sn)^{122}Sn

However, the coupled channel calculation does not give large absolute transfer cross sections. The results are summarized in table 1. Listed are the total cross sections for one to three-pair stripping reactions with the corresponding probabilities for the grazing partial wave. (Powers of ten are indicated.) Similar results[2)] hold for the pick-up reactions, as expected from eq. (7). The rows of table 1 correspond to two choices for the imaginary part of

ImU / ReV	one pair		two pair		three pair	
	σ(mb)	$\|C\|^2$	σ(mb)	$\|C\|^2$	σ(mb)	$\|C\|^2$
1/5	9.-01	6.-03	1.-03	2.-05	1.-06	1.-08
1/30	3.-00	5.-02	1.-02	5.-04	2.-05	8.-07

Table 1 Total cross sections and probabilities for multipair transfer

the nuclear potential. (The real part was fixed according to systematics[5]) The first choice may be called an "educated guess". The second corresponds to virtually no absorption in the surface region. It thus gives an upper limit on the cross sections to expect from grazing collisions. It is seen that even these numbers are quite small. We conclude that there is no indication for a supercurrent transferring many correlated neutron pairs during the Sn + Sn collision.

This work has been done in collaboration with R.A. Broglia, C.H. Dasso, B.S. Nilsson and A. Winther.

References

1. V.I. Goldanski and A.I. Larkin, Sov. Phys. JETP 26 (1968) 617
2. R.A. Broglia, C.H. Dasso, S. Landowne, B.S. Nilsson and A. Winther, Phys. Lett. 73B (1978) 401
3. S. Landowne, C.H. Dasso, B.S. Nilsson, R.A. Broglia and A. Winther, Nucl. Phys. A259 (1976) 99
4. R.A. Broglia, R. Liotta, B.S. Nilsson and A. Winther, Phys. Rep. 29C (1977) 291
5. P.R. Christensen and A. Winther, Phys. Lett. 65B (1976) 19

PHASE CORRELATIONS IN HEAVY ION SCATTERING

E. Hentschel, D. Wohlfarth, H.J. Thomas and D. Grambole
Zentralinstitut für Kernforschung Rossendorf, DDR - 8051 Dresden
V.I. Manko, G.B. Novatzki, S.B. Sakuta, D.N. Stepanov and V.I. Tshuev
IAE "Kurtschatow" Moscow, USSR

It is shown how in one-step processes the asymptotics of the incoming and the outgoing channel are related by the transferred energy and angular momentum. As a consequence of it we get new informations concerning the inelastic angular distribution: a small- and large angle limit of the Fresnel diffractive region and corrected phase relations between the elastic and inelastic channel.

1. Estimate of the outgoing asymptotic angle

The transfer of energy, angular momentum and masses plays an important role in heavy ion reactions. Generally, however, it is difficult to see the consequences directly in the measured distributions. At energies well above the Coulomb barrier many channels are involved and complicate the situation. Also at low energies around the Coulomb barrier the problem still exists. The relation between the incoming and the outgoing asymptotics is hidden in the numerical solution of coupled-channel equations and a lot of parameters is used to describe the forces and couplings. In our paper we present a simple and rigorous method to construct the outgoing asymptotical angle. We reduce the reaction to the most simple case of only two coupled channels and use the following assumptions:

(I) The process is only a one-step excitation of the one colliding particle. That means the transfer of energy and angular momentum occurs in one single act.

(II) The relative motion can be described in terms of classical trajectories.

(III) The excitation process is a sudden transition from the initial quantal state to the final one. It occurs at that point where the colliding nuclei have the closest distance which is allowed by the conservation laws.

Obviously these assumptions are quite rigorous ones and should be commented. Assumption (I) should be reasonable where DWBA-calculations are successful. Assumption (II) is valid at large distances with a more or less pure Coulomb force. That means according to ref.[1,2] the region of the angular distribution where Fresnel diffraction is the dominating oscillation structure. Problems can arise for very light nuclei where the nuclear surface is more transparent. Assumption (III) contains the essential geometrical aspects and has to be tested by the experimental data. It will be shown that the consequences of (III) directly can be observed in the measured elastic and inelastic angular distributions.

The incoming and outgoing channel are defined by the quantum numbers $[E,l,m_l,I,m_I)$ and $[E',l',m_l',I',m_I')$. Here E,l are the energy and angular momentum of the relative motion, I is the intrinsic nuclear angular momentum and m_l,m_I are the projections according to the Basel convention. Unprimed and primed quantities label the incoming and outgoing channel respectively. The excitation is characterized by the transferred quantities $\Delta E=E'-E$ and $\Delta\vec{l}=\vec{l}'-\vec{l}$. If the relative motion is formed by central forces then

$$\Delta l=m_I-m_I' \tag{1}$$

The geometrical meaning of (I),(II) and (III) is shown in fig.1. The particles are "inscattered" till to the reaction"point".There the sudden transition occurs and after that the particles are."outscattered". Only if we can be sure to have the possible states completely specified by the given set of quantum numbers we are allowed to identify this scattering classically in terms of an elastic scattering. Let rmin.and rmin' be the closest distance and θ and θ' be the classical deflection function in the initial and final channel respectively. The essential point of fig.1 is that the outgoing asymptotical scattering angle of the transition process θ_f is not identical with θ' but given by

(2) $$\theta_f = (1/2)(\theta+\theta') + \varphi$$

Classical descriptions existing so far[3] have neglected the turn of the symmetry axis given by φ .This angle φ,however, is important to understand the experimental data. To show that we assume for a first approximation the nuclear force to be zero and obtain for pure Coulomb hyperbolae the result

(3) $$\mathrm{ctg}(\theta'/2) = (1-\Delta l/l)\sqrt{1-\Delta E/E}\ \mathrm{ctg}(\theta/2)$$

(4) $$\cos\varphi = \sin(\theta/2)[1+(1-\Delta l/l)^{-2}((1/\sin(\theta'/2))-1) \quad \text{for rmin'>rmin}$$

(4a) $$\varphi = 0 \quad \text{for rmin'<rmin}$$

The last equation is an empirical result obtained from the experimental data. It reflects a quantum mechanical feature: the creation-"point" is at the symmetry axis of the "outscattering" trajectory.

Note that for $l \to \infty$ the angle θ' is vanishing but φ converges to the nozero limit

(5) $$\lim_{l\to\infty}\theta_f(\theta,\Delta l/l,\Delta E/E) = \lim \varphi(\theta,\Delta l/l,\Delta E/E) = \arccos\sqrt{1-\Delta E/E}$$

which depends only on $\Delta E/E$.

The addition of the nuclear force produces in the elastic channel the well known rainbows. For numerical calculations we use the real part of the optical-model potential which fits the elastic scattering data. According to (1) we obtain for each m-substate a deflection function $\theta_f(l,\Delta l/l,\Delta E/E)$. This is a new and important feature. It will be shown in the next section that the different m-substates give significantly different results.

3. Consequences for the inelastic angular distribution

Fig. 2 presents a typical result from which the conclusions for the inelastic angular distribution can be shown. In this figure all deflection functions for the Rochester data[4] $^{56}Fe(^{16}O,^{16}O'\gamma)^{56}Fe(2^+,0.841\ MeV)$ are shown. In fig. 3 the experimental data and the coupled-channel results from ref.[3] are displayed. From our construction (2) of the asymptotic angle θf we obtain the following conclusions:

3.1. Corrected 180°-phase rule

For the so called reversed Fresnel oscillations[1] and the nuclear-Coulomb interference[1,5] exists a 180°-phase rule between the elasic and inelastic angular distribution.We obtain by (2) a modified formulation: the 180°-phase rule exists between all pairs θ,θ_f related by (2). Figs. 3,4 and 5 show how accurate this corrected phase rule describes the experimental data.The m-dependence in fig.3 is reproduced nicely and the nuclear-Coulomb interference minima in figs. 4,5 are also well located by the arrows calculated from (2),(3) and (4) (ref.[6]) .

3.2. The m-dependence of the rainbow

The classical first rainbow angle corresponds approximately to that region where the Fresnel-diffraction pattern converges into the exponential decrease of σ/σ_R.

From figs. 2 and 3 we see in the inelastic scattering the m-dependence of this behaviour. Thus we find with sufficiently accuracy the upper limit of the Fresnel diffraction region in the inelastic scattering. Besides the strong $\Delta l/l$-dependence we find also a considerable $\Delta E/E$-dependence of the rainbow. This can be seen in fig. 4. The measurement and coupled-channel parameters are described elsewhere [7].

3.3. A small-angle limit of the inelastic Fresnel diffractive region

This effect is a consequence of (5) and illustrated in fig. 2. Unfortunately it is difficult to obtain experimental data. We confirmed the effect by coupled-channel calculations. Typical results are displayed in fig.4. In spite of the quite different behaviour all calculated curves are cutted according to (5). At energies well above the Coulomb barrier this effect is disturbed by the waves from the nuclear interiour.

3.4. A small-angle rainbow for $m<0$-excitations

The interplay between $\Delta l/l$ and $\Delta E/E$ in (3),(4) produces for sufficiently small values $\Delta E/E$ the rainbowlike behaviour of only the $m<0$-deflection function shown in fig.2. The diffraction pattern in the corresponding angular distribution is concentrated in a narrow angular region. An experimental confirmation is given by data recently published by Chait and Sinclair [8].

4. Conclusions

The examples given in sect.3 are part of an extensive analysis of all the available inelastic scattering data. We only summarize here the main results and refer for a detailed discussion to [9]. In particular we investigated the Fresnel diffractive region which provides the most clear test of our assumptions. In general we can state: if the process surely is a one-step excitation the relation between θ_f and θ given in eqs. (1) - (5) describe the experimental data with a surprising accuracy. All consequences can be confirmed by experimental data and, therefore, this description is a consistent one. Limitations occur if the excitation is not a pure one-step process. In some cases the coupling of other excitation channels [10,11] or of reaction channels [12,13] is of importance. In all these cases we find a typical behaviour: the experimental data are not in accordance with the values θ_f calculated by our estimate (2) but are shifted to smaller angles [9]. Therefore, the phase relations contain informations about the simplicity of the excitation process.

Acknowledgement

We are indebted to Dr.F.Videbaek (NBI Copenhagen) for important discussions especially concerning the limitations of our model coming from the coupling of additional channels. We thank him also for making available a coupled-channel code and a lot of experimental data. We are also indebted to Prof. A.Winther (NBI Copoenhagen) and Dr.S.Landowne (Univ.Muenchen) for valuable discussions. In the beginning of our work we had the help of Dr.H.U.Gersch and Dr.J.Moesner (ZfK Rossendorf) and Dr.M.Shukow (IAE Moscow). We would like to thank also Prof.A.A.Ogloblin (IAE Moscow) for encouraging us to investigate the nuclear-Coulomb interference.

References

[1] W.E.Prahn, Nucl.Phys. A273 (1976) 413
[2] W.E.Prahn and K.E.Rehm, Phys.Reports C37 (1978)
[3] P.F.Christensen,V.I.Manko,F.D.Becchetti and J.R.Nickles, Nucl. Phys. A207 (1973)
K.Alder and A.Winther, "Electromagnetic Excitation" North Holland Publ., Amsterdam, 1975
[4] S.G.Steadman, T.A.Belote, R.Goldstein, L.Grodzins, D.Cline, M.J.A. de Voigt and F.Videbaek, Phys.Rev.Lett. 33 (1974) 499
[5] R.A.Malfliet, S.Landowne and V.Rostokin, Phys.Lett. 44B (1973) 283
[6] D.Grambole et.al., Proc.Tokyo Conf. 1977, Contr.p., 597
[7] D. Wohlfarth et.al. to be published
[8] B.T.Chait and D.Sinclair Nucl.Phys. A279 (1977) 517
[9] E.Hentschel et. al. to be published
[10] F. Videbaek, private communication
[11] D.L.Hillis, E.E.Gross, D.C.Hensley, L.D.Rickertsen, C.R.Bingham, A.Scott and F.T.Baker, Phys.Rev.Lett. 36 (1976) 304
[12] K.S. Low, Journ. Phys. Soc. Jap. Suppl. 44 (1978) 267
[13] S. Landowne, private communication

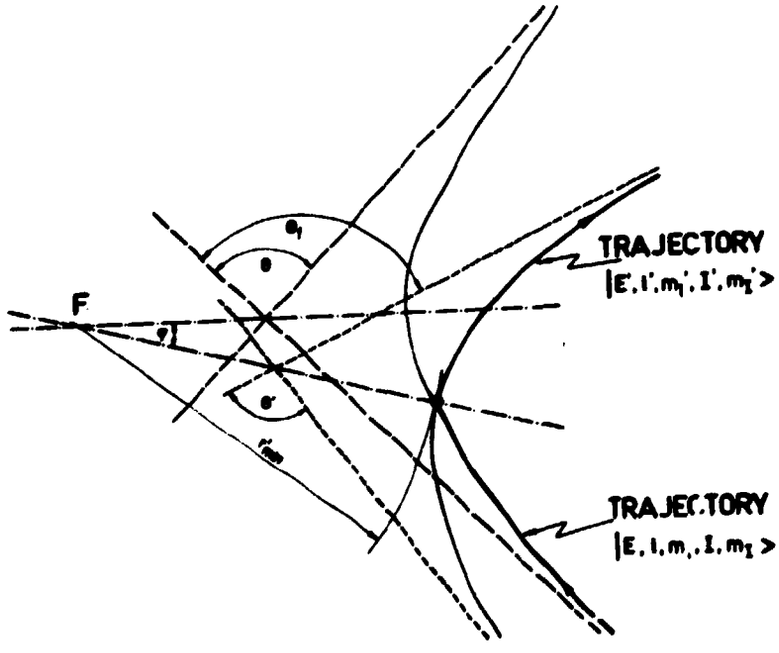

Fig. 1
Construction of the outgoing asymptotical angle

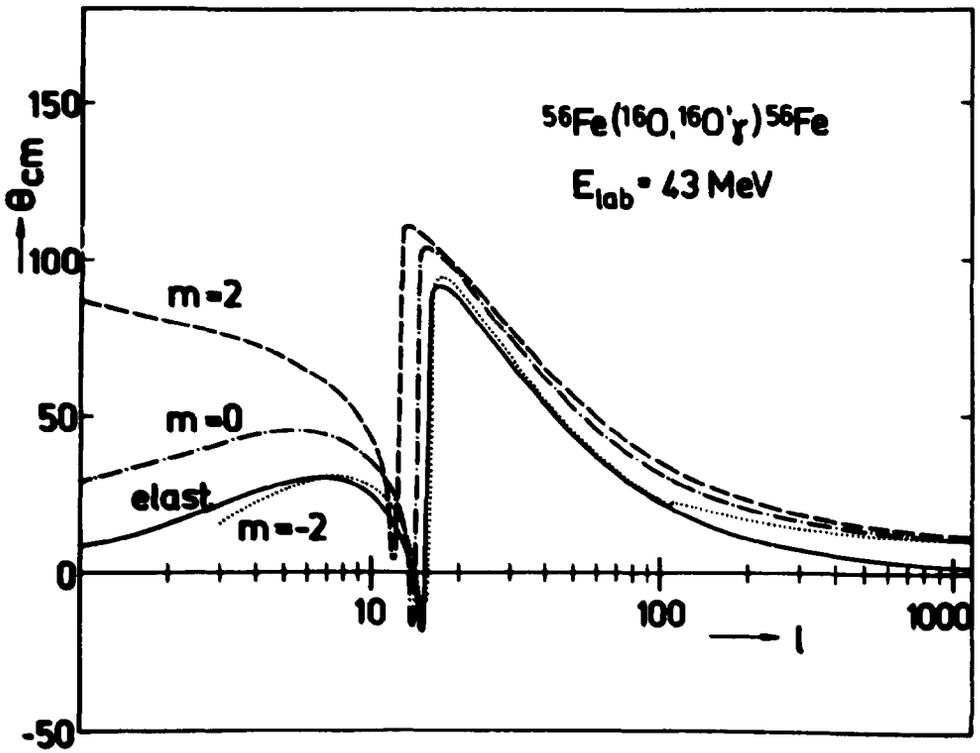

Fig. 2
Deflection functions for the $^{56}Fe(2^{+})$-excitation. The optical potential has been taken from ref. [4] .

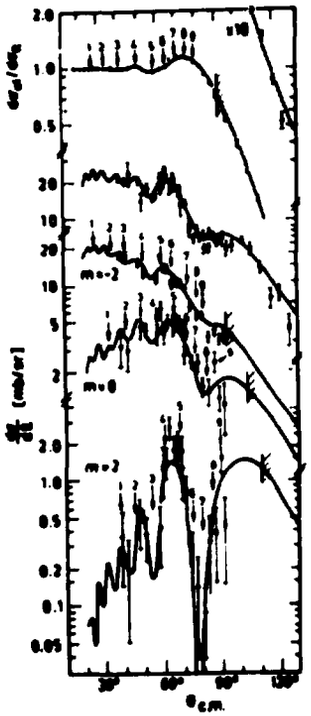

Fig. 3

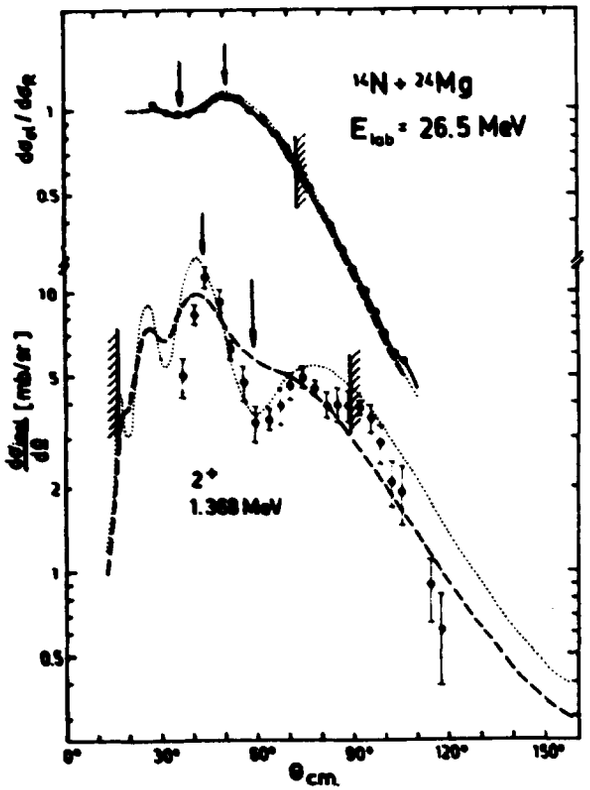
$^{14}N + ^{24}Mg$
E_{lab} = 26.5 MeV
$d\sigma_{el}/d\sigma_R$
$d\sigma_{inel}/d\Omega$ [mb/sr]
2^+
1.368 MeV
$\Theta_{cm.}$

Fig. 4

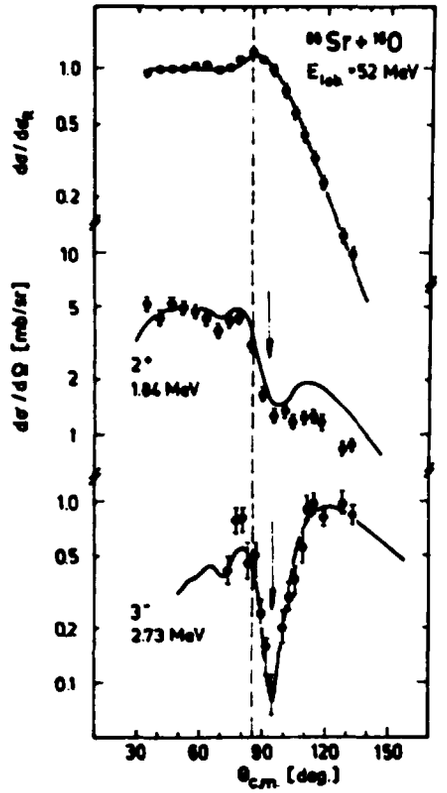
$^{88}Sr + ^{16}O$
E_{lab} = 52 MeV
$d\sigma/d\sigma_R$
$d\sigma/d\Omega$ [mb/sr]
2^+
1.84 MeV
3^-
2.73 MeV
$\Theta_{c.m.}$ [deg.]

Fig. 5

STRUCTURES IN THE ENERGY DEPENDENCE OF NUCLEAR REACTION CROSS SECTIONS

I. Rotter
Zentralinstitut für Kernforschung Rossendorf, DDR - 8051 Dresden

Abstract: The results of calculations in the continuum shell model for overlapping resonance states are given and discussed.

Structures with different widths have been observed for many years over a very broad energy range in different types of nuclear reactions. Besides the well known gross structure, substructures are observed in some isobaric analog resonances [1]. In heavy ion reactions, gross and substructures have also been observed [2]. In these cases, the level density is high and the single resonance states overlap. Therefore, an investigation of the properties of overlapping resonance states is necessary in order to explain the structures observed experimentally.

An investigation of the properties of overlapping resonance states is possible in the framework of the continuum shell model formulated by Barz et al.[3]. The advantage of this model is the unified description of nuclear structure and nuclear reaction aspects. In a first step, the usual shell model problem is solved and the shell model energies and wavefunctions of the discrete states (QBSEC) are obtained. In a second step, the coupling of the discrete states to the continuum is calculated by a coupled channels method. The wavefunctions, widths and energies of the resonance states are obtained by a diagonalizing procedure. The reaction cross section is calculated by means of the wavefunction ψ obtained as the solution of the Schrödinger equation $(H - E)\psi = 0$. This method working for isolated as well as for overlapping resonance states allows to investigate the resonance picture of the cross section.

Numerical calculations have been performed for the $^{15}N+n$ reaction with realistic nuclear structure wavefunctions. The results show that even for $\Gamma \approx D$ individual resonance states cannot always be identified in the cross section (Γ - average width, D - average distance between the resonance states). In dependence on the ratio Γ/D different types of structures may appear. While structures which are caused by only one resonance state appear at the same energy in all channels this is not necessarily the case for structures which are generated by several overlapping resonance states. The centre of these structures may be shifted in the different channels because of the different partial widths. The "widths" of the structures are determined, to a great deal, by the distance of the single resonance states which lie close together by chance due to fluctuations in the level density.

For illustration, the cross section for elastic and inelastic neutron scattering on ^{15}N is shown in fig. 1 in dependence on the number of resonance states (0^+, 1 states with 2p-2h structure). In the first case, there is only one resonance state which determines the shape of the cross section. Then two resonance states with $\Gamma < D$ are added. The number, positions and widths of the resonance states are shown in the middle of the figure. The shape of the cross section becomes intermediate-like.

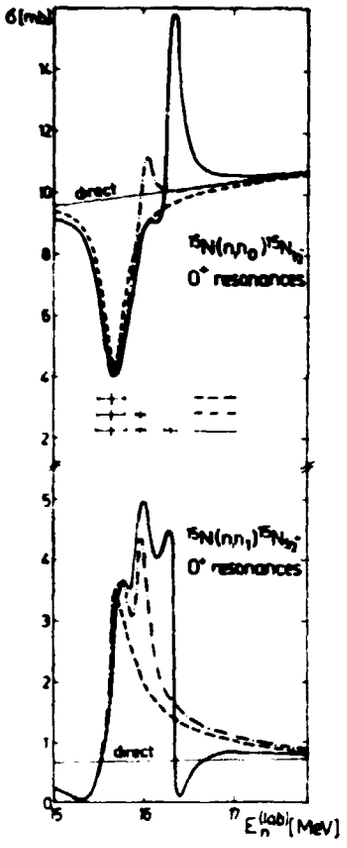

Fig. 1

The calculations in the continuum shell model show further that substructures as well as fine structures may appear under a gross structure created by a doorway state. The conditions for the different types of structures under the gross structure are also determined by the ratio Γ/D for the overlapping resonance states. The appearance of substructures in isobaric analog resonances [1] seems to fulfill the condition $\Gamma \lesssim D$ formulated in the framework of the continuum shell model. Furthermore, recent experimental investigations [4] of the $g_{9/2}$ isobaric analog resonance in ^{53}Mn have shown that it is hard to imagine the existence of other doorways in this case as it is proposed in the schematic model calculations by Cole et al. [5] for explaining the fragmentation problem. But the condition $\Gamma \lesssim D$ is fulfilled.

In heavy ion reactions, the observation of groups of resonances with the same spin testifies to the existence of a doorway state (nuclear molecular state). This state belongs, from the point of view of deformed nuclei, to a potential with large deformation in contrast to the other compound-nucleus states. From the point of view of cluster models, it consists of clusters which are isolated to a high degree. The ratio Γ/D of the single resonance states overlapped by the nuclear molecular state characterizes the type of the structure under the gross structure. If $\Gamma \lesssim D$ then substructures can appear. These substructures as well as the gross structure may show an energy shift in the different reaction channels which is however not larger than the "width". Experimentally, this condition seems to be fulfilled [6].

Although the nuclear molecular states are considered here as special states of a nucleus this does not mean that the nuclear molecular resonances in heavy ion reactions are believed to be susceptible to inclusion within a statistical framework. It follows from the continuum shell model that nuclear states like the single-particle resonances or nuclear molecular states do not allow neither a pure statistical interpretation nor a pure nonstatistical interpretation since they belong partly to the direct reaction part and partly to the resonance reaction part. This conclusion from the detailed discussions in the framework of the continuum shell model means that the question "statistical" or "nonstatistical" is not important for the nuclear molecular resonances since it is not connected with any physical contents. More interesting is the question what the nuclear structure and the asymptotic behaviour of the nuclear molecular state is.

References

1) G.M. Temmer et al., Phys. Rev. Letters 26 (1971) 1341
2) N.R. Fletcher et al., Phys. Rev. C13 (1976) 1173
3) H.W. Barz et al., Nucl. Phys. A275 (1977) 111
4) P. Kleinwächter et al., to be published
5) B.J. Cole et al., Phys. Rev. Letters 39 (1977) 3
6) T.M. Cormier et al., Phys. Rev. Letters 40 (1978) 924

HADRON CHEMISTRY IN HEAVY ION REACTIONS

J. Zimányi
Central Research Institute for Physics, Budapest, Hungary

A statistical model for the time development of fireballs is presented showing the possibility of the production of pion condensatum of Bose-Einstein type.

Introduction

In the central collision of energetic heavy ions a piece of very dense and hot nuclear matter is formed. This process being the only one for producing matter with such enourmos energy density in the laboratory, its investigation is important for nuclear physics, elementary particle physics for statistical physics too.

An exact, relativistic quantum mechanical treatement of the heavy ion collisions seems practically impossible. Therefore theoretical descriptions has to be guided strongly by empirical observations. In the energetic heavy ion research one of the most important fact is the success of the fireball model[1]. Thus the main idea of the fireball concept can serve as a good basis for further theoretical investigations.

The reaction model

The main purpose of this paper is the investigation of time development of the compressed and hot nuclear matter. (A more detailed description is given in ref.[2].) For the description of the nuclear reaction mechanism part of the heavy ion collision process a very simple model is used. Only central collisions between heavy ions of equal masses are considered. The exact treatment of the problem is naturally impossible. The model presented here contains crude approximations but it is believed to describe the main properties of the reaction.

The reaction is described as the collision of two interpenetrating spheres originally filled with cold nucleon gas. The assumptions of the model are summarized as follows:

a/ The target and projecticle nuclei having $A_p = A_t = A$ nucleons originally are represented by moving sphere of volumes $V_p = V_t$ /constant in time/. Their sum is denoted by $V_0 = V_p + V_t$. Before the collisions the number density of the cold nucleons ν_∞ is uniform within the two spheres, thus $\nu_\infty V_0 = 2A$. As the reaction proceeds the two spheres begin to overlap. The overlap volume is denoted by V_{pt}. It is assumed that nucleons outside V_{pt} /the "collision zone"/ are not influenced, thus retain the original ν_∞ density. The cold nucleons within the collision zone are assumed to have a spatially uniform time dependent density $\nu_0(t)$ in the whole volume $V_{pt}(t)$

b/ As the spheres representing the target and projectile nuclei begin to overlap the nucleons in V_{pt} begin to collide with each other. There are elastic scattering as well as Δ resonance production. The scattered out nucleons and produced Δ's are considered as the constituents of a hot gas cloud at rest in the c.m. system and with given temperature T and volume V_g

The overlap of volume V_g with the volumes of nuclei is denoted by V_{gpt} . In the first period of the reaction $V_g(t) = V_{pt}(t) = V_{gpt}(t)$. The particles of the cloud collide with each other and with the fast moving cold nucleons, too. During the collisions resonances are also produced, hence the hot gas consists of nucleons N , Δ -resonances , π -mesons and ρ -mesons Denoting the "cold" nucleons in the original nuclei by N_c the list of different "inelastic" /from the point of view of the model/ processes we take into account is the following:

$$N_c N_c \to NN\,,\quad N_c N_c \to N\Delta\,,\quad N_c N \to NN\,,\quad N_c N \to N\Delta\,,\quad N_c \pi \to N\pi\,,$$

$$NN \to N\Delta\,,\quad \Delta \leftrightarrow N\pi\,,\quad \rho \leftrightarrow \pi\pi$$

c/ The hot gas cloud is described as a multicomponent ideal relativistic Boltzmann gas. However, the interaction between the particles is accounted for to a large extent by allowing the production of resonances. The gas is assumed to be in thermal but not in a chemical equilibrium. /This corresponds to the assumed predominance of elastic collisions. /The time evolution of the densities of different particles are described in terms of statistical equations taking into account the effect of changing volumes. The time dependence of the temperature of the gas is determined from an equation expressing energy conservation.

d/ At the moment t_m of maximum overlap of the colliding spheres ($V_g(t_m) = V_{pt}(t_m) = V_{gpt}(t_m) = V_p = V_t$) the gas decouples from the incident nuclei and the volume $V_g(t)$ of the spherical gas cloud begins its adiabatic expansion. For the approximate description of the expansion the time dependence of the radius $R(t)$ of the sphere is borrowed from a simple hydrodynamic model[3]. The kinetic energy of the hydrodynamic flow is subracted from the total thermic energy. The densities and teperature are kept spatially constant within $V_g(t)$ also in the expansion period.

The division of the process into initial "ignition period" /when nucleons are scattered out from the original cold nuclei and the hot gas is constrained to the overlap and a subsequent "expansion period" when cold nucleons are already ignored/ is, of course, somewhat artifical. In reality the two processes go over into each other smoothly and there is some overlapping period. Our strategy is to consider the two dominant processes seperately for simplifying things.

On the basis of these considerations one obtains a set of coupled differential equations for the time dependence of the $\nu_\rho(t)$, $\nu_\pi(t)$, $\nu_\Delta(t)$, $\nu_N(t)$ $\nu_\rho(t)$ number densities and for the reciprok temperature, $\beta(t) = 1/kT(t)$. These somewhat lengthy equations are similar to the chemical reaction kinetic equations. Here we reproduce one of them as an example:

$$\frac{d\nu_\pi(t)}{dt} = -\frac{1}{V_g(t)}\frac{dV_g(t)}{dt}\nu_\pi + \left[\nu_\rho(t) - \nu_\pi(t)^2 \frac{d_\rho Q_\rho(\beta)}{(d_\pi Q_\pi(\beta))^2}\right] 2\Gamma_\rho \frac{K_1(m_\rho\beta)}{K_2(m_\rho\beta)} +$$

$$+\left[\nu_\Delta(t) - \nu_N(t)\,\nu_\pi(t)\frac{d_\Delta Q_\Delta(\beta)}{d_N Q_N(\beta)\; d_\pi Q_\pi(\beta)}\right]\Gamma_\Delta \frac{K_1(m_\Delta\beta)}{K_2(m_\Delta\beta)}\,,$$

where $K_n(x)$ is the modified Bessel function, $\beta = 1/kT$, Γ_Δ and Γ_ρ are the width of the Δ and ρ resonances, $d_i = (2J_i+1)(2I_i+1)$ is the multiplicity of the i-type particle, and $Q_i(\beta)$ is the single particle partition function:

$$Q_i(\beta) = \frac{m_i^2}{2\pi^2 \beta} K_2(m_i \beta).$$

According to assumption d), the time dependence of volume $V_g(t)$ is given as follows:

$$V_g(t) = \begin{cases} V_{gk}(t), & \text{if } t \le t_m, \\ \frac{4\pi}{3} R(t-t_m)^3, & \text{if } t \ge t_m. \end{cases}$$

The radius of the isentropically expanding sphere of uniform density has the time dependence [3]

$$R(t) = \frac{R_0}{t_0} (t^2 + t_0^2)^{1/2}.$$

The densities multiplied by the corresponding volumes yielded the number of different particles as a function of time. They are displayed in Fig. 1. The chemical potentials μ_i for all the particles were also calculated on the basis of the expression valid for Boltzmann gases:

$$e^{\mu_i(t)\beta(t)} = \frac{\nu_i(t)}{d_i Q_i(\beta(t))} = A_i(t).$$

<u>The analysis of the reaction model</u>

The calculation shows that, while the pions play a negligible role at $E_{lab} \le 400$ MeV/nucleon bombarding energy, they have to be taken into account from about $E_{lab} = 800$ MeV/nucleon. Above the energy of about 2 GeV/nucleon the highly excited nucleon and meson states become presumably more and more important. Their excitation may lead to a maximum temperature.

The inspection of Fig. 1 shows that the Δ resonances and pions are produced mainly in the "ignition period" of the reaction and their sum does not change appreciably during the explosion period. The ratio of pions to Δ's /or to ρ -mesons/, however, varies strongly during the expansion. This ratio--if it were possible to measure it - would give the break up time of the fireball.

The greatest part of the fast moving cold nucleons suffers scattering for the time the spheres interpenetrated each other completely. This suggests that in central collisions of heavy ions of equal masses all the nucleons participate in some way in the formation of the fireball. Peripheral collisions of

unequal mass nuclei are clearly less advatageous from this point of view.

On fig. 1 it can be seen, that even before the complete overlap of the spheres the density of "gas" exceeds that the "cold nucleons". Besides, the cross sections are larger for the "cold nucleon" - "gas" scattering because of lower energy. These facts show, that the collisions of the "cold nucleons" with the constituents of the hot gas play an important role in the "ignition" of the fireball.

The fig. 1 show, that the time necessary to reach the chemical equilibrium is of the same order of magnitude as the total reaction time. Therefore, although the ratios of particle numbers of different "chemical products" don't reach the equilibrium value, they are not very far from them.

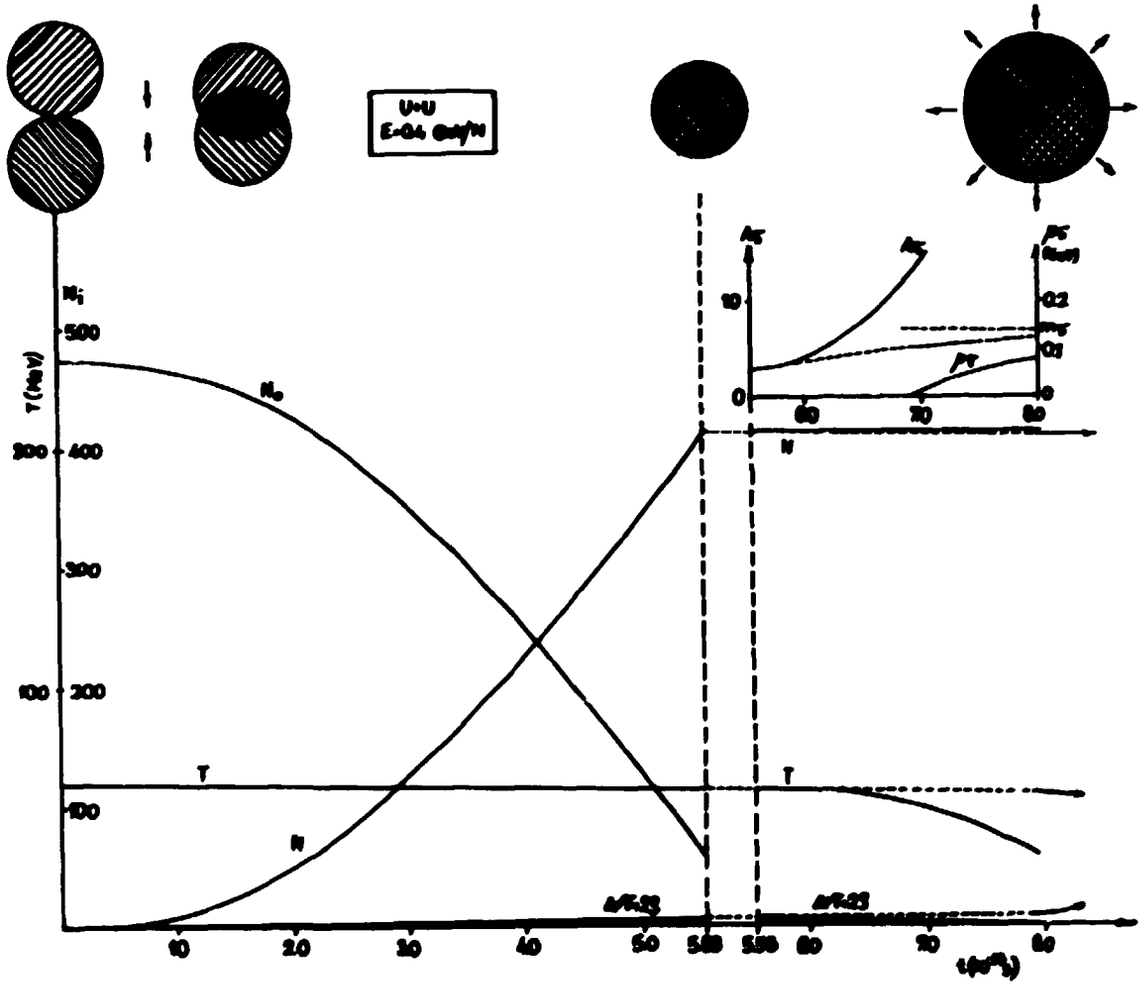

Figure 1a.

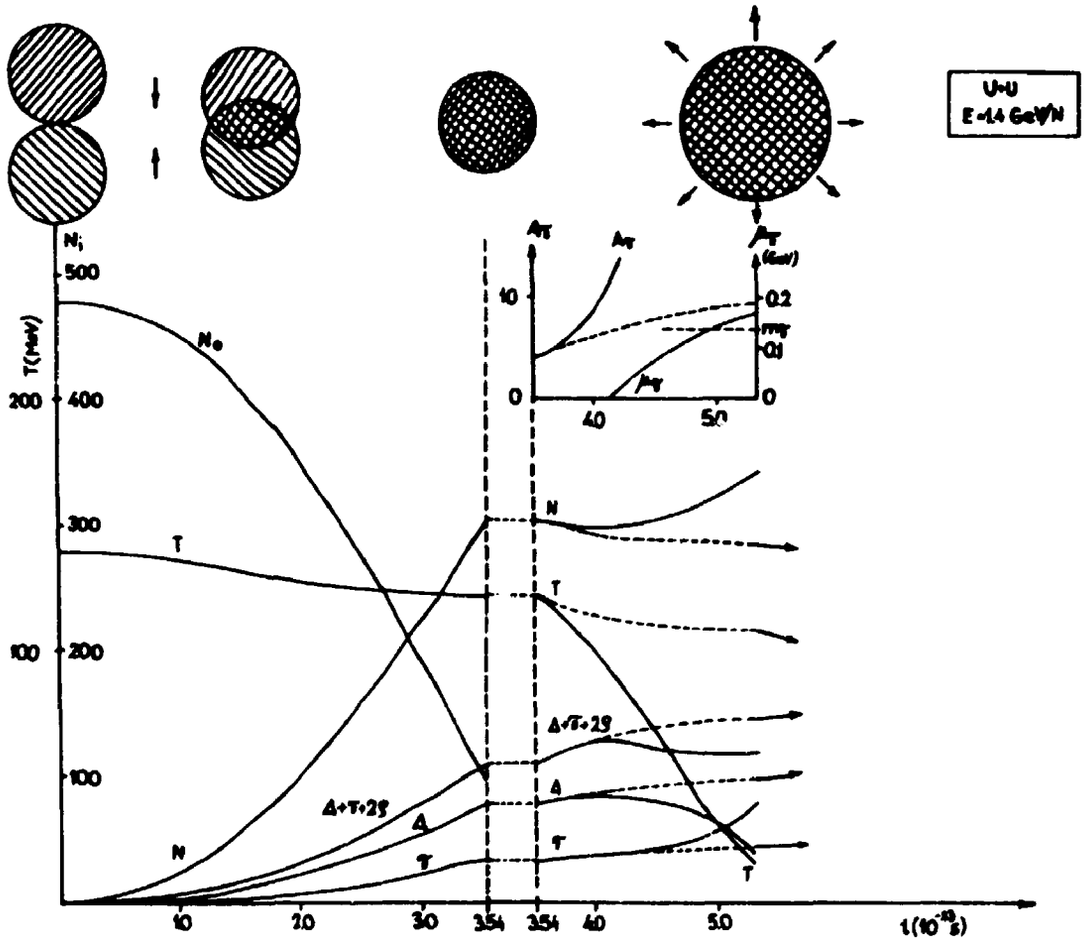

Figure 1b.

Figure 1.

The dynamics of the U+U heavy ion reaction at 1.4 and 0.4 GeV/nucleon bombarding energies. The number of particles and the gas temperature in the overlap region is plotted as a function of time. The shaded spheres on the top of the Figures indicate the geometry of the process: The interpenetration and eventually the expansion of the projectile and target nuclei. The vertical dashed lines separate the "ignition" part from the expansion part. The particle numbers and temperature shown by the dashed branch of the curves correspond to the case, when no expansion was allowed after the complete overlap of the two spheres. The arrows at the end of these curves point to the equilibrium values of the corresponding quantities. The insert in the upper right part show the chemical potential, μ_π and activity, A_π for pions as a function of time. The horizontal line marks the $\mu_\pi = m_\pi$ value, where the possibility of Bose-Einstein pion condensation appears.

Is Bose-Einstein pion condensate formed in the reaction?

Inspecting the inserts in Fig. 1 one can observe a very interesting point on the plot of the pion chemical potential μ_π versus time. Namely, near the break-up time it reaches the value $\mu_\pi = 0{,}14$ GeV i.e. $\mu_\pi = m_\pi$! This is a singular point in the present description. If the gas mixture were large enough and it were spending long enough time in this state then it would correspond to a phase transition implying the creation of a pion condensate. In ideal quantum gases this is the Bose-Einstein condensation. It is important to note that this condensate is a hot one! Its existence is not restricted to near zero temperatures. A remarkable feature is that this condensation /if it occurs/ is just in the last part of the fireball's history, therefore, directly observable. /Events that occur earlier in the fireball's life are "washed out" to a large extent from its "memory" by the later thermal history./ This may provide us with a rather unique tool to study the properties of dense hot and condensed hadronic matter. One has to realize, however, that the intermediate state in the energetic heavy ion reactions has a short lifetime. Therefore the formation of this new type of pion condensate /different from the much discussed pion condensation in cold nuclear matter/, is to be regarded presently more as a question towards experiments than a firm theoretical prediction. The question, how strongly this tendency of momentum space clusterization of pion will manifest itself in the heavy ion reaction is to be answered by further theoretical and experimental investigations.

REFERENCES

[1] G.D. Westfall, J. Gosset, P.J. Johansen, A.M. Poskanzer, W.G. Meyer, H.H. Gutbrod, A. Sandoval and R. Stock;
Phys. Rev. Lett. 37 /1976/ 1202

[2] I. Montvay and J. Zimányi,
preprint, KFKI-1978-45

[3] J.P. Bondorf, S.I.A. Garpman, J. Zimányi,
Nucl. Phys. A296 /1978/ 320

LEPTON- AND MESON-INDUCED EXCITATIONS IN NUCLEI

R.A.Eramzhyan
Laboratory of Theoretical Physics, JINR Dubna, 101000 Moscow, P.O.Box 79, USSR
M.Gmitro
Laboratory of Theoretical Physics, JINR Dubna, 101000 Moscow, P.O.Box 79, USSR
and Institute of Nuclear Physics ČSAV, CS250 68, Řež, Czechoslovakia
H.R.Kissener
Zentralinstitut für Kernforschung Rossendorf, DDR - 8051 Dresden

Examples are collected to show how a broad range of the intermediate-energy nuclear processes involving the continuum excitations may be understood from a unified point of view if the hypothesis of the resonance domination is admitted. Similarly, the evidence is brought forward that the nuclear structure details are vital for the understanding of the meson- and lepton-induced reactions to the low-lying nuclear states.

1. Introduction

There is a lot of nuclear physicists who would argue that the intermediate energy region is a strongly specialised subfield that could safely be ignored by majority. I will have succeeded in my task if in the course of this presentation of a few selected results I can convince you that we are gaining considerable insight when combining the modern understanding of the nuclear structure with the richness of the excitation mechanisms provided by the medium energy projectiles.

The major part of this talk will be devoted to the resonance excitations in the light nuclei. In that part I shall try to be slightly more systematic. Let me, however, start with two examples of the transitions to the low-lying nuclear levels. The examples, in my opinion, show nicely the nature of the questions which we may study by using the intermediate-energy techniques.

2. Nuclear partial transitions

The pion charge-exchange (CEX) process has invoked a lot of theoretical work. In some cases like e.g. CEX on ^{7}Li and ^{10}B the calculation did not find a marked disagreement between experiment and theory. At the same time we have a puzzling discrepancy for the $^{13}C(\pi^+,\pi^0)^{13}N$ charge-exchange reaction. Experimentally, the cross section is known with very reasonable accuracy to be almost constant, σ = 1 mb, for the pion energies 80 MeV < T_π < 220 MeV. The numerous calculations performed in the framework of DWIA (or equivalent) systematically underestimate this cross section by a factor of 3-4 at least. In spite of the repeated attempts to improve this result by e. g. changing the $p_{1/2}$ single-particle orbital, introducing the spin-flip effects, two-step processes, constructing the second-order optical potential, the discrepancy remains still unresolved[1]. It was, however, proposed by Auerbach[2] that the isobar doorway approach may be successfully applied to the problem. In this model the incoming pion forms with a nucleon a Δ_{33} particle bound in the nucleus. The resulting Δ-particle - nucleon-hole configurations are intermediate states serving as doorways in the pion-nucleus scattering. In the charge-exchange reaction on ^{13}C the incoming π^+ interacts with the $p_{1/2}$ neutron forming a Δ^+N^{-1} configuration. Subsequently the Δ decays into a $p_{1/2}$ proton while a Δ^0 escapes. Auerbach, with some plausible parameter values which simultaneously account for the total elastic π^- - ^{12}C cross section in the same energy region,

has obtained the only theoretical result for the CEX cross section on ^{13}C which is in agreement with the experimental data. It remains to be seen whether or not this turns to be the case with a more realistic treatment of the isobar-hole idea.

The second example which I want to discuss comes from the double-charge-exchange (DEX) reactions (π^+,π^-) on the A=16 and A=18 nuclei. The measured ratio of the total cross sections at T_π = 140 MeV for the two DEX reactions is

$$R = \sigma(18) / \sigma(16) = 2.3 \pm 1.0.$$

Qualitatively it looks strange since the A=18 case should be very strongly enhanced. As a matter of fact the $^{18}O(\pi^+,\pi^-)^{18}Ne$ reaction proceeds via a chain of isobar-analogue states, within such a model it is easy to perform an estimation, one reaches the value R = 16 ! It was shown by Lee, Kurath and Zeidmann[3] that taking into account the realistic wave functions of the respective nuclei one observes, despite the very small (about 20% only) admixture of the non-closed-shell configurations present in these wave functions, a substantial change of the result: the new value is R = 3 in a very good agreement with the experiment. The detailed analysis performed in ref.[3] has shown that actually a strongly coherent addition of the small contributions of the 2p-2h configurations is responsible for the enhancement effect.

Charge-exchange, double-charge-exchange, pion elastic and inelastic scattering processes on nuclei may all be simultaneously studied by the powerful coupled-channel method. Such a project has been started by us in Dubna. The first results concerning the $\pi - {}^4He$ processes are available [4], further investigations, including the two mentioned examples of the charge-exchange reactions, are in progress.

3. Resonance excitation mechanism

Let us proceed now to slightly higher nuclear excitations, to excitations of the giant-resonance type. Such states can be created e. g. in

(i) the photoabsorption and photodisintegration processes ($E_\gamma \lesssim 40$ MeV),
(ii) the inelastic electron scattering ($E_e \sim 10^2$ MeV),
(iii) the muon capture reactions $\mu^- A(Z) \rightarrow \nu A(Z-1)$,
(iv) the radiative pion capture reactions $\pi^- A(Z) \rightarrow \gamma A(Z-1)$,
(v) the inelastic scattering of protons, deuterons, and heavier ions (^3He, ^4He, ...)

.....

One may ask what is common for these dissimilar exciting agents? Anticipating slightly the discussion we may state that the most important common ingredient here is just a moderate energy- and momentum-transfer to the nucleus. In all the above cases a particle-hole configuration is formed under the influence of the external field. And it is then the particle-hole interaction which controls the further evolution of the system. The external field is responsible for the type, i.e. the spin, parity and isospin, of the corresponding nuclear excited mode. To be specific, we shall go through the above list once again. There we may see that the photoabsorption leads to the creation of the isovector E1 resonance, the electrons can excite, depending on the scattering angle and the value of the momentum-transfer, a whole set of collective states. In the (μ^-,ν) and (π^-,γ) reactions on the light nuclei the isovector spin-dipole mode strongly dominates. In the radiative pion capture on heavier nuclei the higher spin-

multipole resonances start to dominate the process since pions, being absorbed from the higher mesoatomic orbitals, contribute the non-zero orbital momentum. The inelastic scattering of the protons ($\sim 10^3$ MeV) and ions ($\sim 10^2 - 10^3$ MeV), due to a peculiar nature of the nucleon-nucleon interaction, cause mainly the creation of the isoscalar resonances.

A. Approximation to the unified reaction theory

The giant resonances are nuclear states embedded in the continuum. The nuclear disintegration amplitude pertaining to the above named processes may be written, within the unified theory of nuclear reactions, in the following form

$$M_{0j}(E) = \langle \phi^{(-)}_{jE} | H | 0 \rangle + \sum_s \frac{\langle \phi^{(-)}_{jE} | V | \psi_s \rangle \langle \psi_s | H | 0 \rangle}{E - E_s + \frac{1}{2}\Gamma_s} \qquad (1)$$

The first term on the right-hand side corresponds to an immediate transition of a nucleon into the (j,E) channel. The second term describes a two-step process; the creation and the subsequent decay of the nuclear states $|\psi_s\rangle$.

Presently it is not feasible to take into account simultaneously both the continuum and the complex nuclear structure phenomena. It was therefore an important development when the hypothesis of the giant resonance domination was formulated for the class of reactions under consideration. Then it became possible to omit the first term of eq.(1) and to proceed further by analogy with the usual treatment of the nuclear collective states which lie below the nucleon emission threshold. On this path we were able to consider in a substantial detail the nuclear intermediate states $|\psi_s\rangle$.

Using the hypothesis just formulated it was already possible to understand from a unified point of view a broad range of the phenomena which occur in the above named processes. These are first of all

(a) the localization of the giant resonance,

(b) the resonance structure: quantum numbers of the individual resonances which form the giant resonance,

(c) the general regularities of the resonance excitation and the specific features which are connected with the particular incoming particles,

(d) the main decay channels, the type and spectra of the outgoing particles, population of the individual levels in the daughter nuclei.

Certainly not all of the reactions (i) - (v) which we wish to discuss are investigated to the same extent and detail. In some cases we shall not speak of all the above points.

B. The isoscalar quadrupole resonances

Let me turn to the selected examples. Fig. 1 depicts the energy spectrum of the ^{3}He ($E(^3He) = 130$ MeV) inelastic scattering on ^{16}O. According to the experiment[5] there is about 37% of the isoscalar quadrupole energy-weighted sum rule (EWSR) exhausted in the region 17 - 25 MeV. The calculation performed in a simple one-particle one-hole configuration mixing model has shown 50 - 80% of the EWSR in this energy region. We have performed a more complete calculation in which also the 2p-2h ($2\hbar\omega$) configurations were taken into account both in the ground state and in the final 2^+0 states of ^{16}O. The result[6] is much closer to the experimental value: 34% of the EWSR was located in the giant quadrupole region. Since the nuclear model just mentioned shall appear still several times

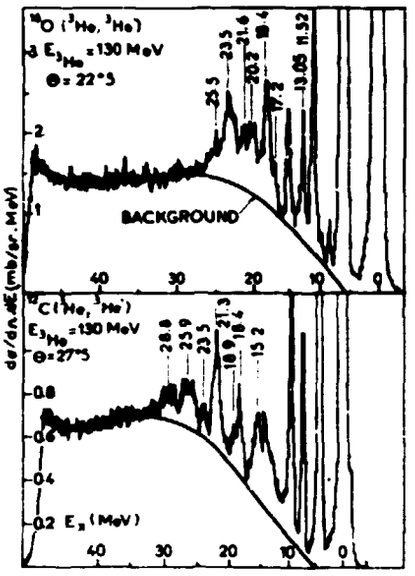

Fig. 1

Measured spectra in the ^{3}He inelastic scattering[5]. Excitation energies of the 2^+ states above 10 MeV are indicated.

in this talk I would like to add also a critical comment already at the very beginning. However fine are the results for the giant resonances, the model does not provide any explanation of the low-lying collective states in ^{16}O.

Now I wish to discuss the isospin selectivity observed in the inelastic scattering of 1 GeV protons. The upper part of fig. 2 shows the B(E2) values of the ^{58}Ni and ^{90}Zr nuclei as calculated in a large-scale semi-microscopic model[7]. Three regions of 2^+ levels are clearly seen in these nuclei. Besides the low-lying collective levels and the isoscalar giant quadrupole resonance lying around 12-15 MeV, we find also the isovector GQR in the region 24 - 30 MeV. The lower part of fig. 2 depicts the cross sections for the scattering of 1 GeV protons calculated in the framework of the Glauber theory using the same wave functions as for the B(E2) values. Since the (p,p') high energy scattering prefers the T=0 transitions, the reaction may serve, e.g., to disentangle the dipole (T=1) and quadrupole (T=0) resonances.

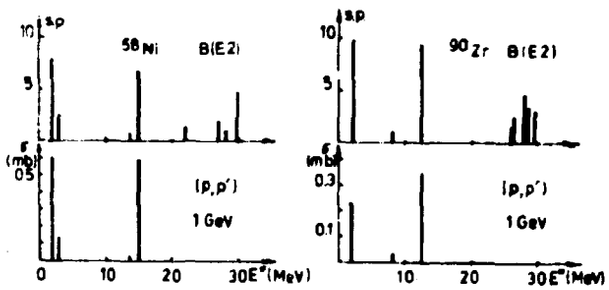

Fig. 2

Reduced probabilities of E2 transitions from the ground to excited states in single-particle units for ^{58}Ni and ^{90}Zr. The $J^\pi = 2^+$ levels with $B(E2)_{s.p.} > 1$ are plotted in the top part. The total cross sections for excitation of the same levels by 1 GeV protons are shown in the bottom part of the figure.

C. Radiative pion capture

Now I would pass to the mesonic excitations announced in the title. In the radiative pion capture the pion from a mesoatomic orbital is captured by the nucleus. The elementary act on a single nucleon is assumed, this is the so called impulse approximation. From the experiment we have the spectrum of the hard gamma rays from these reactions. Two examples of such spectra are shown in figs. 3 and 4 together with the corresponding theoretical results.

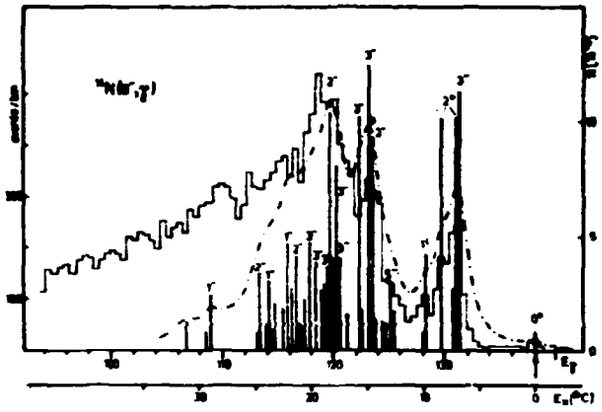

Fig. 3
Radiative pion capture yield on ^{14}N. The histogram is from Alder et al. (Zürich conference 1977, C14). Theoretical branches (vertical bars) are spreaded over Breit-Wigner shapes (dot-dashed curve).

^{14}N: In the calculation[8] only $0\hbar\omega$ and $1\hbar\omega$ nuclear excitations were included. This (monopole and) dipole part of the excitation is responsible for the appearance of the most energetic gamma rays. There is no explanation of the gamma spectrum near $E_\gamma \approx 100$ MeV.

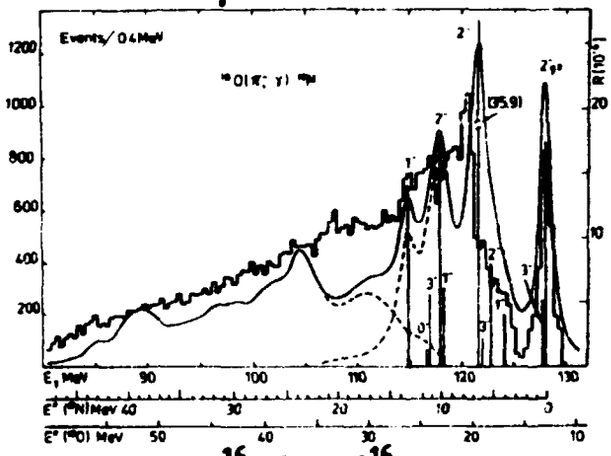

Fig. 4. Calculated yields of the γ rays in the $^{16}O\,(\pi^-,\gamma)\,^{16}N$ reaction. A Breit-Wigner shape of 2 MeV (1.25 MeV) width for resonance (bound) states of ^{16}N was ascribed to each line. The broken curves are for the separate contributions from the spin-dipole ($E_\gamma > 105$ MeV) and spin-quadrupole ($E_\gamma < 118$ MeV). The experimental histogram is from Alder et al. (Zürich conference 1977, C16).

^{16}O: Here we were able to apply a more rich nuclear model. As I have mentioned already, it contains up to 2p-2h configurations. The subspaces $1\hbar\omega$, $2\hbar\omega$ are included fully, some important $3\hbar\omega$ configurations are added, too. It can be seen that this model provides a very good explanation of the observed gamma spectrum. The dipole and quadrupole branches of excitation correspond to the high- and low-energy gamma quanta. Again, a simple 1p-1h model overestimates the total gamma yield (R=3.2%). In the "full" calculation we have obtained[9] R=2.1%. The experimental result is R = (2.27 ± 0.24)%.

^{32}S: As soon as the nuclear charge grows, the gamma spectrum of the (π^-,γ) reaction acquires a more complex character. In ^{16}O about a half of the gamma yield has corresponded to the dipole excitation mode. In

^{32}S we may observe already a domination of the quadrupole and the octupole excitation mode[10], see table 1.

Table 1.
Distribution of the gamma yield in the $^{32}S(\pi^-,\gamma)$ reaction.

Excitation branch	$0\hbar\omega$	$1\hbar\omega$	$2\hbar\omega$	$3\hbar\omega$
R_γ	0.23%	0.55%	0.63%	0.28%
			R_γ (total)=	1.69%

D. Muon capture at rest, the neutron spectra

It seems to be instructive to compare the muon capture and the radiative pion capture processes. I should limit the discussion of the (μ^-,ν) reaction to the case of ^{16}O. In ref.[9] we have been able to show that the ^{16}O nuclear model with 2p-2h correlation provides a good, quantitative understanding of the observed muon capture rates. Once again I shall break the flow of the "resonance" discussion to show in table 2 the partial capture rates for the ^{16}N bound states. They seem to agree nicely with the experiment. I wish to stress the very reasonable result for the $0^+ \to 0^-$ transition which was frequently discussed as a possible source of information on the numerical value of the pseudoscalar (induced) coupling constant G_p. Presently, there is a strong suspicion[11] that the mesonic exchange currents have to be invoked in order to explain fully the situation which includes also the rate of the inverse beta decay ($^{16}N(0^-) \to {}^{16}O(g.s.)$).

Table 2.
The partial muon capture rates for transitions to the ^{16}N bound states in 1/sec.

Model	$J^\pi=$ 0^-	1^-	2^-
no correlations[9]	2690	2830	17990
including 2p-2h[9]	1730	1840	7720
"coexistence"[12]	1270	1640	8320
	Experiment		
Columbia[13]	1100 ± 200	1730 ± 100	6300 ± 700
Berkeley[14]	1600 ± 200	1400 ± 200	——
Williamsburg[15]	1560 ± 170	1310 ± 100	8200 ± 120
Saclay[16]	1570 ± 130	1360 ± 130	——

The total muon capture rate which is indeed mainly due to the excitation of unbound nuclear levels of the giant-resonance type are shown in table 3. Unlike the (π^-,γ) reaction, for the muon capture we observe the strong (90%) dominance of the dipole transition mode. Indeed, majority of the captures proceeds from the mesoatomic s-orbital, therefore zero angular momentum is brought in by the captured meson.

Table 3.
Muon capture rates in the $^{16}O(\mu^-,\nu)^{16}N$ reaction in 10^3 sec^{-1}.

	$\|0\rangle \to \|1p\text{-}1h\rangle$	$\|corr\rangle \to \|1p\text{-}1h\rangle + \|2p\text{-}2h\rangle$
J^- (bound)	23	11
J^- (unbound)	110	91
J^+	9	9
Total	142	111
Experiment	Columbia[13]	93±10
	CERN[17]	98± 5
	Williamsburg[15]	109±13

Instructive and maybe even slightly unexpected is the comparison of the muon capture and the radiative pion capture reactions for the ^{208}Pb target as calculated by Ebert and Meyer-ter-Vehn[18]. Here again, the muon capture proceeds predominantly from the mesoatomic s-state, the radiative pion capture, however, from an f-state (ℓ=3). Indeed, the ^{208}Pb $(\pi^-,\gamma)^{208}$Tl reaction shows markedly more rich picture of the excitations which contains many higher-multipole states including those with $J=6^-$ and $J=7^+$.

Going back to the ^{16}O I wish to compare the spectra of the outgoing neutrons in the (μ^-,ν) and (π^-,γ) reactions. They were calculated[19] in both cases in the framework of the R-matrix theory. The typical peak near E_n= 4 MeV is well reproduced in both the cases. The two spectra, however, differ considerably in their high-energy part. In fig. 5 we may see the long "tail" of the high-energy neutrons from the ^{16}O$(\pi^-,\gamma n)$ reaction, which is absent in the muon-induced decay. In the calculation this tail comes out very nicely because of the strong quadrupole excitation branch of the radiative pion capture reaction.

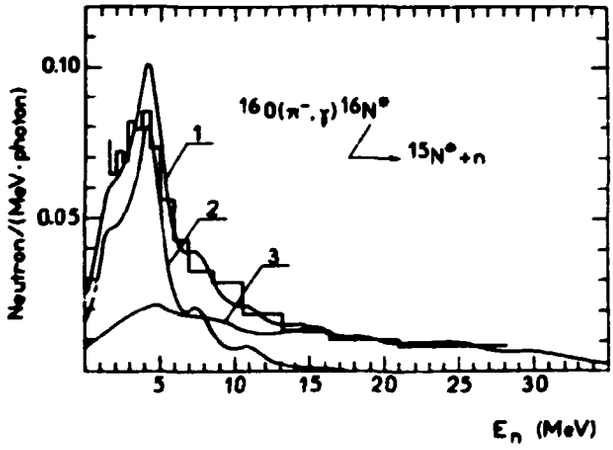

Fig. 5

Spectrum of neutrons following the radiative pion capture on ^{16}O. Experimental data are given in the form of histogram (W.C.Lam et al. Phys.Rev. C10 (1974), 72). Curve 1 is the calculated spectrum, curves 2 and 3 are for the contributions of spin-dipole and spin-quadrupole excitations in ^{16}N, respectively.

E. Backward electron scattering

Among the leptonic excitations, which we have already started to discuss, the electron scattering is indeed the best understood process. In a sense most interesting by now (and almost unexploited as yet) appears to be the 180° scattering, since the kinematics here is such that only the transverse part of the transition survives. This means that the structure of the active part of the transition operator is strongly similar to the structure of the effective Hamiltonian acting in the radiative pion capture reaction. We are able therefore to study the two complementary processes with the additional advantage that the value of the transferred momenta can be controlled in the (e,e') scattering. Fig.6 shows the decomposed spectrum for the backward inelastic scattering of 70 MeV electrons on ^{13}C. This theoretical spectrum gives us an appropriate possibility to look back on the list of questions (a)-(d) which we have put down at the beginning of this talk. The program looking for the localisation of the giant resonances and for their structure seems to reach an accomplishment: In fig. 6 we may follow the envelopes of the individual peaks which provide the position and spreading of the resonances of each multipolarity. We can see very clearly the structure of the giant peaks, their quantum numbers, the very interesting isospin splitting in particular.

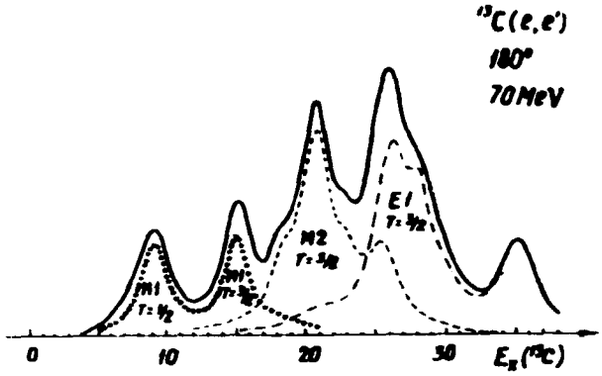

Fig. 6
Calculated form factor of the 180° inelastic electron scattering. The groups of levels of the given spin, parity and isospin are visualised by their envelopes. The individual families are clearly separated in energy.

4. Discussion and outlook

In conclusion I would like to recall once again the only formula of this talk, eq. (1). Now it is time to mention the other line of investigation which was advanced strongly by the group of Zentralinstitut für Kernforschung in Rossendorf and Moscow State University. They have worked in the framework of the unified theory of nuclear reactions in which the nuclear continuum and the bound states are treated on an equal footing. Numerically this approach is indeed very difficult, therefore the calculation (I shall only mention the $^{16}O(\pi^-,\gamma)$ results[20]) were performed in the simplest 1p-1h nuclear model. Naturally in this approach they found an overestimation of the total gamma ray yield. On the other hand that approach gives the possibility to consider certain additional characteristics of the reaction, e.g., the γ - n correlation functions.

Presently the two approaches to the reactions involving the nuclear continuum excitations should be considered in their complementarity. The unified theory provides the general understanding of the problem and also suggests the way of calculation of the angular characteristics, high-energy neutron spectra, etc. The conception of the dominant role played by the giant resonance excitations permits the incorporation of rather complicated nuclear structure models. In this way several important characteristics, especially those connected with the resonance fragmentation may be cleared up. Simultaneously this approach makes it possible to compare the theory with the experimental data for a broad range of the intermediate-energy reactions.

References

1. K.P. Lohs and A. Gal, Nucl. Phys. A292 (1977) 375
2. E. Amerbach, Phys. Rev. Lett. 38 (1977) 804
3. T.S.H. Lee, D. Kurath and B. Zeidman, Phys. Rev. Lett. 39 (1977) 1307
4. M. Gmitro and R. Mach, JINR preprint, Dubna E4-11946, 1978 and to be publ.
5. M. Buenerd et al., Journ. Phys. (Paris) 38 (1977) L-53
6. M. Gmitro, E. Tinková, A. Rimini and T. Weber, Lettere Nuovo Cim. 20 (1977) 449
7. R.A. Eramzhyan, S.I. Fedotov, V.P. Shpakov, Ch. Stoyanov and V.I. Vdovin, Nucl. Phys. A290 (1977) 397
8. G.E. Dogotar, R.A. Eramzhyan, H.-R. Kissener and R.A. Sakaev, JINR preprint E2-11275, 1978
9. R.A. Eramzhyan, M. Gmitro, R.A. Sakaev and L.A. Tosunjan, Nucl. Phys. A290 (1977) 294
10. R.A. Eramzhyan, L. Majling, J. Rizek and R.A. Sakaev, JINR preprint Dubna E2-11234 (1978)
11. P. Guichon, M. Giffon and C. Samour, Phys. Lett. 74B (1978) 15
12. O. Malcioglu, A. Goswami and R.D. Graves, Lettere Nuovo Cim. 7 (1973) 897
13. R.S. Cohen, S. Devons and A.D. Canaris, Nucl. Phys. 57 (1964) 255
14. A. Astbury et al., Nuovo Cim. 33 (1964) 1020
15. P.R. Cane et al., Phys. Lett. 45B (1973) 292
16. M. Giffon et al., Zurich Conference 1977, abstract Q13
17. J. Barow, J.C. Sens, P.J. Duke and M.A.R. Kemp, Phys. Lett. 9 (1964) 84
18. K. Ebert and J. Meyer-ter-Vehn, preprint 1977
19. R.A. Eramzhyan, M. Gmitro and L.A. Tosunjan, Journal of Physics G: Nucl. Phys. 4 (1978) L233; Czech. J. Phys. B29 (1979) to be published
20. R.A. Winsch, JINR preprint, Dubna E4-11592 (1978) and to be published

INVESTIGATION OF PROTON-NUCLEUS INTERACTIONS AT 640 MeV ACCOMPANIED BY BACKWARD EMISSION OF ENERGETIC PROTONS

V.I. Komarov, G.E. Kosarev, D. Netzband and V.D. Toneev
Joint Institute for Nuclear Research Dubna, USSR
H. Müller, T. Stiehler and S. Teech
Zentralinstitut für Kernforschung Rossendorf, DDR - 8051 Dresden
K.K. Gudima and S.G. Mashnik
Institute of Applied Physics Kishinev, USSR

Protons of energies between 50 and 145 MeV ejected from carbon have been measured at angles 105° to 160° with respect to the 640 MeV proton beam. The measurements have been carried out both inclusively and in coincidence with protons emitted at forward angles up to ± 40° with energies from 255 to 330 MeV chosen in accordance with the kinematics of quasifree scattering on two-nucleon groups. Inclusive cross sections at 140° and coincidence cross sections at the angle pair (-12°, 122°) have also been measured with Be, Al, Cu and Pb targets. The data have been compared with the predictions of several models.

There has been considerable recent interest in nuclear reactions leading to the production of backward-emitted energetic protons (BEP). Such reactions can be realized with medium-energy protons under the conditions of large momentum or energy transfers to the struck few-particle systems (clusters) in the target nucleus. Only detailed investigation of the BEP production can help to find out to what extent these processes are caused by short-range nucleon-nucleon correlations. The scaling characteristics of the BEP production are also widely discussed at present. It is known (see e. g. [1]) that this regularity ("nuclear scaling") appears at incident energies of the order of 1 GeV, i. e. much earlier than the scaling behaviour in elementary particle interactions. Therefore, BEP production studies at medium energies allow the scaling outset to be traced out and may lead to a more profound understanding of the physical nature of the scale-invariant regularities in relativistic nucleus-nucleus collisions [2].

Inclusive BEP measurements have been carried out over a wide range of energies and angles for incident medium-energy protons [3-6]. A number of different models [7-10] have been proposed which rather successfully explain inclusive BEP data of certain backward angles. To select the most adequate model, more detailed experimental information is obviously necessary. The aim of this paper is to report on investigations of the angular dependence of inclusive BEP production and of correlations between BEP and accompanying energetic protons in the forward hemisphere.

Fig. 1 shows the BEP angular dependence for three representative energies (carbon target). The data are given in the relativistic invariant representation $f = E/(p^2 \cdot \sigma_{tot}) d^2\sigma/d\Omega dp$. Our calculations according to the (A-1) nucleon exchange mechanism [9] show that rather good agreement with the data is obtained [5] if the incident proton interacts with a two-nucleon group (curve c). A similar result was obtained in ref. [11], were a correlation mechanism of the interaction between the proton and the [2N]-cluster was proposed (dashed line).

The results of most of the reaction models proposed to describe the BEP production depend very strongly on the high-momentum behaviour of the target wave function. On the other hand, it is expected [12] that multiple scattering processes can considerably contribute to the BEP spectra. We have simulated such

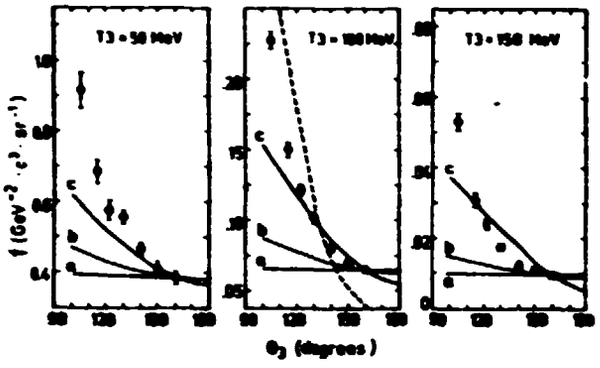

Fig. 1

BEP angular distributions from 640 MeV protons incident on carbon. Full lines - calculations according to the model of ref. [9] (a) (A-1)-nucleon exchange, (b), (c) interactions with [3N]- and [2N]-clusters, respectively. Dashed line - result of calculation[11].

multiple scatterings by using the Monte Carlo method. These calculations are based on the Dubna version of the cascade model [13,14]. In fig. 2 the calculated results together with our BEP data are presented. As is seen, the inclusive cross sections in dependence on angle and target mass number are fairly well reproduced. The contributions of the preequilibrium processes estimated in the framework of the cascade-exiton model [15] are also shown (dashed lines). The detailed analysis of the cascade results in comparison with our BEP data indicates that

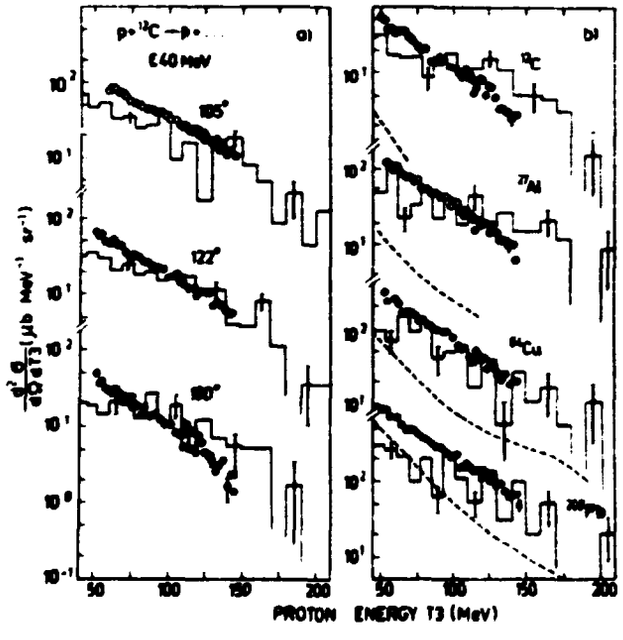

Fig. 2

Measured inclusive BEP spectra and cascade model calculations without preequilibrium emission (histograms).
(a) Results with C target. (b) Results with C, Al, Cu and Pb targets at 140°. Dashed lines - spectra due to preequilibrium emission of protons.

(i) only a small number of nucleons participates effectively in the cascade process,

(ii) in one of the cascade collisions a pion is produced which is absorbed by a nucleon pair in the same nucleus.

As inclusive data do not allow to distinguish between the different models proposed, it is obviously necessary to carry out coincidence experiments in which the characteristics of fast particles accompanying BEP are studied [11,16]. The experimental conditions were chosen to cover just that T1 - T3 energy region which includes the quasielastic scattering on two-nucleon clusters according to process

$$p + [pN] \rightarrow (p_1N)_{\Delta=0} + p_3 \; . \qquad (1)$$

Here, p_1, p_3 are the forward and backward emitted protons, respectively, measured in coincidence and N is the other cluster member not observed [17] or measured in a triple-coincidence experiment [18]. The main features of the two-proton coincidence yield can be summarized as follows:

(i) A strong correlation between the two protons is observed in the θ_1-dependence of the cross section (fig. 3). The fit by a Gaussian gives the mean value $\bar{\theta}_1 = -(10.9^\circ \pm 1.1^\circ)$ for T3 = 105 - 145 MeV. This value should be compared with $\theta_1 = -12.6^\circ$ following from the kinematics of process (1) for $\theta_3 = 122^\circ$.

(ii) The T3 energy spectra decrease monotonically with increasing T3 for all angle pairs (θ_1, θ_3) measured (fig. 4a, b). The difference spectrum shown in fig. 4c does not contradict the existence of a broad maximum expected at about 75 MeV for process (1).

(iii) The θ_3-distributions are strongly asymmetric with respect to $\theta_3 = 180^\circ$ and depend noticeably on the BEP energy (fig. 5b). Again we note that the value $\theta_3 = 124^\circ$ follows from the kinematics of process (1) for $\theta_1 = -12^\circ$.

(iv) The cross section $d^4\sigma/d\Omega_1 dT1 d\Omega_3 dT3$ depends weakly on the energy T1 of the forward outgoing proton (fig. 5c).

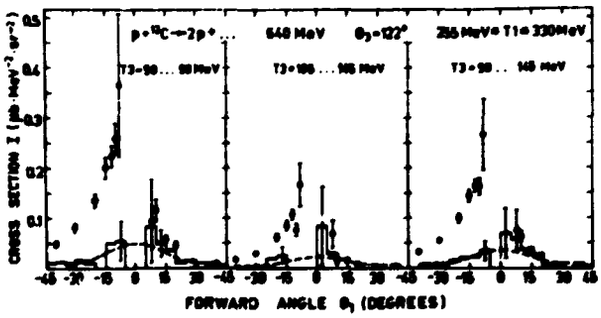

Fig. 3

Two-proton coincidence cross section for three intervals of BEP energies T3 versus angle θ_1. Histograms and dashed curves - cascade model calculations.

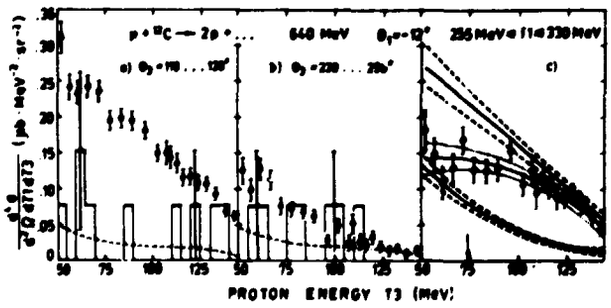

Fig. 4

Differential cross section versus BEP energy T3. (a), (b) - Spectra for two BEP angular intervals. Histograms and dashed lines - cascade model calculations. (c) - Polynomial fits to the data given in (a), (b) and to their difference (full circles). The arrow indicates T3 expected for process (1).

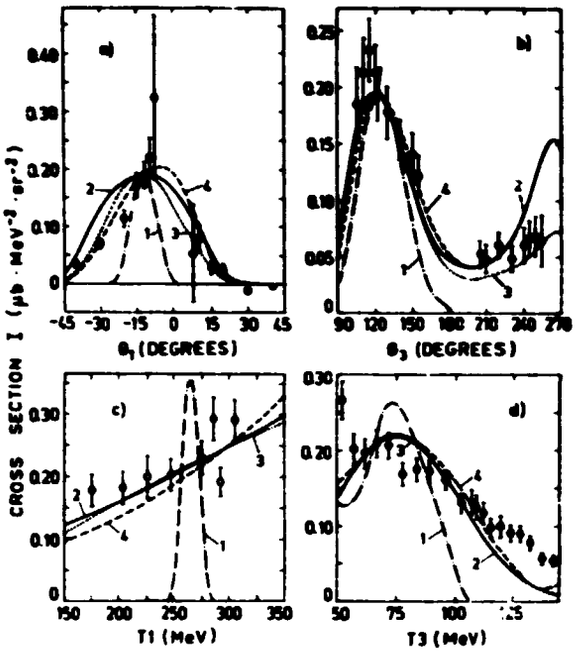

Fig. 5

Comparison of two-proton coincidence data with calculations according to the model of scattering on [2N]-clusters. Data points - the difference of experimental cross sections and cascade calculations. Cross sections integrated over T3 from 50 - 90 MeV.
(a) $\theta_3 = 122^o$, (b) $\theta_1 = -12^o$, (c) $\theta_1 = -12^o$, $\theta_3 = 122^o$, (d) differential cross section $d^4\sigma/d^2\Omega\, dT1\, dT3$ for the angle pair $(-12^o, 122^o)$. The curves 1 - 4 represent the calculations (see text).

(v) Two-proton coincidence measurements have been carried out also at $(-12^o, 122^o)$ using Be, Al, Cu and Pb targets. It has been found that the cross section per target nucleon decreases with increasing A. The A^n-fit of the integrated cross section (T3 = 50 - 145 MeV) results in n = 0.39 ± 0.7.

The cascade model calculations of the coincidence cross sections (i) - (v) turn out to be considerably smaller than the experimental ones and seem to be symmetric relative to the incident beam axis.

The character of the measured two-proton distributions indicate that an essential contribution seems due to process

$$p + [pN] \rightarrow p_1 + N + p_3 \; . \qquad (2)$$

The calculations assuming proton scattering on two-nucleon clusters in carbon according to process (2) are shown in fig. 5. First we note that the calculation with relative momentum $\Delta = 0$ in the p_1N-system results in distributions which are considerably narrower than the experimental ones (curves 1). This may indicate that the correlated cluster model [10] is not supported by the experiment. The three-particle phase space calculations for reaction (2) reproduce the general behaviour of the distributions (curves 2). Moreover, two versions of weight functions introduced in the phase space integral have been considered in the calculations for process (2). These versions A, B correspond to a backward scattering mechanism and to a small-angle scattering mechanism, respectively (curves 3, 4 in fig. 5).

Version A is characterized by large mean four-momentum transfers (≈ 7 fm^{-1}) and low mean excitations ($\approx$ 12 MeV) of the nucleon pair, and the corresponding values for version B are ≈ 2 fm^{-1} and $\approx$250 MeV. The considerably smaller values of transferred momenta and high excitations according to version B favour the small-angle scattering mechanism.

From our inclusive and two-proton data we were able to estimate the quantity

$$\varkappa = \frac{(d\sigma_{coinc}/d\Omega_1 d\Omega_3)d\Omega_1}{d\sigma_{incl}/d\Omega_3} \approx 0.2 .$$

This value can be regarded as the lower limit of the contribution to the inclusive BEP yield not caused by the quasi-two-particle process [7,8].

In conclusion we believe that two mechanisms are quite sufficient to describe our data of inclusive as well as coincidence measurements - the cascade process with intranuclear pion absorption and the projectile scattering associated with considerable energy transfer to a nucleon pair. The common attribute of both mechanisms is the large energy transfer (of the order of the pion mass) deposited by the incident proton into the struck few-nucleon group. Therefore, it seems that the BEP production at medium incident energies is determined first of all by the properties of highly excited few-nucleon systems in the nucleus.

References

1) G.A. Leksin; Proc. XVIIth Int. Conf. on High Energy Physics, Tbilisi, 1976

2) A.M. Baldin; Fiz. Ehlem. Chastits At. Yadra 8 (1977) 429

3) S. Frankel et al.; Phys. Rev. Lett. 36 (1976) 642

4) V.I. Komarov et al.; Phys. Lett. 69B (1977) 37

5) V.I. Komarov et al.; JINR report E1-11513 (1978)

6) J. Källne et al.; Phys. Lett. 74B (1978) 170

7) R.D. Amado and R.M. Woloshyn; Phys. Rev. Lett. 36 (1976) 1435

8) S. Frankel; Phys. Rev. Lett. 38 (1977) 1338

9) H.J. Weber and L.D. Miller; Phys. Rev. C16 (1977) 726

10) T. Fujita; Phys. Rev. Lett. 39 (1977) 174

11) T. Fujita and J. Hüfner; submitted to Nucl. Phys.

12) V.B. Kopeliovich; Yad. Fiz. 26 (1977) 168

13) V.S. Barashenkov and V.D. Toneev; in: Interactions of high-energy particles and atomic nuclei with nuclei (Atomizdat, Moscow, 1972) (in Russian)

14) K.K. Gudima et al.; JINR report E2-11307 (1978)

15) K.K. Gudima and V.D. Toneev; JINR report E4-9489 (1976)

16) R.M. Woloshyn; Nucl. Phys. A306 (1978) 333

17) V.I. Komarov et al.; submitted to Phys. Lett. B, JINR report E1-11564 (1978)

18) V.I. Komarov et al.; Proc. European Symposium on Few-Particle Problems in Nuclear Physics, Potsdam, 1977, ZfK-347 (1977) 185; JINR report E1-11354 (1978)

STRUCTURE INVESTIGATIONS IN THE NUCLEAR CONTINUUM BY MEANS OF HIGH-ENERGY (e,e'N) AND (p,p'N) REACTIONS

V.V.Balashov, E.P.Kislyakov, V.L.Korotkikh
Institute of Nuclear Physics, Moscow State University, USSR
R.Wünsch
Zentralinstitut für Kernforschung Rossendorf, DDR-8051 Dresden

The efficiency of a correlation experiment, in which the scattered high-energy projectile is detected simultaneously with the product of nuclear disintegration is demonstrated in a calculation on the basis of the unified theory of direct and resonance processes.

The nuclear structure in the continuum, i.e. above the disintegration threshold, is being studied on a ever increasing scale. For the excitation of the nucleus in this energy region nearly all kinds of projectiles available from the accellerator can be used. However, the actual structure of the nucleus can only be observed, if the interaction of the projectile with the nucleus is sufficiently weak (in the sense of the perturbation theory). The incoming particle transfers only a certain amount of energy, momentum, spin, isospin or other quanta to the nucleus.

The weak coupling between the projectile and the nucleus can be realized

(i) by a projectile with a high kinetic energy, or

(ii) by a weakly (in comparison with the nucleon-nucleon interaction inside the nucleus) interacting projectile.

In the first case the reaction time is too small to disturb the nuclear structure, e.g. in the inelastic scattering of high-energy hadrons with a small energy and momentum transfer. A projectile interacting electromagnetically (photon, electron) or weakly (muon) fulfils the weak coupling condition also for a longer reaction time, e.g. in a capture reaction from the atomic orbit.

The use of high-energy projectiles can be a promising tool for the spectroscopy of the nuclear states in the continuum [1]. However, many important theoretical questions of applying this method have not been developed sufficiently so far. Among these is the question about the relation between the direct and resonance processes of nuclear disintegration by means of high-energy particles. In the spectra of inelastically scattered electrons and protons, as well as other high-energy particles, the inhomogeneities of the nuclear continuum associated with the excitation of collective states manifest themselves against the background of intense direct transitions. It is commonly assumed that the direct transitions due to the quasi-elastic scattering of the projectile on the individual nucleons of the nucleus and possible on nucleon clusters as well, and the giant resonance excitation are caused by entirely different mechanisms. Their contributions to the nuclear excitation probability are assumed to be additive. However, there is a wide region of momentum transfer where a correct understanding of the reaction is not possible unless using a unified theory of direct and resonance processes.

Coincidence experiments like (e,e'N) and (p,p'N), in which the scattered

projectile is detected simultaneously with the product of nuclear disintegration may yield much more information about the nuclear structure in the continuum than the conventional scattering experiments.[1-3] The characteristics of the correlation between the scattered and ejected particles are determined not only by the intensity of the transitions of various multipolarities but also by the phase relations between the transition amplitudes. Therefore, the description of correlation characteristics is only possible in the framework of a unified theory describing simultaneously all contributions to the transition probability.

In order to demonstrate the efficiency of a correlation experiment and its interpretation on the basis of a unified theory we have calculated the spectra and angular correlation functions for the inelastic scattering of electrons and protons on the nucleus ^{12}C. Our main purpose is to forecast the new, unrelated to the chosen nucleus, general problems to be encountered by the experimentalist while applying the coincidence technique not as a conventional method of studying the direct process of quasi-elastic knock-out, but as a method for investigating the structure of the nuclear continuum. This enables us to use the rather simple particle-hole basis for the description of the states of ^{12}C.

The numerical calculations have been performed in a continuum shell model version described in ref.[4] For the description of the electron scattering the plane wave impulse approximation has been used. Considering small scattering angles we restrict ourselves to the Coulomb component of the electron-nucleon interaction. The scattering of the proton ($E_p \approx 1$ GeV) has been described in Glauber's theory using the approximation of a single inelastic collision [5]. The details of the calculation are described in refs.[6,7].

For fixed values of the transferred momentum q we have calculated the spectra R(E,q) of inelastic scattered electrons and protons, as well as the differential quantities $dR(E,q,\hat{k}_N)/d\hat{k}_N$, either as a function of the excitation energy E of the nucleus ^{12}C for definite ejection angles $\hat{k}_N$ ("differential" spectra), or for definite excitation energies as a function of the ejection angle (angular correlation function).

The main results of our calculations can be summarized as follows:

1. Varying the absolute value of the momentum transferred to the nucleus, resonances of a definite multipolarity can be either pronounced or suppressed. Higher multipolarities are favoured by a larger momentum, lower ones by a smaller momentum.
   The used projectile can also imply special selection rules for the excitation of certain resonances. In the scattering of protons practically only resonances with isospin T=0 are excited while electrons excite both T=0 and T=1 resonances. (Fig.1)
   Thus, informations completing each other may be extracted.

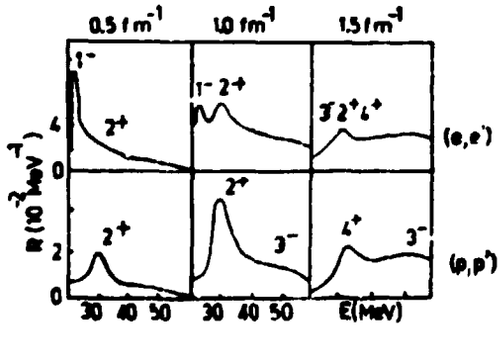

Fig.1 Spectra of inelastic scattered electrons (top) and protons (bottom) on ^{12}C for three values of the transferred momentum (q=0.5, 1.0, 1.5 fm^{-1})

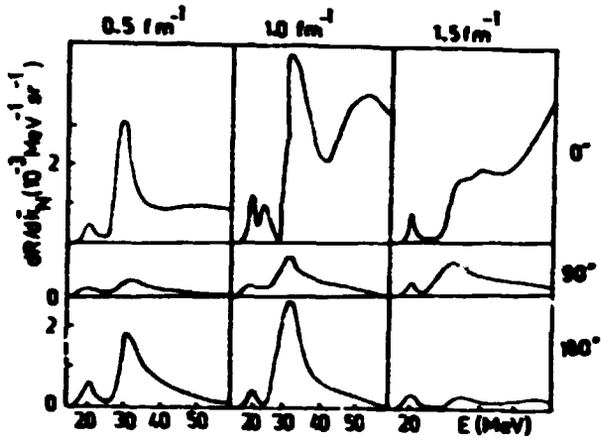

Fig.2 "Differential" spectra of the $^{12}C(p,p'p)^{11}B$ reaction for ejection angles $\theta = 0°, 90°, 180°$ (measured from the momentum transfer vector $\vec{q}$) in the scattering plane.

2. The coincidence experiments (e,e'N) and (p,p'N) may yield valuable additional informations about the nucleus and the reaction mechanism. At Fig.1 the resonances at 30 - 40 MeV are overleped by a strong direct contribution which manifest themselves as a quasi-elastic knock-out of a nucleon in the direction close to the vector $\vec{q}$ ($\theta = 0°$) (see Fig. 2) In the opposite direction (anti-quasi-elastic kinematics) the direct contribution vanishes. Further informations can be extracted by studying seperately the ejection of protons, neutrons and alpha clusters from the ground state or a definite excited state of the residual nucleus.

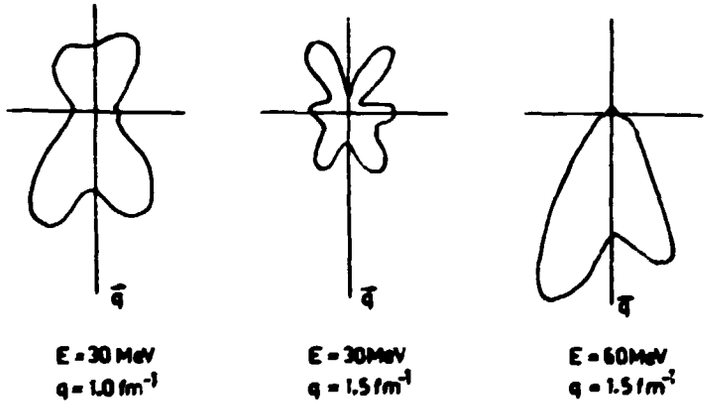

Fig.3
Polar diagram of the angular correlation function of the reaction $^{12}C(p,p'p)^{11}B$ in the scattering plane.

3. For the inelastic scattering of protons the influence of the distortion of the projectile wave function on the correlation function has been investigated. Our calculations predict a strong violation of the azimuthal symmetry around the vector $\vec{q}$. (Figs. 3 and 4)

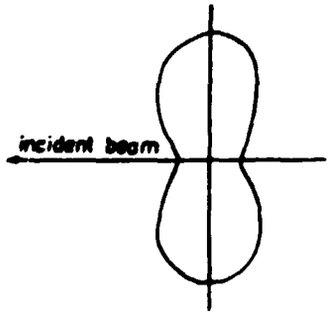

Fig.4
Polar diagram of the azimuthal dependence of the angular correlation function for the reaction $^{12}C(p,p'p)^{11}B$ around the momentum transfer vector q.

References

1. V.V.Balashov, Proc. VIth Int. Conf. on High-energy physics and nuclear Structure, Dubna, 1971, p.167
2. V.V.Balashov et al., Nucl. Phys. A216 (1973) 574
3. N.N.Titarenko, Yad. Fiz. 21 (1975) 730
4. H.W.Barz, I.Rotter, J.Höhn, Nucl. Phys. A275 (1977) 111
5. V.V.Karapetyan et al., Nucl. Phys. A203 (1973) 561
6. R.Wünsch, V.L.Korotkikh, N.N.Titarenko, Yad. Fiz. 28 (1978)
7. V.V.Balashov et al., JINR P4-11565 (1978); submitted to Nucl. Phys.

CONTINUOUS PARTICLE SPECTRA FROM DIRECT BREAK-UP REACTIONS*

G. Baur

Institut für Kernphysik, Kernforschungsanlage Jülich, D-5170 Jülich, West Germany

F. Rösel and D. Trautmann

Institut für Theoretische Physik, Universität Basel, CH-4056 Basel, Switzerland

A review of the theory of break-up reactions is presented, which was developed in recent years in the frame of direct nuclear reaction theory. Elastic and inelastic break-up modes, both contributing to inclusive spectra, are discussed. Recently measured (d,p), (α,^{3}He) and (^{9}Be,^{8}Be) spectra over a wide range of target nuclei are compared with our theory. Contributions from preequilibrium and evaporation processes to these spectra are also considered, but in most cases the break-up is the dominant reaction mechanism.

I. Introduction

A typical spectrum of particles emitted in nuclear reactions can be explained by different reaction mechanisms: at the high energy end of the spectrum (see Fig. 1) isolated peaks occur which are due to fast one-step transitions to discrete states of the residual nucleus. The low energy part of the spectrum is usually described by preequilibrium processes, where more collisions in the target are necessary to loose energy. For even lower energies the spectrum is dominated by the evaporation from the compound nucleus.

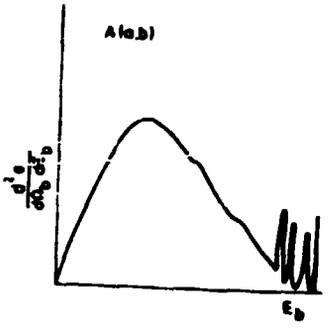

Fig. 1: Spectrum of particles emitted in a nuclear reaction.

The topic of this talk is the break-up process (fragmentation) of the projectile a into its constituents b and x (a=b+x) in the nuclear and Coulomb field of the target nucleus. This reaction mode contributes substantially to the total reaction cross section. Over the last years this break-up process has been studied rather extensively both theoretically and experimentally. We present here the distorted wave theory of the break-up process. We distinguish two modes, the elastic [1] and inelastic [2-4] break-up, depending on whether the target remains in the ground state or not during the collision. We apply this theory to (d,p) spectra measured [2] over a wide range of target nuclei. Quite recently, also the break-up reaction of the tightly bound α-particle has been observed [3,5]. Furthermore we study the break-up of the very weakly bound ^{9}Be under subcoulomb conditions [4,6]. Although there is a great activity in this field at the present time, it should be mentioned that the break-up process has quite a long history in nuclear physics. The break-up of the deuteron in the Coulomb field of the nucleus was first considered theoretically by Oppenheimer [7]. A partial solution of that problem which is quite close to the starting point of our investigations was given by Landau and Lifshitz [8]. The early experiments of Helmholtz, McMillan and Sewell [9] in 1947 of high energy deuteron break-up could be well accounted for by the Serber model [10]. Nowadays the "abrasion process" also plays a dominant role in the new field of high energy heavy ion physics [11] as well as in relativistic deuteron-nucleus interactions [12]. Deuteron-nucleus collisions in the multi-GeV region were studied theoretically by Fäldt and Pilkuhn [13].

---

* Invited talk presented by D. Trautmann at the 8th Symposium on Interaction of Fast Neutrons with Nuclei, held at Gaussig, DDR, November 13-17, 1978

2.1 Coincidence Cross Section

We consider the reaction

$$A + a \rightarrow A + b + x \ , \qquad (1)$$

where the projectile a disintegrates in the Coulomb and nuclear field of the target nucleus into the constituents b and x which are supposed to be both detected. If the nucleus A remains in the ground state during the collision, the reaction is called the elastic break-up, for which the T-matrix element is given by the expression (post-interaction form):

$$T_{\vec{q}_a \rightarrow \vec{q}_b \vec{q}_x} = \iint d^3r_{bx} d^3R_a \chi_b^{(-)*}(\vec{R}_b)^* \chi_x^{(-)*}(\vec{R}_x)^* V_{bx}(\vec{r}_{bx}) \phi_{bx}(\vec{r}_{bx}) \chi_a^{(+)}(\vec{R}_a) \ . \qquad (2)$$

The scattering wave solutions of the particles a, b and x generated by appropriate optical potentials are denoted by χ and the momenta of the particles in the initial and final states are given by $\vec{q}_a$, $\vec{q}_b$ and $\vec{q}_x$. The interaction between b and x is described by the potential $V_{bx}(\vec{r}_{bx})$ and the wave function of the particle a is denoted by ϕ_{bx}. It is expected that the DWBA expression (2) is a good approximation if the elastic scattering is the dominant channel.

Let us first study the (d,pn) break-up process for lower energies in the zero range approximation, where an especially "clean" situation arises for deuteron bombarding energies well below the Coulomb barrier. In this case, the distorted waves of the deuteron and of the proton are given by the pure Coulomb wave functions, whereas the neutron wave function is always distorted by the nuclear interaction of the neutron and the target nucleus [14]. Due to the Coulomb repulsion, the contributions to the integral in eq. (2) are strongly suppressed for distances $R<R_0$ where R_0 denotes the nuclear interaction radius. Therefore, only the asymptotic neutron wave function $\chi_{\ell_n}(q_n R)$ enters into expression (2). This wave function can be expressed entirely in terms of the S-matrix elements S_{ℓ_n} of elastic n-A scattering, which leads to the following expression for the break-up T-matrix element:

$$T_{\vec{q}_d \rightarrow \vec{q}_p \vec{q}_n} = T_{p.c.} + \sum_{\ell_n} \frac{1}{2} (S_{\ell_n} - 1) T_{\ell_n} \ . \qquad (3)$$

The first term, $T_{p.c.}$, describes that part of the T-matrix which corresponds to a plane wave of the neutron [8,15], the second term takes the scattered part of the neutron wave function into account. The matrix elements $T_{p.c.}$ and T_{ℓ_n} can be calculated either analytically [1,8,15] or with the Vincent-Fortune integration method [16]. Calculations [17] based on eq. (3) lead to a very good agreement with experimental data [18]. This is very gratifying since the theoretical calculation was performed with essentially no free parameter. (The S_{ℓ_n}'s were calculated with a standard optical model potential.)

Above the Coulomb barrier the nuclear interaction is taken into account by means of the appropriate optical potentials. In Fig. 2, taken from ref. [17], the theoretical calculations are compared with experiment [19], again the agreement is good. Corrections due to "finite range" are found to be small, but they seem to further improve the agreement with experiment.

2.2 Elastic and Inelastic Break-Up

Now we want to treat this kind of cross sections where only particle b is detected ("inclusive cross section"). The contribution of the elastic break-up to that cross section can simply be obtained by an integration over the angle of the unobserved particle x. This can be done analytically by virtue of the orthogonality of the spherical harmonics leading to the following expression for the elastic part of double differential cross section:

$$\frac{d^2\sigma(el)}{d\Omega_b d\Omega_b} = \frac{m_a m_b m_x}{4(2\pi\hbar^2)^3}\frac{q_b q_x}{q_a}\sum_{\ell_x m_x}|T_{\ell_x m_x}(\theta_b)|^2 . \tag{4}$$

Note that the sum over ℓ_x-values has become incoherent. Hereby we have introduced the "reduced" T-matrix

$$T_{\ell_x m_x}(\theta_b) = D_0 \int d^3r\, \chi^{(-)*}_{\vec{q}_b}(\vec{r})\chi_{\ell_x}(q_x,r)Y_{\ell_x m_x}(\hat{r})\chi^{(+)}_{\vec{q}_a}(\vec{r})A(r)P(r) . \tag{5}$$

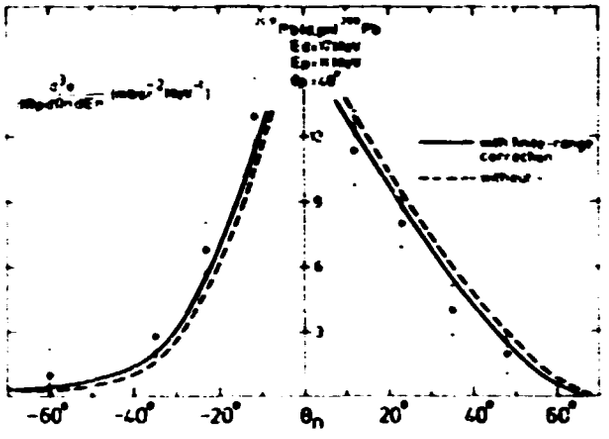

Fig. 2: Comparison of theory and experiment [19] in the deuteron break-up reaction above the Coulomb barrier.

By deriving expression (4) we have used again the zero-range approximation (the zero-range constant D_0 corresponds to the vertex a+b+x). Finite range- and non-locality effects are given by the functions A(r) and P(r), respectively [2].

For the inclusive type of spectra we also have to consider all kinds of inelastic processes between particle x and target A, i.e. we have to consider processes of the type A+a→b+c, where c is some specific two-body final state of the system B=A+x. The form factor for such a transition can be written as

$$\int d\xi_A \phi^{(-)*}_{Bc}\phi_A = 4\pi\sum_{\ell_x m_x} i^{\ell_x}\chi^c_{\ell_x}(r)Y_{\ell_x m_x}(\hat{r})Y_{\ell_x m_x}(\hat{q}_c)^* , \tag{6}$$

where ϕ_A denotes the ground state wave function of nucleus A and $\phi^{(-)}_{Bc}$ describes a complete scattering state of the system B with the boundary condition c. The internal coordinates of nucleus A are denoted by ξ_A. In principle, it would be possible to calculate this form factor with the help of a model wave function for $\phi^{(-)}_{Bc}$. However, this would be very difficult and impracticable if there are many open channels. But fortunately, there is an approximative procedure which allows us to make use of the unitarity of the S-matrix (for the system B=A+x). This simplifies the whole calculation enormously. We note (see ref. [17]) that the main contribution to the DWBA integral comes from the region outside the nuclear interaction $r>R_0$. There we can express the radial form factor $\chi^c_{\ell_x}$ entirely in terms of the scattering matrix elements $S_{\ell_x,c}$ which connects the elastic channel ℓ_x and the inelastic channel c. In complete analogy to the situation for the elastic break-up the integration over the angle of $\vec{q}_c$ can be carried out in order to obtain from the triple differential cross section the double differential cross section for the (a,b) reaction. Somehow arbitrarily the radial form factor $\chi_{\ell_x}(r)$ is extended into the interior region $r<R_0$, however it is expected that the contribution of this region is small compared to the whole DWBA integral, so this is not expected to be a serious approximation. The entire dependence on the channel index c rests then in the S-matrix element $S_{\ell_x,c}$. With the help of the unitarity of the S-matrix

$$\sum_{c\neq\ell_x}|S_{\ell_x,c}|^2 = 1 - |S_{\ell_x,\ell_x}|^2 , \tag{7}$$

the summation over all states $c\ell_x$ can be carried out, leading to the inelastic break-up cross section in the following compact form:

$$\frac{d^2\Omega(\mathrm{inel})}{d\Omega_b dE_b} = \frac{m_a m_b m_x}{4(\hbar c)^2 (2\pi)^3} \frac{k_b k_x}{k_a} \sum_{\ell_x m_x} \frac{\sigma^{\mathrm{reaction}}_{\ell_x}}{\sigma^{\mathrm{el}}_{\ell_x}} |T_{\ell_x m_x} - T^{0}_{\ell_x m_x}|^2 \quad . \tag{8}$$

Here we have introduced the elastic and total reaction cross section $\sigma^{\mathrm{el}}_{\ell_x}$ and $\sigma^{\mathrm{reaction}}_{\ell_x}$, respectively and $T^{0}_{\ell_x m_x}$ denotes the reduced T-matrix eq. (5), where the radial wave function of particle x is replaced by the spherical Bessel function $j_{\ell_x}(q_x r)$.

For the (a,b) double differential cross section, the elastic and inelastic contributions, eqs. (4) and (8), have to be added up.

3. Results and Discussion

3.1 The Break-Up of a Heavy Ion: The (^{9}Be,^{8}Be)-Reaction

The break-up of ^{9}Be was studied experimentally in ref. [6] for subcoulomb conditions and it was shown in ref [4] that the measured spectra can be well described within the present theory. However, for a close agreement of the experimental data with the theoretical calculation the effect of the recoil has to be taken into account, as can be seen in Fig. 3. Since the numerical

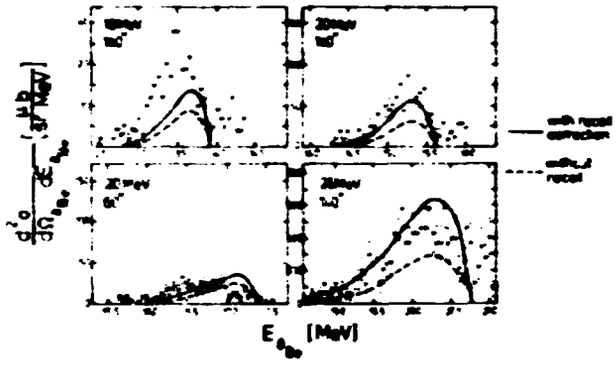

Fig. 3: Comparison of the theoretical inclusive spectra with the experimental results [6] for the reaction ^{197}Au(^{9}Be,^{8}Be). The theoretical curves are the sum of the elastic and inelastic break-up modes. The spectroscopic factor for the ^{9}Be ground state was taken to be S=0.55.

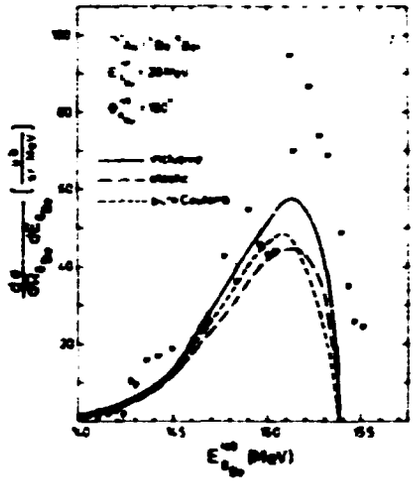

Fig. 4: Comparison of the theoretical spectra with the experimental data of ref. [6]. The recoil correction is included.

evaluation of the T-matrix, eq. (2), is too cumbersome, the recoil effect is approximated by the Buttle-Goldfarb prescription [20]. Although the elastic break-up gives the largest contribution to the inclusive cross section, the inelastic break-up cannot be neglected. This can be seen in Fig. 4, where also the pure Coulomb break-up cross section, obtained by neglecting the n-Au-interaction is shown for comparison.

In ref. [6] it is claimed that the Coulomb excitation of the $1/2^+$ resonance just above the neutron threshold is the main reaction mechanism, but according to ref. [4] this is only a small additional effect at these low bombarding energies. In principle, however, this mechanism cannot be excluded. For the break-up of ^{6}Li it is expected that the Coulomb excitation of the ^{6}Li-projectile will be very important.

3.2 The Break-Up of the Deuteron: The (d,p)-Reaction

As a next example we consider proton spectra in deuteron induced reactions which have been measured quite recently at a deuteron bombarding energy E_d = 25.5 MeV 2). In Fig. 5 angle inte-

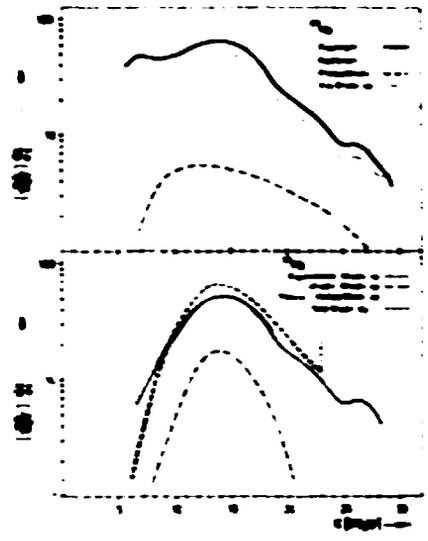

Fig. 5: Experimental angle integrated proton spectrum, together with the equilibrium, pre-equilibrium and experimental break-up contributions (E_d = 25.5 MeV). For further details see ref [2]. In the bottom part, the experimental break-up spectrum is compared to the elastic, inelastic and total break-up calculation.

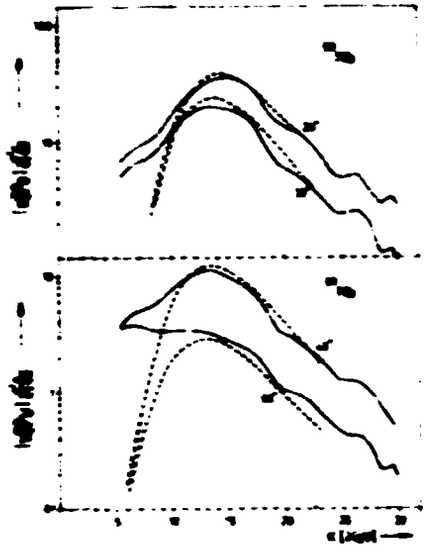

Fig. 6: Comparison of experimental and theoretical proton spectra at forward angles for the (d,p) reaction on ^{93}Nb (E_d = 25.5 MeV). The continuous lines denote the experimental results, the dashed lines are the theoretical calculations.

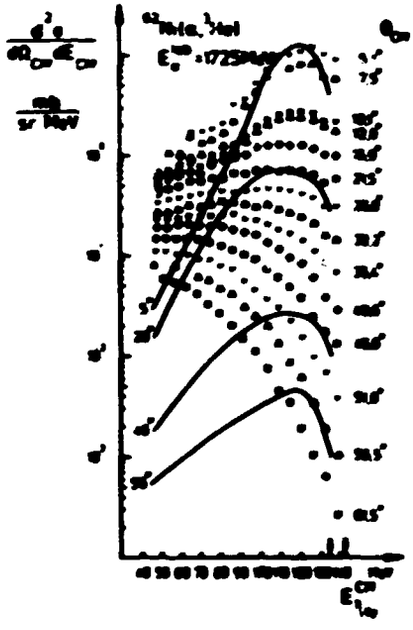

Fig. 7: Double differential cross sections for the ^{62}Ni(α,^{3}He) reaction at E_α = 172.5 MeV. Full lines indicate theoretical calculations. The energies corresponding to the ground state transition and the three-body threshold are indicated by arrows.

grated (d,p)-spectra on ^{93}Nb are shown and compared with our theory, where the "experimental break-up curve" is obtained by subtracting preequilibrium and evaporation processes from the measured cross section. Note that at around half of the incident deuteron energy a prominent bump is found. In Fig. 6 experimental data are compared for several proton angles with the theoretical calculations. The agreement is satisfactory, especially in the bump region. For lower proton energies the experimental data lead to higher cross section, since there are additional contributions from preequilibrium and compound processes.

3.3 The Break-Up of the α-Particle: The (α, ^{3}He)-Reaction

Let us finally consider the (α,^{3}He) break-up process 3). In Fig. 7 the double differential cross section for the ^{62}Ni(α,^{3}He) reaction at E_α = 172.5 MeV is shown. Agreement between experiment and theory is found for large $E_{^3He}$ energies, whereas for decreasing energy discrepancies occur, especially for larger ^{3}He angles. This is caused by multistep processes, which will become important for ^{3}He particles emerging with lower energies. It was furthermore shown in ref. [3] that the (α,^{3}He)-reaction excites favoured ℓ_n-values. This selectivity makes this reaction a useful tool for studying single neutron strength distributions in nuclei for high ℓ_n-values and high excitation energies.

4. Conclusion

We have seen that a wealth of data on continuous particle spectra can be explained by the break-up mechanism. Our theory is formulated in the frame of direct reaction theory. This mechanism is especially important for loosely bound particles like deuteron or ^{9}Be. The agreement of the theory with (d,pn) coincidence measurements is very good, this is especially important in the "clean" subcoulomb region. Also for the most tightly bound particle, the α-particle, a substantial fraction of the total reaction cross section at higher α-energies is due to the break-up mechanism. When the cross section for break-up is a large part of the total reaction cross section, its influence on other channels (e.g. the elastic one) cannot be neglected. The inelastic break-up mode is responsible for a substantial part of the experimental break-up yield. The stripping reaction to unbound states is an interesting tool to study the hitherto unexplored high lying single particle properties, much in the same way as inelastic scattering probes the giant resonances and pickup reactions the deep lying hole structure of nuclei.

References

[1] For a review see G. Baur and D. Trautmann, Phys.Rep. 25C (1976) 293 and further references contained therein.
[2] J. Pampus, J. Bisplinghoff, J. Ernst, T. Mayer-Kuckuk, J. Rama Rao, G. Baur, F. Rösel and D. Trautmann, Nucl.Phys.A (1978), in press
[3] A. Budzanowski, G. Baur, C. Alderliesten, J. Bojowald, C. Mayer-Böricke, W. Oelert, P. Turek, F. Rösel and D. Trautmann, Phys.Rev.Lett. 41 (1978) 635
[4] G. Baur, M. Pauli, F. Rösel and D. Trautmann, Nucl.Phys. A (1978), in press
[5] J.R. Wu, C.C. Chang and H.D. Holmgren, Phys.Rev.Lett. 40 (1978) 1013
[6] J. Unternährer, J. Lang and R. Müller, Phys.Rev.Lett. 40 (1978) 1077
[7] J.R. Oppenheimer, Phys.Rev. 47 (1935) 845
[8] L. Landau and E. Lifshitz, JETP 18 (1948) 750 (English translation in: Collected papers of L. Landau)
[9] A.C. Helmholtz, E.M. McMillan and D.C. Sewell, Phys.Rev. 72 (1947) 1003
[10] R. Serber, Phys.Rev. 72 (1947) 1008
[11] H.H. Heckmann, D.E. Greiner, P.J. Lindstrom and F.S. Bieser, Phys.Rev.Lett. 28 (1972) 926
[12] L.S. Ashgirey, M.A. Ignatenko, V.V. Ivanov, A.S. Kusnetsov, M.G. Mescheryakov, S.V. Razin, G.D. Stoletov, I.K. Vzorov and V.N. Zhmyrov, Nucl.Phys. A305 (1978) 404
[13] G. Fäldt and H. Pilkuhn, Ann.Phys. 58 (1970) 454
[14] G. Baur and D. Trautmann, Nucl.Phys. A199 (1973) 218
[15] G. Baur and D. Trautmann, Nucl.Phys. A191 (1972) 321
[16] C.M. Vincent and H.T. Fo[illegible] Phys.Rev. C2 (1970) 782
[17] G. Baur, F. Rösel and D. [illegible]mann, Nucl.Phys. A265 (1976) 101
[18] L. Jarczyk, J. Lang, R. M[illegible]ler, D. Balzer, R. Viatte and P. Marmier, Phys.Rev. C8 (1973) 68
[19] C.L. Fink, B.C. Cohen, J.L. van der Waerd and R.J. Petty, Phys.Rev. 185 (1969) 1568
[20] B.J. Buttle and L.J.B. Goldfarb, Nucl.Phys. A176 (1971) 299

CONTINUUM SHELL-MODEL DESCRIPTION OF EXCITED STATES IN LIGHT DEFORMED NUCLEI

H.W. Barz
Zentralinstitut für Kernforschung Rossendorf, DDR - 8051 Dresden

During recent years much effort has been done to extend the range of applicability of the continuum shell-model to nuclei consisting of a non-magic number of nucleons. In a spherical basis one is forced to handle a complicated mixture of shell-model configurations [1]. The difficulties increase the more the nucleon number differs from the magic number. But, it is well known that the states of statically deformed nuclei can be described in a good approximation by a single Slater determinant built from deformed single-particle orbits. This suggests the idea to describe the excited states of a deformed nucleus in the frame work of the 1p-1h model which has been applied succesfully for spherical nuclei.

Recently [2] the giant dipole resonance in ^{20}Ne has been analysed using a discrete deformed single-particle basis and taking into account the coupling to a spherical one-particle continuum. We aim to apply the 1p-1h model to very light nuclei where most of the unoccupied single-particle orbits already belong to the continuum. We restrict us to strongly deformed nuclei which are assumed to exist for mass numbers 7, 8 and 9.

The model proposed is based on the adiabatic approximation in which it is assumed that the Hamiltonian can be decomposed in an intrinsic Hamiltonian H' and a rotational term $H_{rot} = \hbar^2/2\mathcal{J}\,(I(I+1) - 2K^2)$ with $\mathcal{J}$, I and K being the total angular momentum, its projection on the body-fixed symmetry axis and the momentum of inertia. Then in the strong coupling limit [3] the wave function of the target nucleus reads

$$\mathcal{C}^{I_T}_{M_T K_T} = \left(\frac{2I_T+1}{16\pi^2(1+\delta_{K0})}\right)^{1/2} \left[D^{I_T}_{M_T K_T}(\theta)\,\chi_{K_T}(\kappa') + (-)^{I_T-\hat{I}}\, D^{I_T}_{M_T -K_T}(\theta)\,\chi_{-K_T}(\kappa') \right] \quad (1)$$

The Wigner D-function depends on the orientation θ of the deformed nucleus with respect to the space fixed frame and projects out the spin I_T as well as its projections K_T (M_T) on the body (space) fixed z-axis. The intrinsic state wave function χ_{K_T} is an antisymmetrized product of single-particle states obtained as solutions of a Schrödinger equation with a deformed potential well given in the body fixed frame

$$V_{def} = V(r,R) + V_{s.o}(r,R)\,\vec{l}\vec{\sigma} + \beta\, R\frac{d}{dR}V(r,R)\,Y_{20}(\kappa') \quad (2)$$

The potential contains a Woods-Saxon potential V, a spin-orbit potential V_{so}, the nuclear radius R and the deformation parameter β.

Now, assuming the adiabatic approximation the continuous states of the nucleus are described [4] by wave functions similar to eq. (1). But now the intrinsic wave function χ_K does not vanish asymptotically because one nucleon is promoted into the continuum. Therefore we expand the wave function χ_K in 1p-1h components in the intrinsic system:

$$\chi_K = \frac{1}{r}\sum_{h\ell j} i^{\ell}\, \mathcal{J}_{\ell j,\, K-K_T+m_h}(\kappa'_g)\, \xi^{(K)}_{h\ell j}(r)\quad |(h,m_h)^{-1}\rangle, \quad (3)$$

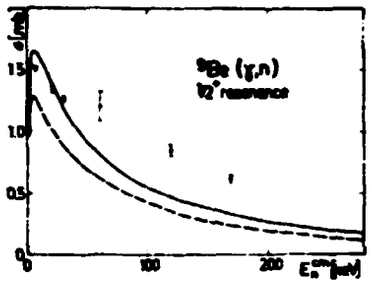

Fig. 1. Photo-neutron cross section near the neutron threshold of 1.67 MeV with $I = 1/2^+$. Experimental data are taken from ref. [6] (—— 9 channel, - - - 1 channel).

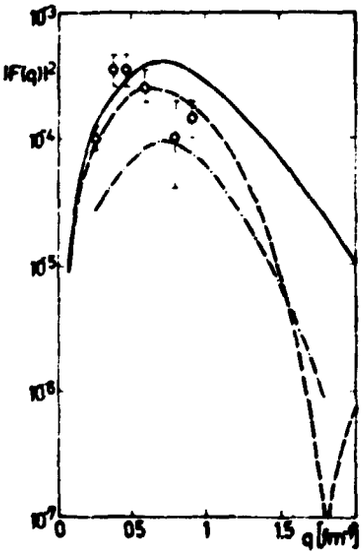

Fig. 2. Longitudinal formfactor for the electro-excitation of the $1/2^+$ resonance near the threshold compared with experiment [7] and the result of a molecular orbital model [8] (—·—).

where the symbol $|h\, m_h^{-1}\rangle$ means the residual nucleus with a hole in the orbit h. The radial wave functions $\xi^{(K)}_{hlj}(r)$ represent the motion of the escaping nucleon carrying the angular momenta l, j and the projection $K - K_T + m_h$. The radial wave function are calculated by solving a system of coupled-channels equations [5] which is derived from the Schrödinger equation $(E'-H')\,\chi_K = 0$ where the intrinsic energy is connected with the lab. energy via $E = E' + \hbar^2/2\mathfrak{J}\,[I(I+1) - 2K^2]$. The radial wave function are coupled due to both the deformed potential and the residual force of H'.

Now, the model is applied to the nucleus ^{9}Be. The single-particle energies can be derived from the experimental energy spectra of ^{9}Be and the neighbouring nuclei ^{8}Be and ^{8}Li. Then we adapt the potential parameters and use V = 52/44 MeV for l = 1/0,2 and V_{so} = 5 MeV. A deformation parameter of β = 1.3 is needed to obtain the correct splitting of 16 MeV of the spherical $p_{3/2}$ orbit. The parameters of the potential depths for l = 0,2 are chosen to produce the first $1/2^+$ resonance near the threshold energy of 1.67 MeV. For the residual interaction a strength of 650 MeV fm^3 $(0.7 + 0.3\, P^{\sigma}_{12})\delta_{\mu}$ is assumed. In fig. 1 the calculated (γ,n) cross section with I = 1/2 near the threshold is compared with experiment [6]. The broken line results from a one-channel calculation in which only the weakly bound neutron is regarded. Taking into account all the nine nucleons (heavy line) the cross section increases by 25 %. The B(E1, $3/2^- \to 1/2^+$) value of 0.25 e^{2}mb obtained from the energy integrated cross section is well compatible with experiment. We also calculated the longitudinal formfactor for excitation of the $1/2^+$ resonance in inelastic electron scattering (fig. 2). A recoil corrected effective charge

$$\hat{e}_i = e_i\, e^{i\frac{A-1}{A}\vec{q}\vec{r}} + \sum_{j(\neq i)} e^{-\frac{i}{A}\vec{q}\vec{r}} \langle j|e_j j_0(qr)|j\rangle$$

has been used (e_i - charge, $\vec{q}$ - transferred momentum).

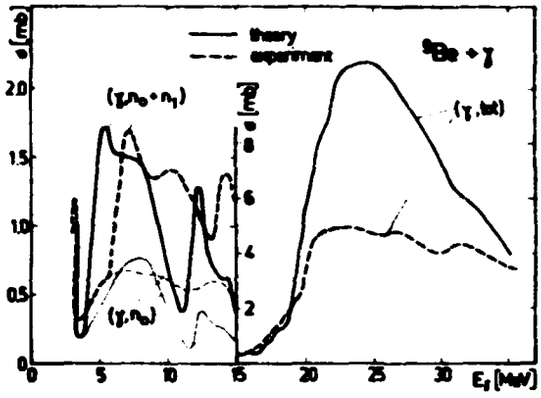

Fig. 3. The calculated photo-nucleon cross sections compared with the experimental data.

The total photo-absorption cross section for ^{9}Be is represented in fig. 3. Below 12 MeV the weakly bound neutron determines the cross section. However, the giant dipole resonance at 25 MeV is formed by excitation of the 1s and the $p_{3/2}$ nucleons with $m_{z'} = \pm 1/2$. The resonance structures calculated resembles that found in experiment although the calculated giant resonance appears to narrow which may be a hint to neglected ground state correlations. The calculations proof the ability of the 1p-1h model to describe the continuous states in deformed nuclei.

References

1) H.W. Barz, I. Rotter and J. Höhn, Nucl. Phys. A275 (1977) 111
2) K.W. Schmid and G. Do Dang, Phys. Rev. C15 (1977) 1515
3) A. Bohr, Dan. Mat. Fys. Medd. 27 (1952) No. 14
4) S.I. Drozdov, Zh ETF 28 (1955) 734; T. Tanura, Rev. Mod. Phys. 37 (1965) 679
5) H.W. Barz, Proc. of the Int. Symp. on Nuclear Reactions, Balatonfüred 1977, p. 378
6) B. L. Berman et al., Phys. Rev. 163 (1967) and ref. here in
7) A.G. Slight et al., Nucl. Phys. A208 (1973) 157 and ref. here in
8) S. Okabe and Y. Abe, Proc. of the 3rd Int. Conf. on Clustering Asp. of Nucl. Structure and Nucl. Reactions, Manitoba 1978, B 10

FINITE-RANGE DWBA ANALYSIS OF THE $^9Be(n, \alpha_0)^6He$ REACTION

I.M.Turkiewicz, S.Burzyński, K.Rusek, A.Trzciński, J.Turkiewicz, P.Żuprański
Institute of Nuclear Research, Warsaw, Poland

The subject of the present paper is to study the influence of cluster structure of ^9Be on the multinucleon-transfer reactions induced by fast neutrons on the ^9Be nucleus. The angular distributions of the $^9Be(n,\alpha_0)^6He$ reaction were measured by us at 12.2, 14.1 and 18.0 MeV 1). Zero-range DWBA analysis has provided a good description of the shapes of the angular distributions but could not be considered as satisfactory because of too crude approximations used. The present paper uses finite-range DWBA analysis in the hope to obtain more reliable spectroscopic informations. As main contributions to the $^9Be(n,\alpha_0)^6He$ reaction we consider the two following processes:

1. light particle pick-up (direct process): $n + (^3He + {}^6He) \rightarrow (n + {}^3He) + {}^6He$
2. heavy particle pick-up (exchange process): $n + (^5He + {}^4He) \rightarrow (n + {}^5He) + {}^4He$

These two pick-up modes are related to three-nucleon and four-nucleon cluster components of the ^9Be ground state wave-function. We have calculated the $^9Be(n,\alpha_0)^6He$ differential cross-section as a coherent sum of both these transfers. Knock-on process was omitted as its contribution is expected to amount to less than 5% of pick-up contributions 2). The cross-section for a cluster pick-up can be calculated from a familiar DWBA expression equivalent to that applied in one-nucleon transfer. For the reaction $B + b \rightarrow A + a$ where $B = A + x$ and $a = b + x$ in the relative states with radial quantum numbers N_1L_1 and N_2L_2 respectively, the cross-section can be written in terms of a structural part A and dynamical part β as

$$\frac{d\sigma}{d\Omega} = \frac{2s_a+1}{2s_b+1} \sum_{lm} \left| \sum_{N_1L_1N_2L_2} A^{l}_{N_1L_1N_2L_2} \, \beta^{lm}_{N_1L_1N_2L_2}(\theta) \right|^2$$

where the symbols and the coordinate system are those used in the paper of Austern et al. 4 and in the finite range DWBA programme "Lola" of DeVries 3).

$$\beta^{lm}_{N_1L_1N_2L_2}(\theta) = \iint d\tau_{bB}\, d\tau_{aA}\, \chi^*_a(\tau_{aA}) \left| f^{lm}_{N_1L_1N_2L_2} \right| \chi_b(\tau_{bB})$$

is a finite range amplitude with two-dimentional form factor $f^{lm}_{N_1L_1N_2L_2}$ containing the product of the effective interaction potential and the wave functions of the relative motion of the cluster pairs in the initial $\psi_{N_1L_1}$ and final $\psi_{N_2L_2}$ states. The χ are distorted waves. The coherent sum

$$\sum'_{N_1L_1N_2L_2} A^{l}_{N_1L_1N_2L_2} \, \beta^{lm}_{N_1L_1N_2L_2}(\theta)$$

is taken over all $N_1L_1N_2L_2$ quantum numbers compatible with an orbital angular momentum transfer l. $(N_1L_1) \rightarrow (N_2L_2)$ contributions allowed by angular momentum selection rules for $^9Be + n \rightarrow \alpha + {}^6He$ g.s. are given in Table I.

The values of radial quantum numbers for the relative motion of cluster pairs were determined by the relation of oscillator energy conservation in a Talmi-Moshinsky transformation from single nucleon to cluster coordinates assuming clusters in their ground states. The wave functions ψ_{NL} used as bound states to calculate the form factors were generated in Saxon-Woods potential so as to reproduce the separation energy of the clusters. The parameter values that were used to calculate bound state wave functions are listed in Table II.

TABLE I

Bound states participating in ^3He and ^5He cluster transfer for the $^9Be(n,\alpha_0)^6He$ reaction

initial state	N_1	L_1	final state	N_2	L_2	l
$^3He + ^6He$	2	1	$^3He + n$	1	0	1
$^5He + ^4He$	3	0	$^5He + n$	1	1	1
$^5He + ^4He$	2	2	$^5He + n$	1	1	1

TABLE II

Bound states potential parameters $\left[R = r_o\left(A_1^{1/3} + A_2^{1/3}\right)\right]$

State	E_{SE} MeV	r_o fm	a fm	V MeV
$^3He + ^6He$ 2p	21.172	1.12	0.65	67.2
$^4He + ^5He$ 3s	2.524	1.12	0.65	46.5
$^4He + ^5He$ 2d	2.524	1.12	0.65	46.9
$n + ^5He$ 1p	1.919	1.03	0.65	53.6
$n + ^3He$ 1s	20.568	0.93	0.65	57.0

The interaction potentials responsible for ^3He and ^5He transfer are Woods-Saxon bound state potentials of $n + ^3He$ and $n + ^5He$ respectively.

Geometric parameters of the Saxon-Woods well in which bound state wave functions were solved should be discussed. Generally speaking these parameters are not well determined for clusters. We have tried several values of R from 2.9 fm to 5.3 fm i.e. from the range suggested by different optical potential fits to ^3He and ^4He elastic scattering on light nuclei 5,6) and applied in cluster transfer calculations. In this range we have observed the dependence of the differential cross section on R not only in absolute value but also in its shape. We have chosen $R(^3He + ^6He) = 3.65$ fm and a = 0.65 fm to reproduce experimental root-mean-square radius of the ^9Be nucleus and we kept the same parametrization for $^4He + ^5He$ bound state. The optical model parameters for calculation of the distorted waves in the entrance and exit channels are shown in Table III. The optical potential for $n + ^9Be$ was obtained from an analysis of the available elastic scattering data of Lutz et al. 7) at 14 MeV. For the exit channel, since no data exists for α scattering on ^6He, potential from an analysis of the scattering of 18.54 MeV alpha particles on ^6Li 6) was used. From different parameters given by authors we have chosen two sets without spin-orbit term. They are listed as AI and AII in Table III.

TABLE III

Optical model parameters for the entrance and exit channels

	system	V MeV	R fm	a fm	W MeV	W_D MeV	R_I fm	a_I fm
	$n + ^9Be$	48.76	2.49	0.65	0	11.42	2.91	0.28
AI	$^4He + ^6He$	167.6	2.29	0.61	0	8.6	2.29	0.61
AII	$^4He + ^6He$	193.3	3.64	0.45	0	17.9	3.64	0.45

The potential AII gave cross sections one order of magnitude smaller than the experimental values. The results presented below have been obtained with potential AI.

The transition amplitudes $\beta^{lm}_{N_1 L_1 N_2 L_2}$ for the possible transfers were computed with the aid of a finite range DWBA code "Lola" 3). The structure factors weighting the contributions of each reaction amplitude $\beta^{lm}_{N_1 L_1 N_2 L_2}$ are

$$A^{l}_{N_1 L_1 N_2 L_2} = (-1)^{L_1+L_2+S_x-J_2}\, i^{l}(2l+1)\, W(L_1 J_1 L_2 J_2; S_x l)\; S^{1/2}_{B\to A+x}\; S^{1/2}_{a\to b+x}$$

S_x is the spin of transfered cluster, $J_1 = L_1+S_x$, $J_2 = L_2+S_x$. $S^{1/2}_{B\to A+x}$ and $S^{1/2}_{a\to b+x}$ are the spectroscopic amplitudes, as defined in ref. 8), for the break up of nucleus B into A and x clusters, and outgoing particle a into b and x. The three-nucleon and four-nucleon structure amplitudes for ^{9}Be ground state have been calculated by Kurath 9) and Kurath and Millener 10). The ^{6}He $\to$ ^{5}He + n amplitude we have calculated using the definition and phase convention of ref. 8). Firally the structure factors for the three transfers listed in Table I are the following:

- 0.201 for ^{3}He pick-up
+ 0.230 for ^{5}He pick-up from 3s state
+ 0.123 for ^{5}He pick-up from 2d state.

The differential cross-sections of ^{9}Be(n, α_0)^{6}He transition have been calculated using these structure factors. Contributions to the cross-sections from the various processes are plotted in fig.1 together with their coherent sum. It is evident that interference has a very important influence on the final result. The comparison of calculated differential cross-sections with 12.2 and 14.1 MeV experimental angular distributions is shown in fig.2 and 3. The angular distributions as well as the absolute magnitudes of the cross sections are reproduced fairly well by the theoretical curves. The fact that the agreement between data and calculations have been obtained with the spectroscopic amplitudes not adjusted but taken from the independent predictions offers the indication that the applied finite-range analysis was appropriate.

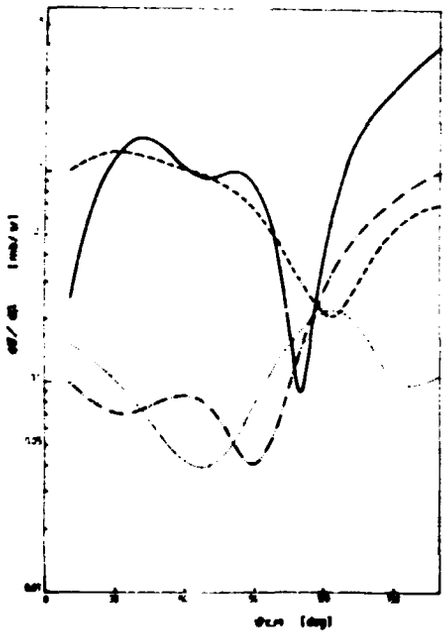

Fig.1 Separation of the complete cross-section predicted by the pick-up mechanisms (solid curve) into ^{3}He pick-up component (dashed curve) and ^{5}He components (3s - dash-dot and 2d - dotted curve).

It has to be mentioned, however, that to perform the complete analysis of this type of reaction it would be desirable to use a code without the usual DWBA potential cancellation assumption.

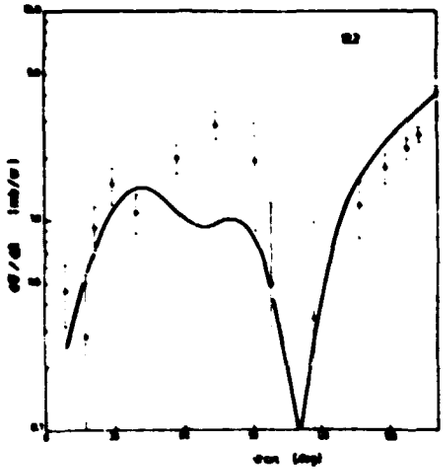

Fig.2 Angular distribution of the $^{9}Be(n,\alpha_0)^{6}He$ reaction at 12.2 MeV. The curve is the sum of finite-range DWBA calculations for ^{3}He and ^{5}He pick-up mechanism.

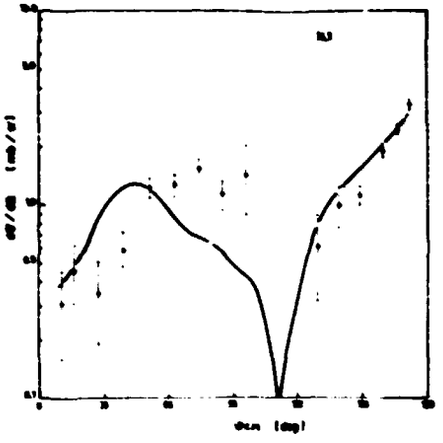

Fig.3 The same as in Fig.2 but for 14.1 MeV.

REFERENCES

1. W.Smolec, S.Burzyński, K.Rusek, I.M.Turkiewicz, J.Turkiewicz and P.Żuprański, Nucl.Phys., A257 1976 397
2. R.DeVries, University of California, PhD Thesis, 1971
3. R.DeVries, Lola a DWBA Program
4. N.Austern, R.M.Drisko, E.C.Habbert and G.R.Satchler, Phys.Rev.,133 1964 B3
5. E.B.Carter, G.L.Mitchell, R.H.Davies, Phys.Rev., 133 1964 B1421
6. H.G.Bingham, K.W.Kemper and N.R.Fletcher, Nucl.Phys., A175 1971 374
7. H.F.Lutz, J.B.Mason and M.D.Karvelis, Nucl.Phys., 47 1963 521
8. N.Anyas-Weiss et al. Physics Reports 12C 1974 203
9. D.Kurath, Phys.Rev., C7 1973 1390
10. D.Kurath and D.J.Millener, Nucl.Phys., A238 1975 269

FINITE-RANGE DWBA ANALYSIS OF THE $^{14}N(n,\alpha)^{11}B$ REACTION

K.Rusek, S.Burzyński, I.M.Turkiewicz, J.Turkiewicz, A.Trzciński, P.Zupranski
Institute of Nuclear Research, Warsaw, Poland

In continuation of our previous studies of (n, α) reactions on light nuclei we have measured at 12.2, 14.1 and 18.0 MeV neutron energies the angular distributions of the $^{14}N(n,\alpha)^{11}B$ reaction going to the ground and the first excited state of the ^{11}B nucleus. An attempt has been made to analyse the data using a simple three nucleon pick-up mechanism. In this process three nucleons from 1p shell of ^{14}N are transferred to 1s shell of ^{4}He. As it has been proved by Rotter 1), the transition strength is determined in this case by the spectroscopic amplitude for the transfer of a ^{3}He - like cluster with spatial symmetry [3] , spin 1/2 and isospin 1/2. The spectroscopic amplitudes for the separation of such a cluster from 1p shell nuclei have been calculated by Kurath and Millener 2). Decomposition of the ^{14}N into the ^{11}B g.s. and the cluster ^{3}He contains three states of relative motion: $2P_{1/2}$, $2P_{3/2}$ and $1P_{5/2}$ with the spectroscopic amplitudes equal + 0.017, + 0.463 and - 1.292, respectively. For the $^{14}N \rightarrow {}^{11}B_{1exc} + {}^{3}He$ only two states are possible: $2P_{1/2}$ (+ 0.901) and $2P_{3/2}$ (+ 0.086). According to the angular momentum selection rules and energy conservation and assuming that the directions of spins $\vec{j}_{\alpha_0}$ and $\vec{s}_n$ do not change in the reaction, one obtains the transfers listed in Table 1.

TABLE 1

$^{3}He + {}^{11}B_{g.s.}$ $N_1L_1J_1$	$^{3}He + n$ $N_2L_2J_2$	angular momentum transfer l s j	$^{3}He + {}^{11}B_{1exc}$ $N_1L_1J_1$	$^{3}He + n$ $N_2L_2J_2$	angular momentum transfer l s j
$2P_{1/2}$	$1S_{1/2}$	1,1/2,1/2	$2P_{1/2}$	$1S_{1/2}$	1,1/2,1/2
$2P_{3/2}$	$1S_{1/2}$	1,1/2,3/2	$2P_{3/2}$	$1S_{1/2}$	1,1/2,3/2
$1P_{5/2}$	$1S_{1/2}$	3,1/2,5/2			

From Table 1 one can see that different bound state contributions result in different orbital angular momentum transfer. As the transfer amplitudes $\beta^{lm}_{N_1L_1N_2L_2}$ for different l and j transfers contribute to the cross section incoherently 3) the general expression DWBA for the differential cross section can be in this case rewritten as 4):

$$\frac{d\sigma}{d\Omega} = (2s_n+1)\sum_{lm}(2l+1)W(L_1j_1L_2j_2;sl)\, S_{^{14}N\to{}^{11}B+{}^{3}He}\, S_{^{3}He\to{}^{3}He+n}\, \left|\beta^{lm}_{N_1L_1N_2L_2}(\theta)\right|^2$$

The transition amplitudes β^{lm} have been calculated with the finite range DWBA code LOLA supplied us kindly by DeVries 4). The optical-model potential used in our calculations had the form

$$U = -V(e^{x}+1)^{-1} + 4iW_D\frac{d}{dx'}(e^{x'}+1)^{-1} + V_c$$

$$X = \frac{r - r_{oR} A^{1/3}}{a_o} \qquad X' = \frac{r - r_{oI} A^{1/3}}{a_I}$$

V_c - the Coulomb potential of a uniformly charged sphere of radius $1.34\ A^{1/3}$.

The parameters of the optical-model potential for incident channel n + ^{14}N were obtained by fitting the elastic scattering data at 12.25 and 13.96 MeV neutron energies 7). Fits were performed using the optical-model search code SNOOPY 8). The parameters for E_n= 18.0 MeV were obtained by linear extrapolation. Distorting potential in the exit channel for 18.0 MeV calculation was obtained from the analysis of the α + ^{11}B elastic scattering data at E = 21.9 MeV 9). As there is no available data at lower energies we used the same set of parameters for 12.2 and 14.1 MeV calculations decreasing only surface absorption. Optical model potential parameters used in calculations are listed in Table 2.

TABLE 2

Entrance channel							Exit channel					
E_n	V	r_{oR}	a_o	W_D	r_{oI}	a_I	V	r_{oR}	a_o	W_D	r_{oI}	a_I
12.2	51.91	1.2	0.65	4.75	1.2	0.558	213.8	1.343	0.492	2.0	2.565	0.507
14.1	50.55	1.2	0.65	4.71	1.2	0.603	213.8	1.343	0.492	3.25	2.565	0.507
18.0	47.76	1.2	0.65	2.80	1.2	0.696	213.8	1.343	0.492	4.0	2.565	0.507

Units are MeV and fm

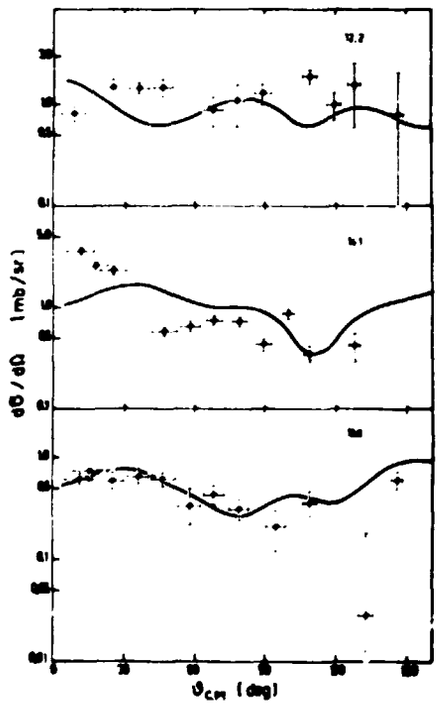

Fig.1 The angular distributions of alpha particles leading to the ground (α_0) state of ^{11}B at three neutron energies

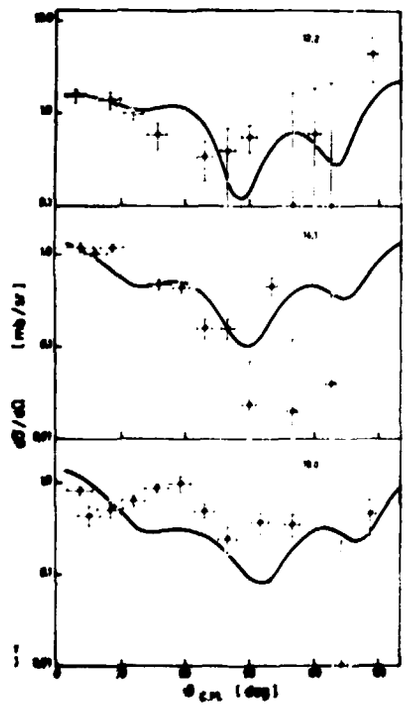

Fig.2 The angular distributions of alpha particles leading to the first excited (α_1) state of ^{11}B at three neutron energies.

The bound state wave functions were calculated in the Saxon-Woods well with the depth adjusted to reproduce the corresponding ^{3}He separation energies. The geometrical parameters for the ^{3}He + ^{11}B g.s. bound state were chosen to give the experimental root-mean-square radius of the ^{14}N nucleus 10). The same parameters were used for $^{11}B_{1exc}$ + ^{3}He. The ^{3}He + n parameters were taken from 6). All parameters used in the form factor calculations are listed in Table 3.

TABLE 3

state	E_{SE} MeV	r_o fm	a fm
^{3}He + n	20.58	0.9	0.5
^{3}He + ^{11}B	20.70	1.08	0.65

$$R = r_o\left(A_1^{1/3} + A_2^{1/3}\right)$$

In figs. 1 and 2 the comparison of the measured cross sections with the calculated ones is shown. The fairly good agreement obtained for the shapes and for the absolute values as well seem to indicate that finite range DWBA calculations for ^{3}He pick-up process are adequate to describe $^{14}N(n,\alpha)^{11}B$ reaction in the studied neutron energy range. The contributions of other mechanisms cannot however be excluded.

REFERENCES

1. I.Rotter, Nucl.Phys., A135 1969 378
2. D.Kurath, D.J.Millener, Nucl.Phys., A238 1975 269
3. N.Austern, R.M.Drisko, E.C.Halbert and G.R.Satchler, Phys.Rev.133 1964 B3
4. R.M.DeVries, Code LOLA, unpublished, The University of Rochester
5. R.M.DeVries, Thesis, unpublished, University of California, Los Angeles
6. R.M.DeVries, J.L.Perrenoud, J.Slaus, J.W.Saunier, Nucl.Phys.A178 1972 424
7. R.W.Bauer, J.D.Anderson, M.P.Lutz, C.Wong, J.W. McClure, B.A.Pohl, Nucl. Phys., A93 1967 673
8. P.Schwandt, Report 8/5/69, University of Wisconsin
9. J.Steyaert, Thesis, unpublished, Universite Catholique de Louvain
10. Atomic Data and Nuclear Data Tables, 14 No 3

ENERGY AND ANGULAR DISTRIBUTIONS OF ALPHA PARTICLES EMITTED IN THE $^{149}Sm(n,\alpha)^{146}Nd$ REACTION INDUCED BY FAST NEUTRONS

W.Augustyniak, L.Głowacka, M.Jaskóła, J.Turkiewicz, L.Zemło, Le Van Khoi[+]
Institute of Nuclear Research, Warsaw, Poland

The interest in the (n,α) reactions is mainly due to the possible role of the clustering phenomena in the emission of the alpha particles. The (n,α) reaction could be a tool for quantitative determination of the four-particle correlation in nuclei, of course if the reaction mechanism is known sufficiently well to describe correctly the whole process including the tested elements of the nuclear structure.

In the recent years a number of investigations of rare-earth nuclei have been performed [1,2]. In many cases it is extremely difficult to state a priori what should the reaction mechanism be. This is especially true for the study of the (n,α) reactions induced by fast neutrons on heavy nuclei. The cross sections for these reactions is quite low, also the level density in this atomic mass region is high and the energy resolution of our measurement does not allow a separation of the single levels except for the $^{147}Sm(n,\alpha)$ and $^{143}Nd(n,\alpha)$ reactions where we observed excitation of the isolated levels.

In this work the energy spectra and angular distributions of the α-particles emitted in the $^{149}Sm(n,\alpha)^{146}Nd$ reaction have been measured for neutron energies 12.3, 14.1 and 18.2 MeV. The relatively large level spacing in the ^{146}Nd nucleus make it possible to separate some of the levels.

The experimental arrangement was similar to that used in our earlier work [3]. Neutrons were produced in the $^{3}H(d,n)^{4}He$ reaction with deuterons accelerated in a Van de Graaff accelerator. The neutron flux was determined by counting the protons recoiled from a thin polyethylene foil in a CsI(Tl) scintillation counter.

The alpha particle spectra were measured at an average angle of 34° with a large angular spread of $\pm 20^{o}$. The target was made of Sm_2O_3 (samarium enriched to 97% with ^{149}Sm) which was deposited onto a thick carbon backing by sedimentation method. The target thickness was about 3 mg/cm^2.

The angular distributions of the alpha particles were measured at E_n=14.1 and 18.2 MeV. These distributions contain all α-particles with energies corresponding to the excitation of the final nucleus up to 5.0 MeV.

The results have been analysed in terms of statistical, pre-equilibrium and knock-on models.

The predictions based on the Hauser-Feshbach theory [4,5] are shown in fig.1. In the calculations the channels with n,p and α as a first particle were taken into account. The results of the calculations show that the experimental spectra are shifted considerably towards higher energies and the measured values of the cross sections are greater by a factor of about 100 as compared with the predictions of the Hauser-Feshbach theory.

[+] On leave from University of Hanoi, Vietnam

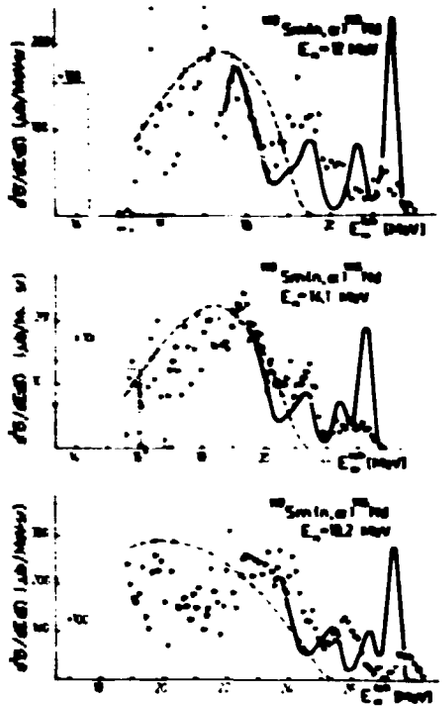

Fig.1 Comparison of the measured and calculated cross sections. The solid lines are the predictions based on the knock-on model with the parameter b = 0.1. The dashed and dotted lines are the predictions based on the pre-equilibrium and Hauser-Feshbach models, respectively. The experimental resolutions (FWHM) are 360 keV for E_n = 12.3 and 18.2 MeV and 440 keV for E_n = 14.1 MeV.

In the pre-equilibrium calculations the formula given by Colli and Marcazzan [6] was used. This model implies some probability for four nucleons to be correlated in a α -particle-like structure in the target nucleus. The calculations show that the pre-equilibrium model reproduces the shape of the experimental spectra quite well except for the high energy part. This model does not reproduce the structure which we observed in our spectra.

The existence of high-energy α-particles in the experimental spectra and the fact that the angular distributions of the emitted alpha particles are strongly forward peaked suggest a significant contribution from a direct mechanism. Following Shapiro [7] we assume the amplitude of the direct reaction to be described by a set of nonrelativistic Feynman diagrams. Analysis of the location of the singularities of the amplitude of the (n,α) reaction led to the conclusion that for rare-earth nuclei the knock-on mechanism dominates. In accordance with ref.[2] the differential cross section for the (n,α) reaction can be written as:

$$\frac{d^2\sigma}{d\Omega dE_\alpha} = \sum_i \int_{-\infty}^{\infty} \frac{d\sigma_i}{d\Omega} \frac{1}{2\pi} \frac{\Gamma_i}{(E_i - E_x)^2 + \frac{1}{4}\Gamma_i^2} N(E_x, E_\alpha) dE_x$$

where: $d\sigma_i/d\Omega$ describes the differential cross section for the population of states in the final nucleus: $N(E_x, E_\alpha)$ describes the energy resolution of the experiment, the fragmentation width $\Gamma_i = bU_i$ was assumed according to [8] dependent linearly of excitation energy U_i.

The level structure of the doubly-even final nucleus calculated by Vdovin and Stoyanov [9] were used. As calculations dit not give the absolute values of the cross sections, normalization to the experiment was performed up to the 4 MeV excitation energy of the final nucleus. In this excitation energy region the

knock-on model gives a fairly good description of the measured energy spectra. In fig.2 the calculated and measured angular distributions of α-particles are compared. The measured angular distributions of α-particles show distinct forward peaking and this feature is well reproduced by the knock-on calculations. The fact that theoretical forward-backward asymmetry is smaller that that experimentally observed is probably due to the approximation made in the calculations, where the isotropy of neutron-alpha scattering was assumed.

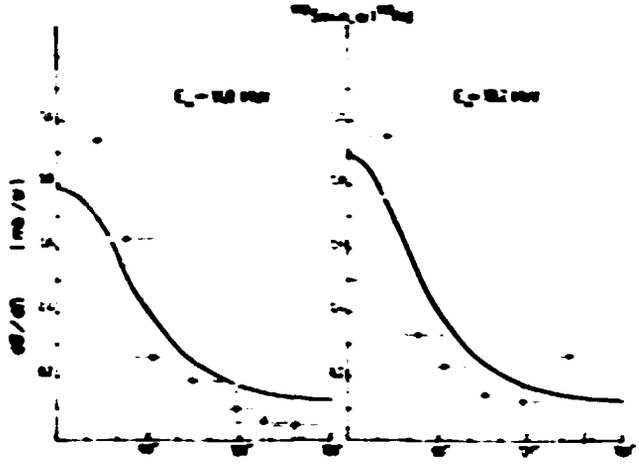

Fig.2 Comparison of the measured angular distributions of α-particles with the calculated ones based on the knock-model.

References

1. H.Kitazawa, Nucl.Phys. A149 (1970) 513
2. L.Głowacka, H.Jaskóła, J.Turkiewicz, L.Zemło, K.Kozłowski, W.Oenkiewicz, Nucl.Phys. A262 (1976) 205
3. H.Jaskóła, J.Turkiewicz, L.Zemło, W.Oenkiewicz, Acta Phys.Pol., B2 (1971) 521
4. W.Heneer, H.Feshbach, Phys.Rev., 87 (1952) 366
5. W.R.Smith, Computer Phys.Commun. 1 (1969) 106; 1 (1969) 181
6. L.Colli-Milazzo, C.M.Marcazzan-Braga, Phys.Lett., 38B (1972) 155
7. I.S.Shapiro, Theory of direct nuclear reactions (Gosatomizdat, Moscow, 1963)
8. B.B.Back, J.H.Bung, S.Bjørnholm, J.Hattula, P.Kleinheinz, J.R.Lien, Nucl.Phys. A222 (1974) 337
9. P.I.Vdovin, Ch.Stoyanov, Izv.Ak.Nauk SSSR Ser.phys. 39 (1975) 1618

CONFIGURATION MIXING EFFECT IN THE α-TRANSFER REACTIONS

B. Apagyi
Technical University, Budapest, Hungary
T. Vertse
ATOMKI, Debrecen, Hungary

In the past ten years much attention has been devoted to the α-transfer experiments. This interest can be explained by the fact that the α-particle transfer reactions represent important tool for studying α-clusterization in nuclei, thereby, they furnish us with new type of informations on the wave functions of the nuclear states involved in the α-transferring processes. This information cannot be obtained from any other experiment (with the exception of detecting α-decay from the states lying above the α-threshold energy). All the works aimed at getting information about the /^{6}Li,d/ reactions (e.g. [1,2]) made use of phenomenological method for calculating the reaction form factor (FF). It means that they neglected the contributions arising from the configuration mixing effect being present in the nuclear states. One of the first attempts to include the configuration mixing effect into the description of the α-transfer reaction was the calculation of Apagyi and Vertse [3] who showed on the ^{12}C/^{6}Li,d/^{16}O$_{gs}$ example that the neglect of the contributions arising from the microscopic structure of the ^{16}O$_{gs}$ wave function may lead to incorrect conclusions.

To estimate the importance of the configuration mixing effect in the α-transfer reactions, five of these have been investigated systematically by making use of phenomenological FF /PFF/ as well as microscopical FF /MFF/ in the theoretical description. The five reactions investigated are the ^{12}C/^{6}Li,d$_{i=0-4}$/^{16}O* reactions [2,4] at bombarding energies 18, 20 MeV. In these reactions the first five states of ^{16}O* are populated, namely, the 0^+_1/0/, 0^+_2/6.05/, 3^-/6.13/, 2^+/6.92/, 1^-/7.12/ states which lie below the α-threshold energy of 7.16 MeV. Apart from the MFF calculation, the standard method has been applied for the description, i.e., one-step α-cluster transfer mechanism has been assumed, and the ZR DWBA computer code DWUCK [5] has been adopted for the differential cross section calculation. The optical potentials in the entrance and exit channels have been taken from elastic scattering analyses [6,7] as described in ref.[3].

To calculate the PFF, the usual way is to write it in a form

$$F_L(r) = S_\alpha^{1/2} \; /^{16}O/ \; \varphi_{NL}^{/WS/}(r) \qquad (1)$$

consisting of the absolute value of the square root of the α-spectroscopic factor and a normalized eigenfunction of a real Woods-Saxon /WS/ potential. Usually, the parameters of the WS potential are chosen as follows: the depth parameter V_0 is determined by the separation energy /SE/ condition method, the diffuseness a is equal to 0.65 fm, and the radius is calculated generally from two types of forms; in certain cases from that which does not include the α-particle mass number /$R^{WSI} = r_0 A_{target}^{1/3}$ /, in other cases from that which does it include /$R^{WSII} = r_0(A_{target}^{1/3} + 4^{1/3})$ /. According to these two choices, two

theoretical curves have been obtained for the angular distributions of the reactions investigated. These phenomenological results denoted by WSI and WSII are presented in the upper part of fig. 1, where also the experimental findings [2,4] are shown (dots). We see that neither the WSI PFF-s (broken lines), nor the WSII PFF-s (dotted-broken lines) are able to describe the experimental angular distributions in the c.m. scattering angle region between 0° and 90°. It is suspected therefore that beside possible other effects (mechanism, ZR and so on), the simple PFF calculation may be responsible for the lack of agreement. For that reason, all the calculation have been repeated by making use MFF-s.

To calculate the MFF, one has to start from the overlap integral

$$F_L(r) = \langle \Psi_{^{12}C}\, \Psi_{\alpha}\, Y_{LM} | \Psi_{^{16}O} \rangle = \sum_N A_{NL}^{/ZBM/}\, \varphi_{NL}^{/HO/}(r) \qquad (2)$$

which can be expanded in terms of any orthonormal set of functions. The appearance of more than one term with different N-s in the MFF is a direct consequence of the configuration mixing effect in the ^{16}O wave function. The expansion coefficients A_{NL} (the α-spectroscopic amplitudes) have been calculated by Apagyi and Fái [8] using harmonic oscillator /HO/ basis set and Zuker wave functions /ZBM/ as $\Psi_{^{16}O}$. Applying these amplitudes, one can determine the MFF-s which include the configuration mixing effect. As a result of this effect, the internal part of the MFF is diminished, the outer part is enhanced when comparing them with the PFF case. The MFF calculated in such a way is denoted by HO indicating the HO basis set. It is well known, however, that the asymptotical behaviour of the HO functions is not appropriate for the reaction calculation. Therefore, a WS tail with proper asymptote has been matched to the outer part of the MFF beyond its last maximum/minimum to ensure the physical external behaviour of the MFF. In such a way, one obtains the MFF denoted by SE remembering of the separation energy condition imposed on the tail. According to these two choices in the MFF-s, two theoretical angular distributions have been obtained in each case of the five reactions investigated.

These microscopic results denoted by HO and SE are presented on the bottom of fig. 1. It can be seen from the figure that, compared to the PFF case, a significant improvement could be achieved in all the cases considered. These improvements are entirely due to the microscopical or configurational mixing aspect of the FF calculation. (All the theoretical curves of fig. 1 are multiplied by a factor n (less than ten) to get the magnitude agreement with the experimental points at $\Theta_{cm} = 20^{\circ}$. In the normalization procedure D_0^2 $S/^6Li/ = 3.7\ 10^3$ MeV^2fm^3 [9], $S/^{16}O^{\alpha}/$ are taken from [8].)

In summary, it has been demonstrated in a systematic way that the configurational mixing property of the nuclei has an important effect in the α-transfer reactions. Its inclusion into the theoretical calculations is, therefore, desirable.

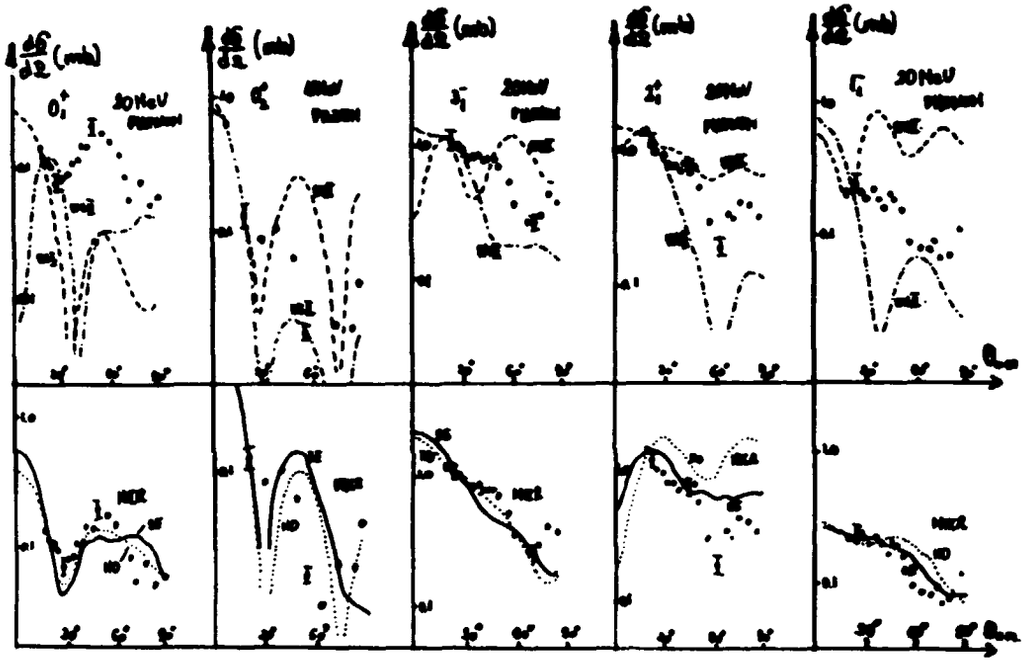

Fig. 1

References

[1] U. Strohbusch et al., Phys. Rev. C9 (1974) 965;
H.W. Fulbright et al., Nucl. Phys. A284 (1977) 329;
K.I. Kubo and N. Hirata, Nucl. Phys. A187 (1972) 186

[2] K. Bethge et al., Phys. Rev. C2 (1970) 395

[3] B. Apagyi and T. Vertse, Proceeding of the Int. Symp. on Nuclear Reaction held in Balatonfüred (Hungary) 1977 Ed. L.P. Csernai, p. 219

[4] K. Meier-Ewert et al., Nucl. Phys. A110 (1968) 142

[5] P.D. Kunz, University of Colorado, COO - 535 - 606

[6] K. Bethge et al., Z. Phys. 208 (1968) 486

[7] E. Newman et al., Nucl. Phys. A100 (1967) 225

[8] B. Apagyi and G. Fái, J. Phys. G3 (1977) L 163

[9] M.P. Bornand et al., Nucl. Phys. A294 (1978) 492

ПОДХОДЫ И МОДЕЛИ ДЛЯ ОПИСАНИЯ УГЛОВОЙ ЗАВИСИМОСТИ ПРЕДРАВНОВЕСНОГО ИСПУСКАНИЯ ЧАСТИЦ СПЛОШНОГО СПЕКТРА

Д. Зелигер и С. Сасонов
Technische Universität Dresden, Sektion Physik, DDR - 8027 Dresden

1. Введение

Описание механизма ядерных реакций при средних энергиях в рамках представлений об образовании долгоживущего состояния статистического равновесия , т.е. так называемого компаунд-ядра приводит, как известно, к определенным расхождениям с экспериментом. Это, в частности, касается относительно высокого вклада высокоэнергетических частиц в экспериментальных спектрах испускания а также их угловой ассимметрии. Учёт так называемых предравновесных процессов в дополнении с в.н. механизмов дает значительное улучшение согласия с экспериментом.

Для теоретического описания таких процессов в прошлые годы были разработаны разные формализмы на основе экситонной модели [1-4]. Они позволили успешно описать сечения реакций, функции возбуждения а также спектры испускания частиц, интегрированные по углам.

Однако, эти подходы не позволили описать также и угловые распределения испущенных частиц в процессах, в которых остаточное ядро является высоко возбужденным. Лишь в последнее время появился ряд работ, исходящих из экситонной модели, которые ставили задачу включения угловых распределений в данный формализм.

Параллельно появились работы на основе хорошо разработанных теорий прямых ядерных реакций, в которых также предпринималась попытка описания угловых распределений в сплошной части спектра испущенных частиц.

Наконец, использовались независимо от выше названных подходов, возможности классической термодинамики и неравновесной статистики для получения результатов в желанном направлении.

Многообразие подходов с одной стороны и очевидный интерес многих авторов в данной проблематике, по-видимому, связаны не только с практическим значением её в связи с расчётом ядерных данных, но и с фундаментальной задачей выяснения механизма ядерных реакций.

В данном докладе принимается попытка, сравнить и критически оценить разные подходы.

2. Подходы на основе экситонной модели

Существенным недостатком исходной экситонной модели [1-4] состоит в том, что в ней учитывается только закон сохранения энергии но не учитывается сохранение угловых моментов, откуда вытекает непригодность этой модели к описанию угловых распределений. Разные усовершенствования этой модели сохраняют статистический одночастичный

характер описания, а путем введения дополнительных предположений предпринимается попытка расширить область применений этой модели [5,6,7].

Таким образом, Мантцуранис и др. [5,6] исходят из дополнительного предположения о том, что угловое распределение предравновесной эмиссии определяется только направлением движения "лидирующей частицы", т.е. падающей частицы. Авторы [5,6] рассматривают процесс двухчастичного остаточного взаимодействия между частицей и ядром, классифицируя состояния промежуточной системы не только /как в исходной экситонной модели/ числом экситонов и энергии возбуждения но и направлением движения "лидирующей частицы". Основываясь на этом, авторы расчитывают предравновесные вероятности заселения n-экситонных состояний либо на базе т.н. обобщенных мастер - уравнений [5] либо в рамках аналитической формулы, сходной с гибридной модели [6]. Из вероятностей заселения получаются энергетические спектры а также угловые распределения предравновесной эмиссии, причем в ряде случаев получено хорошее согласие с экспериментом.

В другой работе [7] экситонные состояния классифицируются числом экситонов, энергией возбуждения и спином. При этом предполагается, что состояния с равным числом экситонов и спином, но с разными орбитальными моментами и полными спинами между собой интерферируют только лишь в простейшей экситонной конфигурации с $n=n_0$. Кроме того пренебрегаются корреляции между состояниями с разным экситонным числом и полным спином. Т.е. предполагается, что n-экситонные состояния, за исключением состояний с $n=n_0$, являются относительно долгоживущими квазистационарными квантовыми состояниями. Расчитанная таким путем анизотропия угловых распределений, как и ожидается, зависит от начального числа экситонов n_0 а также от энергии испускания.

3. Расчёт на основе теорий прямых ядерных реакций

В ряде работ для описания начальной стадии предравновесных реакций с возбуждением континуума состояний остаточного ядра применяются соответствующие образом усреднения по энергии расчёты в рамках теорий прямых ядерных реакций. Так, в работе [8] предполагается, что дважды дифференциальное сечение испускания нейтронов состоит из испарительной и прямой части. В [9] в подобии к этому, но более последовательно, предполагается, что это сечение складывается из равновесной, предравновесной /кроме самой простой реакции/ и прямой реакции. Разделение предравновесной компоненты делается для того, чтобы использовать простую экситонную модель для описания процессов испускания из более сложных состояний /$n \geq 5$/. Ассимметричную часть углового распределения приписывается только тем продуктам реакции, которые покидают составную систему после первого акта взаимодействия /соответствующего $n=3$/. Для расчёта их вклада используют феноменологические выражения, основанные на хорошо известном приближении с плоскими волнами PWBA, учитывая немногие характерные для данного ядра одночастичные переходы в модели оболочек. Расчитанные таким образом угловые распределения показывают хорошее согласие с экспериментом.

Своего рода "гибрид" между экситонной моделью и PWBA-теории представлена в работе [10]. В рамках экситонной модели вводятся скорости испускания зависящие от углового момента и таким образом получаются предравновесные спектры испускания для каждого орбитального момента эмитированной частицы. Угловая зависимость дается

сечением PWBA для соответствующей величину переданного орбитального момента. С таким формализмом авторы [10] также достигают хорошего описания углового распределения для ряда ядерных реакций.

Микроскопическое описание в приближении DWBA для дважды дифференциальных сечений испускания частиц в континууме состояний было предложено в работе [11]. В рамках этого подхода из полных волновых функций рассматриваются 1p1h-компоненты, так как только они могут возбудиться путем одного частично-дырочного остаточного взаимодействия. Матричные элементы усредняются по энергетическому интервалу, соответствующему эксперименту, получая таким образом усредненные сечения по многим состояниям остаточного ядра. Результаты согласуются с экспериментом. Описанный формализм однако, неприменим для энергий возбуждения остаточного ядра выше нескольких Мэв вследствие пренебрежения многократных соударений а также испускания из квази-связанных состояний, что приведет к недооценке абсолютного вклада таких процессов и превышению их угловой анизотропии.

Дальнейший шаг в этом направлении представляет работа Тамуры и др. [12]. Также в приближении DWBA, но на основе одно- и двухступенчатых прямых возбуждений вычисляются спектры и угловые распределения предравновесной эмиссии. Возбуждаются 1p1h- и 2p2h-состояния остаточного ядра, что позволяет охватить экспериментально найденное поведение также и при более высоких энергиях возбуждения остаточного ядра /по сравнению с теорией с одноступенчатыми возбуждениями/.

Общим недостатком всех предложенных методов в рамках теорий прямых ядерных реакций /помимо математических трудностей, связанные с микроскопическим описанием/ является необходимость их стыковки с расчётом по другой, коренным образом отличающейся теории /в первую очередь это статистическая модель/. Только в этом случае удается удовлетворительное описание всего спектра и угловых распределений при всех энергиях.

4. Применение геометрических представлений о траектории частиц

В т.н. каскадно-экситонной модели [13] объединяются полу-классические представления из каскадной и экситонной моделей с полной статистической теории ядерных реакций. С помощью формализма каскадной модели описываются соударения налетающей частицы с нуклонами ядра, приводящие к образованию возбужденных частиц и дырок в начальной фазе ядерного процесса. Этот формализм дает также анизотропное угловое распределение испущенных частиц. Дальнейшее "развитие" составной системы описывается с помощью экситонной модели, начиная с тем числом n_0 частиц плюс дырок, которое образовалось во время "каскадной", быстрой фазы процесса. После достижения статистического равновесия, дальнейшая "судьба" ядерной системы описывается в рамках полной статистической теории. И в расчётах с экситонной моделью и со статистической теорией угловая зависимость принимается изотропной. Расчитанные сечения находятся в хорошем согласии с экспериментом.

5. Применение классической термодинамики

Вейнер и Вестрэм [14] разработали метод описания предравновесного развития составной системы на основе классических термодинамических представлений. Идро в на-

чальной фазе ядерной реакции принимается локально нагретым. Путем процесса диффузии ядерное возбуждение во время конечного временного интервала распространяется по всему ядру пока не достигается термодинамического равновесия. Локальная ядерная температура зависящая от времени определяет спектр и угловое распределение испущенных из "нагретого" ядра частиц, она определяется путем решения уравнения диффузии со соответствующими краевыми и начальными условиями. Время реакции определяется постоянной транспорта энергии в ядерной материи. Нужно отметить, что данной формализм, так-же как и каскадно-экситонная модель, применим лишь при достаточно высоких энергиях, при которых полу-классическое рассмотрение оправдано. Сравнение с экспериментом данного метода пока ещё предстоит.

6. Заключение

Разнообразие возникших за последние годы подходов и моделей для описания угловых распределений предравновесных спектров указывает на актуальность этого вопроса и значительный интерес к нему со стороны многих групп. Это связано с одной стороны с желанием, более полно понять и описать механизм ядерных реакций при средних энергиях а с другой стороны с необходимостью расчета ядерных данных для прикладных целей.

Окончательная оценка и сравнение разных подходов пока трудно вследствие разной степени разработки этих методов и выбора авторами различных случаев их применения. По чисто физическим соображениям, кажется, пока нельзя выбрать тот или иной "единственно правильный" подход к решению рассмотренной проблематики. Наоборот, ситуация скорее указывает на то, что экспериментально хорошо известный факт наличия предравновесной эммиссии преимущественно в переднюю полусферу можно в той или иной мере хорошо описывать совершенно разными модельными представлениями. Поэтому, хотя бы из эвристических соображений целесообразно дальше развивать и усовершенствовать разные направления описания. Для широких практических применений конечно, критерий простоты приобретает особое значение. В будущее для большей наглядности сравнений требуется проведение анализов одних и тех-же экспериментов в рамках разных подходов.

Литература

[1] J.J.Griffin, Phys. Lett. 17(1966)478
[2] C.K.Cline, M.Blann, Nuc . Phys. A 172(1971)225
[3] M.Blann, A.Mignerey, Nucl. Phys., A 186(1972)245
[4] К.Зайдель, Д.Зелигер, Р.Райф, В.Д.Тонеев, ЭЧАЯ 7/1976/13
[5] G.Mantzouranis et al., Phys. Lett. 57 B (1975)220; Z. Phys. A 276(1976)145
[6] G.Mantzouranis Phys. Lett. 63 B (1976)25
[7] В.А.Плюйко, ЯФ 27/1978/1175
[8] А.А.Лукьянов и др., ЯФ 21/1975/67
[9] H.Jahn, in Nuclear Theory in Nuclear Data Evaluation, Vol. 2 p.515, 1975
[10] Y.Irie et al., Phys. Lett. 62 B (1976)9
[11] R.Reif, Kernenergie 20(1977)177
[12] T.Tamura et al., Phys. Lett. 66 B (1977)109
[13] K.K.Odima, V.D.Toneev, Preprint JINR E4-9489(1976)
[14] R.Weiner, K.Westrom, Nucl. Phys. A 286(1977)282

ANALYSIS OF 3.4 MEV NEUTRON SCATTERING FROM 2s-1d-SHELL NUCLEI IN THE FRAMEWORK OF STATISTICAL AND DIRECT REACTION MODELS

T. Schweitzer, D. Seeliger and S. Unholzer
Technische Universität Dresden, Sektion Physik, DDR - 8027 Dresden

The interpretation of our differential cross section experimental data in neutron scattering from Na-23, Mg-24, Al-27, Si-28 is improved by inclusion of coupled channel effects in the calculation of the direct reaction parts. We have succesfully explained differences in the shape and amplitude of experimental angular distributions from statistical calculations for scattering of 3.4 MeV neutrons from Na-23, Mg-24, Al-27, Si-28, Mn-55, Fe-56 by way of direct reaction contributions [1]. Direct parts were then calculated by use of Distorted Wave Born Approximation.

The physical reaction model of our investigation is all the same an incoherent superposition of statistical and direct reaction parts. There is not any general model to calculate such problems for nuclei more complicated as 1p-shell nuclei. Because of that, we can use only limited models as statistical and direct theories. Applications within the bounds of these models are standard techniques and yield a description of experimental data, which is succesfull , but our problem lies near or behind the limits of validity for such models.

We have mainly two reasons for physical reliability in our investigations:
- consistence in the experimental data
- the absolute basis of theoretical calculations.

The basis of our calculations is absolutely because of resignation of any fitting together theoretical curves and experimental data. All free parameters of the theoretical models are fixed by use of a generalized optical model parameter set [2] about the full range of nuclear masses and for all theoretical calculations and by use of β-deformation parameters from reliable literature values.

Hauser-Feshbach-calculations corrected for level width fluctuations (HFC) were carried out with the computer code ELIESA [3]. The codes CHUCK [4] and JUPITOR 1 [5] were used for coupled channels calculations (CC). Two examples of our analysis are given in figs. 1 and 2. The correspondence between experiment and theory is very well for an absolute model. We can explain the gross structure and amplitude of the experimental angular distributions in the frame of our reaction model. Fine structure is probably caused by violation of the statistical assumptions in the compound nucleus.

Summary
- We have carried out a systematical study of the nuclear reaction mechanism by neutron scattering experiments at 3.4 MeV neutron incident energy about a wide range of nuclear masses.
- It gives experimental evidence for direct reaction contributions in the excitation of all low-lying collective 2^+-states (and such states which are

coupled to that 2^+)

- We can succesfully describe our experimental results in the framework of a simple reaction model of incoherent superposition of statistical and direct reaction parts.
- The base of our calculations is absolutely because of no fitting experimental and theoretical results together.
- Coupled channels effect must be considered for the excitation of rotational states. Such inclusion leads to further improvements in the conformity of our experimental and theoretical curves.
- The used optical model parameter set enables a good overall representation over a wide range of nuclear masses.

References

[1] T. Schweitzer, D. Seeliger and S. Unholzer, Proc. of the VII. Int. Symp. on Interactions of Fast Neutrons with Nuclei, Gaussig 1977, to be published

[2] B. Holmquist, T. Wiedling, Journal Nucl. Energy 27 (1973) 543

[3] G. Kießig, Thesis, Technical University Dresden, Phys. Department (1974)

[4] P. Kunz, unpublished

[5] T. Tamura, report ORNL-4152 (1967)

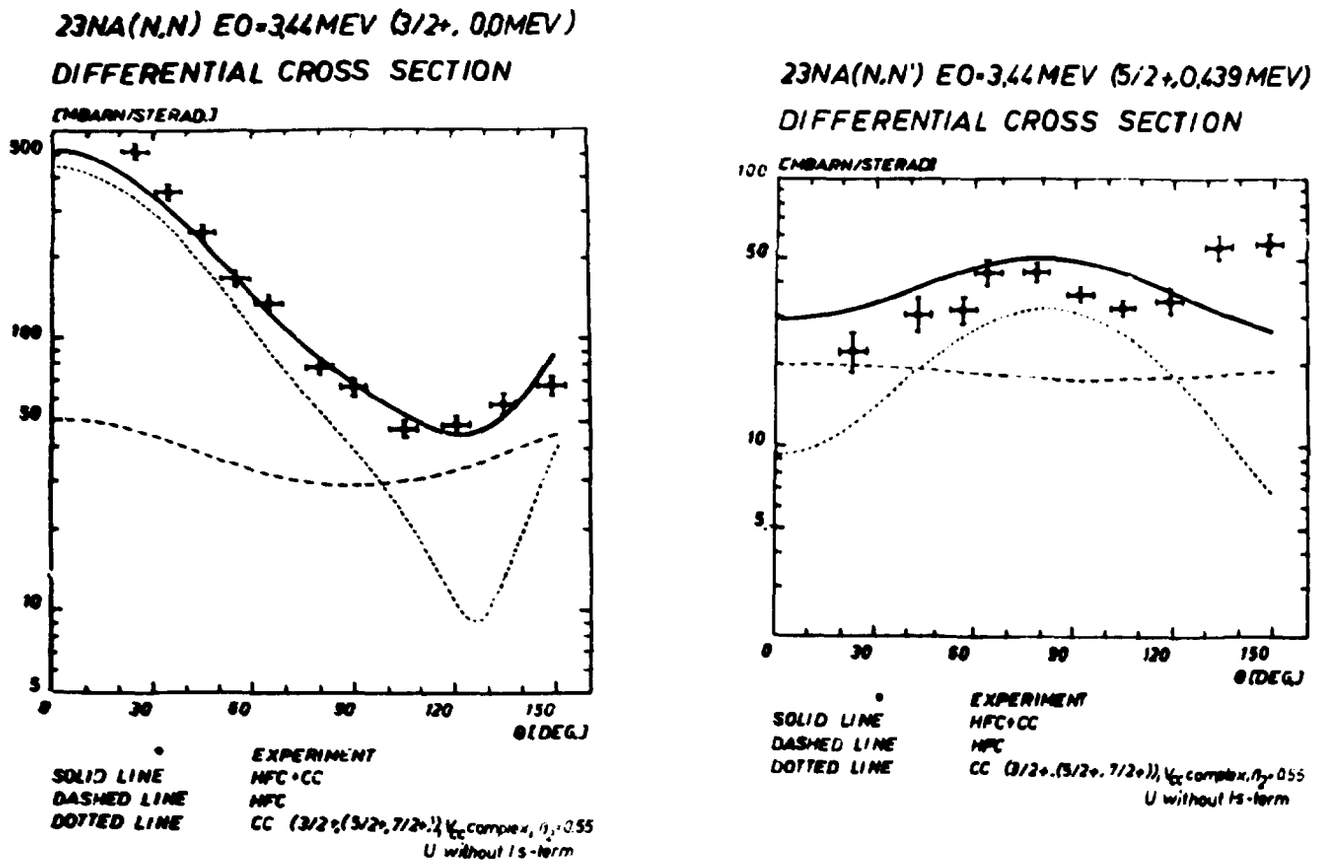

Fig. 1

Analysis of 3.4 MeV neutron scattering data from Na-23 by incoherent superposition of statistical (HFC) and direct reaction parts (CC). Level properties and coupling modes are indicated. CMS-angular distribution

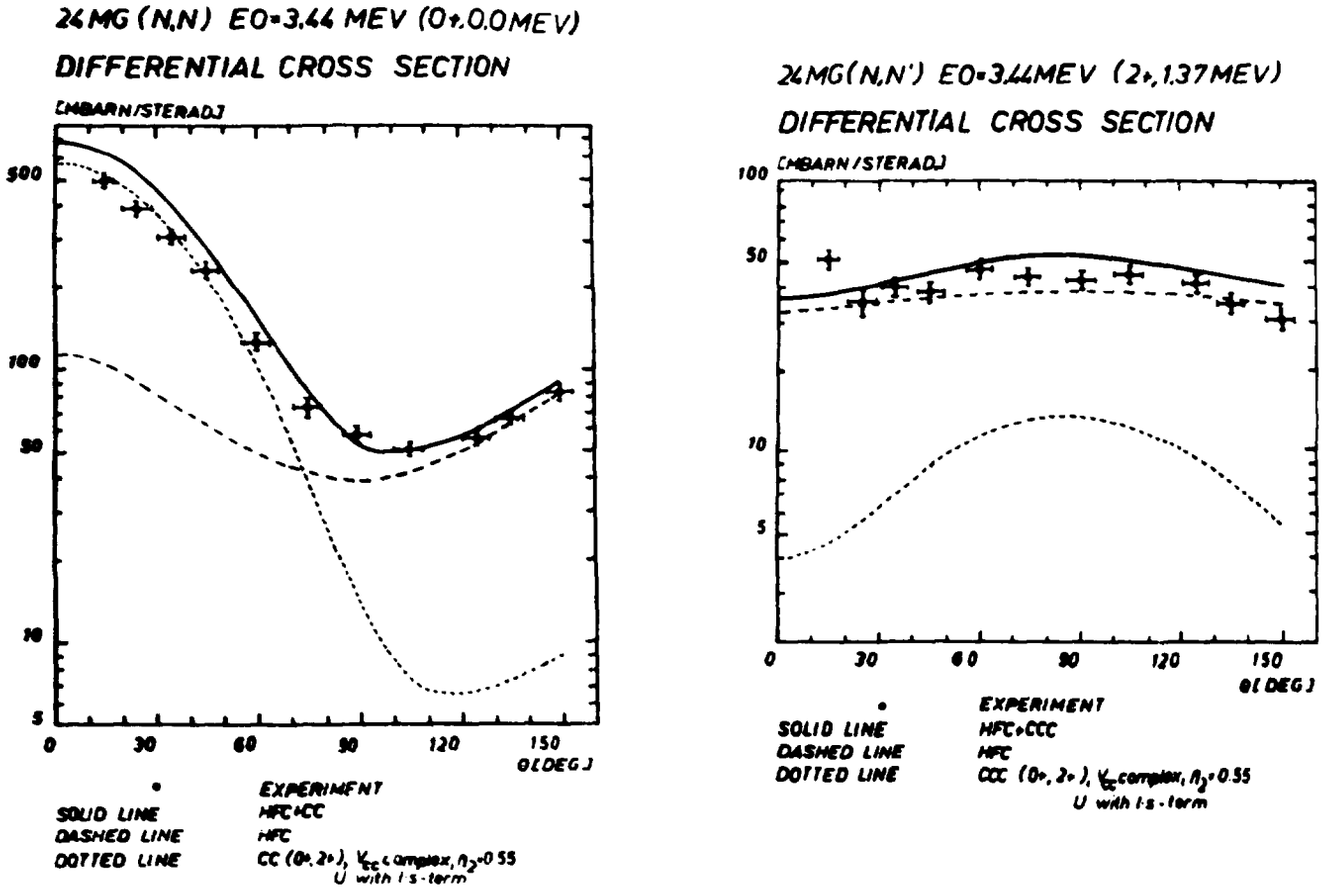

Fig. 2
Analysis of 3.4 MeV neutron scattering data from Mg-24 by incoherent superposition of statistical (HFC) and direct reaction parts (CC).

FIRST RESULTS FROM INVESTIGATION OF THE $^{28}Si(n,n')$ REACTION IN THE ENERGY RANGE BETWEEN 6.8 AND 12 MEV

Adel-Fawzy, H. Förtsch, W. Pilz, D. Schmidt, D. Seeliger and T. Streil
Technische Universität Dresden, Sektion Physik, DDR - 8027 Dresden

Experimental results and first theoretical analysis are represented for elastic and inelastic scattering of neutrons in a larger energy range on ^{28}Si.

1. Introduction

In earlier time the investigation of the reaction mechanism on light nuclei was done for small energy range only, in the most cases near 3 MeV and 14 MeV, respectively. These experiments differ regarding the measuring technique and also the models and parameters of the theoretical analysis used.
The work given here has been begun with the aim to measure and describe the $^{28}Si(n,n')$ reaction in a wide energy range uniformly. The model is a incoherent superposition of compound and direct reaction part. Furthermore, such measurements are important for nuclear data requirement.

2. Experimental procedure

The measurements were performed with tandem facilities in the ZfK Rossendorf, using a computer-coupled multi-angle TOF-detector system with 8 detectors.
For the neutron production it was used a deuterium gas target.
As monitor another TOF-detector was inserted in the whole system.
For determination of absolute cross sections the neutron flux with monitor detector was checked, that means the product flux times monitor efficiency is determined. Additionally by measurement the efficiency ratio of the monitor and measuring detector the monitor efficiency is eliminated.
The flight path is in order of 3 meters, the time resolution is about 3 ns.
The sample consists of natural silicon with a diameter of 3 cm and a height of 3 cm. The incident neutron energy spread depends slightly on the bombarding energy and was near 120 keV.
Suitable computer programs for peak area determination and multiple scattering correction were commonly used.

3. Analysis of the experimental data

The elastic scattering is described as a sum of shape and compound part (see also fig.1). The calculation of the shape elastic scattering is deduced from the spherical optical model with parameters from OBST et al. 1) slightly varied in the spin-orbit term.

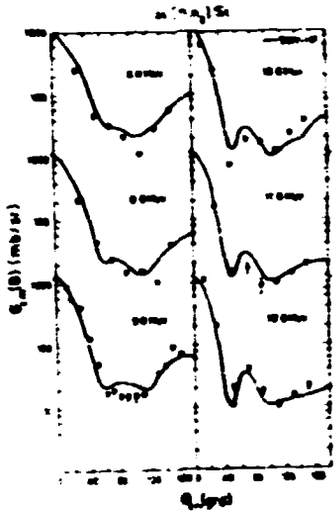

fig.1
Angular distributions of the elastic scattering on ^{28}Si

The compound elastic scattering was calculated with the HAUSER-FESHBACH program "ELIESE" 2) with the same parameters including alpha-particle and proton channel, respectively. The agreement as well as seen shows the parameters to be usefull for the calculation of the direct reaction part.

For analysing the inelastic scattering cross section data were compared up to now with HAUSER-FESHBACH calculations (HFC) and additionally for 10 MeV only adding a direct reaction part using the coupled channel method (CCC). This CCC has been based on the collective model with rotational excitation including coupling between the first four excited states of ^{28}Si, but excluded the 3^+ anomalous parity state.
Fig.2 shows the angular distributions for the first excited state (2^+). As expected the difference between experimental points and the calculated compound contributions increases with energy. As it can be seen, for 10 MeV the shape and absolute value of the distribution can be described quite well by including of the direct reaction part.

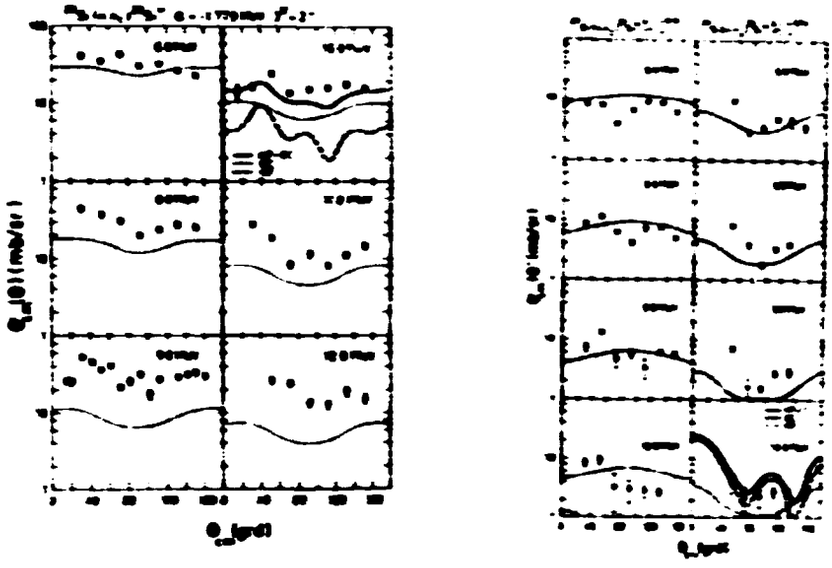

fig.2 and 3
Inelastic scattering on ^{28}Si : angular distributions of the n_1-, n_2- and n_3-group for several energies

Fig.3 gives firstly the angular distributions of the second excited state (4^+) in comparison with the HFC results. The order of magnitude of the experimental points is reproduced in general by this compound reaction part only, unexpected up to the highest energies.
On the other hand the structure cannot be described as well as nessecary. The CCC preliminarely done gives a very small contribution to the cross section.
This theoretical analysis will be continued.

4. Literature

1) H. Obst, private communication
2) G. Kießig, thesis, Technische Universität Dresden (1975)

ИССЛЕДОВАНИЕ ГАММА СПЕКТРОВ И СЕЧЕНИЙ ОБРАЗОВАНИЯ ГАММА-КВАНТОВ ИЗ РЕАКЦИЙ $^{56}Fe+n$ И $^{93}Nb+n$ В РАМКАХ СТАТИСТИЧЕСКОЙ ТЕОРИИ ХАУЗЕРА-ФЕШБАХА

Б. Базаррагчаа[+)], Д. Хермсдорф
Technische Universität Dresden, Sektion Physik, DDR - 8027 Dresden

I. Введение

При решении многих практических задач, в частности при конструкции ядерных реакторов и расчете защиты от излучений, требуются точные сведения о полном сечении производства γ-квантов из конструктивных материалов и продуктов реакций, а также о γ-спектрах. Эффективное сечение образования сплошной части γ-излучения из реакций с нейтронами высокой энергии на тяжёлых ядрах, как показывают результаты некоторых экспериментов, является преобладающим по сравнению с сечениями образования дискретных γ-линий. Однако, в связи с экспериментальной трудностью определения таких спектров, обусловленной наличием фона рассеянных на образце нейтронов и сложностью обработки результатов эксперимента, теоретическое исследование сечения производства и спектров γ-излучений различных ядер в реакциях с нейтронами с помощью той или иной модели приобретает большое актуальное значение.

При взаимодействии нейтронов высоких энергий/до 20 Мэв/ со средними и тяжёлыми ядрами, средняя энергия возбуждения остаточного ядра лежит в области большой плотности уровней и снятие возбуждения происходит, главным образом, каскадным излучением гамма-квантов, носящим статистический характер. Поэтому для описания данного процесса будет более разумным привлечение статистической теории ядерных реакций.

В данной работе вычислены сечения возбуждения некоторых дискретных γ-линий, сечения производства и спектры непрерывного γ-излучения из реакций $^{56}Fe+n$ и $^{93}Nb+n$ на основе теории Хаузера-Фешбаха/I/ с коррекцией на флуктуацию ширин /2/ и детального рассмотрения γ-каскадов, идущих из высоковозбужденных состояний. На начальном этапе испарительного каскада учитывалась предравновесная эмиссия нейтронов по экситонной модели/3-8/.

При этом были исследованы влияние учета предравновесного распада, вклад излучений высокой мультипольности и других возможных каналов реакции на эти величины. Расчет проводился с помощью программы "STAPRE"/9/ на ЭВМ БЭСМ-6 вычислительного центра Дрезденского Технического Университета.

2. Входные данные для расчета

Проведение вычислений эффективных сечений производства и спектров γ-квантов по программе "STAPRE" требует знания коэффициентов проникновения ядер Fe, Mn Cr или Nb, Zr, Y для нейтронов, протонов, альфа-частиц, соответственно, и коэффициента проникновения γ-кванта, а также информации об энергетических уровнях и схемах распада ядер, участвующих в реакциях.

2.I. Коэффициенты проникновения для частиц и γ-лучей

Коэффициенты проникновения ядер для нейтронов, протонов и α-частиц получены с помощью программы "DMO" путём решения уравнения Шредингера с оптическим потенциалом. Параметры потенциала выбирались из сопоставления вычисленных и -

[+)] Гос. университет Улаанбаатор, Монголия

экспериментальных дифференциальных сечений.

Для вычисления коэффициентов проникновения γ-лучей были использованы одночастичная модель Вайскопфа/10/ и гипотеза Бринка-Акселя/11/. В работе Бартоломева и др./12/ силовая функция $f^{In}_{\gamma XL}(\varepsilon_\gamma)$ γ-излучения определена как

$$f^{In}_{\gamma XL I'\pi'}(\varepsilon_\gamma) = \frac{1}{\varepsilon_\gamma^{2L+1}} \frac{1}{D^{In}} \langle \Gamma_{\gamma XL}(E,I,\pi;E',I',\pi') \rangle \quad , \qquad (1)$$

где $\langle \Gamma_{\gamma XL}(E,I,\pi,E'I'\pi') \rangle$ -средняя ширина распада из состояния (E,I,π) к состоянию (E',I',π') путём γ-эмиссии с мультипольностью XL и энергией $\varepsilon_\gamma = E-E'$.

Усреднение берется по начальному состоянию (E,I,π), средняя ширина которого равна D^{In}. Если предположить независимость силовых функций от спина и чётности состояний, то коэффициент проникновения γ-лучей имеет следующий вид:

$$T_{\gamma XL}(\varepsilon_\gamma) = 2\pi \varepsilon_\gamma^{2L+1} f_{\gamma XL}(\varepsilon_\gamma) \quad . \qquad (2)$$

Силовые функции для M1, E2, M2, E3, M3-излучений вычислены из одночастичной модели и нормированы относительно E1-излучения, а E1-силовая функция находилась из среднего сечения фотопоглощения $\langle \sigma^I_{\gamma E1}(\varepsilon_\gamma) \rangle$ посредством гипотезы Бринка-Акселя:

$$f_{\gamma E1}(\varepsilon_\gamma) = \frac{1}{2(\pi\hbar c)^2} \frac{1}{g_I} \frac{1}{\varepsilon_\gamma} \langle \sigma^I_{\gamma E1}(\varepsilon_\gamma) \rangle \quad . \qquad (3)$$

Предполагается, что $\langle \sigma^I_{\gamma E1}(\varepsilon_\gamma) \rangle$ может выражаться через параметры E1 гигантского резонанса. Для его зависимости от энергии принималась следующая Лоренц-форма:

$$f_{\gamma E1}(\varepsilon_\gamma) = \frac{1}{6(\pi\hbar c)^2} \cdot \sigma_R \cdot \frac{\Gamma_R^2 \varepsilon_\gamma}{(\varepsilon_\gamma^2 - E_R^2)^2 + \Gamma_R^2 E_R^2} \quad , \qquad (4)$$

где E_R, Γ_R -энергия и ширина E1 резонанса, σ_R -сечение его в пике.

Глобальные значения этих параметров взяты из работы/11/. E1-силовая функция может быть нормирована также на среднюю радиационную ширину при энергии возбуждения, равной энергии связи нейтрона, полученную по формуле Гартнера/13/.

2.2. Плотность уровней и схемы распада

Плотность уровней является важной величиной в статистической теории, от которой результаты её предсказания чувствительно зависят. В данной работе плотность уровней вычислялась согласно модели Ферми-газа с смещённым основным состоянием /14/. Значения параметров плотности уровней взяты из работ/15-18/, а схемы распада и соотношения разветвления из /19/.

3. Результаты вычисления и обсуждение

На рис.1-2 представлены вычисленные значения функции возбуждения некоторых дискретных γ-квантов, возникающих при неупругом рассеяния нейтронов на ядре. Вклады от γ-излучений высокой мультипольности/Рис.1/ и предравновесной эмиссии нейтронов/Рис.2/ на эти величины начинают сказываться при энергии бомбардирующих нейтронов около 14-15 Мэв. На спектрах γ-эмиссии из $^{56}Fe+n$ и $^{93}Nb+n$ /Рис.3-4/ видны роль различных каналов реакций и влияние предравновесной эмиссии нейтронов. Функции возбуждения производства гамма-квантов в этих реакциях показаны на графиках 5-6 .

Из результатов вычисления и их сравнения с новейшими экспериментальными данными можно сделать следующие заключения:

- Вклад излучения высокой мультипольности приводит к росту функции возбуждения при больших энергиях
- Влияние предравновесной эмиссии нейтронов на форму эмиссионных γ-спектров начинается при $E_n > 14-15$ Мэв и её учет улучшает описание экспериментальных

данных. Это ещё раз подтверждает важную роль предравновесной эмиссии в механизме протекания ядерных реакций/20/.

- При энергиях нейтронов до 20 Мэв доминирующим процессом в производстве гамма-квантов для этих ядер является неупругое рассеяние нейтронов, затем при больших энергиях налетающих нейтронов начинает конкурировать (n,2n) реакция.
- Путём выбора значений параметров в рамках статистической теории можно достигнуть хорошего описания эффективного сечения производства и спектров γ-квантов из реакций с нейтронами на средних и тяжёлых ядрах при энергии падающих нейтронов до 20 Мэв.

References

/ 1/ W. Hauser, H. Feshbach, Phys. Rev. 87 (1952) 336

/ 2/ P.A. Moldauer, Revs. of Mod. Phys. 36 (1964) 1079

/ 3/ J.J. Griffin, Phys. Lett. 17 (1966) 478

/ 4/ C.K. Cline, M. Blann, Nucl. Phys. A172 (1971) 225

/ 5/ G.M. Braga-Marcazzan, E. Gadioli-Erba, L. Millazzo-Colli and P.G. Sona, Phys. Rev. C6 (1972) 1398

/ 6/ C. Kalbach, Acta phys. slov. 25 (1975) 100

/ 7/ C. Kalbach-Cline, Nucl. Phys. A210 (1973) 590

/ 8/ F.C. Williams Jr., Nucl. Phys. A166 (1971) 231

/ 9/ M. Uhl, A Computer Code for Particle Induced Activation Cross Sections and Related Quantities, IKR76/01, Vienna, 1976

/10/ J. Blatt, B. Weisskopf, Theoretical Nuclear Physics, Chap. 12, New York, 1952

/11/ P. Axel, Phys. Rev. 126 (1962) 671

/12/ G.A. Bartholomev et al., Advances in Nuclear Physics, Vol. 7, Ch. 4, Plenum Press, N.Y. (1973)

/13/ D.G. Gardner, invited paper presented at the "Conference Nuclear Cross Sections and Technology", Washington, D.C., March 3-7, 1975

/14/ D.W. Lang, Nucl. Phys. 77 (1966) 545

/15/ W. Dilg et al., Nucl. Phys. A217 (1973) 269

/16/ M. Uhl, Acta Phys. Aust. 31 (1970) 245

/17/ J.N. Shubin, Byull. Centra po Yad. Dan. 4 (1967) 305

/18/ P. Rösner, Diplomarbeit, TU Dresden, 1978

/19/ M.N. Rao, Nucl. Data B3-3, 4-46,
R.L. Auble and M.N. Rao, Nucl. Data B3-5, 6-129;
Nucl. Data Sheets Vol. 7-8, 1972;
I.J. van Heerden et al., Z. Physik 260 (1973) 9

/20/ К. Зайдел, Д. Зелигер, Р. Рай, В.Д. Тонеев, ЭЧАЯ 7 (1976) 499

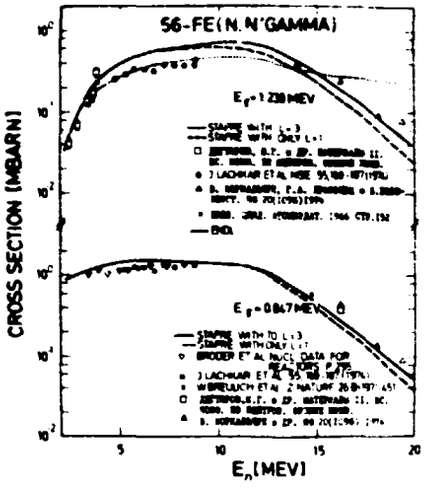

Рис. 1

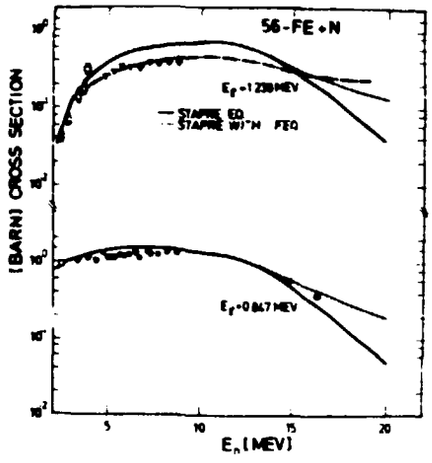

Рис. 2

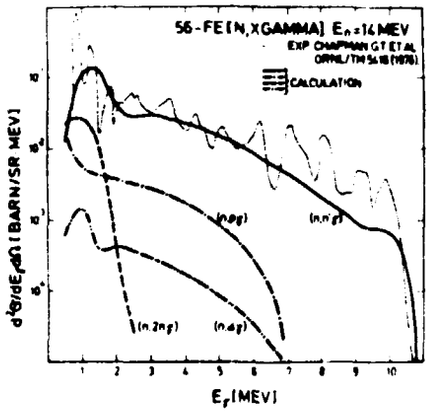

Рис. 3

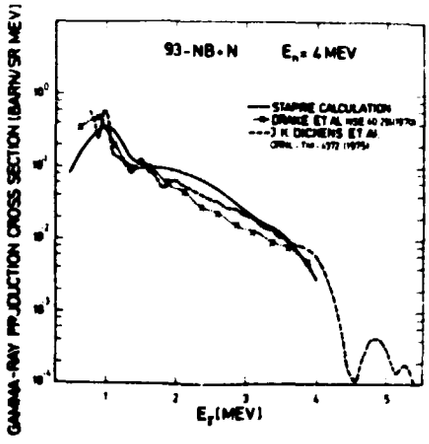

Рис. 4

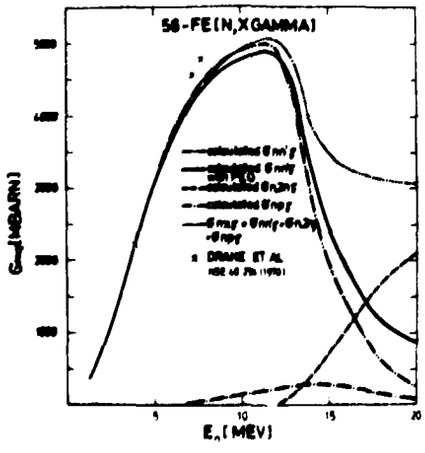

Рис. 5

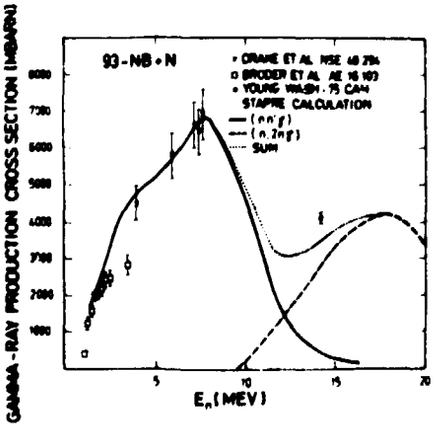

Рис. 6

НЕЙТРОНЫ ИЗ (p,n) РЕАКЦИЙ НА ЯДРАХ $^{90,91,94}Zr$.

Н.С. Бирюков, Б.В. Журавлев, А.П. Руденко, О.А. Сальников, В.М. Трыкова
Физико-энергетический институт, Обнинск, СССР

Спектры нейтронов из (p,n) реакций на ядрах $^{90,91,94}Zr$ измерялись при энергии протонов 11,2 ± 0,1 МэВ под углами 30^0, 60^0, 90^0, 120^0, 150^0. Измерения проводились на спектрометре нейтронов по времени пролета на 150 см циклотроне ФЭИ. Определены параметры плотности ядерных уровней. Показано, что учет вклада прямых процессов, определенных как асимметричная компонента наблюдаемых угловых распределений нейтронов, приводит к более согласованным значениям параметров плотности ядерных уровней.

Данная работа является продолжением исследований [1 - 6] по изучению энергетических и угловых распределений нейтронов из реакций (n,n') и (p,n) с целью выяснения особенностей их механизма и структуры исследуемых ядер. В работе измерялись спектры нейтронов из реакций $^{90,91,94}Zr(p,n)^{90,91,94}Nb$ при энергии протонов 11,2 ± 0,1 МэВ под углами 30^0, 60^0, 90^0, 120^0, 150^0. Энергия протонов выбрана так, чтобы в реакциях $^{91}Zr(p,n)^{91}Nb$ ($Q_{p,n}$ = -1,920 МэВ) и $^{94}Zr(p,n)^{94}Nb$ ($Q_{p,n}$ = -1,704 МэВ) реализовать такой же интервал энергий возбуждения, как и в ранее исследованной нами реакции $^{93}Nb(n,n')^{93}Nb$[1].

Измерения проводились спектрометром нейтронов по времени пролета на 150 см циклотроне ФЭИ, разрешающая способность которого составляла 1,1 нсек/м при пролетной базе 2,5 м. В качестве мишеней использовались металлические фольги толщиной 2,43 мг/см^2, 2,04 мг/см^2, 4,91 мг/см^2, соответственно для ^{90}Zr(96,8 %), ^{91}Zr(63,63 %), ^{94}Zr(91,2 %). Основной примесью в мишенях из ^{91}Zr и ^{94}Zr был исследуемый в данной работе изотоп ^{90}Zr, что позволило сделать соответствующие поправки. Более подробно техника эксперимента, процедура измерения и обработки данных описаны в работах [6, 7].

Результаты измерений представлены на рис. 1, 2. Видно, что спектры нейтронов из (p,n) реакций не имеют характерного для неравновесных процессов высокоэнергетичного хвоста, наблюдаемого в реакциях неупругого рассеяния нейтронов, хотя асимметрия в угловом распределении указывает на их наличие.

Предварительно интегральные спектры нейтронов из реакций $^{91,94}Zr(p,n)^{91,94}Nb$ были проанализированы в рамках предравновесной модели распада ядер [8], аналогично тому, как это было сделано в работе [1] для спектра нейтронов, неупругорассеянных на Nb, также представленного на рис. 1.

$$N(E_n)dE_n=\left\{A_1\cdot E_n\cdot\sigma_c(E_n)\cdot exp(-E_n/T)+A_2\cdot E_n\cdot\sigma_c(E_n)\cdot\sum_{\substack{n_0\\(\Delta n=+2)}}p\cdot(n-1)(n+1)\cdot\left(\frac{U}{E^*}\right)^{n-2}\right\}\cdot dE_n \qquad (1)$$

где: U - энергия возбуждения остаточного ядра,
E - энергия нейтронов, $\sigma_c(E_n)$ - сечение обратной реакции
T - ядерная температура,
E^* - энергия возбуждения составного ядра,
n,p - число возбужденных квазачастиц и частиц, соответственно
A_1,A_2 - константы

Использование приближения "постоянной ядерной температуры" для описания равновесной части спектра исследуемых ядер представляется нам наиболее оправданным, такой характер изменения плотности ядерных уровней около магических чисел является следствием дискретной структуры спектра одночастичных состояний [9, 10]. Чтобы избежать вклада нейтронов из реакции (p,pn) и $(p,2n)$, анализ спектра начинался с E_n = 2,3 МэВ. Сечение обратной реакции принималось независящим от энергии нейтронов. Начальное число возбужденных квазичастиц n_0= 3. Результаты анализа представлены на рис. I и в таблице I.

Таблица I

Реакции	Параметр		
	T (МэВ)	α (%)	$\sigma_{нес}$ (мбарн)
$^{91}_{40}Zr^{51}(p,n)^{91}_{41}Nb^{50}$	0,83 ± 0,01	1,9	816 ± 65
$^{94}_{40}Zr^{54}(p,n)^{94}_{41}Nb^{53}$	0,94 ± 0,01	1,6	840 ± 67
$^{93}_{41}Nb^{52}(n,n')^{93}_{41}Nb^{52}$	0,73 ± 0,01	18,2	1740 ± 140

Из таблицы видно, что наблюдаемое отличие в доле нейтронов, испущенных до наступления равновесия, в реакциях (p,n) и (n,n') существенно превышает предсказываемое моделью предравновесного распада ядер отличие в 2 раза [11]. Это согласуется с результатом, полученным нами в работах [4, 6] для реакций $^{181}Ta(p,n)^{181}W$ и $^{181}Ta(n,n')^{181}Ta$. Однако, в данном случае наблюдается противоречащее известным представлениям изменение ядерной температуры вблизи магических чисел (N = 50). Для ядра $^{94}_{41}Nb^{53}$ ядерная температура должна быть приблизительно на 10 % меньше, чем для магического по нейтронам $^{91}_{41}Nb^{50}$ [12], а из анализа спектров получается на 12 % больше. Такое аномальное поведение ядерной температуры может быть связано с некорректным выделением в рамках модели предравновесного распада спектра нейтронов, испущенных до наступления статистического равновесия.

Нам представляется физически более правильным выделить такие процессы на основе имеющейся информации об асимметрии в угловом распределении [2, 7].

Для этого угловое распределение нейтронов по энергетическим интервалам 0,5 МэВ аппроксимировалось разложением по полиномам Лежандра до второго порядка включительно, вклад асимметричной компаненты при таком представлении определяется коэффициентом при первом полиноме. Полученные таким образом интегральные спектры (гистограммы) асимметричной части угловых распределений в реакциях $^{91}_{40}Zr^{51}(p,n)^{91}_{41}Nb^{50}$ и $^{94}_{40}Zr^{54}(p,n)^{94}_{41}Nb^{53}$ представлены на рис. I

Характерной особенностью этих спектров является то, что они резче изменяются с энергией, чем спектры предравновесной эмиссии. Кроме того, спектр асимметричной части углового распределения нейтронов в реакции $^{94}_{40}Zr^{54}(p,n)^{94}_{41}Nb^{53}$ по абсолюту вдвое больше, чем спектр предравновесной эмиссии и спектр асимметричной части в реакции $^{91}_{40}Zr^{51}(p,n)^{91}_{41}Nb^{50}$.

Однако, хотя асимметрия в угловом распределении несомненно указывает на наличие прямых процессов, она позволяет определить лишь нижнюю границу их вклада. Процессы, отличные от равновесного, по-видимому, более часты, чем указывает этот критерий, они могут иметь и изотропное угловое распределение. Оценки вкла-

да изотропной составляющей этих процессов, сделанные из анализа угловых распределений неупругорассеянных нейтронов в работах [2, I3], показали, что он равен вкладу асимметричной части. В первом приближении можно предположить, что такое же соотношение между асимметричной и изотропной компонентами имеет место и в (p,n) реакциях, и что полный интегральный спектр нейтронов, испущенных до достижения равновесия, равен удвоенному спектру асимметричной части.

Интегральные спектры нейтронов из реакций $^{91}_{40}Zr(p,n)^{91}_{41}Nb$ и $^{90}_{40}Zr(p,n)^{90}_{41}Nb$ после вычитания асимметричной компоненты и удвоенной асимметричной компоненты анализировались в рамках статистической теории равновесного распада ядер и определялись параметры плотности ядерных уровней.

$$N(E_n)dE_n = const \cdot E_n \cdot \sigma_c(E_n) \cdot \rho(U)\, dE_n \qquad (2)$$

где:

$$\rho(U) \begin{cases} \exp(-E_n/T) & \text{- приближение постоянной ядерной температуры,} \\ U^{-5/4} \cdot \exp(2\sqrt{aU}) & \\ U^{-2} \exp(2\sqrt{a'U}) & \text{- модель ферми-газа,} \end{cases}$$

a, a' - параметры плотности ядерных уровней в модели ферми-газа,

$U = E_0 - E_n + Q - \Delta$ - энергия возбуждения остаточного ядра,

Δ - энергетическое смещение, значения этого параметра взяты из работы [I4].

Результаты анализа представлены на рис. 3 и в таблице 2.

Видно, что учет вклада прямых процессов приводит к более согласованным значениям параметров плотности ядерных уровней. Ядерная температура для $^{90}_{41}Nb^{53}$ после вычитания удвоенной асимметричной компоненты становится меньше (параметр a - больше), чем для $^{91}_{41}Nb^{50}$, как это и следует из оболочечной модели ядра. При этом значение параметров плотности ядерных уровней в модели ферми-газа для $^{91}_{41}Nb$ хорошо согласуется с данными по нейтронным резонансам [I5, I6, I7], являющимися наиболее прямой экспериментальной информацией. Хорошее согласие получается также с параметрами плотности ядерных уровней $^{93}_{41}Nb^{52}$, определенными по мягкой части спектра неупругорассеянных нейтронов [I], и $^{90}_{41}Nb^{49}$, средняя энергия возбуждения которого была вдвое меньше, чем для $^{91}_{41}Nb^{50}$ и $^{93}_{41}Nb^{53}$. Спектр нейтронов из реакции $^{90}_{40}Zr(p,n)^{90}_{41}Nb$ анализировался без учета прямых процессов, так как характер углового распределения, практически, не указывает на их наличие.

В таблице 2 приведены также сечения поглощения протонов, определенные как сумма равновесной части спектра нейтронов из (p n) реакции (площадь под кривой) и соответствующей доли прямых процессов, вклад прямых процессов в энергетическом интервале (0 - 0,5)МэВ, где нет экспериментальной информации, предполагался равным нуля. Величина определенного так сечения существенно зависит от того, с каким значением параметра плотности ядерных уровней (в данном случае, ядерной температуры) производится экстраполяция спектра в нуль. Результаты показывают, что лучшее согласие с расчетами по оптической модели с потенциалом Беччети-Гриниаса [I8], дающими для ^{90}Zr, ^{91}Zr, ^{94}Zr, соответственно 930, 950, 990 мбарн, получается опять же при вычитании из интегрального спектра нейтронов удвоенной асимметричной компоненты.

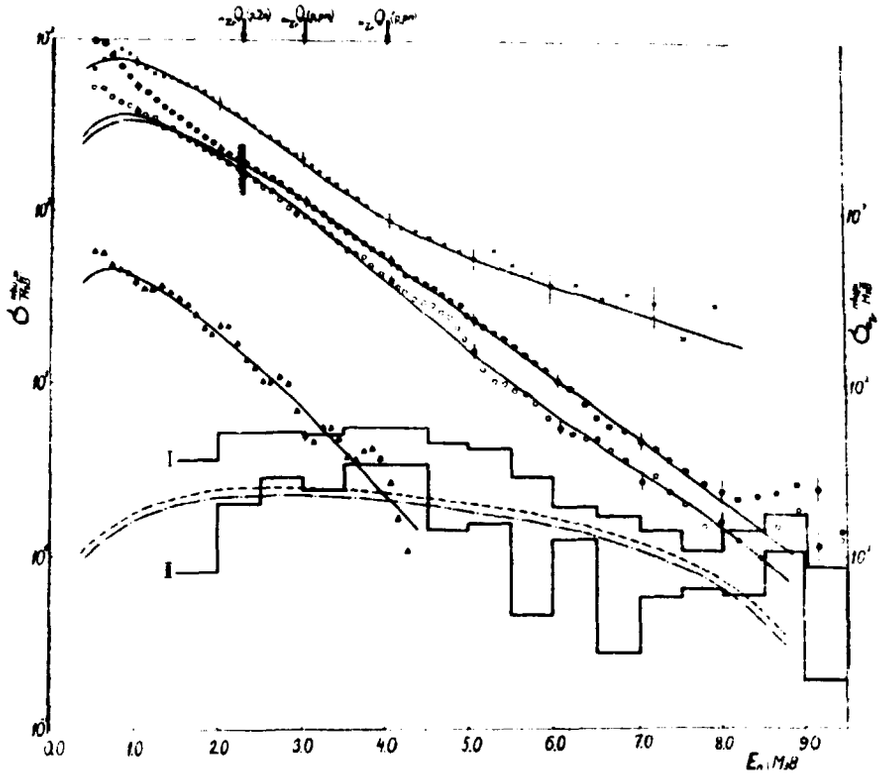

Рис. I Интегральные спектры нейтронов: • - $^{94}Zr(p,n)^{94}Nb$(I), o - $^{91}Zr(p,n)^{91}Nb$ (2), ▲ - $^{90}Zr(p,n)^{90}Nb$(3), x - $^{93}Nb(n,n')^{93}Nb$(4). Сплошные кривые - расчет по модели предравновесного распада для реакций I, 2, 4 и равновесного распада для реакции 3. Пунктирная и штрихпунктирные кривые - спектры предравновесной эмиссии, соответственно, для реакций 2, I. Гистограммы - асимметричная компонента интегральных спектров в реакциях $^{94}Zr(p,n)^{94}Nb$(I) и $^{91}Zr(p,n)^{91}Nb$(II). ↑ - нижняя граница анализируемого участка спектра в реакциях I и 2.

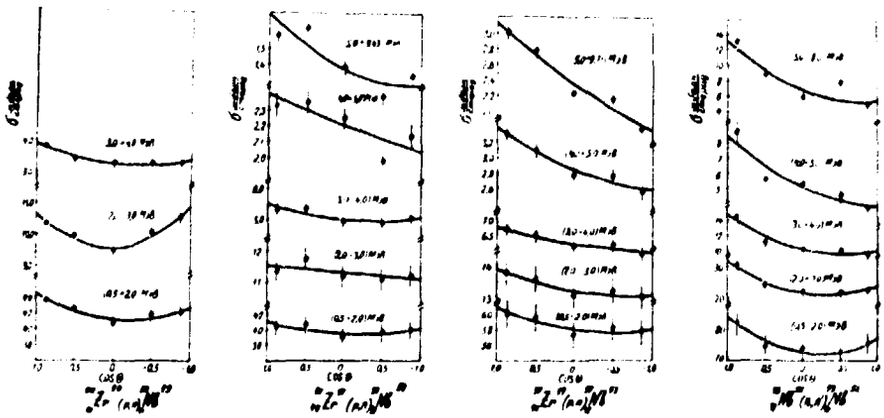

Рис. 2 Угловые распределения нейтронов. Кривые - аппроксимация экспериментальных данных разложением по полиномам Лежандра.

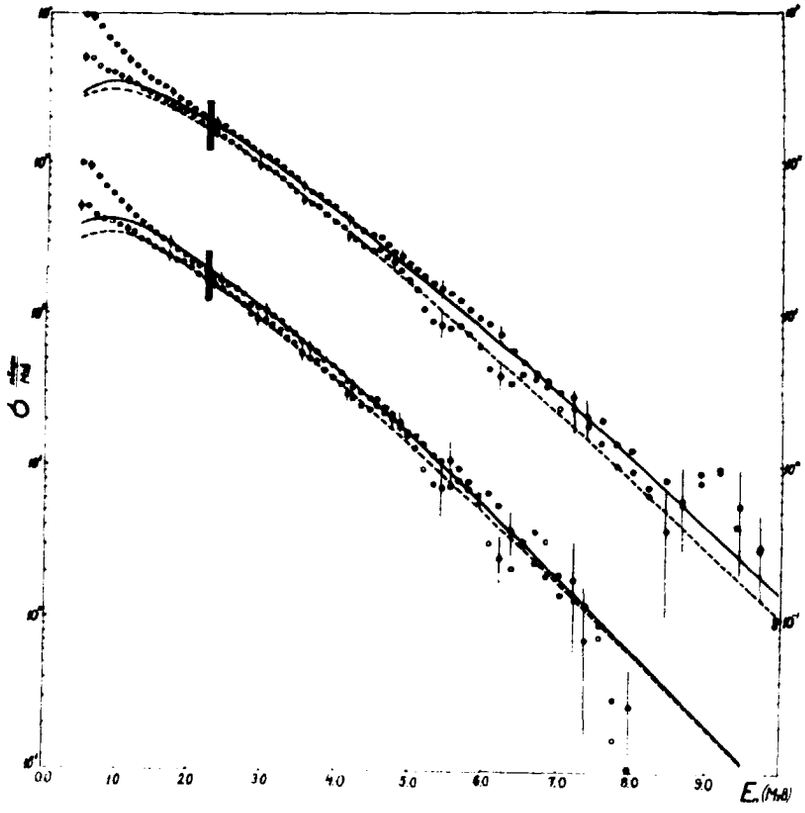

Рис. 3 Спектры нейтронов из реакций $^{91}Zr(p,n)^{91}Nb$(o) и $^{94}Zr(p,n)^{94}Nb$(•) после вычитания асимметричной компоненты (вверху) и после вычитания удвоенной асимметричной компоненты (внизу, шкала для σ справа). Кривые - расчет в рамках "приближения постоянной температуры".

Таблица 2

Ядро	Тип анал.	T МэВ	a МэВ$^{-1}$	a' МэВ$^{-1}$	$\tilde{U}=E_0-\bar{E}_n+Q$ МэВ	$a_{рез}$ МэВ$^{-1}$	σ_{abs} мбарн	α неравн. (%)
$^{91}_{41}Nb^{50}$	I	0,91±0,01	8,5±0,2	10,1±0,2			702±58	0
	2	0,87±0,01	9,1±0,2	10,8±0,3	6,01		755±68	1,5
	3	0,81±0,01	10,2±0,3	12,1±0,3			871±85	2,6
$^{94}_{41}Nb^{53}$	I	0,99±0,01	8,8±0,2	10,2±0,2		$13,15^{+0,18}_{-0,16}$ [15]	789±63	0
	2	0,91±0,01	9,2±0,2	11,4±0,3	6,12	12,81±0,25 [16]	882±79	3,1
	3	0,78±0,01	12,0±0,3	14,4±0,3		12,86 [17]	1061±100	5,1
$^{90}_{41}Nb^{49}$	I	0,70±0,01	11,2±0,3	14,0±0,4	3,00		852±69	0
$^{93}_{41}Nb^{52}$	I	0,77±0,03	14,7±0,9	18,4±1,1	7,56			

Примечание:

I - анализ без вычитания неравновесных процессов, 2 - вычтена асимметричная компонента спектра, 3 - вычтена удвоенная асимметричная компонента.

Литература

[I] Н.С. Бирюков, Б.В. Журавлев и др. Я.Ф. т. I9, II90-I206, (I974)
[2] Н.С. Бирюков, Б.В. Журавлев и др. Я.Ф. т. 25, 767, (I977)
[3] Н.С. Бирюков, Б.В. Журавлев и др. Препринт ФЭИ-457, (I973)
[4] Н.С. Бирюков, Б.В. Журавлев и др. "Нейтронная физика", (Материалы 4-й Всесоюзной конференции по нейтронной физике, Киев) ч. I, 260, (I977)
[5] Н.С. Бирюков, Б.В. Журавлев и др. Доклад на Международном симпозиуме по взаимодействию нейтронов с ядрами, Гауссиг, ГДР, (I977)
[6] Н.С. Бирюков, Б.В. Журавлев и др. Я.Ф. т. 26, II46, (I977)
[7] Н.С. Бирюков, Б.В. Журавлев и др. Препринт ФЭИ-I67, (I969)
[8] J.J. Griffin, Phys. Rev. Lett. 17 (1966) 478
[9] А.В. Игнатюк, В.С. Ставинский, Ю.Н. Жубин, Препринт ФЭИ-I67, (I969)
[I0] M. Maruyama, Nucl. Phys. A131 (1969) 145
[II] D. Seeliger, Proc. of the third intern. seminar on interact. of fast neutrons with nuclei, Gaussig, ZfK-261 (1973) 77
[I2] А.В. Игнатюк, К.К. Истеков и др. "Нейтронная физика", (Материалы 4-й Всесоюзной конференции по нейтронной физике, Киев) ч. I, 60, (I977)
[I3] А.В. Игнатюк, В.П. Лунев, В.Г. Проняев, Препринт ФЭИ-682, (I976)
[I4] W. Dilg, W. Schantl et al., Nucl. Phys. A217 (1973) 269
[I5] H. Baba, Nucl. Phys. A159 (1970) 625
[I6] A. Gilbert, A.G.W. Cameron, Can. J. of Phys. 43 (1965) 1446
[I7] G. LePoittevin et al., Nucl. Phys. 70 (1965) 497
[I8] А.Б. Пащенко, Ядерно-физические исследования в СССР, вып. 20, 39, (I973)

ПАРАМЕТР СПИНОВОЙ ЗАВИСИМОСТИ ИЗ УГЛОВЫХ РАСПРЕДЕЛЕНИЙ НЕЙТРОНОВ В (p,n) РЕАКЦИЯХ

Н.С. Бирюков, Б.В. Журавлев, А.П. Руденко, О.А. Сальников, В.И. Трыкова
Физико-энергетический институт, Обнинск, СССР

Из Анализа спектров и угловых распределений нейтронов из (p,n) реакций на ядрах $^{52,53,54}Cr$, $^{56,57}Fe$, $^{60,62}Ni$, $^{90,91,94}Zr$, ^{113}Cd, ^{115}In, ^{122}Sn, ^{181}Ta, ^{197}Au при энергии протонов 11,2 ± 0,1 МэВ определены параметры спиновой зависимости.

Изучение спиновой зависимости плотности ядерных уровней, одной из фундаментальных характеристик ядра, представляет принципиальный научный интерес и необходимо для практических задач при вычислении сечений взаимодействия в рамках статистических моделей ядерных реакций. Одним из путей получения информации о спиновой зависимости является изучение угловых распределений частиц, испускаемых в ядерных реакциях, так как характер углового распределения существенно зависит от того, в какой степени угловой момент частицы связан с угловым моментом составного ядра вследствие закона сохранения углового момента. Степень этой зависимости определяется параметром спиновой зависимости, пропорциональным среднему квадрату углового момента нуклонов вблизи поверхности ферми $\langle m^2 \rangle$.

$$\sigma^2 = \langle m^2 \rangle g t = J \cdot t \qquad (1)$$

где: g - плотность одночастичных состояний вблизи поверхности ферми,
t - термодинамическая температура,
J - момент инерции ядра.

Эриксон и Струтинский [1] показали, что для равновесных процессов в приближении не слишком сильной связи спина составного ядра со спином остаточного ядра и орбитальным моментом испущенной частицы, т.е. при малой анизотропии, угловое распределение имеет вид

$$W(E_n,\Theta) \sim 1 + \frac{\bar{J}^2 \cdot \bar{\ell}^2}{12 \cdot \sigma^4} P_2(\cos\Theta), \qquad (2)$$

где: E_n - энергия испущенных частиц,
Θ - угол в системе центра масс,
$\bar{J}^2$ и $\bar{\ell}^2$ - среднее квадратичное значение углового момента составного ядра и испущенных частиц, соотвественно.

Из сравнения отнормированных на P_0 коэффициентов при P_2 в разложении по полиномам Лежандра экспериментальных угловых распределений с аналогичным коэффициентом в выражении (2) можно определить параметр спиновой зависимости.

В данной работе измерялись спектры и угловые распределения нейтронов из (p,n) реакций на ядрах $^{52,53,54}Cr$, $^{56,57}Fe$, $^{60,62}Ni$, $^{90,91,94}Zr$, ^{113}Cd, ^{115}In, ^{122}Sn, ^{181}Ta, ^{197}Au при энергии протонов 11,2 ± 0,1 МэВ. Измерения проводились на спектрометре нейтронов по времени пролета на 150 см циклотроне ФЭИ, разрешающая способность которого составляла 1,1 нсек/м при пролетной базе 2,5 м. Подробно

техника эксперимента, процедура измерения и обработки экспериментальных данных описаны в работе [2] . На рис. I представлены угловые распределения нейтронов для соответствующих интервалов энергий.

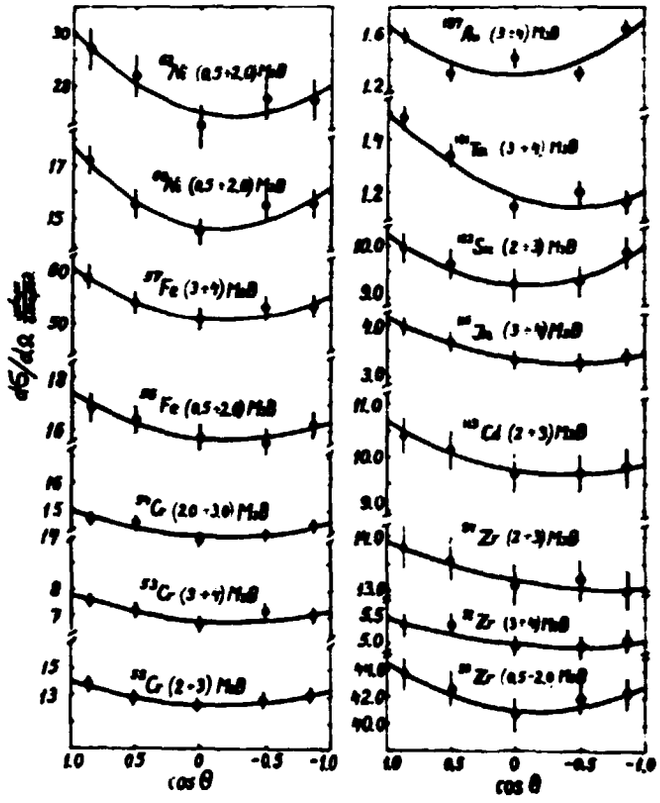

Рис. I Угловые распределения нейтронов. Кривые - аппроксимация экспериментальных данных разложением по полиномам Лежандра до 2-го порядка методом наименьших квадратов.

Выбор указанных интервалов энергий обусловлен стремлением избежать вклада нейтронов из (p,pn) и (p,2n) реакций и нейтронов, испущенных до наступления статистического равновесия. Характерной чертой наблюдаемых угловых распределений нейтронов является малая анизотропия, что отвечает основному требованию применимости выражения (2). Средние квадраты угловых моментов составных ядер и нейтронов определялись с использованием коэффициентов проницаемости, вычисленных по программе КОП [3].

$$\bar{\ell}^2 = \sum \ell(\ell+1)\cdot(2\ell+1)\cdot T_\ell(E_n) / \sum (2\ell+1)\, T_\ell(E_n)$$
$$\bar{J}^2 = \sum_\nu J_\nu(J_\nu+1)\cdot(2J_\nu+1)\cdot T_{\ell\nu}(E_p) / \sum_\nu (2J_\nu+1)\, T_{\ell\nu}(E_p) \qquad (3)$$

На рис. 2 представлены значения параметра спиновой зависимости, определенные в данной работе.

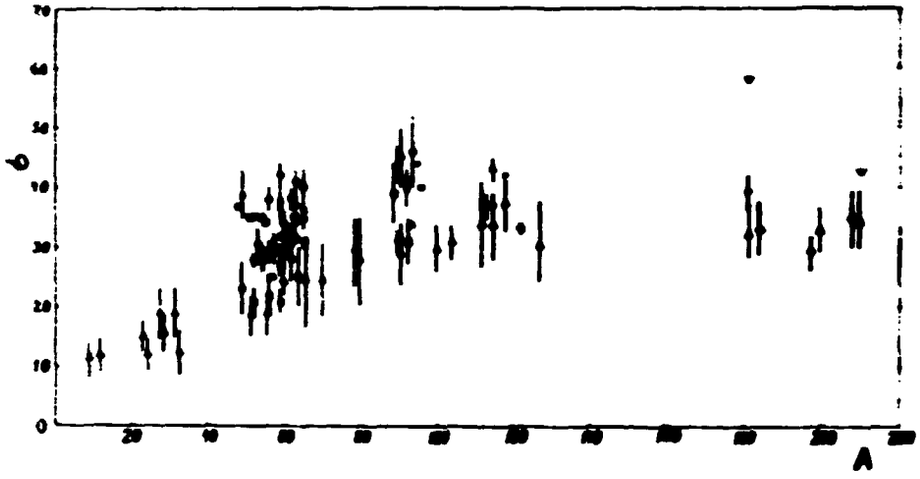

Рис. 2 Зависимость параметра σ от массового числа. ● - данная работа, ■ - 4, × - 5, ○ - 6, Δ - 7, □ - 8, ▲ - 9, ▽ - 10.

Указанные ошибки обусловлены только ошибками эксперимента. Из сравнения с результатами других работ [4, 5, 6, 7, 8, 9, 10] видно, что наши данные находятся в определенном согласии с параметрами спиновой зависимости, полученными в этих работах. Однако, разброс экспериментальных значений параметра, определенных из угловых распределений частиц, испущенных в различных ядерных реакциях, достаточно велик; в области $A \simeq 60$, где имеется максимальное количество данных, он составляет 30 %. Такой разброс связан с рядом систематических ошибок, вызванных присутствием частиц, испущенных до наступления статистического равновесия, частиц, испущенных в сопутствующих реакциях типа $(n,2n)$, $(p,2n)$, (p,pn) и др., а также из-за нарушений условий применимости выражения (2). Как показано в работе [11] для неравновесного распада входных состояний ожидается существенно большая анизотропия в угловом распределении по сравнению с угловым распределением равновесных процессов и наблюдаемая на эксперименте анизотропия может быть в значительной степени вызвана неравновесным распадом. Этим, предположительно, можно объяснить заниженные значения σ, полученные в работах [8, 9]. Так как энергия возбуждения остаточного ядра после испарения второй частицы мала, то присутствие частиц из упомянутых сопутствующих реакций в исследуемом диапазоне энергий тоже может привести к уменьшению параметра спиновой зависимости из-за влияния парных корреляций сверхпроводящего типа. Определенные систематические ошибки могут быть связаны с применением приближения (2) для анализа угловых распределений с достаточно глубокой анизотропией [7].

Общий результат, тем не менее, указывает на постоянство параметра спиновой зависимости от массового числа для $A > 40$, в то время как модель ферми-газа предсказывает $\sigma(A) \sim A^{7/12}$.

На рис. 3 показано отношение моментов инерции ядер, соответствующих экспериментальным значениям параметра спиновой зависимости, к твердотельным, предсказываемым моделью невзаимодействующих частиц.

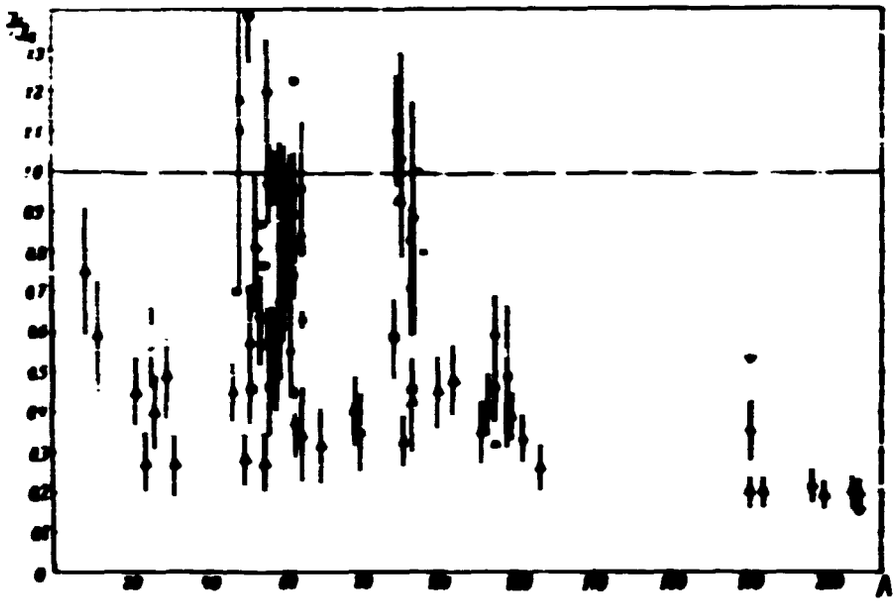

Рис. 3 Зависимость отношения наблюдаемого момента инерции к твердотельному от массового числа. Обозначения те же, что и на рис. 2. Жирно-пунктирная кривая - предсказание модели невзаимодействующих частиц.

Эффекты, связанные с влиянием парных корреляций сверхпроводящего типа и оболочечной структуры ядра, оценены аналогично тому, как это сделано нами в работе [8] и введены соответствующие поправки. Результаты других работ, представленных на рис. 3 переопределены на значения твердотельного момента инерции с r_0 = 1,25 Фм. Наблюдается плохое согласие с модельными предсказаниями для A < 100 данных, полученных в данной работе ($J/J_{тв}$ = 0,97) и в работах [4, 5, 6, 7]. Результаты, полученные из анализа угловых распределений неупругорассеянных нейтронов [8, 9], как это уже отмечалось, дают заниженные значения параметра спиновой зависимости, и, соответственно, момента инерции ядер для этой области массовых чисел. Для A > 100 вся совокупность представленных на рис. 3 работ указывает на отличие моментов инерции ядер от твердотельного в (2 ÷ 5) раз.

Уменьшение момента инерции может быть обусловлено, помимо уже учтенного влияния парных корреляций и оболочечной структуры, наличием асимметричного по спину ядерного взаимодействия [12]. Полученное в работе [12] выражение для момента инерции с учетом такого взаимодействия указывает на возможное уменьшение момента инерции в (1,5 ÷ 2,0) раза, однако, область его применимости распространяется преимущественно на легкие и средние ядра.

Возможно, что наблюдаемое на эксперименте уменьшение момента инерции для тяжелых ядер является указанием на то, что энергия фазового перехода не остается постоянной с ростом A, как это следует из модели сверхпроводимости [13], а увеличивается, в результате чего усиливается влияние остаточных взаимодействий на структуру возбужденных ядер в целом и на момент инерции ядра в частности.

Литература

[I] T. Ericson and V. Strutinski, Nucl. Phys. 8 (1958) 284
T. Ericson, Adv. Phys. 9 (1960) 425
[2] Н.С. Бирюков, Б.В. Журавлев и др. Я.Ф., т.26, вып.6, II46, (I977)
[3] А.Б. Пащенко, Ядерно-физические исследования в СССР, вып.20, 39, (I973)
[4] S.M. Grimes, J.D. Anderson et al., Phys. Rev. C10 N6 (1974) 2373
[5] P. Hille, P. Sperr et al., Nucl. Phys. A232 (1974) 157
[6] C.C. Lu, L.C. Vaz and J.R. Huizenga, Nucl. Phys. A197 (1972) 321
[7] M. Bormann, W. Schmidt et al., Nucl. Phys. A186 (1972) 65
[8] Н.С. Бирюков, Б.В. Журавлев и др. Нейтронная физика, (материалы 3-й Всесоюзной конференции по нейтронной физике, Киев), часть 4, I23, (I976)
[9] Д. Хермсдорф, А. Майстер и др. Нейтронная физика, (материалы 4-й Всесоюзной конференции по нейтронной физике, Киев), часть 2, III, (I977)
[I0] T. Akiyoshy et al., J. Nucl. Science and Technology 11 (1974) 523
[II] А.В. Игнатюк, В.П. Лунев, В.Г. Проняев, Изв. АН. СССР, серия физ., т. 39, № I0, 2I44, (I975)
[I2] А.В. Игнатюк, Изв. АН. СССР, серия физ., т. 38, № I, I72, (I974)
[I3] А.В. Игнатюк, Ю.Н. Шубин, Изв. АН. СССР, серия физ., т.37, I955, (I973)

ЗАВИСИМОСТЬ СЕЧЕНИЙ РЕАКЦИЙ (n,p) И (n,2n) ПРИ ЭНЕРГИИ I4-I5 МЭВ ОТ ПАРАМЕТРА $(N-Z)/A$

В.М. Бычков, А.Б. Пащенко, В.И. Пляскин
Физико-энергетический институт, Обнинск, СССР

На основе теоретических представлений о протекании ядерной реакции получены простые формулы, связывающие сечения реакций (n,p) и $(n,2n)$ при энергии нейтрона I4 - I5 Мэв с параметром $(N-Z)/A$.

I. Сечение реакции (n,p).

Исходя из предположения, что сечение реакции (n,p) пропорционально произведению вероятности образования составного ядра на вероятность эмиссии из него протона, можно получить следующую формулу:

$$\sigma_{np} \simeq \sigma_{ne} \exp\left\{\sqrt{\frac{a}{E_n}}\left(-S_p - B_K + \delta'\right)\right\}, \quad (1)$$

здесь: σ_{ne} -сечение поглощения нейтрона, S_p -энергия связи протона в составном ядре, B_K -кулоновский барьер ядра, a -параметр плотности уровней, $\delta' = \delta_p - \delta_c$, где δ_c, δ_p - поправки на спаривание в составном и остаточном ядрах, E_n -энергия нейтрона.

Определив энергию связи S_p по формуле Вайцзеккера, получим зависимость сечения реакции (n,p) от числа протонов и нейтронов ядра-мишени:

$$\sigma_{np} = \sigma_{ne} \exp\left\{\sqrt{\frac{a}{E_n}}\left(-C_1 \frac{N-Z+1}{A} + C_2 \frac{Z-1}{A^{1/3}} - \Delta\right)\right\}, \quad (2)$$

Параметры этой формулы, определённые из сравнения с экспериментальными данными при энергии нейтрона I4 - I5 Мэв, имеют следующие значения

$\sigma_{ne} = 7{,}06\,\pi r_0^2 (A^{1/3}+1)^2$ мбарн, $r_0 = 1{,}4\ 10^{-13}$;

$C_1 = 50$ Мэв, $C_2 = 0{,}58$ Мэв, $\Delta = 3{,}26$ Мэв, $a = A/10$ Мэв$^{-1}$.

Полученные соотношения можно сравнить с эмпирической формулой Левковского /I/, которая часто используется для оценки сечений /2,3/:

$$\sigma_{np} = \sigma_{ne} \exp\left\{-33\,(N-Z)/A\right\}; \quad (3)$$

Из приведённых соотношений видно, что экспериментально обнаруженная зависимость сечения от параметра $(N-Z)/A$ является следствием зависимостиот этого параметра энергии связи протона в составном ядре. Сравнение изотопической зависимости сечений, предсказываемых формулой (2) и формулой Левковского, приводится на рис. I,2. Результаты расчёта по формуле (2) согласуются с экспериментальными данными по сечению реакции (n,p) в пределах 20% отклонения для 80% рассмотренных ядер.

2. Сечение реакции $(n,2n)$.

Аналогичный подход был использован для вывода зависимости сечения $(n,2n)$ при энергии налетающего нейтрона I4 - I5 Мэв. При выводе формулы использовалось предположение о последовательном испускании двух

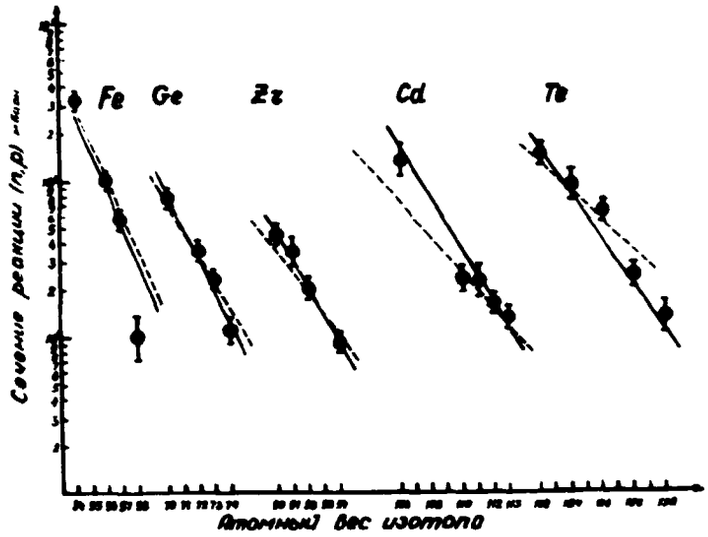

Рис.I. Изотопическая зависимость сечения реакции (n,p) в области масс ядер 50 -I20. Сплошной линией показан расчёт по формуле (2), пунктирной - по формуле Левковского.

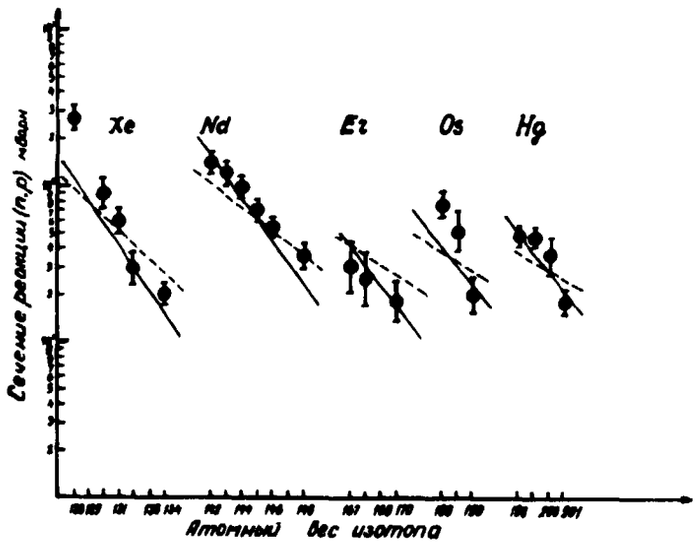

Рис.2. Изотопическая зависимость сечения реакции (n,p) в области масс ядер I20 - 200. Обозначения те же, что и на рис. I.

нейтронов составным ядром с учётом предравновесной эмиссии первого нейтрона; при этом конкуренцией заряженных частиц и гамма - квантов во втором каскаде пренебрегалось. Полученная в результате этих предположений формула имеет следующий вид:

$$\sigma_{n2n} = \sigma_{nM}\left[0{,}68 + \frac{N-Z}{A} - 5{,}2\left(47{,}4\frac{N-Z}{A} - 1\right)\exp\left\{-47{,}4\frac{N-Z}{A}\right\}\right]; \qquad (4)$$

$$\sigma_{nM} = \sigma_{ne}\left(1 - \exp\left\{-33\frac{N-Z}{A}\right\}\right);$$

Соотношение (4) по своей форме совпадает с эмпирической формулой

$$\sigma_{n2n} = \sigma_{ne}\left[1 - k\exp\left\{-m\frac{N-Z}{A}\right\}\right];$$

из работ /2,4/, если пренебречь зависимостью предэкспоненциального множителя от параметра $(N-Z)/A$. Предсказания формулы (4) согласуются с экспериментальными данными в пределах приводимой ошибки в 75% случаев. Большинство ядер, для которых соотношение (4) и (5) плохо описывают экспериментальные сечения, лежат в области значений параметра $(N-Z)/A < 0{,}1$. Более строгий расчёт с учётом конкуренции каналов (n,np), $(n,n\alpha)$, $(n,n\gamma)$ показывает, что это расхождение связано с пренебрежением вероятностью распада по каналу (n,np).

В таблице I приведены результаты расчётов для ядер с $(N-Z)/A < 0{,}1$, из которых видно, что сечение реакции (n,np) на этих ядрах сравнимо с величиной σ_{n2n}, а в некоторых случаях значительно превосходит её.

Таблица I.

Элемент	$\frac{N-Z}{A}\,10^3$	σ_{n2n} расчёт	σ_{nnp} расчёт	σ_{n2n} эксперим.
^{58}Ni	34	50	454	34,8 ± 1,7
^{54}Fe	34	3,5	469	10,7 ± 2,2
^{50}Cr	40	47	333	27,9 ± 1,8
^{46}Ti	43	39,2	254	17,8 ± 7,5
^{45}Sc	67	346	374	322 ± 25
^{63}Cu	80	549	185	501 ± 36

Предложенные нами формулы могут применяться для оценки сечений с точностью порядка экспериментальной ошибки / 10 - 15% для сечения σ_{n2n} и 20% для $\sigma_{n,p}$ /. Границы применимости этих формул вытекают из упрощений, сделанных при их выводе.

Литература

1. Э.Н. Левковский, Ядерная физика 18 (1973) 705
2. N.I. Molla and S.M. Qaim, Nucl. Phys. A283 (1977) 265
3. S. Pearlstein, Nucl. Sci. and Eng. 23 (1965) 238; Nucl. Data, A3 (1967) 327; J. Nucl. Energy 27 (1973) 81
4. W. Lu, N. Ranakumac and R.W. Pink, Phys. Rev. C1 (1970) 350

ON /n,2n/ EXCITATION FUNCTIONS

Z.T. Bödy
Institute of Experimental Physics, Kossuth University, Debrecen, Hungary

A systematics is recommended to obtain the parameters for describing /n,2n/ excitation functions by the constant temperature Weisskopf formula.

In order to describe /n,2n/ excitation functions, the formula

$$\sigma_{n,2n} = \sigma_0 \left[1-\left(1+\frac{\xi}{T}\right)e^{-\frac{\xi}{T}}\right], \quad \xi = \frac{A}{A+1} E_n + Q_{n,2n}$$

was chosen and a search was made for a systematics of the parameters σ_0 and T.

The following formulae for T were tested:

1/ The result of the simple statistical model using free Fermi gas

$T_1 = \sqrt{\frac{U}{a}}$ with a = const.A [1]

2/ The shell model approach to level densities

$T_2 = \sqrt{\frac{U}{a}}$ with a from the Newton formula [2]

3/ $T_3 = \sqrt{\frac{U}{a}}$ with a from a systematics [3]

U was taken at 14.7 MeV in each case.

4/ A new formula /see Appendix/ has also been developed as

$$T_4 = \frac{6.7}{A^{1/3} N^{1/6}} \text{ /MeV/}, \qquad \text{where } N = N_Z + N_N$$

is the number of nucleons outside the closed shells /subshells/ with the prescription that N_N can not be zero /if it would be the case then the last but one shell must be taken into account/. This formula is derived, in fact, in the spirit of Izumo's partial equilibrium statistical model [4], namely that in calculating the equilibrium system only a part of the nucleons would be taken into account. However, the way of deduction, the A and N dependence as well as the prescription for obtaining N is different from that of Izumo.

5/ Finally, the T_5= constant choice is also tested.

The $T_{exp.}$ values were extracted by least square fitting from experimental excitation functions. Two different methods were followed to do this:

a/ Each experimental excitation function was used separately, the weights were the reciprocal squares of the errors. The resulting $T_{exp.}$ values were finally averaged with equal weights omitting highly deviating values.

b/ The former method has the disadvantages that the number of experimental points and the energy intervals -- which these points lie within -- are very different for the different measurements. This introduces additional fluctuations. Therefore, to handle uniformly the data the following procedure was followed:

first -- each excitation function was normalized to the same value at 14.7 MeV;
second -- they were plotted on the same graph;
third -- an eye-guided curve was drawn through these points;
fourth -- equally spaced and an equal number of points were taken from these curves in such a way that the first point was at ≈1 MeV above the threshold;

fifth -- with these sample points and with equal weights the least square fitting for T was performed.

For testing the 1/ - 5/ suggestions for T a selected set of $T_{exp.}$ values obtained by method b/ was used /see fig./. In the figure only the temperatures T_1 and T_4 were plotted. The "order of goodness" has been found to be: T_4, T_5, T_1 and T_2. However, when considering higher mass number region only, the above sequence changes to T_5, T_4, T_2 and T_1.

T_3 could have been calculated only for a limited number of cases due to the lack of a complete a value list and the results were not too good. This is not surprising because the suggested "matching energies" were well below the ones used here [3].

Because there is a belief [3] that the value of the a parameter depends rather on neutron than on proton number, the formula for T_4 was tested also by using N_N instead of $N=N_Z+N_N$. This improves the fit in the higher mass region /but its quality still does not surpasses that of T_5 here/ and makes it worse for $A \lesssim 120$. So, this is in concordance with the above expectation that the level density parameter depends mostly on neutron number, at least for heavier nuclei, but shows the importance of proton shells for $A \lesssim 120$. Here, being the neutron excess not so high, proton single particle states, too, would play a role in populating the neighbourhood of the Fermi level.

Owing to the fact that mostly the same /odd-even/ type of nuclei provided the data for the selected set of $T_{exp.}$ values, no odd-even effects were taken into account. If one wants to take this into correction he could use approximately

$$T_{even-even} = T_{odd-even}\left(1+0.37A^{-1/2}\right) \qquad \text{and}$$

$$T_{odd-odd} = T_{odd-even}\left(1-0.37A^{-1/2}\right).$$

Being only a few percent in most cases, this correction is neglected in calculating the temperatures for the figure, but -- in fact -- it generally improves the fit with experimental data.

So, the use of

$$T_4 \quad \text{for } 20 \lesssim A \lesssim 120, \text{ and}$$

$$T_5 = 1.16 \quad \text{for } 120 < A \lesssim 200$$

can be recommended for odd-even nuclei /and also the use of the correction mentioned for the others/, in such cases when no experimental values are available.

Neither of these formulae can reproduce some exceptional temperetures, e.g. that for ^{14}N, ^{19}F, ^{64}Zn, ^{204}Pb which nuclides are near to closed shells.

For calculating σ_0 the use of $\sigma_{n,2n}$ values at 14.7 MeV [5] and the T values obtained before could be recommended.

A preliminary test was also performed for the investigation of the formula

$$\sigma_{n,2n} = \sigma_0\left[1 - \frac{B(\eta)}{B(1)}\right]$$

with $B(\eta) = \sum_{l=0}^{n} \binom{n}{l} \frac{\eta^{2l+2}}{2l+2}\left(\frac{\eta^{2l+3}}{2l+3} + 1 - \eta\right)$ and $\eta = \frac{|Q_{n,2n}|}{\varepsilon}$

obtained as a statistical equilibrium limit in pre-equilibrium formalism [7].

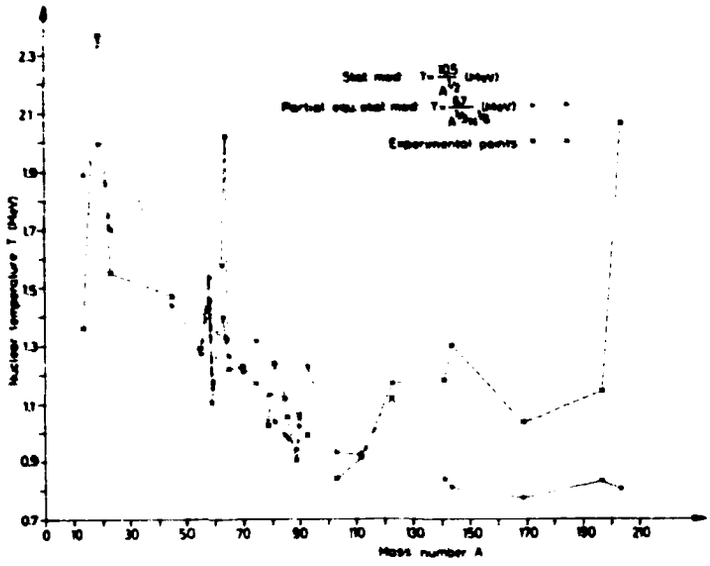

The parameter n here is in close relation with the nuclear temperature, it is approximately a linear function of 1/T. It seems that this formula with fitted σ_0 and n can not be distinguished from the Weisskopf formula within experimental errors.

Appendix

In the case of a strongly degenerate nonrelativistic and non-interacting Fermi gas [6] one obtains for the total energy

$$E=E_0\left[1+\frac{5\pi^2}{12}\left(\frac{kT}{E_F}\right)^2+\ldots\right],$$

where the E_F Fermi energy

$$E_F=\frac{1}{8}\left(\frac{3}{\pi}\right)^{2/3}\frac{h^2}{m}\left(\frac{N}{V}\right)^{2/3} \qquad \text{and } E_0=\frac{3}{5}NE_F$$

being N the number of particles and $V=\frac{4\pi}{3}r_0^3A$ is the nuclear volume. Introducing the excitation energy $U=E-E_0$ one obtaines

$$kT\sim\frac{\sqrt{U}}{A^{1/3}N^{1/6}}$$

If no degrees of freedom are supposed to be frozen in, then N can be identified with A and thus the ordinary statistical model result will follow

$$kT\sim\frac{\sqrt{U}}{A^{1/2}}$$

References

[1] P.Marmier, E.Sheldon: Physics of Nuclei and Particles, Vol.II,Acad.Press 1970
[2] T.D.Newton, Can.J. Phys. 34 /1956/ 804
[3] G. Reffo: Parameter systematics for statistical theory calculations of neutron reaction cross sections, IAEA Winter Courses on Nucl.Phys. and Reactors, Part I., SMR/43-17 ICTP, Trieste, 1978 /Unpublished/
[4] K.Izumo, Partial Equilibrium Statistical Model for Nuclear Reactions I.N.S.J. 59, 1963 and Nucl.Phys. 62 /1965/ 673.
[5] Z.T. Bödy, J. Csikai, Atomic Energy Rev. 11 /1973/ 153, and Z.T. Bödy, INDC /HUN/-10, Vienna, 1973
[6] P. Gombás, D. Kisdi: An Introduction to the Theoretical Physics, Vol.II. Akadémiai Kiadó Budapest, 1971 /in Hungarian/
[7] To be published in ATOMKI Közl.

ВОПРОСЫ ТЕОРИИ НЕЙТРОННОФИЗИЧЕСКОГО ЭКСПЕРИМЕНТА

В.Н. Дунин
Радиевый институт им. Хлопина, Ленинград, СССР

Необходимость точных расчетов параметров ядернофизических устройств привела в последнее время к заметному росту требований к точности и достоверности ядерных данных [I]. Как известно, (например [2]) расчеты, проводимые с использованием различных библиотек не обеспечивают необходимой точности. Проводимые корректировки данных по результатам интегральных экспериментов позволяют повысить точность предсказания параметров до необходимого уровня. Однако наличие погрешностей и приближений расчетной модели и другие причины неадекватности эксперимента и расчета делают задачу корректировки внутренне противоречивой, а результаты - всегда до некоторой степени формальными [I, 2]. Как показывает анализ, основную погрешность в значения ядернофизических констант (ЯФК) вносит неопределенность вводимых поправок. Повышение точности поправок связано с увеличением их количества и требует полного рассмотрения процесса получения экспериментальных данных и их связи с измеряемыми ЯФК. Кроме введения поправок, важным моментом при определении ЯФК является оценка ковариационной матрицы результата [2, 3]. Такая оценка может быть не простой ввиду сложного и не всегда явного характера поправок и способов их учета. Поэтому следуя [4], представляется целесообразным описать искажения экспериментальных результатов с единой точки зрения, рассматривая задачу извлечения значений ЯФК, как обратную задачу теории переноса излучения. Такой подход может оказаться полезным при планировании экспериментов по уточнению ЯФК с учетом корреляционных свойств экспериментальных методик [5].

Большинство экспериментов по измерению ЯФК описывается системой уравнений (I).

$$L_i F^i_{(x)} = S^i_{(x)} \qquad (1а)$$

$$S^i_{(x)} = \sum_j \left(\Sigma^{j\to i}_{(x)} , F^j_{(x)} \right) \qquad (1б)$$

$$A\left\{ \left(F^k_{(x)} , \Sigma_{(x)} \right) \right\} = \Phi_{(x)} \qquad (1в)$$

Здесь (Iа)-уравнения переноса излучения типа i, (Iб)-уравнение описывающее рождение излучения типа i, уравнение (Iв) связывает свойства детектора (оператор A) и измеряемое значение ЯФК ($\Sigma_{(x)}$) с показаниями детектора $\Phi_{(x)}$. Так как для определения операторов системы (I) привлекается большое количество оцененных ранее констант, вновь получаемые ЯФК уже не будут независимыми и следует оценивать ковариационные свойства ЯФК. Отметим, что интегральное уравнение (Iв) является некорректным [6], кроме того в системе (I) присутствует также в общем случае некорректное уравнение переноса (Iа). Таким образом решение обратной задачи (I) требует, вообще говоря, применения методов регуляризации [6, 7].

Можно выделить два больших класса обратных задач. Задачи первого типа (нелинейные) характеризуются тем, что неизвестные параметры входят не только в уравнение (Iв). Ко второму типу (линейные задачи) отнесем задачи, в которых уравнения (Iа) и (Iб) полностью определены априорной информацией.

Из физических соображений следует вывод о существовании решения системы (I). В тоже время так как система (I) может не быть полностью адекватна условиям эксперимента, и $\Phi_{(x)}$ известна с ошибкой, может не существовать решения обратной задачи в обычном смысле. Согласно [6] будем искать обобщенное решение $\Sigma'_{(x)}$ обратной задачи как

$$\varphi(\Sigma') = \inf\left\{ \| \Phi_{(x)} - \Phi^{э}_{(x)} \|^2 : \Sigma_{(x)} \in U \right\} \qquad (2)$$

Здесь $\Phi_{(x)}$ вычисленные показания детектора, $\Phi^{э}_{(x)}$ экспериментальные показания. Область определения Σ, U задается классом физически допустимых значений и может быть дополнительно ограничена априорной информацией. Определение решения с помощью соотношения (2) эквивалентно некоторому методу регуляризации [7]. Для поиска экстремума (2) можно рекомендовать метод стохастического квазиградиента [8]. Это вызвано тем, что для решения уравнения переноса в условиях произвольной геометрии эксперимента наиболее удобно применять метод Монте-Карло, статистическая природа результатов которого делает невозможным точное вычисление функции цели и ее градиента, что не влияет на результаты поиска методом стохастического квазиградиента. Как можно видеть, линейные задачи сводятся к интегральным уравнениям, которые после дискретизации имеют вид

$$\sum_j R_{ij} \Sigma_j = \Phi_i \qquad (3)$$

При решении (3) применяют различные методы [9, IO, 7, 8], основанные на формуле (2) или аналогичных соотношениях [7].

Корреляционные свойства ЯФК удобно определить с помощью коэффициентов чувствительности S, вводимых как

$$\delta \Sigma = \sum_j S_j \, \delta \sigma_j$$

Тогда ковариационная матрица будет

$$\varepsilon = S^T \varepsilon_\sigma S$$

и коэффициент корреляции

$$R = \varepsilon / (D(\sigma_i)\,(S^T D(\sigma) S))^{1/2}$$

Для вычисления S можно применять различные методы: I. конечноразностный метод, 2. формулу

$$S_j = \frac{\partial \Sigma}{\partial \sigma_j} + \left(\frac{\partial \Sigma}{\partial F}, \frac{\partial F}{\partial \sigma_j} \right)$$

где $\frac{\partial F}{\partial \sigma_j}$ удовлетворяют уравнению переноса вида

$$L \frac{\partial F}{\partial \sigma_i} = \left(\frac{\partial S}{\partial \sigma_i} - \frac{\partial L}{\partial \sigma_i} F \right)$$

производные $\frac{\partial F}{\partial \sigma_i}$ можно вычислять одновременно с определением потока F методам работ [II],

3. с помощью теории возмущений [I2]

$$S_j = \frac{\partial \Sigma}{\partial \sigma_j} + \left(F^*, \frac{\partial S}{\partial \sigma_j} \right) - \left(F^*, \frac{\partial L}{\partial \sigma_j} F \right)$$

где $L^* F^* = \frac{\partial \Sigma}{\partial F}$

Зная коэффициенты S с помощью методов работы [5] можно решать экстремальные задачи планирования дифференциальных экспериментов.

Описанная математическая схема нейтронно-физического эксперимента и методы решения обратных задач теории переноса излучения были использованы при составлении пакета прикладных программ TEST для ЭВМ БЭСМ-6 для обработки экспериментальной информации с целью уточненного определения ЯФК в экспериментах проводимых в Радиевом институте им. В.Г. Хлопина г. Ленинград и Техническом университете г. Дрезден. В пакете TEST для решения некорректных уравнений [3] линейных обратных задач используется метод статистической регуляризации [10], который заключается в том, что дополнительная информация о решении, сообщающая свойство устойчивости вводится в виде априорного распределения вероятности некоторого функционала от решения (например гладкости $\varphi = (\frac{\partial^2 \Sigma}{\partial x^2}, \frac{\partial^2 \Sigma}{\partial x^2})$ или ограниченности $\varphi = (\Sigma, \Sigma)$).

Пакет TEST был использован при решении таких задач как определение:

1. сечений неупругого рассеяния ряда элементов методом времени пролета,
2. сечений деления нейтронами 14,7 МэВ и нейтронами делительного спектра,
3. множественности мгновенных нейтронов деления,
4. спектра нейтронов деления ^{252}Cf и
5. сечений и положений уровней неупругого рассеяния делящихся изотопов.

Литература

[1] Усачев Л.Н., Nuclear data for reactors, Paris 1966, Proc. conf., V. 1, Vienna, IAEA, 1967, p. 310

[2] Ваньков А.А., Воропаев А.И., Юрова Л.Н., Анализ реакторнофизического эксперимента, М., Атомиздат, (1977)

[3] Усачев Л.Н., Ядерные константы, вып. 20, С. 3-12, (1975)

[4] Марчук Г.И., ДАН СССР, т. 156, № 3, (1963)

[5] Бобков Ю.Г., Манохин В.Н., Усачев Л.Н., Ядер. конст. вып. 27, с.3-8,(1977)

[6] Тихонов А.Н., Арсенин В.Я., Методы решения некорректных задач, М., Наука, (1974)

[7] Иванов В.К., Васин В.В., Танана В.П., Теория линейных некорректных задач и ее приложения, М., Наука, (1978)

[8] Ермольев Ю.М., Методы стохастического программирования, М., Наука. (1976)

[9] Ваньков А.А., Ядерные константы, вып. 16, с. 11-19 (1974)
Ваньков А.А., Воропаев А.И., Тараско М.З., Ядерные константы, вып. 21, с. 32-48 (1976)

[10] Турчин В.Ф., Козлов В.П., Малкевич М.С., УФН, т. 102, вып.3, с. 345-386, (1970)

[11] Золотухин В.Г. и др., Прохождение излучений через неоднородности в защите, М., Атомиздат, (1968)
Плетников Е.В., Труханов Г.Я., Ядерные константы, вып. 16, с. 106-111, (1974)

[12] Усачев Л.Н., Атомная энергия, т. 15, вып. 6, с. 472-481, (1968)

ОТНОСИТЕЛЬНЫЕ ИНТЕНСИВНОСТИ РЕНТГЕНОВСКИХ ЛУЧЕЙ К-СЕРИИ НЕКОТОРЫХ ЭЛЕМЕНТОВ С $Z = 53 - 96$

Ц. Вылов (ОИЯИ), В.М. Горожанкин (ОИЯИ), А.Н. Иванов (ВНИИМ, Ленинград), Г. Музиоль (ТУ, Дрезден), Е.А. Фролов (ВНИИМ, Ленинград), В.Г. Чумин (ОИЯИ), Г. Морнак (ТУ, Дрезден), М.Ф. Юдин (ВНИИМ, Ленинград)

С помощью Ge(Li) - и Ge- детекторов измерены относительные интенсивности рентгеновских лучей К-серии для 24 элементов с $Z = 53 - 70$, 73, 81, 82, 84, 94 и 96, а также энергий K_2-лучей для $Z = 82$, 83, 94 и 96. Полученные результаты сравниваются с расчетными данными.

С помощью разработанной нами методики [1] измерены относительные интенсивности рентгеновских лучей К-серии для 24 элементов с $Z = 53 - 70$, 73, 81, 82, 84, 94, 96. Использовались полупроводниковые детекторы со следующими характеристиками: 25 мм^2 x 5 мм Ge(энергетическое разрешение $\Delta E = 150$ эВ при $E \sim 5$ кэВ), 100 мм^2 x 7 мм Ge($\Delta E = 150$ эВ при $E \sim 5$ кэВ) и 200 мм^2 x 5 мм Ge(Li) ($\Delta E = 240$ эВ при $E \sim 5$ кэВ). Измерения проводились с учетом эффектов, искажающих форму аппаратурного спектра, а именно:

а) для снижения роли обратного рассеяния источники изготавливались на алюминиевой (18 мкм) подложке,
б) для устранения вклада самопоглощения и возбуждения флюоресценции большая часть источников приготавливалась с помощью электромагнитного масс-сепаратора (энергия внедрения ионов 25 кэВ),
в) все измерения проводились на расстоянии не более 6 см, причем более низкие измерялись на детекторах с малым диаметром, так как при этом энергетическое разрешение лучше и, кроме того, устранялись до минимума эффекты поглощения в воздухе и эффекты суммирования L_x- и K_x- лучей.

Проведены более 100 серий измерений с помощью 44 различных нуклидов. Предварительные результаты экспериментов приведены в таблице. Погрешности рассчитаны по формулам, приведенным в [1] , причем погрешность калибровки спектрометра на узком энергетическом участке не учтена.

Полученные результаты сравниваются с расчетами Скофильда [2]. На данном этапе анализа можно константировать систематическое превышение экспериментальных отношений $I_{K\alpha 2}/I_{K\alpha 1}$ над расчетными на величину ~0,6 %. Обращает на себя внимание значение $I_{K\alpha 2}/I_{K\alpha 1}$ для $Z = 82$, которое ниже расчетного на величину ~1,4 %. Дополнительные эксперименты требуют также данные с $Z = 94$ и $Z = 96$.

В предположении E_γ (411,8 - ^{198}Hg) = 411,794 ± 0,007 кэВ измерены также энергии K_x - лучей для $Z = 82$, 83, 94 и 96. В частности, получены следующие результаты: $E_{K\alpha 2}(Z = 82) = 72{,}806$ (4), $E_{K\alpha 1}(Z = 82) = 74{,}972$ (4), $E_{K\alpha 2}(Z = 83) = 74{,}818$ (2), $E_{K\alpha 1}(Z = 83) = 77{,}110$ (2), $E_{K\alpha 2}(Z = 94) = 99{,}532$ (3), $E_{K\alpha 1}(Z = 94) = 103{,}734$ (2), $E_{K\alpha 2}(Z = 96) = 104{,}573$ (2) и $E_{K\alpha 1}(Z = 96) = 105{,}255$ (2).

Таблица: Экспериментальные данные об относительных интенсивностей рентгеновских лучей K-серии.

Z	$K_{\alpha_2} / K_{\alpha_1}$	$K_{\beta_1'} / K_{\alpha_1}$	$K_{\beta_2'} / K_{\alpha_1}$	K_{β} / K_{α}
53	0,5408 ± 0,0030	0,2823 ± 0,0017	0,0632 ± 0,0005	0,2242 ± 0,0014
54	0,5430 ± 0,0014	0,2864 ± 0,0007	0,0669 ± 0,0003	0,2290 ± 0,0005
55	0,5452 ± 0,0023	0,2920 ± 0,0070	0,0707 ± 0,0023	0,2350 ± 0,0070
56	0,5459 ± 0,0021	0,2926 ± 0,0010	0,0745 ± 0,0005	0,2378 ± 0,0007
57	0,5504 ± 0,0015	0,2995 ± 0,0010	0,0772 ± 0,0005	0,2429 ± 0,0007
58	0,5477 ± 0,0032	0,2992 ± 0,0017	0,0771 ± 0,0007	0,2432 ± 0,0012
59	0,5527 ± 0,0026	0,2975 ± 0,0008	0,0754 ± 0,0009	0,2400 ± 0,0014
60	0,5532 ± 0,0020	0,3032 ± 0,0011	0,0785 ± 0,0005	0,2458 ± 0,0008
61	0,5554 ± 0,0010	0,3016 ± 0,0018	0,0760 ± 0,0004	0,2425 ± 0,0014
62	0,5577 ± 0,0020	0,3059 ± 0,0009	0,0784 ± 0,0004	0,2467 ± 0,0007
63	0,5613 ± 0,0031	0,3127 ± 0,0034	0,0809 ± 0,0014	0,2506 ± 0,0031
64	0,5633 ± 0,0030	0,3121 ± 0,0021	0,0810 ± 0,0006	0,2507 ± 0,0013
65	0,5637 ± 0,0010	0,3102 ± 0,0013	0,0796 ± 0,0004	0,2490 ± 0,0012
66	0,5630 ± 0,0015	0,3127 ± 0,0027	0,0810 ± 0,0009	0,2516 ± 0,0020
67	0,5654 ± 0,0021	0,3207 ± 0,0013	0,0838 ± 0,0006	0,2584 ± 0,0009
68	0,5660 ± 0,0028	0,3219 ± 0,0020	0,0846 ± 0,0010	0,2599 ± 0,0015
69	0,5724 ± 0,0036	0,3198 ± 0,0019	0,0848 ± 0,0009	0,2568 ± 0,0017
70	0,5745 ± 0,0022	0,3211 ± 0,0020	0,0840 ± 0,0005	0,2589 ± 0,0014
73	0,5780 ± 0,0070	0,3242 ± 0,0030	0,0888 ± 0,0010	0,2618 ± 0,0020
81	0,5960 ± 0,0033	0,3440 ± 0,0040	0,1026 ± 0,0009	0,2793 ± 0,0025
82	0,5870 ± 0,0050	0,3450 ± 0,0070	0,1033 ± 0,0009	0,2830 ± 0,0040
84	0,5960 ± 0,0080	0,3530 ± 0,0060	0,1109 ± 0,0014	0,2900 ± 0,0060
94	0,6160 ± 0,0070	0,3660 ± 0,0050	0,1335 ± 0,0018	0,3109 ± 0,0035
96	0,6122 ± 0,0019	0,3936 ± 0,0029	0,1411 ± 0,0090	0,3310 ± 0,0120

Литература

[1] Н. Зилов, ОИЯИ, Р6-10417, Дубна, 1977
[2] J.H. Scofield, Phys. Rev. A9 (1974) 1041

STUDY OF NEUTRON INDUCED REACTIONS AT THE INSTITUT FÜR RADIUMFORSCHUNG UND KERNPHYSIK DER ÖSTERREICHISCHEN AKADEMIE DER WISSENSCHAFTEN

H. Vonach

Institut für Radiumforschung und Kernphysik der Österreichischen Akademie der Wissenschaften, Wien

A survey is given of our present program for studying 14 MeV neutron induced reactions consisting of measurements of elastic and inelastic neutron scattering cross-sections, measurements of energy and angular distributions of protons and α-particles from (n,p) and (n,α) reactions, comparison of the results with coupled channel and statistical model calculations and cross-section evaluations for some important threshold reactions.

1) Measurement of differential elastic and inelastic scattering cross-sections with good energy resolution (6 m flight path)

G. Winkler, K. Hansjakob, G. Staffel

In order to study elastic scattering of 14 MeV neutrons with clear separation from all inelastic events and also for measuring the high energy part of the inelastic neutron spectra with good energy resolution a time of flight system using about 7 m flight path has been set up at our accelerator as shown in fig. 1.

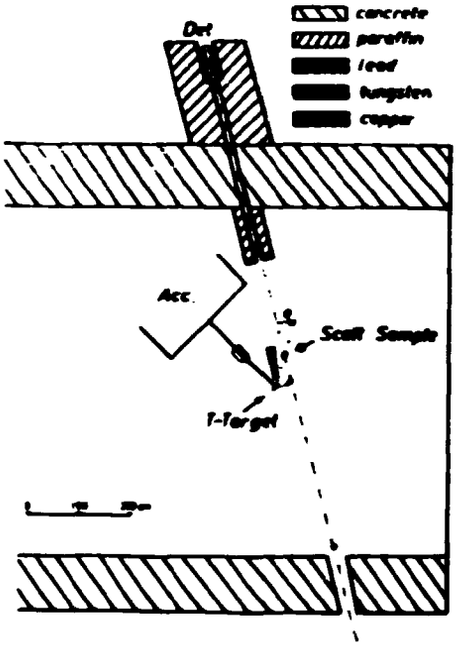

Fig.1. Experimental set up for measurement of differential elastic and inelastic scattering cross-sections for 14 MeV neutrons with good energy resolution

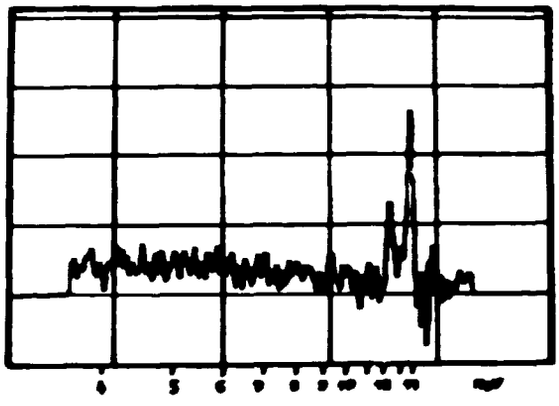

Fig.2. Time-of-flight spectrum from 14 MeV neutron scattering on Chromium at 115°. Background subtracted, Chromium sample 40 x 120 x 4 mm, measuring time 300 min 665 counts in elastic peaks.

Pulsed 14 MeV neutrons (pulse width 1-2 nsec) are produced by means of a 250 keV d.c. accelerator by means of the T(d,n) reaction. Neutrons scattered into the

direction of the collimator are detected by means of a 5" ø, 2" thick NE 213 scintillator. The scattering angle is determined by the sample position which is varied along the collimator axis by means of a precision laser-based positioning system. A shadow bar is used to shield the collimator entrance against direct source neutrons. The efficiency calibration of the neutron detector is done by measuring the scattering on hydrogen in a polyethylene sample using the well-known n-p cross-section.

Using this system scattering of 14 MeV neutrons for both natural Barium and Chromium has been investigated in the angular range 20° - 130° in 5° steps with an energy resolution of about 0.5 MeV at 14 MeV. Fig. 2 shows a typical time of flight spectrum. As apparent from the figure the scattering to the first 2^{+} level of ^{52}Cr can be clearly resolved, likewise this was possible for the first 2^{+} level in ^{138}Ba.

Data analysis is still in progress, cross-sections will be available within a few months, the overall accuracy is expected to be about 15%. For Barium, which is of technical importance as shielding material, this is the first measurement of elastic and inelastic neutron scattering at 14 MeV. For Chromium, which is even more important technically up to now only one elastic scattering measurement existed at 14 MeV /1/ which according to our preliminary analysis is in good agreement with the present results.

2) Measurement of the angle-integrated secondary neutron spectra from interaction of 14 MeV neutrons with various nuclei for secondary neutron energies 0.3 - 4 MeV

A. Chalupka, H. Vonach, F. Wenninger

The high energy parts (E_n > 2 MeV) of the secondary neutron spectra from the interaction of 14 MeV neutrons with nuclei are rather well known at present for most materials of practical interest, a large part of this information being due to the work of Prof. Seeliger and co-workers /2/. The low energy parts of the secondary spectra, however, are rather poorly known in most cases due to experimental difficulties especially with n-γ discrimination background and multiple scattering at low secondary neutron energies. Therefore an experimental program to determine those spectra for a large number of elements has been initiated last year. Fig. 3 shows the experimental set up. Pulsed neutrons are produced by means of the 250 keV Cockroft-Walton accelerator of the institute in an extremely small low mass TiT target construction. The scattering samples (hollow cylinders) surrounded the target and the neutron time of flight spectrum is measured at a distance of 1 m by means of a NE 213 liquid scintillator . The scintillator is operated at a very low threshold (equivalent to about 200 keV proton recoil energy) and a pulse-shape (PSD) method is used to discriminate between neutrons and photons. As reported earlier /3/ the application of the PSD method is possible down to the very low threshold. Time of flight, recoil proton energy and pulse shape detector output for each event is recorded on disc in order to enable optimal off-line analysis with respect to n-γ discrimination and background reduction. Both the direct neutrons and the neutrons from inelastic scattering and (n,2n) reactions are detected simultaneously in the NE 213 detector and thus absolute production spectra can be derived directly from the measured time of flight spectra, the target sample geometry and the energy dependence of the detector effi-

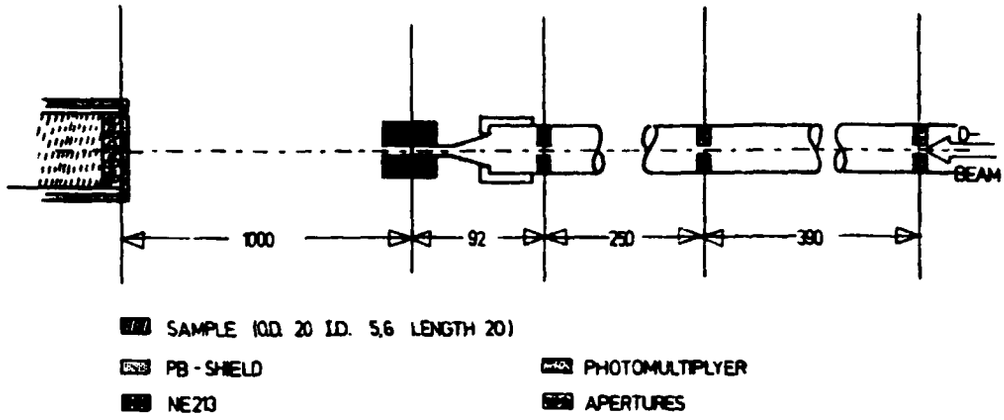

Fig. 3. Experimental set up for measurement of the angle-integrated low energy parts of the secondary neutron spectra from the interaction of 14 MeV neutrons with nuclei (Tritium target is located in the center of the scattering sample)

ciency. The latter is determined at low energies (0.3 - 4 MeV) by means of a ^{252}Cf calibration measurement, whereby the T:T target is replaced by a fast ionization chamber containing a ^{252}Cf source. The special low-mass chamber developped in this way exhibits a time resolution of about 0.5 nsec and an efficiency of about 99% for detection of fission products. For 14 MeV neutrons the scintillator is calibrated by means of the well-known Al(n,α)^{24}Na activation cross-sections. Neutron spectra measurements of the described kind have very recently been performed on Al, Ti, Cr, Fe, Ni, Cu, Zn, Zr, Nb, Mo, Ag, Sn, Ba, W, Ta, An, Pb and Bi. Data analysis has just started. As an example of the data, fig. 4 shows the background-subtracted time of flight spectrum for the ^{93}Nb(n,n') and ^{93}Nb(n,2n) reactions from a preliminary data analysis. It is hoped that reliable cross-sections with 1σ uncertainties of 5-10% can be extracted from the data over most of the investigated energy range.

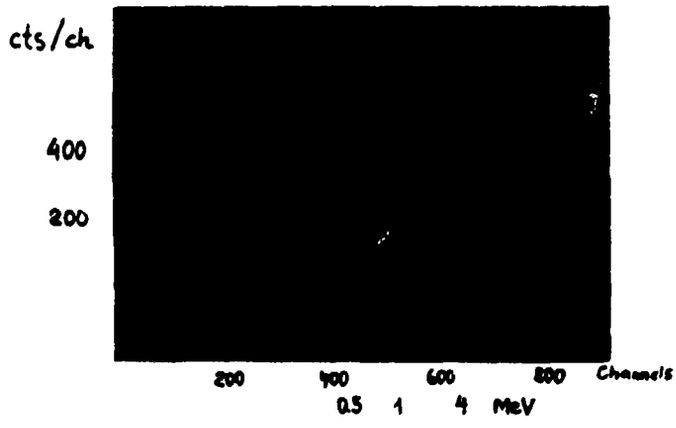

Fig. 4. Secondary neutron spectrum from the interaction of 14 MeV neutrons, with ^{93}Nb (background subtracted, Nb sample hollow cylinder 20 mm o.d., 5 mm i.d., 20 mm high, measuring time 1 h detector threshold approximately 30 keV electron energy)

3) Investigation of the energy and angular distributions of protons and α-particles from (n,p) and (n,α) reactions.

C. Derndorfer, R. Fischer, P. Hille, G. Stengl, H. Vonach

A new combination of a small multiwire proportional counter and a scintillator has been constructed, which allows simultaneously the measurement of the energy and angular distributions of charged particles of neutron induced nuclear reacions and the determination of the background.

In a cylindrical chamber (20 cm diameter, 12 cm height) (fig. 5) 32 sense wires, 32 shielding wires and a grid of 64 wires are arranged around a central scintillator. The thin target foil is laid in a semicircle outside the sense wires. A graded shield, consisting of a graphit ring and a gold foil is put behind the target foil as well as on the other half of the chamber to reduce background from the construction materials.

The origin of a charged particle is traced by a coincidence between the central crystal and one of the sense wires. As the direction of the incoming neutrons is known, the reaction angle can be derived. On the average the angular resolution is 13 degrees at FWHM, which is sufficient for experiments studying compound and precompound reactions.

The energy resolution is mainly determined by the thickness of the target, the pressure of the filling gas, the distribution of path length in the chamber and the properties of the scintillator. The resolution varies between 0.5 and 1 MeV depending on the energy the type of the particle and the target thickness necessary for sufficient count-rate.

The central scintillator is a CsJ(Tl) crystal (1 inch diameter, 1 mm height) and has good pulse shape properties for particle identification. Charged particles up to an energy of 20 MeV are stopped.

The proportional chamber is operated with a mixture of 95% argon and 5% CO_2 at a pressure of approximately 100 mbar and uses 20 μ gold coaled tungsten wires as sense wires. The chamber is operated at a voltage of + 650 volts, the field on the wire therefore is approximately 1.0×10^5 V/cm and the gas amplification approximately 1500.

The chamber has been tested with an Am-241 foil in the place of the target foil. The outputs of 16 wires were connected to a charge sensitive preamplifier and an energy resolution of the proportional counter (in coincidence with the scintillator) of 15% was obtained in accordance with calculations.

Fig. 6 shows the block diagram of the associated electronics. Each wire produces both an analog and a logical signal (Time-out). The logical signals are fed to an address logic which transforms them to 5 bit address characterizing the different sense wires, simultaneously they are used as timing signals in a fast coincidence with the photomultiplier anode signals to identify the coincidences between the proportional counter and the scintillator pulses.

The analog pulses from the proportional counters are at first combined in 4 summing amplifiers summing 8 preamplifier outputs each. The output of these summing amplifier are fed into linear gates, which are opened in case of coincidence with the scintillator and eventually all proportional counter signals are combined in a final summing amplifier. By means of this arrangement 4 times higher counting rates can be admitted to the proportional counters than in case of direct summing of all proportional counter outputs (DE signals) in one summing

amplifier. The CsJ scintillator is used to produce a timing signal, an energy (E) signal and a pulse-shape-signal (PSI) which allows to discriminate between photon, proton and α-particles.

Finally for each event the E, PS and DE signals and the wire address are stored sequentially in an on-line computer enabling simultaneous measurement of the energy and angular distribution of all kinds of charged particles emitted by the investigated target. Particle identification can be done both by means of PSD information in the CsI scintillator and the $\frac{dE}{dx}$ information of the proportional counters.

The counter with the complete electronic system is non being tested with α-particles and will be used for studies of the (n,p), (n,d) and (n,α) reactions on ^{50}Cr and ^{93}Nb in the first half of next year.

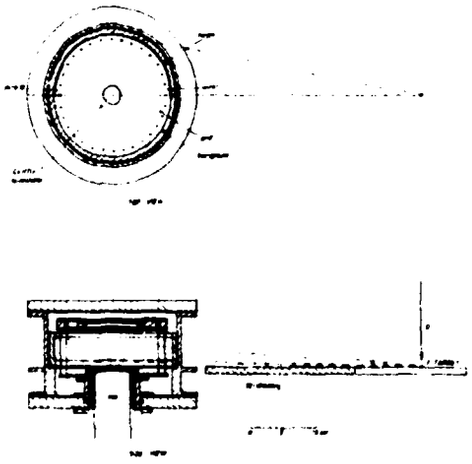

Fig. 5. Multiwire proportional-counter-scintillator-system for study of (n, charged particle) spectra and angular distributions.

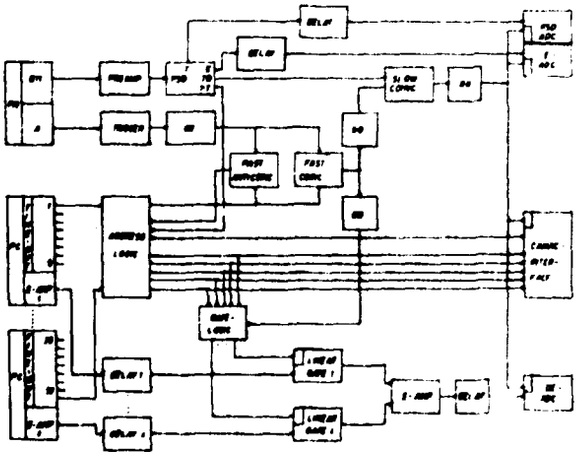

Fig. 6. Block diagram of the electronics for the multi-wire proportional-counter-scintillator-system.

4) Comparison of the results of 1-3 with nuclear reaction calculations including coupled channel calculations preequilibrium and statistical model

B. Strohmaier, M. Uhl

For comparison of an neutron cross-section measurement and for cross-section predictions in general the computer code STAPRE /4/ based on the preequilibrium and equilibrium model of nuclear reactions has been developped.
This code is designed to calculate cross-sections for particle induced nuclear reactions with several emitted particles and γ-rays under the assumption of sequential evaporation.
Each evaporation step is treated within the framework of the statistical model of nuclear reactions with consideration of spin and parity conservation. For the evaporation of the first particle preequilibrium emission is taken into account . For a specified sequence of up to six emitted particles the following quantities can be obtained for all nuclei involved in the cascade.

1) activation cross-sections
2) population of isomeric states
3) production cross-sections for gamma-rays from low-lying excited levels
4) angle integrated energy spectra for all emitted particles and γ-rays.

Recently the program has been extended to include fission. In addition the coupled channel code JUPITOR has been set into operation at the Vienna University computer and is used to calculate cross-sections for elastic scattering and inelastic neutron scattering to low lying levels and to generate the neutron transmission coefficients needed as input for the STAPRE program.
Using these code complete evaluations of all neutron cross-sections on Barium /5/ and Phosphorus /6/ have been performed, demonstrating its ability to fit a large variety of different cross-section data simultaneously with one set of parameters.
At present calculations concentrate on neutron, proton and α-spectra from those (nn'), (n,2n), (n,p) and (n,α) reactions which are simultaneously studied experimentally (see section 1-3) and on calculations of excitation functions in connection with our evaluation work on dosimetry reactions (see section 5).

5) Cross-section evaluations for neutron dosimetry reactions

S. Tagesen, H. Vonach

In order to fullfill an increasing demand of the users of evaluated neutron cross-sections, an evaluation program for threshold neutron reactions has been started which includes also both calculations of the uncertainties of the evaluated cross-sections and of the correlation coefficient between these cross-section uncertainties. In this year evaluations of the $^{24}Mg(n,p)$, $^{63}Cu(n,2n)$, $^{64}Zn(n,p)$ and $^{90}Zr(n,2n)$ reactions have been completed /7/, evaluation of the $^{103}Rh(nn')^{103}Rh^{m}$, $^{31}P(n,p)$, $^{19}F(n,2n)$, $^{93}Nb(nn')^{93}Nb^{m}$ and $^{27}Al(n,\alpha)$ reactions will be performed next year.
As an example of this work fig. 7 shows the results of our $^{63}Cu(n,2n)$ evaluation in comparison with previous evaluations /8, 9/.

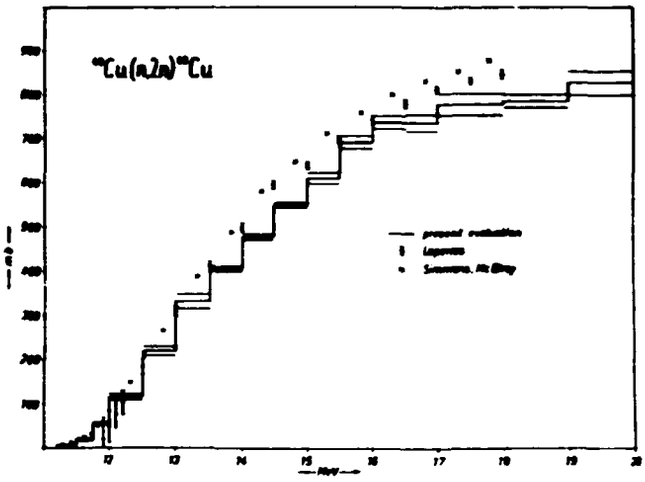

Fig. 7. Comparison of the present evaluation with the previous evaluations of Lapenas /8/ McElroy and Simmons /9/

References

/1/ P. Stelson et al., Nucl. Phys. 68 (1965)

/2/ D. Hermsdorf et al., 97 ZfK 277(U), INDC (GDR)-2/L 1975

/3/ A. Chalupka, G. Stengl, M.R. Maier and P. Sperr, Nucl. Instr. Meth. 150 (1978) 209

/4/ M. Uhl, B. Strohmaier, Proc. Winter Course on Nuclear Physics and Reactors, Trieste 1978 in press

/5/ B. Strohmaier and M. Uhl, Nucl. Sci. Eng. 65 (1978)

/6/ B. Strohmaier, Proc. Int. Conf. on Neutron Cross-Sections Harwell 1978, in press

/7/ S. Tagesen, H. Vonach and B. Strohmaier, Proc. Int. Conf. on Neutron Cross Sections, Harwell 1978 in press and Physics Data, ZAED in press

/8/ A.A. Lapenas et al., Izmerenie Spektrov Nejtronov Aktivycionnym Metodom, Zinatne, Riga, USSR, 1975 (1975)

/9/ R.L. Simmons and W.L. Mc Elroy BNWL-1312 (1970)

ВРЕМЕНА ЖИЗНИ КОМПАУНД-ЯДЕР ^{236}U И ^{239}U ПРИ ЭНЕРГИИ ВОЗБУЖДЕНИЯ 6,7 - 10 МэВ

П.Е. Воротников, О.В. Груша, Ю.В. Мелков, Н.А. Морозов,
Ю.Д. Отставнов, Л.Н. Сеткина, А.Ф. Тулинов, Н.Г. Чеченин, О.А. Шишков
Институт ядерной физики Московского государственного университета,
Институт атомной энергии им. И.В. Курчатова, СССР

Методом основанным на эффекте теней, измерены времена жизни ядер ^{236}U и ^{239}U в интервалах энергии возбуждения E^* = 6,7 - 11,2 МэВ и 6,4 - 9,1 МэВ, соответственно. Полученные значения сравниваются с результатами расчетов, использующих зависимость плотности уровней $\rho(E^*)$ в модели ферми-газа в эмпирическую $\rho(E^*)$, вычисленную на основе анализа сечений (n,γ) и (n,n') реакции.

В работе [1] на основании анализа реакций $n\gamma$ и nn' был сделан вывод о возможном существовании в тяжелых ядрах при энергии возбуждения $E^* \sim 8$ МэВ фазового перехода, при котором происходит изменение зависимости плотности состояний $\rho_{комп}$ от E^*. Так как выше $E^*_{кр}$ $\rho_{комп}(E^*)$ должна была расти быстрее, чем до этой энергии, можно было ожидать замедления скорости распада, т.е. увеличения времени жизни τ компаунд-ядра по сравнению с расчетной или экстраполированной снизу величиной. Уникальную, по-видимому, возможность проверки этого явления представляет метод измерения с помощью эффекта теней, наблюдающегося в ядерных реакциях на монокристаллических мишенях [2]. Метод основан на том, что форма углового распределения заряженных продуктов ядерной реакции в окрестности кристаллографической оси зависит от среднего смещения компаунд-ядра из узла решетки кристалла под действием импульса налетающей частицы, т.е. в конечном итоге от времени жизни компаунд-ядра. Нами были предприняты такие измерения с использованием монокристаллов $^{238}UO_2$ и $^{235}UO_2$.

2. Монокристаллы UO_2 изготовлялись электролитическим разложением уранилхлорида из его расплава в хлориде калия и свинца при контролируемой величине тока на единицу поверхности растущего фронта кристаллов. В качестве источников моноэнергетических нейтронов, бомбардирующих монокристалл UO_2(1) (рис. 1), использовались реакции $^7Li(p,n)$, $^3H(p,n)$ и $^2H(d,n)$. Регистрация осколков деления стеклянными детекторами (2) производилась в окрестности двух кристаллографических осей III, одна из которых составляла угол 10^0 с направлением пучка (3) налетающих заряженных частиц, а другой угол 80^0. На основе измеренного распределения плотности треков на стеклах-детекторах строились профили теней от названных осей, два из которых приведены на рис. 2. Видно, что тени от двух осей, отличающихся лишь величиной нормальной составляющей импульса компаунд-ядра, имеют различную форму и разные значения относительной интенсивности частиц в минимуме χ. Разность $\Delta\chi = \chi_{min}(80^0) - \chi_{min}(10^0)$ представляет собой наблюдаемый эффект конечного времени жизни компаунд-ядра. Эта величина, а также соответствующие изменения "площади сечения" и "объема" теневой лунки были использованы для определения среднего времени жизни τ [3].

3. Результаты измерений $\tau_{комп}$ для ядер ^{239}U и ^{236}U приведены на рис. 3 и 4, соответственно. На этих же рисунках показаны результаты, полученные при охлаждении монокристалла до температуры жидкого азота нами (темные точки) и группой физиков в Орхусе, Дания (треугольники) [4, 5]. Видно, что тепловое движение атомов кристалла не сильно влияет на результаты. Сплошными линиями на рисунках показаны зависимости

$$\tau(E^*) = \hbar / \Gamma(E^*)$$

где полная ширина распада Г вычислена по Хаузеру и Фешбаху [6] с использованием ферми-газовых ($2\Delta_0$ = I,I МэВ, a = 25,7, жирная линия) и эмпирических (тонкая линия) $\rho(E^*)$. Эти $\rho(E^*)$ воспроизведены на рис. 5. Как следует из работы [I], для четно-четных по Z и N ядер эмпирическая $\rho(E^*)$ совпадает с ферми-газовой зависимостью, а для А-нечетных ядер существенно отличается от нее, но хорошо соответствует расчетам работы [7], результаты которой изображены на рис. 5 квадратами. Подтверждают эмпирическую $\rho(E^*)$ для А-нечетных ядер и данные по плотности резонансов этих ядер, показанные на рис. 5 точками. При малых E^* кружками обозначены $\rho(E^*)$ оцененные по прямому подсчету числа уровней в α-спектрах [8] и спектрах неупруго рассеянных нейтронов [9].

Как видно из приведенных рисунков, экспериментальные результаты согласуются с расчетом, использующим эмпирические $\rho(E^*)$ до $E^* \sim$ 2,5 МэВ для ^{239}U и $E^* \sim$0,5 МэВ для ^{236}U. При больших E^* измеренные τ_{239} и τ_{236} лежат значительно выше расчетных. В рамках статистической теории

$$\Gamma(E^*) = \hbar / \sum_k \Gamma_k(E^*) = 2\pi\rho_{комп}(E^*) / \sum_k \int |M^k_{E^*,E_{fin}}|^2 \rho^k(E_{fin})\, dE_{fin}$$

где M^k и $\rho^k(E_{fin})$ - парциальный матричный элемент и плотность конечных состояний для -того способа распада составного ядра, и такое поведение $\tau_{комп}$ можно объяснить либо изменением матричного элемента, либо изменением зависимости $\rho(E^*)$ выше $E^*_{крит}$ = 7,5 ± 0,2 МэВ. Заметим, однако, что при этих E^* ядра ^{239}U и ^{236}U распадаются со сравнимыми вероятностями двумя путями - испусканием нейтронов и делением, - причем сохраняющееся с точностью до нескольких процентов "плато" сечения деления показывает, что отношение ширин Γ_f / Γ_n для конкурирующих процессов не меняется. Если считать их независимыми, то представляется маловероятным, чтобы матричные элементы для столь разных процессов изменялись сильно и одинаково. Более вероятной причиной такого поведения (E^*) представляется соответствующее изменение $\rho_{комп}(E^*)$, общей для обеих ветвей распада.

Зависимость $\rho_c(E^*)$, позволяющая объяснить полученные результаты выше $E^* \simeq$7,5 МэВ, показана на рис. 5 штриховой линией. Изменение зависимости ρ_c, т.е. энтропии $S = \ln \rho_c$, от E^* можно трактовать как фазовый переход в ядре при $E^*_{крит} \simeq$ 7,5 МэВ. Интересно отметить, что выше этой энергии возбуждения зависимость $\rho_c(E^*)$, по-видимому, одинакова для ядер обоих типов четности по N, и относительный ход $\rho_c(E^*)$ очень близок к $\rho_c(E^*)$ для А-нечетных ядер при малых E^*. Такое объяснение, однако, требует осторожности, так как ядерная температура $T = dE^*/d\ln\rho_c(E^*)$ при переходе через $E^*_{крит}$ довольно резко уменьшается до величины ~300 КэВ. Сам этот факт и столь низкое значение T при $E^* \sim$ 8 МэВ трудно понять. Быть может, мы имеем дело лишь с некоторой имитацией этой характеристики более сложным процессом.

Другое возможное объяснение может быть связано с возбуждением при $E^* > 7,5$ МэВ некоторых новых состояний, сильно замедляющих распад ядра, например, типа гигантского резонанса. В этом случае $E^*_{крит}$ является пороговой энергией для возбуждения таких состояний. Выбор между этими возможностями может быть сделан, например, после аналогичных измерений на ^{237}Np. Можно ожидать, что появление новых состояний произойдет при таких же энергиях возбуждения, в то время как фазовый переход - при близких значениях энтропии, т.е. $\rho(E^*)$, достигаемой для нечетно-нечетного ^{238}Np при E^* примерно на I МэВ. Данные по $\sigma_{n\gamma}$ для ^{237}Np[IO] показывают как-будто, что соответствующие явления наблюдаются при $E^* \sim 6,3$ МэВ, т.е. свидетельствуют в пользу фазового перехода. Однако, более определенный ответ могут дать только прямые измерения $\tau_{ионизации}(E^*)$ для этого ядра.

Литература

[I] П.Е. Воротников, Изв. АН СССР (сер. физ.) 36. I75. (I972)

[2] А.Ф. Тулинов, ДАН СССР I62. 546. (I965)

[3] P.E. Vorotnikov et al., Nucl. Phys. A281 (1977) 295

[4] J.U. Andersen et al., Nucl. Phys. A241 (1975) 317

[5] Й.У. Андерсен, Ю.В. Меликов и др. Предв. прогр. и тезисы докладов 9 Всесоюзного совещания по физике взаимодействия заряженных частиц с кристаллами. Изд. МГУ. (I978)

[6] П.Е. Воротников, О.В. Груша и др. Предв. программа и тезисы докладов 9 Всесоюзного совещания по физике взаимодействия заряженных частиц с кристаллами. Изд. МГУ. (I978)

[7] В.Г. Соловьев, Л.А. Малов. Препринт ОИЯИ Р4-6346, (I972)

[8] В.М. Горбачев, Ю.С. Замятнин, А.А. Лбов. Основные характеристики изотопов тяжелых элементов. Атомиздат, (I975)

[9] E. Bernard, A.T.G. Fergusson et al., Nucl. Phys. 80 (1966) 46

[IO] R.J. Nagle, J.H. Landrum, M. Lindner, Proc. III. Conf. Neutr. Cross Sect. and Technology, Knoxvill. 1971

Рисунки

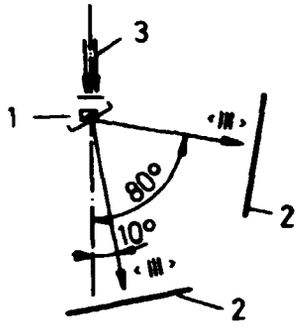

Рис.1

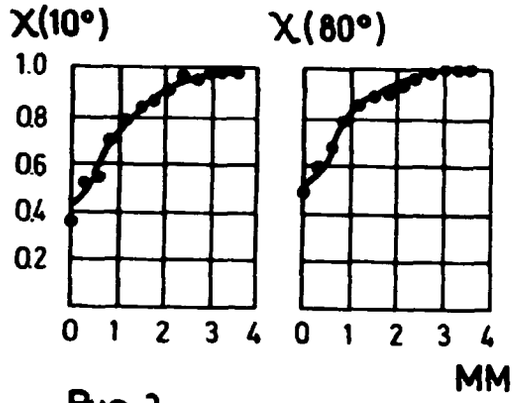

Рис. 2

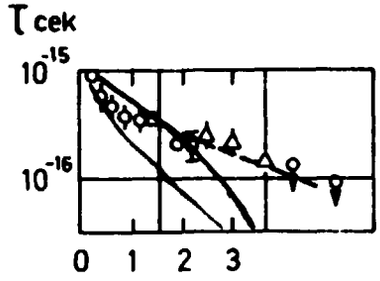

Рис.3 E_n Мэв

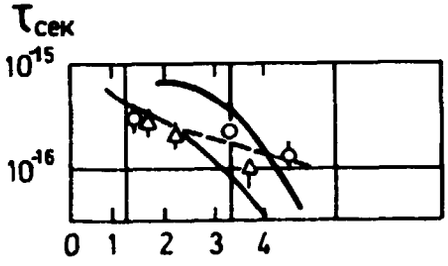

Рис. 4 E_n Мэв

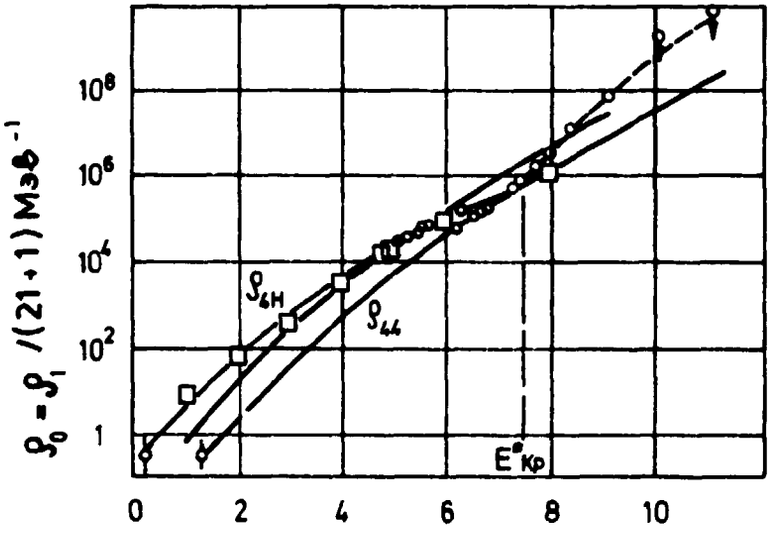

Рис. 5 E^* Мэв

ИЗОМЕРНЫЙ СДВИГ НЕЙТРОННЫХ РЕЗОНАНСОВ

К.Зайдель, А.Майстер, Д.Пабст, Л.Б.Пикельнер
Объединенный институт ядерных исследований, ЛНФ, Дубна, СССР.

На импульсном реакторе ИБР-30 методом времени пролета измерены спектры пропускания различных химических соединений урана-238. Получены предварительные данные об изомерном сдвиге нейтронного резонанса и изменении среднеквадратичного радиуса ядра.

В 1973 г. в работе [1] было предложено использовать изомерный сдвиг нейтронного резонанса для определения изменения среднеквадратичного радиуса ядра $\Delta\langle r^2\rangle$ при возбуждении ядра, обусловленном захватом нейтрона. Изомерный сдвиг уровня происходит в результате сверхтонкого электрического взаимодействия электронов с ядром. Изменение энергии нейтронного резонанса можно представить в виде

$$\Delta E_0^{IS} = \frac{1}{6\varepsilon_0} e^2 Z \Delta|\psi_e(0)|^2 \Delta\langle r^2\rangle \qquad (1)$$

где $\Delta|\psi_e(0)|^2$ – разность плотности электронов на месте ядра для двух различных химических соединений.

Сложность эксперимента по измерению изомерного сдвига обусловлена малостью ожидаемого эффекта: ΔE_0^{IS} порядка 10^{-4} эв при ширине резонанса около 10^{-1} эв. Кроме того, различие кристаллических решеток у разных химических соединений приводит к изменению формы резонанса, что необходимо учитывать при обработке. Для определения изомерного сдвига измерялось пропускание нейтронов через различные соединения урана. Схема эксперимента приведена на рис. 1. Для обеспечения постоянства экспериментальных условий измерения велись с тремя образцами, вводимыми в пучок поочередно на 5 минут. Управление и контроль в ходе измерения велись с помощью малой ЭВМ ТРА-i. В пучке постоянно находился образец из тербия, резонансы которого служили как реперные для объективного контроля спектров. На рис. 2 показан один из спектров, полученных за 10 часов измерений. Величина изомерного сдвига резонанса урана 6,67 эВ определялась при совместной обработке на ЭВМ спектров разных химических соединений, как это описано в нашей работе [3]. Процедура отделения изомерного сдвига от эффектов, связанных с кристаллической структурой образцов, подробно рассмотрена в работе [4]. Для расчета разности плотности электронов, которую необходимо знать для перехода от ΔE_0^{IS} к $\Delta\langle r^2\rangle$, были использованы данные о химическом сдвиге рентгеновской L_{α_1}-линии в уране, зависимость константы распада урана-235 от вида химической связи, а также некоторые теоретические расчеты. Подробнее этот вопрос рассмотрен в работе [5].

В результате обработки экспериментальных данных для нескольких химических соединений урана получены предварительные данные об изомерных сдвигах, из которых выведена величина $\Delta\langle r^2\rangle$, составляющая $(-0{,}6 \pm 0{,}3)\cdot 10^{-26}$ см^2. Полагая, что параметр деформации урана-238 в основном состоянии $\beta = 0{,}24$, заряд распределен по ядру равномерно, а диффузность края ядра не меняется при возбуждении, можно получить для возбужденного состояния ядра ^{239}U $\beta \simeq 0{,}20$, т.е. деформация несколько уменьшается. Эти результаты находятся в качественном согласии с теоретическими оценками Бунатяна [6].

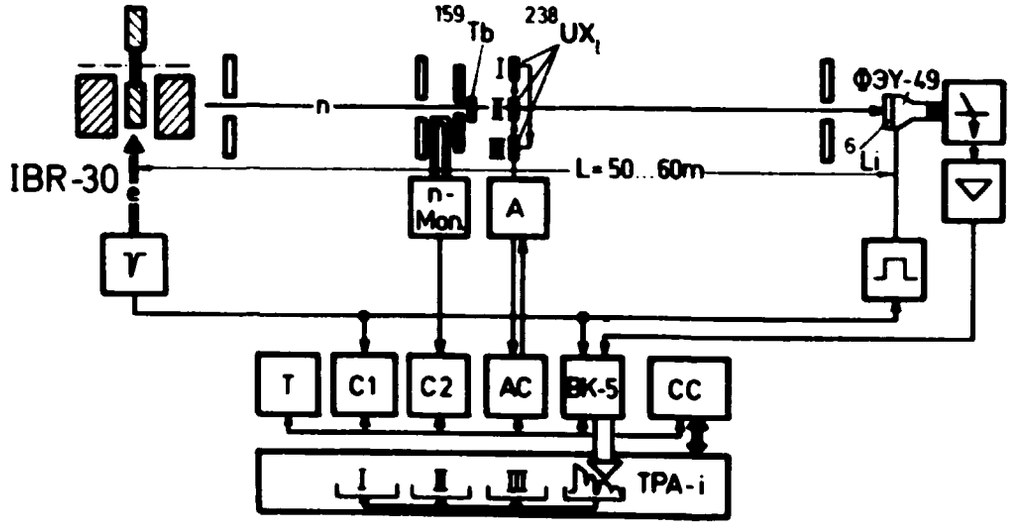

Рис. I. Схема эксперимента. *IBR* -30 - импульсный реактор ИБР-30 в бустерном режиме[2]; I,II,III - образцы из трех разных химических соединений урана и принадлежащие им накопленные спектры по времени пролета; ^6Li + ФЭУ-49 - сцинтилляционный детектор нейтронов; *T* - таймер; C1 и C2 - счетчики; A и AC - блоки управления для смены образцов; ВК-5 - временной кодировщик; CC - контролер камаковского каркаса; ТРА- *i* - малая ЭВМ.

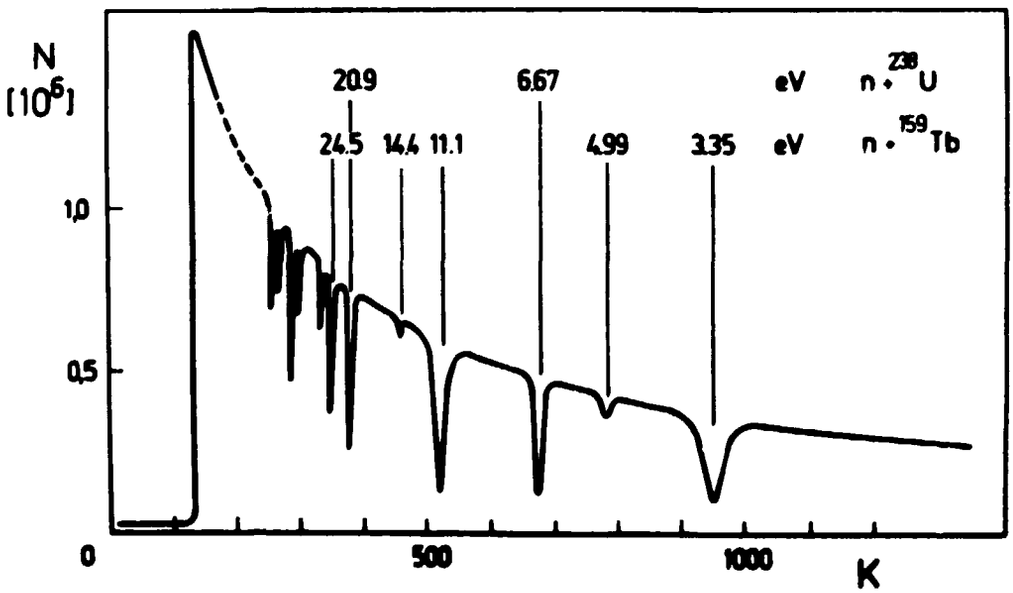

Рис. 2. Экспериментальный спектр одного образца. K - номер временного канала с шириной 2 мксек, *N* - число отсчетов.

Литература

1. В.К.Игнатович, Ю.М.Останевич, Л.Чер. ОИЯИ, Р4-7296, Дубна, 1973.
2. В.В.Голиков и др. ОИЯИ, 3-5736, Дубна, 1971.
3. Г.Г.Акопян, В.А.Вагов, К.Зайдель, А.Майстер, Д.Пабст, Л.Б.Пикельнер, Ш.Салай. ОИЯИ, Р3-11740, Дубна, 1978.
4. К.Зайдель, А.Майстер, Д.Пабст, Л.Б.Пикельнер. ОИЯИ, Р3-11741, Дубна, 1978.
5. К.Зайдель, А.Майстер, Д.Пабст. ОИЯИ, Р3-11742, Дубна, 1978.
6. Г.Г.Бунатян. Ядерная физика 26, вып.5, 979 (1977).
   Г.Г.Бунатян. ОИЯИ, Р4-11131, Дубна, 1977.

THE USE OF THE TIME CORRELATED ASSOCIATED PARTICLE METHOD FOR ABSOLUTE FISSION CROSS SECTION MEASUREMENTS

R. Arlt
Technische Universität Dresden, Sektion Physik, DDR - 8027 Dresden

1. Introduction

The absolute neutron counting with an accuracy in the order of 1% is a difficult experimental task, which must be resolved in every precise cross section measurement. In many cases it is possible to overcome this problem by counting the charged particles, which are produced together with the neutrons in a two body nuclear reaction. Strong follow from the reaction mechanism correlations in time, energy and angle of the two body nuclear reaction between the neutrons and the associated charged particles (AP).

In one group of experiments the angular and energy correlations are used to produce a well known neutron flux through a target. If the target is a neutron detector with timing properties, the time correlations can be used, too. This time correlated associated particle method /1/ allows a strong reduction of background events induced by unwanted source or scattered neutrons. If the neutron target-detector system is larger than the neutron cone, no geometrical factors must be known if the cross section of a neutron induced nuclear reaction should be determined.

2. The use of the time correlated associated particle method (TCAPM) in fission cross section measurements

One way to succeed a higher accuracy in fission cross section measurements is - as an alternative to measurements in a broad energy range - the precise ($\frac{\Delta\sigma}{\sigma}$ = 1-2%) absolute determination of the fission cross section at few spot point neutron energies /2/. The TCAPM is very suitable for this purpose, if the range of the covered neutron energies could be extended.

Until now this method has been used by Alchazov et al. /3/, Grenier et al. /4/ and later by a joint Dresden - Leningrad group /5/, to measure fission cross sections at 14.7 MeV. The $T(d,n)^4He$ reaction has been used. The associated alpha particles have been registered with a thin film detector /3, 5/ or a surface barriere detector /4/. When a thin film detector coupled to a fast photomultiplier is used, more than 10^5 alpha particles per second could be counted /6/. This is a sufficiently high counting rate to use a single plate fission chamber for cross section measurements.

At the Technical University Dresden a associated particle system has been designed using the $D(d,n)^3He$ reaction /7/. With 130 keV deuterons 2.6 MeV neutrons have been produced and used for fission cross section measurements on ^{235}U /8/. Up to $2 \cdot 10^4$ ^3He particles per second have been counted with a surface barriere detector. This is a lower limit, when working with a single plate

fission chamber.

Bartle et al. /9/ used the TCAPM to produce collimated neutron beams in the energy range from 2 to 2o MeV. Because a fission chamber is a neutron detector with a efficiency of about $1o^{-6}$ it will be difficult, to use his method for fission cross section measurements. The use of multiplate fission chambers could solve this problem.

3. Inaccuracies and errors of the time correlated associated particle method

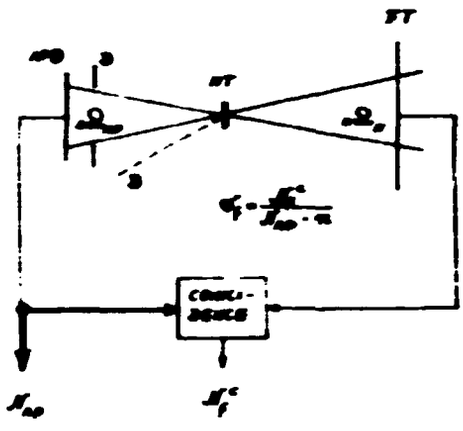

Fig. 1 The basic principle of the TCAPM

The principle of the TCAPM is shown on fig. 1. A charged particle beam (B) is hitting a neutron producing target (NT). The associated particle detector (APD) is counting all charged particles in an angle $\Delta\Omega_{AP}$ defined by the diaphragm D. No background events should be registered in the APD. This detector delievers the zero time point for all neutrons of the cone defined by $\Delta\Omega_N$. The fission target (FT) should be larger than the neutron cone, so that every neutron of the cone has a chance for a fission. If the fission products are counted in coincidence with the associated particles, the fission cross section will be get by the formula $\sigma_f = N_f^c / N_{AP}\, n$ (N_f^c-number of coincident fission products, N_{AP}-number of associated particles, n - number of the fissionable atoms per cm^2). The relative error of the fission cross section is given by the expression:

$$\frac{\Delta\sigma_f}{\sigma_f} = \sqrt{\left(\frac{\Delta N_f^c}{N_f^c}\right)^2 + \left(\frac{\Delta N_{AP}}{N_{AP}}\right)^2 + \left(\frac{\Delta n}{n}\right)^2}$$

3.1 Errors and inaccuracies connected with the registration of the fission products

3.11 Statistical error

The measuring time necessary to get a statistical error of 1% has been estimated for a single plate fission chamber with a 25o $\mu g/cm^2$ target and a fission cross section of 2 barn. The measuring time amounts to about 1.2 - 12 days for AP rates between $1o^4$ and $1o^5$ cps.

3.21 Fission chamber efficiency

In an absolute fission cross section measurement the fission detector efficiency must be known with an accuracy less than 1%. Usually, the fission detector is constructed in such a manner, that the efficiency for fission products is nearly 1oo %, but very small for the alpha particles from the natural alpha

activity of the fission target. The resulting problems will be discussed below in the case, when a parallel plate fission chamber is used.

3.211 Counting losses due to the timing threshold

In the TCAPM the threshold of the timing discriminator usually is determining the counting losses of the fission products. This threshold is set as low as possible, so that some of the alpha particles will trigger the CFT too. This alpha particles will be eliminated by the coincidence between the associated particles and the fission products, so that a small alpha counting rate can be tolerated. On fig. 2 the block scheme used in our experiments /10/ for timing and determining the counting losses due to the CFT bias is shown. In the computer memory the direct and coincidence spectrum of the FP is accumulated as it is shown on fig. 3a, b. If a linear extrapolation to zero bias is carried out, the total FP losses due to the CFT bias have been estimated less than 2%. If the error of this extrapolation is less than 20%, the contribution to the relative error of σ_f due to the CFT bias will be less than 0.4%. This small values can be reached only with a very low CFT bias.

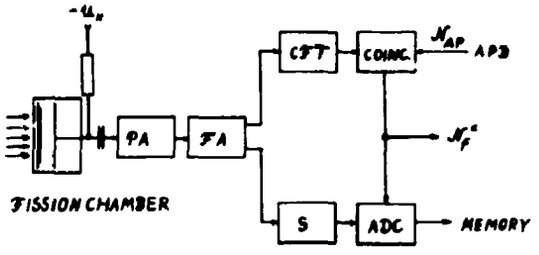

Fig. 2 Block scheme of the fission chamber electronics (PA preamplifier, FA fast amplifier, CFT constant fraction trigger, COINC. fast coincidence, S stretcher, ADC analogue to digital converter

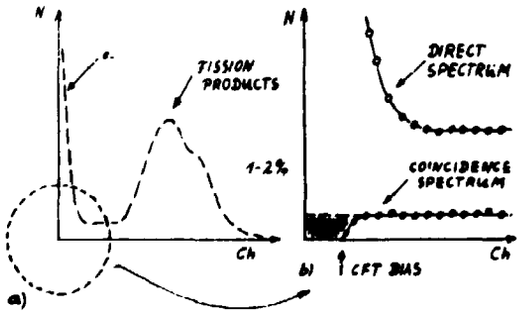

Fig. 3a, b Fission chamber spectrum and low energy cut off due to the CFT bias.

However, it should be mentioned, that the linear extrapolation to zero bias is arbitrary. If the FP spectrum in this region has a more complicated character, an additional error could be appear. Since calculation or measurement of the FP spectrum at very low ($\lesssim$ 10 MeV) energies is difficult, this possible source of an error should be minimized by setting the CFT threshold as low as possible.

3.212 Absorbtion of the fission products in the target material

If the fission product is emitted in a small angle to the target surface, the energy loss in the target can be large, even if a thin target is used. Due to the impuls of the incident neutrons the resulting counting losses are depending on the neutron energy. The resulting inefficiency of the fission chamber has been calculated in dependence on the target thickness, neutron energy and anisotropy of the fission product angular distribution /11, 12, 13/. Although these losses can be calculated with a good accuracy, additional problems can lead to a larger uncertainty as deduced from the calculations. The range of the fission products should be known for the chemical composition of the used

fission target. A further uncertainty is caused by the surface structure of the fission target. As has been shown by P.H. White /14/ the surface roughness of the fission target has a definite influence on the escape of the fission products from the foil.

To get a real value of the fission chamber efficiency - including all the factors discussed above - an experimental test should be carried out. For this purpose the method, described in /15/ for a ^{252}Cf source, has been modified. The fission chamber, loated with a non threshold target f.g. ^{235}U, is irradiated with thermal neutrons or 24 keV neutrons from a Sb-Be photonuclear source. The fission neutrons are counted in coincidence with the fission products. As has been shown in /15/ on this way the inefficiency of a fission chamber - if it is small - can be determined with a high accuracy.

4. Errors and inaccuracies of the associated particle counting

The main source of an error is the background of non-associated particles in the energy window of the associated particles discriminator. Every background particle leads to a higher N_{AP} count and in this way to a smaller fission cross section. On the other hand it is not necessary to know the efficiency of the AP counting system, because only such fission products will be counted, for which a coincident AP has been registered.

For every neutron energy a special AP counting system must be developed. Therefore the errors strongly depend on the special detection system and should be analysed for every system.

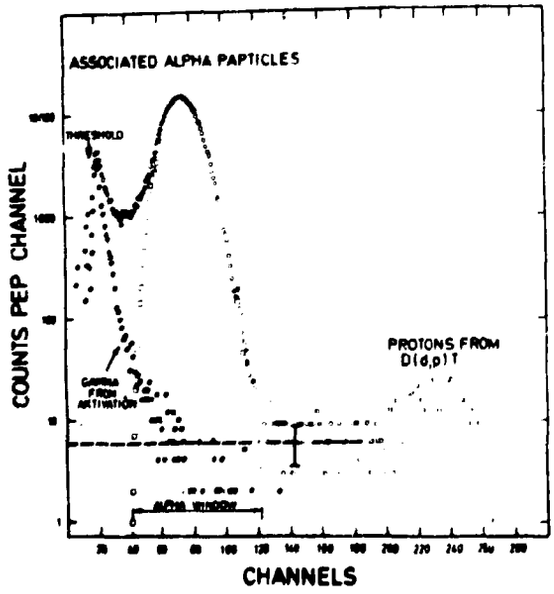

Fig. 4 Alpha particle spectrum of the T(d,n)4He reaction

As two examples we show the AP spectra for the two systems, which have been developed recently at the Technical University Dresden /6, 7/. On fig. 4 the alpha spectrum of the $T(d,n)^4He$ reaction registered with a thin NE 102A scintillator is shown. The background is produced mainly from the protons of the D(d,p)T reaction and from low energy gammas, electrons and elastical scattered deuterons. Because the background is less than o.1% of the alpha counting rate in the window, it can be neglected. However the extrapolation of the background shown on fig.4 has to be checked carefully by test experiments.

In the case of the $D(d,n)^3He$ reaction the situation is more complicated (see fig. 5). The background - mostly caused by the tritons and the protons of the $D(d,p)^3H$ reaction - reaches values of few percents of the ^3He counting rate in the discriminator window. The background spectrum of the tritons and protons is very smooth, so that an extrapolation with an error less than 2o % can be carried out. The background from neutrons, deuterons a.s.o. has been found to be negligible.

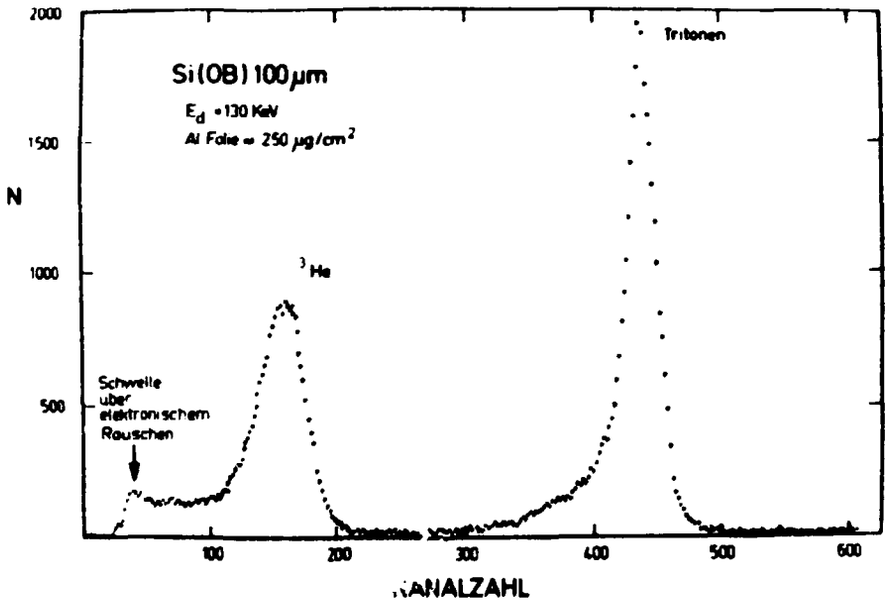

Fig. 5 Charged particle spectrum of the $D(d,n)^3He$ and D(d,p)T reactions (protons out of scale)

5. Errors and inaccuracies connected with the cone

5.1 Neutron scattering

Some of the neutrons will be scattered out of the cone on the neutron target backing, on the fission chamber entrance window, on the fission target backing or on the air. The different cases of neutron scattering schematically are shown on fig. 6. Only in the case 1 the neutron will be scattered out of the

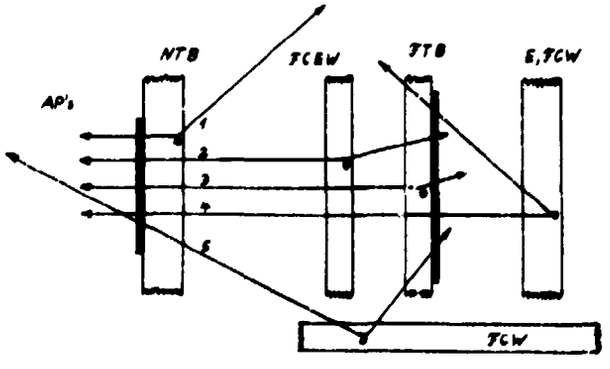

Fig. 6
Schematical drawing of the different neutron scattering processes. (AP associated particles, NTB neutron target packing, FCEW fission chamber entrance window, FTB fission target packing, E electrode, FCW fission chamber wall)

beam. In the cases 2, 3, 4 the neutrons will interact with the fission target with a lower energy (inelastic scattering). The case 5 can be neglected because the correspondent associated particles are not registered. All these cases can be calculated and have found to be less than 2% for 14.7 MeV neutrons and a thickness of the copper between neutron and fission target of about 1 mm /5/. The results of the calculations have been checked, by measuring of the fission cross section with different material layers between the neutrons and the fission targets.

5.2 Scattering of the associated particles

The scattering of the associated particles gives one of the most serious limitation of the accuracy of the TCAPM, because it is very difficult to proof the calculations under realistic conditions. The different cases are classified on fig. 7. The case 1 can be minimized by diaphragmas along the AP channel or by large distancy to the wall. The case 2 cannot influence the result. The most serious problems result from the case 3, if the AP is scattered into the detector, but the corresponding neutron is outside the cone. A careful mapping of the cone with a small (Ø 1 mm) scintillator in coincidence with the associated particles is necessary, to estimate the influence of the different AP scattering processes on the result of the measurement. Moreover, the fission target should be placed very close to the neutron target, so that the central part of the neutron cone delivers only less than about 10% of the total fission counts of the chamber. In this way the chance coincidence rate is higher, but the scattering corrections will be smaller, because small angle scattering is decreased.

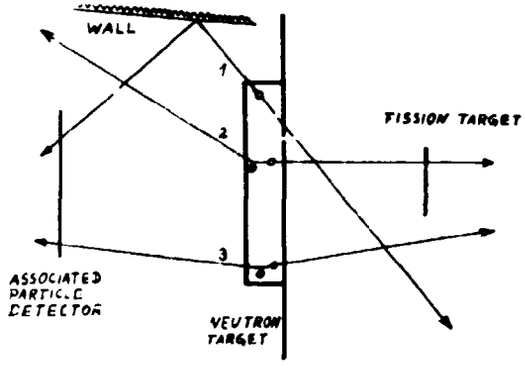

Fig. 7 Schematical drawing of the different associated particle scattering processes

6. Errors and corrections connected with the electronics

The following sources of errors should be carefully analysed, if the electronic block scheme for a precise measurement using the TCPAM is designed: The dead time of the associated particle channel including the fast coincidence, the efficiency of the CFT, the chance coincidence rate.

During the experiment a complete documentation of the following data is necessary: N_{AP}, N_f^c, fission chamber spectrum in coincidence with the associated particles and without (for correction of the counting losses due to the CFT bias), spectrum of the time intervalls between the associated particles and the fission products (to check the function of the fast coincidence and to correct for chance coincidences), spectrum of the associated particles (to estimate the background of non associated particles in the discriminator

window), divers monitor rates. An on line calculation of the uncorrected fission cross section is desirable. to proof the proper function of the equipment during the runs. These requirements can be fullfilled only by a computer coupled experiment. For our fission cross section measurement we use a KRS 4200 minicomputer (VEB ROBOTRON Dresden) together with a CAMAC measurement system /10/.

7. Errors and corrections connected with the fission target

All the problems connected with the target weight are similar as in cross section measurement with other methods and will not discussed here especially. However a high uniformity of the target is required. In the case of targets with a high specific alpha activity the uniformity can be checked easilly by a alpha scanning method. Difficulties arise in the case of ^{238}U. Optical methods have been used, to measure the non uniformity of such targets /13/.

8. Summary and conclusions

The use of the time correlated associated particle method for precise absolute measurements of fission cross sections has been analysed. In comparison to other methods all problems connected with an absolute neutron monitoring are eliminated. As specific problems of the TCAPM, which can give the limitation of the method the following questions have been found: Background of the associated particle detector, small angle scattering of the associated particles in the neutron target and the low counting rate. Further efforts are necessary, if the method should be extended to other neutron energies away from 14 MeV.

The author wish to thank prof. G. Musiol and the doctors I.D. Alkhasov, Drapscinskij, H.-G. Ortlepp, V.I. Spakov, R. Teichner and W. Wagner for valuable discussions.

References

/1/ M.M. Meier, Neutron Standards and Applications, NBS Special Publication 493 (1977) 221

/2/ M.G. Sowerby, Review of Standard Reference Data and important Cross Section Discrepancies, ANL / ND-77-1

/3/ И.Д. Алхазов, В.П. Касаткин, О.И. Косточкин, Л.З. Малкин, А.В. Сорокина, К.А. Петржак, А.В. Фомичев, В.И. Шпаков, Б.Б. Румянцев, А.М. Соколов, Труды Всесоюзного Совещания по Нейтронной Физике, Киев 1975, стран. 13

/4/ M. Cance and G. Grenier, Proceedings of the NEANDC/NEACRP Specialists Meeting on Fast Neutron Fission Cross Sections of U-233, U-235, U-238, and Pu-239; ANL-76-90 (1976) 237

/5/ И.Д. Алхазов, Р. Арльт, В. Вагнер, Ф. Вайдхазе, В. Гриммм, В.Н. Душин, С.С. Коваленко, О.И. Косточкин, Р. Краузе, Г. Музиоль, Х.Г. Ортлепп, К.А. Петржак, Р. Тайхнер, В.И. Шпаков, Препринт ТУ Дрезден 05-37-78 и Атомная Энергия (в печати)

/6/ Р. Арльт, В. Вагнер, Г. Музиоль, Х.Г. Ортлепп, А.М. Соколов, Р. Тайхнер, Препринт ТУ Дрезден 05-3-78

/7/ R. Arlt, H.-U. Heidrich, M. Josch, G. Musiol, H.-G. Ortlepp, R. Teichner, W. Wagner, P. Weidhase, I.P. Alkhazov, O.J. Kostochkin, V.I. Spakov, Gemeinsamer Jahresbericht 1978, to be published as a ZfK-report 1979

/8/ R. Arlt et al., following contribution

/9/ C.M. Bartle, D.W. Gebbie, C.L. Hollas, NJaM 144 (1977) 437

/10/ W. Meiling, R. Arlt, W. Grimm, W. Hirsch, B. Krause, W. Wagner, P. Weidhase, Kernenergie 9 (1978) 292

/11/ P.H. White, Journ. of Nucl. Energy Parts A/B 19 (1965) 325

/12/ G.W. Carlson, NJaM 119 (1974) 97

/13/ G. Pausch, R. Arlt, R. Teichner, W. Wagner, A.V. Pomichev, Gemeinsamer Jahresbericht 1978, to be published as a ZfK-report 1979

/14/ P.H. White, NJaM 79 (1970) 1

/15/ V. Dorlin and V. Mozhaev, NJaM 105 (1972) 277

ИЗМЕРЕНИЕ СЕЧЕНИЯ ДЕЛЕНИЯ НУКЛИДОВ 235,238 УРАН, 237 НЕПТУНИЙ И 239 ПЛУТОНИЙ ПРИ ЭНЕРГИЯХ НЕЙТРОНОВ 14.7 МЭВ И 2.6 МЭВ

Р. Арльт, В. Вагнер, Э. Гримм, Г. Чузколь, Х.-Г. Ортлепп, Г. Паум, Р. Тейхмер, Ч. Ин
Технический Университет Дрезден, Секция Физики, ГДР - 8027 Дрезден
Ч. Х. Алхазов, В. Н. Душин, Л. В. Драпчинский, С. С. Коваленко, О. И. Косточкин, Ю. А. Петржак, Л. Н. Чаков
Радиевый Институт им. Хлопина, Ленинград, СССР

Выполнены абсолютные измерения сечения деления нуклидов урановой области с помощью метода сопутствующих частиц в совпадении с осколками деления. Достигнутая точность лучше 2%.

I. Введение

Оптимальный расчет и экономичная работа ядерных реакторов требуют предоставления ядерных констант по сечению деления важных нуклидов ядерного горючего с точностью 1-2 % /1/.
В частности значение сечения деления около 14 МэВ часто используется в качестве калибровочной для экспериментов с белым спектром нейтронов.
Сечение деления нуклида 235 уран является важным стандартом для относительных измерений /2/. Оно считается известным с точностью около 2.4 - 6 % в области энергии от 1 - 15 МэВ /3/ в то время как в работе /4/ утверждается меньшая [illegible] %.
[illegible] абсолютные значения сечения деления нуклидов 235 уран, 238 уран, 237 нептуний и 239 плутоний, полученные в нескольких сериях [illegible] на нейтронном генераторе Технического университета Дрездена в соответствии с единственной программой абсолютных измерений сечения деления Технического университета Дрездена и Радиевого института им. Хлопина г. Ленинград /5/.

II. Метод измерения

Моноэнергетические нейтроны были получены нейтронным генератором, производящим нейтроны с энергии (14.70 ± 0.10) МэВ по реакции T (d,n) ^{4}He /6/ и с энергии (2.6 ± 0.15) МэВ по реакции D(d,n)^{3}He при установлении соответствующей геометрии /7,8/.
При этих энергиях сечение деления показывает известное плато из-за основной конкуренции каналов реакции, нейтронной эмиссии и деления. Выбор таких энергий для абсолютных измерений калибровочных точек благоприятен тем, что энергетические распределения нейтронов мало влияют на измеренное значение сечения деления.
При абсолютном определении сечения деления применяется метод сопутствующих частиц в сочетании с осколками деления /7,10/, в качестве которых были частицы [illegible] тяжелых ионов.
[illegible] сопутствующих нейтронов ^{3}He- или ^{4}He-частицы и [illegible] в предыдущих работах /8, /.
[illegible] на параметрах [illegible] в таблице I.

Взвешивание мишеней проводилось счетом естественной альфа-активности в малой геометрии и в геометрии 2π и $2/3\pi$. Неоднородность слоев была определена использованием ра лчных диафрагм при альфа-счете и независимо оптическим и микроаналитическими методами /II/ в случае 238 урана.

Таблица I. Параметры мишеней

Нуклид	поверхностная плотность в мкг/см^2	погрешность взвешивания	неоднородность слоя
^{235}U - I	267.2	0.75 %	0.5 %
^{235}U - II	256.7	0.75 %	0.5 %
^{238}U	386.3	0.75 %	5 %
^{237}Np	228.6	0.5 %	0.3 %
^{239}Pu	289.8	0.5 %	0.75 %

III. Поправки и погрешности сечения деления

В работе /IO/ подробно обосновывается необходимость внесения некоторых поправок, связанных со систематическими ошибками этого метода определения вторичных частиц с осколками деления и с регистрацией осколков деления [illegible] ионной камере деления. Это осуществляется, по аналогии с работой /II/, [illegible] контрольных спектров, которые непрерывно фиксируются во время эксперимента **on-line** с малой ЭВМ /I3/.

Поправка на поглощение осколков в слое мишени постулируется в работе /II/. Метод коррекции сечения на рассеяние и поглощение нейтронов в [illegible] материалах аппаратуры и в подложке мишени описан в работе /I5/.

Т.к. эти поправки по величине не больше 3 % в случае 14.7 МэВ и не больше 7 % в случае 2.6 МэВ их погрешности могут достичь 10-20 %.

Погрешности поправок и параметров мишеней, при достаточно большой статистике совпадений, определяют достижимую точность сечения деления. В табл. II приведены отдельные погрешности, входящие в суммарную погрешность сечения.

Результаты при энергии 2.6 МэВ представляют собой предварительные данные, которые были получены в первом эксперименте с применением метода сопутствующих частиц в совпадении с осколками деления /9/. При потоке нейтронов [illegible] 10^4 нейтр$\cdot$с$^{-1}$ время измерения длится около 10 дней. Повышение точности считается доступным совершенствованием разделения ^{3}He-частиц от рассеянных дейтронов и тритонов. Как видно в табл.II, повышение точности сечений при энергии 14.7 МэВ достижимо лишь более аккуратным определением параметров мишеней, что является довольно сложной задачей.

IV. Результаты и дискуссия

Результаты измерений представлены в табл. III. Полученное значение сечения деления при 14.7 МэВ для нуклида 235 урана совпадает со значениями работ /I6/ и /I7/. Расхождение в 7 % наблюдается со значениями сечения деления из работ /I8/ и /I9/, измеренными относительно сечения рассеяния нейтронов на водороде. Сравнение сечения деления других нуклидов с данными работ/I7,I9,20,21,22/

Таблица II. Погрешности поправок и сечений деления в %

энергия	2.6 МэВ	14.7 МэВ			
нуклид	^{235}U -I x)	^{235}U -II	^{238}U	^{237}Np x)	^{239}Pu x)
источник погрешности					
взвешивание мишени	0.75	0.75	0.75	0.75	0.75
неоднородность	0.50	0.50	I.50	0.40	0.75
статистика совпадений	I.60	0.46	0.48	0.58	0.53
случайные совпадения	0.66	0.08	0.I2	0.II	0.I2
экстраполяция к нулевой энергии осколков	0.42	0.04	0.09	0.05	0.05
потери осколков в мишени	0.20	0.20	0.20	0.20	0.20
рассеяние и поглощение нейтр.	0.8 x)	0.20	0.20	0.20	0.20
определение числа сопутств. част.	0.62	$I0^{-3}$	$I0^{-3}$	$I0^{-3}$	$I0^{-3}$
суммарная погрешность	2.3 x)	I.I	I.8	I.I x)	I.2 x)

Таблица III. Значения сечений деления в $I0^{-24}$ $см^2$

энергия	I4.7 МэВ	2.6 МэВ
нуклид		
^{235}U	2.073 ± 0.023	I.2I5 ± 0.028 x)
^{238}U	I.I94 ± 0.022	
^{237}Np	2.I72 ± 0.023 x)	
^{239}Pu	2.360 ± 0.028 x)	

точе показывает, что абсолютно измеренные значения сечения деления на 5 - I0 % меньше тех, которые были получены в относительных измерениях.

В случае непороговых нуклидов это может быть связано с тем, что метод совпадений сопутствующих нейтронам частиц с осколками деления эффективно исключает фон медленных нейтронов. Кроме того возможна корреляция ошибок, если абсолютное значение сечения деления определено из относительных измерений, напр. по отношению к сечению деления 235 урана /23,24/.

Интересно сравнить отношения сечений деления, вычисленные из абсолютно измеренных сечений, со значениями, непосредственно полученными в измерениях отношений сечений деления /см. табл. IV/.

В случае отношений $^{238}U/^{235}U$ и $^{239}Pu/^{235}U$ наблюдается совпадение результатов с данными работ /25,24,26/, полученными в экспериментах с белым спектром нейтронов. Для отношения $^{237}Np/^{235}U$ расхождение выходит за приведенные интервалы ошибок.

Таблица IV. Отношения сечений деления при энергии I4.7 МэВ

отношение	абсолютное измерение	измерение отношения
$^{238}U/^{235}U$	0.576 ± 0.012 xx) 0.557 ± 0.017 /I7/	0.567 ± 0.013 /25/ 0.557 ± 0.009 /24/ 0.574 ± 0.006 /26/ 0.548 ± 0.014 /27/
$^{237}Np/^{235}U$	I.048 ± 0.016 xx)	I.050 ± 0.004 /28/ 0.984 ± 0.026 /23/
$^{239}Pu/^{235}U$	I.I38 ± 0.018 xx)	I.I30 ± 0.005 /25/ I.560 ± 0.009 /24/ I.15 ± 0.05 /29/

xx) настоящая работа

V. Заключения

Метод сопутствующих частиц в совпадении с осколками деления позволяет определить абсолютное сечение деления с хорошим энергетическим разрешением нейтронов с точностью лучше 2 %.

Сечения деления абсолютных измерений на 5-10 % меньше сечений из относительных измерений.

Отношения сечений деления с использованием абсолютно измеренных значений довольно хорошо совпадают с непосредственно измеренными отношениями сечений деления, что можно интерпретировать как признак консистенции измеренных сечений. Чтобы исключить систематических ошибок нужно тщательно изучить все условия метода сопутствующих частиц /I0/, аккуратно ввести поправки и провести выборочные измерения в различных экспериментальных условиях. Особое внимание нужно обратить на изготовление и исследование мишеней.

x) предварительные данные

Литература

/I/ Usachev,L.N.,Manokhin,V.N.,Bobkov,Yu.G., Proc. of the Symp. on Appl. of Nucl. Data in Sci. and Technol.,Paris 1973, IAEA Vienna, Vol. 1,129

/2/ Bowerby,M.G., ANL/ND-77-1, 23

/3/ Konshin,V.A., INDC(CCP)-94/U, 1976,11

/4/ Carlson,G.W.,Czirr,J.B., Proc. of the NEANDC/NEACRP Spec. Meet. on fast Neutr. Fission Cross Sections, Argonne, 1976, ANL-76-90, 258

/5/ Arlt,R.,Krause, R.,Musiol,G.,Teichner,R.,Wagner, W.,Weidhase, F.,Alkhazov,I.D.,Shpakov,V.I., Jahresbericht 1976, ZfK-315, 172

/6/ Raics,P.,Programme NECAL, priv. comm.

/7/ Алхазов,И.Д.,Косточкин,О.И.,Малкин,Л.З.,Петрчук,К.А.,Томичев,А.В.,Шпаков,В.И., Мат. II. Всесоюзн. конф. по нейтр. физ., Киев 1973, часть 4, I3

/8/ Арльт,Р.,Вагнер,В.,Музиоль,Г.,Ортлепп,Х.-Г.,Соколов,А.М.,Тейхнер,Р., препринт Техн. Университета Дрездена 05-3-78, 1978

/9/ Arlt, R.,Heidrich,H.-U., Josch,M.,Musiol,G.,Ortlepp,H.-G.,Pausch,G.,Teichner,R.,Wagner,W.,Weidhase,F.,Alkhazov,I.D.,Dushin,V.N.,Kostochkin,O.I., Shpakov,V.I., Jahresbericht 1978, ZfK-report, to be published

/10/ Arlt,R., "The use of the time correlated ass.particle method...",these proc.

/11/ Arlt,R.,Heidrich,H.-U.,Teichner,R.,Wagner,W.,Schöneich,J.,Kostochkin,O.I., Shpakov,V.I., Jahresbericht 1978, ZfK-report, to be published

/12/ Алхазов,М.Д.,Арльт,Р.,Вагнер,В.,Вайдхазе,Ф.,Гримм,Х., Дузиоль,Г.,Коваленко,С.С., Костючкин,О.И.,Краузе,Р., Ортлепп,Х.-Г., Петржак,К.А., Соколов, С.П., Шпаков,В.И.,Тейхнер,Р., Мат. II. Междун. Симп. по взаимод. быстр. нейтр. с атомн. ядр., Гауссиг 1977, в печати

/13/ Meiling,W.,Arlt,R.,Grimm,H.,Hirsch,W.,Krause,R., Wagner,W.,Weidhase,F., Kernenergie 21,Heft 9, (78) 292

/14/ Pausch,G.,Arlt,R.,Teichner,R.,Wagner,W., Jahresbericht 1978,ZfK,to be publ.

/15/ Гужин,Э.И., Мат. III. Междун. Симп. по взаимод. быстр. нейтр. с атомн. ядр., Гауссиг 1978

/16/ Czirr,J.B.,Sidhu.G.S., Nucl. Sci. Eng. 57 (1975) 18

/17/ Cance,M.,Grenier,G., ANL-76-90, 237

/18/ Soverby,M.G.,Patrick,B.H., Ann. of Nuc. Sci. and Eng. 1 (1974) 409

/19/ Leughers,B.,Cierjacks,S.,Brotz,P.,Erbe,D.,Gröschel,D.,Schmalz,G.,Voß,F., ANL-76-90, 246

/20/ Алхазов,М.Д.,Поваленко,Г.Д.,Костючкин,О.И., Полкин,Е.В.,Петржак,К.А.,Соколов,А.П.,Тонкачев,Ю.Ф.,Шпаков,В.И., Мат. I. Всесоюзн. конф. по нейтр. физ. Киев 1977, часть 3, 155

/21/ Hart,W., AHSB(S)R 109, Risley 1969(and references)

/22/ Carner,M.,Wechsler,S.,Yiftah,S., IA-1346, 1977

/23/ Behrens,J.W., Magana,J.W.,Browne,J.C., UCLD-17370(77)

/24/ Behrens,J.W., Carlson,G.W., UCLD-10981(75)

/25/ Cierjacks,S.W.,Leughers,B.,Kari,K.,Brotz,B.,Erbe,D.,Gröschel,D.,Schmalz,G. Voß,F., ANL-76-90, 94

/26/ Difilippo,F.C.,Perez,R.B.,de Saussure,G.,Olsen,D.,Ingle,R, ANL-76-90,114

/27/ Coats,M.S., Gayther,D.B.,Pattenden,N.J., IV. Conf. on Cross Sect. and Technol.,Washington 1975, NBS 425, Vol.II, 568

/28/ White,P.H.,Warner,G.P.,Journ. Nucl. En. 21 (67) 671

/29/ Uttley,C.A.,Phillips,J.A., AERE-NP/R-1996 (1956)

^{6}Li+d REACTIONS BELOW E_d= 200 keV

J.Szabó, M.Várnagy, Z.T.Bödy
Institute of Experimental Physics, Kossuth University, Debrecen, Hungary

Cross sections were determined for the ^{6}Li/d,n/^{7}Be, ^{6}Li/d,p/^{7}Li and ^{6}Li/d,α/^{4}He reactions between 100 and 180 keV deuteron energy.

1. Introduction.

The investigation of nuclear reactions induced by low-energy charged particles on light nuclei is important from the point of view of nuclear astrophysics as well as for planning controlled thermonuclear reactors /CTR program/. From the present stage of our knowledge, the first prototype will be most probably a DT-reactor. However, there are some other exoergic reactions which can be taken into account as nuclear-fusion reactions. In 1973 a request list was issued for the fusion research asking cross-section data with errors less than 25% for a lot of reactions in the energy range E_d=0.1-5 MeV[1]. Among these the ^{6}Li+d reactions are of the highest priority. On the other hand, since there are only few measurements [2-7] for the /d,n/, /d,p/ and /d,α/ reactions at E_d< 500 keV, it seemed to expedient to measure the cross-section data for this energy region.

2. Experimental techniques.

For the measurements a Cockcroft-Walton generator of 180 kV was used. The intensity of the analysed deuteron beam on the target was about 1-3 μA. Thick targets of ^{6}LiF were prepared by sedimentation onto Cu backing, the enrichment being to 87.9% in ^{6}Li. Measurements were performed in the interval E_d= 100-180 keV in steps of 20 keV.

3. Cross-section determination.

A. ^{6}Li/d,n/^{7}Be

This reaction is exoergic, Q=3.38 MeV. To determine the cross-section data the activation method was used. The decay scheme can be seen in fig.1.

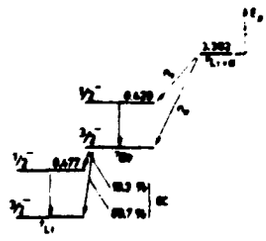

Fig.1. Energy levels involved in the ^{6}Li/d,n/^{7}Be reaction.

With the knowledge of the branching ratio of 477.6 keV γ-line one can determine the number of ^{7}Be nuclei produced and the value of the cross section. The 477.6 keV γ-rays from the decay of ^{7}Be /$T_{1/2}$=53 days/ were detected by a 40 cm^3 Ge/Li/ detector fed to a 4000-channel pulse-height analyser. For this γ-line the energy resolution and the photopeak efficiency were 2.8 keV

and 9.57×10^{-3}, respectively. The cross-section values were calculated by the formula:

$$\sigma(E_0) = \frac{1}{N}\left(\frac{dY}{dE}\right)_{E_0}\left(\frac{dE}{dx}\right)_{E_0} \qquad /1/$$

which is valid for a thick target, where N is the number of ^{6}Li nuclei per cm^3 in the target. $(dY/dE)_{E_0}$ is the slope of the yield curve at E_0 and $(dE/dx)_{E_0}$ is the stopping power of the bombarding particles in the target material[8]. Cross-section values are plotted in fig.2 vs. bombarding energy.

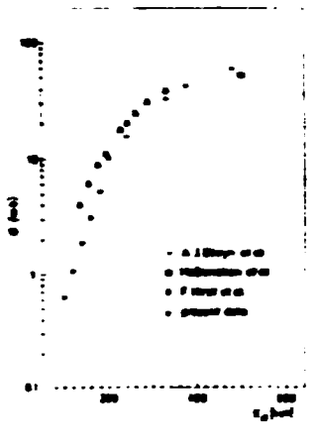

Fig.2. Cross-section values for ^{6}Li/d,n/^{7}Be vs. bombarding energy

Owing to the peculiarities of thick-target measurements, it is not easy to separate the uncertainties into purely statistical and systematic: one can generally estimate a 10 or 20% error for cross-section data. The real errors are possibly between these values.

B. ^{6}Li/d,p/^{7}Li and ^{6}Li/d,α/^{4}He

For these reactions Q values are 5.02 and 22.37 MeV, respectively. To obtain cross-section data for /d,p/ and /d,α/ reactions on ^{6}Li, a new method was developed for the simultaneous determination of the angular distribution of protons and α-particles applying SSNTD. This type of detector has a lot of advantages: the detection efficiency is very high /~100% for protons and

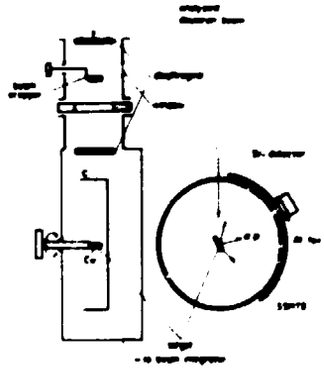

Fig.3. Schematic view of the experimental arrangement used for the angular-distribution measurements.

α-particles/, low background, long stability, to mention only the most important properties of that. The schematic drawing of the experimental arrangement can be seen in fig.3. The SSNTD stacks, bent on the 10 cm diameter cylinder, covered an angular interval of 45-165°. The 2 mm diameter circular holes on the cylinder served as diaphragms for the protons and α-particles to enter the SSNTD at right angles. At 120° there was a 2 mm diameter hole on the SSNTD stacks for a monitoring Si-detector. Two 100 μm thick cellulose-nitrate sheets were used as detectors. In front of the first detector and between the two detectors polycarbonate degrader foils were applied to screen the background particles as well as to reduce the energies of protons and α-particles to the desired values $E_p \sim 600$ keV, $E_\alpha \sim 8$ MeV/. The irradiation time was chosen so that there were a number of tracks of about 2000 at each angle. The angular distributions of protons and α-particles were proved to be isotropic. The cross-section values were calculated by the formula /1/. The results are shown in figs. 4,5. To our knowladge this is the first case of the

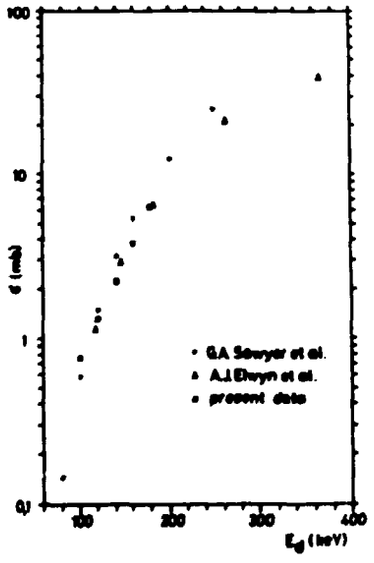

Fig.4. Cross-section values for $^{6}Li/d,p/^{7}Li$ vs. bombarding energy

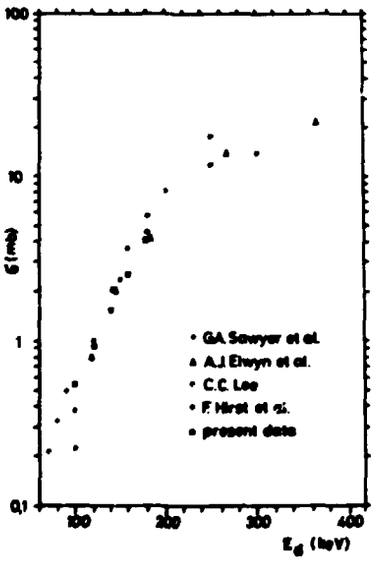

Fig.5. Cross-section values for $^{6}Li/d,\alpha/^{4}He$ vs. bombarding energy

application of SSNTD for cross-section measurement when the outcoming particle is proton. Using the direct detection method applying the SSNTD, the number of the error sources are less than the activation method. So thus, the errors of the cross-section values for the /d,p/ and /d,α/ reactions are $\sim$ 10%.

References

[1] International Nuclear Data Committee, INDC/NDS/-57/U+F/ Dec. 1973/
[2] F. Hirst, I. Johnstone and M.J.Poole, Phil. Mag. 45/1954/ 762
[3] L.M. Baggett and S.J. Bame, Phys. Rev. 85 /1952/ 434
[4] G.A. Sawyer and J.A. Phillips, Los Alamos Sci. Lab. Rep. LA-1578 /1953/
[5] C.C. Lee, J. Korean Phys. Soc. 2 /1969/ 1.
[6] R. McClenahan and R.E. Segel, Phys. Rev. C11 /1975/ 370
[7] J.E. Monahan, A.J. Elwyn and F.J.D. Serduke, Nucl. Phys. A269 /1976/ 61
[8] C.F. Williamson, J.P. Boujet and J.Picard, Report CEA-R 3042 /1966/

CORE POLARIZATION AND MESONIC EFFECTS MANIFESTED BY l-FORBIDDEN M1 TRANSITIONS

W. Andrejtscheff
Bulgarian Academy of Sciences, Inst. for Nucl. Research and Nucl. Energy, Sofia
K.M. Muminov and T.M. Muminov
Joint Institute for Nuclear Research Dubna, USSR

The nucleon-number dependence of l-forbidden B(M1) values is studied. Open problems in the interpretation of the systematics are pointed out.

1. General remarks

Core polarization phenomena and mesonic effects are frequently discussed in the last years in connection with magnetic dipole moments and transition strengths experimentally determined in heavy-ion in-beam investigations as well as in decay studies[1]. The present talk is not intended as an exhaustive review of these subjects. Its aim is merely to present a new systematization of l-forbidden B(M1) values and to call attention to some open problems.

In the pure shell model, M1 transitions between states with $\Delta l=2$ are forbidden as the M1 operator

$$\mathcal{M}(M1)=g_l\vec{l}+g_s\vec{s}$$

does not change the orbital quantum number l by two units. Nevertheless, l-forbidden transitions ($s_{1/2}\longleftrightarrow d_{3/2}$, $d_{5/2}\longleftrightarrow g_{7/2}$ etc.) are often observed in real nuclei, however, with B(M1) values smaller than those of allowed transitions.

Two effects are considered now as mainly responsible for the occurance of such transitions: the spin polarization of the core and mesonic exchange currents.

The spin polarization of the core (illustrated by the graph taken from ref.[2]) arises from a residual interaction of the odd nucleon j with nucleons in open shells of the core. As a result, core nucleons from the orbit $j_1=l_1+\frac{1}{2}$ are excited to the orbit $j_2=l_1-\frac{1}{2}$ giving rise to core excited p-h states $j_1^{(-1)}j_2$ with $I_c^{\pi}=1^+$. In this way, beside the main

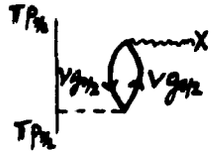

$\pi\,|j\rangle \Rightarrow p_{1/2}$
$\nu\,|j_1\rangle \Rightarrow g_{7/2}$
$\nu\,|j_2\rangle \Rightarrow g_{9/2}$

components of the wave functions, additional configuration admixtures arise allowing the M1 transitions in question:

$$|I\rangle=\alpha_0|j,I_c=0;I=j\rangle+\sum_i\alpha_i|j,(j_1^{(-1)}j_2)I_c=1;I=j\rangle$$

For our present considerations, two features of this interaction are of special importance. (i) Core polarization phenomena should be sensitive to shell effects;

(ii) For quantitative treatment, assumptions for the two-body interaction should be made. Arima and Horie[3] who first performed such calculations used a δ-function force

$$V_0+V_1\vec{\sigma}_i\vec{\sigma}_k\equiv V_s\frac{1-\vec{\sigma}_i\vec{\sigma}_k}{4}+V_t\frac{3+\vec{\sigma}_i\vec{\sigma}_k}{4}$$

with $|V_t| = 1{,}5\,|V_s|$. It is of interest that realistic forces used in later calculations[4] have similar V_t/V_s ratios. With this ratio, the interaction between like particles (e.g. odd proton with core protons) provides a contribution of about four times larger than that of unlike particles (e.g. odd proton with core neutrons).

The influence of mesonic effects on magnetic dipole moments and transitions is associated with the general dependence of the magnetic operator on currents in the nucleus inclusive meson exchange currents. Two of the graphs describing one-pion exchange current contributions[2] should be displayed here. The first of them (A) presents meson exchange

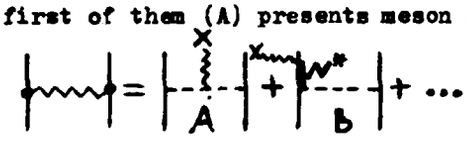

associated with the electromagnetic interaction and graph B describes a pion emitted by the second particle which excites an isobar N^* deexcited by an electromagnetic transition.

Generally, both effects mentioned here: core polarization and meson exchange currents are usually taken into account by a modification of the magnetic dipole operator:

$$\mathcal{M}(M1) = (g_l + \delta g_l)\vec{l} + (g_s + \delta g_s)\vec{s} + g_p[Y_2 s]$$

The core polarization is thereby described by the last term (spin-quadrupole interaction), which allows M1 transitions with $\Delta l = 2$. In the determination of the constants $\delta g_{l,s}, g_p$ the influence of the mesonic effects are taken into consideration.

2. Lifetime measurements. Multidimensional nanosecond analysis with Ge(Li) detectors

Lifetime measurements in the nanosecond region from which B(M1) values were deduced (fig.1) are performed in different laboratories with the delayed coincidence method. Here, a modern variant of this method should be shortly presented[5].

In-beam experiments in heavy-ion reactions with several reaction channels open and off-beam studies of short-lived radioactive isotopes deal with gamma-ray spectra of high line-density. Such spectra can be successfully analyzed only by Ge(Li) detectors which however have modest timing properties. The experience in the last years, e.g. in Rossendorf and Dubna, resulted in a new modification of the delayed coincidence method which enables the multidimensional investigation of nanosecond isomers with half-lives down to ≈ 0.2 ns by the inclusion of the centroid-shift analysis. The real possibilities of this method can be only exploited when the full energy-time information is recorded, e.g. on the basis of a mini-computer (e.g. HP 2116C in the Dubna variant).

Gamma-gamma delayed coincidences are measured by a TAC with a scintillation counter (start) and a Ge(Li) detector (stop). After the experiment, windows are selected in both energy spectra and the corresponding time curves are obtained. The energy dependence of the centroid positions along the gamma-ray Ge(Li) spectrum is deduced in diagram form. Then, "delayed" gamma-rays can be easily identified and quantitatively analysed.

3. Systematics of l-forbidden M1 transitions

The reduced transition probabilities B(M1) of l-forbidden M1 transitions in non-deformed nuclei with $100 < A < 210$ are presented in fig.1. Thereby, the

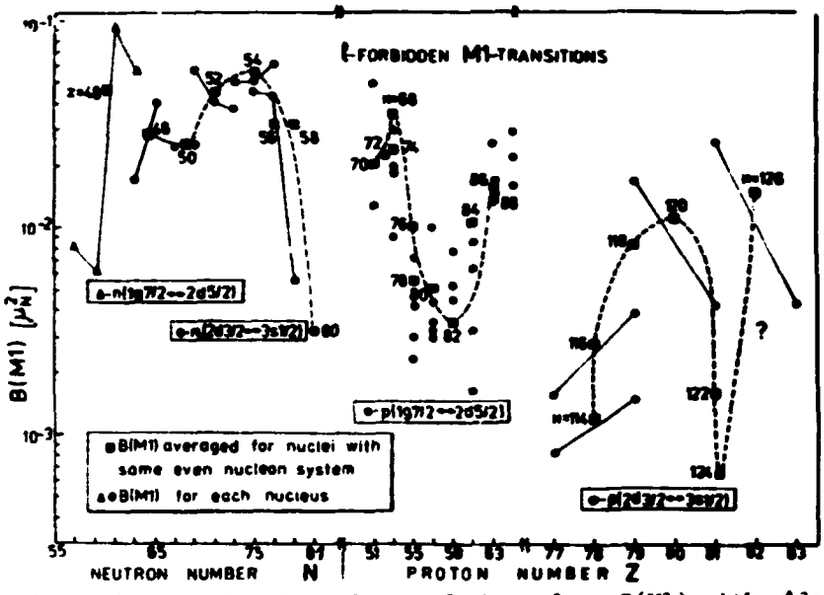

Fig. 1 Nucleon-number dependence of the values B(M1) with $\Delta l=2$. The transition in $^{209}_{83}Bi_{126}$ included is of the type $f_{7/2} \rightarrow h_{9/2}$. The errors are evaluated to be about 20%.

B(M1) values are plotted versus the odd-nucleon number (e.g. transitions of the odd neutron are presented versus the neutron number N). Additionally, average B(M1) values for nuclei with the same even-nucleon number are shown. In this way, the dependence on the neutron number N as well as on the proton number Z can be studied simultaneously. For some nucleon numbers only the B(M1) value in one nucleus is known: for Z=58,60 (N=79,81, respectively), N=68 (Z=53), N=118, 122, 124 (Z=79, 81, respectively). The averaging procedure could not be applied in these cases.

For odd-neutron nuclei with $55 < N \leq 81$, the B(M1) values decrease strongly in the vicinity of $N \approx 82$. A certain decrease is also appreciable for Z=50 nuclei. Unambiguously, these are shell effects. They are expected according to the core polarization picture: the closed shell of like nucleons is stronger "felt" than that of unlike nucleons.

The proton transitions in the region $51 \leq Z \leq 65$ reveal a pronounced minimum for N=82 and considerably less appreciated minimum for $Z \approx 50$. In this case, the filling of the unlike-nucleon shell seems to influence stronger the B(M1) values considered here as a "measure" of core-polarization. This is in surprising contradiction to the V_t/V_s ratio usually assumed (sec.1) which predicts larger contributions from the interaction between like nucleons.

In spite of this contradiction, it should be stressed that both cases discussed so far are in principle to understand in terms of the core polarization theory.

This is not the case for the proton transitions in nuclei with $77 \leq Z \leq 83$. Beside the irregularities in the general tendency with increasing values of N

and Z, the most striking fact is that the average quantity B(M1) for N=126 and Z_{av}=82 (from $^{207}_{81}T_{126}$ and $^{209}_{83}Bi_{126}$) is not the lowest value as expected from the simple core-polarization picture but the highest one in this region.

A simple satisfactory explanation for this dramatic behaviour of the M1, Δ l=2 values in the region $77 \leq Z \leq 83$ is difficult to propose. Arima and Huang Lin[4] found the contributions from mesonic exchange currents for $Z \geq 82$ nuclei to be nearly as large as those from core polarization and with opposite phase. According to Towner et al.[6], higher-order core-polarization contributions and vibrational admixtures[7] turn out to be more important than mesonic corrections in the formation of M1 transition matrix elements in closed shell plus or minus one nuclei. Paar and Brant[8] found that quadrupole vibrational admixtures practically does not influence M1, Δl=2 matrix elements of the operator $[Y_2 \sigma]$.

Two further remarks of more general nature should be added. Recently, Grecksch et al.[9] showed that M1 transitions in different complex nuclei (between ^{12}C and ^{40}Ca) can be significantly influenced by the inclusion of Δ(1236) resonance virtual excitations into the conventional particle-hole model (cf. graph B, sec.1).

Magnetic properties of nuclei, especially l-forbidden M1-transitions are considered in the last years in connection with a possible existence of π-condensate. The investigations reveal that a detailed inclusion of one-pion exchange effects is important for the correct description of these transitions[10].

A talk about l-forbidden M1 transitions should include the information about a M1 "anomaly" in deformed odd-A nuclei concerning transitions between orbitals $5/2^-[402]$ and $7/2^-[404]$, arising from the spherical states $d_{5/2}$ and $g_{7/2}$ (cf. fig.1). For a long time it has been assumed that the strong deviation of the B(M1) value in ^{181}Ta is somewhat like a "pathological" exception. Careful lifetime measurements[11] in Rossendorf and Dubna (^{153}Tb, $^{171,173,175}Lu$, $^{177,179}Ta$) revealed that we have to do with a systematical deviation which is up to now not well understood. Nevertheless, it seems sure that again mesonic currents and spin-polarization effects should be made responsible for this phenomenon[12].

References

/1/ H. Morinaga and T. Yamazaki, In-Beam Gamma-Ray Spectroscopy, North-Holl. 1976, Chapt. 3

/2/ O. Häusser, I.S. Towner, T. Faestermann, H.R. Andrews, J.R. Beene, D. Horn and D. Ward, Nucl. Phys. A293 (1977) 248

/3/ A. Arima and H. Horie, Prog. Theor. Phys. 11 (1954) 509

/4/ A. Arima and L.J. Huang-Lin, Phys. Lett. 41B (1972) 429

/5/ W. Andrejtscheff, N.Z. Marupov, K.M. Muminov, T.M. Muminov, R.R. Usmanov and F. Khamraev, JINR P13-11312 (1978)

/6/ I.C. Towner, F.C. Khanna and O. Häusser, Nucl. Phys. A277 (1977) 285

/7/ I. Hamamoto, Phys. Lett. 61B (1976) 343

/8/ V. Paar and S. Brant, Phys. Lett. 74B (1978) 297

/9/ E. Grecksch, M. Dillig and M.G. Huber, Phys. Lett. 72B (1977) 11

/10/ E.E. Saperstein, S.V. Tolokonnikov and S.A. Fajans, Izv.AN SSSR, ser. fiz. 41 (1977) 2063

/11/ K.D. Schilling et al., Nucl. Phys. A265 (1976) 58

/12/ W. Andrejtscheff, JINR D-9682

ИССЛЕДОВАНИЕ ИЗМЕНЕНИЯ СТРУКТУРЫ АТОМНОЙ ОБОЛОЧКИ ПРИ ИОНИЗАЦИИ АТОМА УРАНА ПО МЕТОДУ ДИРАКА-ФОКА-СЛЕТЕРА

Г. Шорнак
Объединенный институт ядерных исследований, Дубна, СССР

Аннотация

С помощью метода Дирака-Фока-Слетера рассчитано влияние внешних вакансий в атомных оболочках урана на энергетическую структуру оболочек атома и на энергии рентгеновских переходов. Обнаружены, наряду с возрастанием энергий рентгеновских переходов при последовательном удалении электронов с наименьшей энергией связи, отрицательные сдвиги рентгеновских энергий при удалении электронов из подоболочек 4f-уровней атома.

I. Введение

С развитием современных диагностических методов на основе спектроскопии характеристического рентгеновского излучения для анализа плазмы, ряда космических объектов, исследования процесса ионизации атомов в ионных источниках современных ускорителей тяжелых ионов и для диагностики электронно-ионных колец, как они существуют на прототипе коллективного ускорителя тяжелых ионов [I], требуется в растущей мере знание энергетической структуры оболочек атома как функции ионизационного состояния.

В настящей работе исследуется влияние внешних вакансий на энергетическую структуру оболочек атома и на энергии рентгеновских переходов. Рассматриваются изменения энергетической структуры атома урана вплоть до ядра, полностью ободранного от электронов.

2. Энергетическая структура атома урана в зависимости от ионизационного состояния

В данной работе используется программа типа Дирака-Фока-Слетера [2]. Эта программа рассчитывает самосогласованное потенциальное поле и радиальные орбитальные функции для атомов или ионов на основе уравнения Дирака. Как потенциал обмена используется потенциал Слетера [3]. Для больших расстояний от ядра в асимптотическое поведение потенциала внесены поправки по методу, предложенному Латером [4]. При всех расчетах принимается, что между угловыми моментами существует jj-связи.

Расчитанные энергии уровней для всех степеней ионизации атома урана опубликованы в работе Шорнака и др. [5]. На первом рисунке представлена зависимость полной энергии атома E_t и её отдельных компонентов (кинетическая энергия электронов E_k, потенциальная энергия электроны-ядро E_n, средная энергия электростатического взаимодействия между электронами E_e и энергия обмена E_{ex}) от степени ионизации атома.

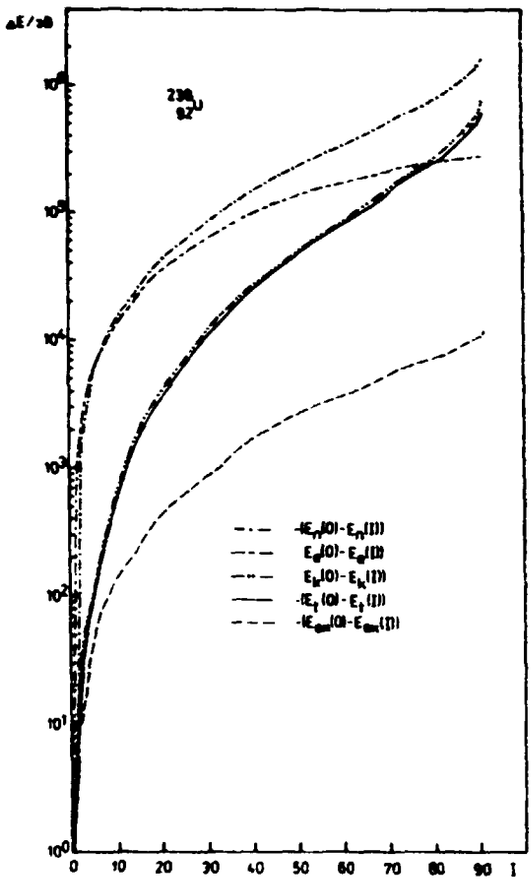

Рис. I Зависимость полной энергии атома урана E_t и её отдельных компонентов от степени ионизации I атома

3. Сдвиги рентгеновских линий

При расчёте сдвигов рентгеновских линий в зависимости от ионизационного состояния атома урана принимается, что как образование дырок во внутренних оболочках атома, так и заполнение из расположенных выше оболочек происходит за время, значительно меньше времени релаксации атомных состояний, т.е. при этом условии можно использовать для расчета энергии рентгеновских линий энергии уровней атомных состояний, имеющихся перед возникновением вакансий внутри атома.

Рассчитанные из энергий атомных уровней урана сдвиги некоторых рентгеновских переходов в зависимости от степени ионизации атома, представлены на рис. 2. Энергии рентгеновских переходов растают при последовательном удалении электронов из O-, P- и Q-уровней. Однако, при удалении электронов из 4f -подоболочек можно наблюдать противоположное поведение сдвигов рентгеновских энергий. Расчеты для ряда других элементов, имеющих заполненные электронами 4 -подоболочки, в том числе свинец и гафний, показывают тот же самый эффект, как обнаружено у урана.

Такое поведение сдвигов рентгеновских переходных энергии можно понимать следующим образом: электроны, занимающие 4f -подоболочки, находятся на относительно большом радиальном расстоянии от ядра. Однако электроны со сравнительно низкими квантовыми числами сконцентрированы ближе к ядру в узком радиальном диапазоне. Так как электроны 4f -подоболочек находятся в сравнении с другими состояниями электронов с большими квантовыми числами, в маленьком радиальном диапазоне, изменение плотности электронов 4f -оболочек меньше влияет на экранирование электронов K-оболочки, чем на выше расположенных состояниях. Вследствие такого эффекта изменение энергии связи электронов K-оболочки будет меньше, чем для выше расположенных уровней, что является причиной отрицательных сдвигов энергии рентгеновских переходов, потому что вообще изменение энергии связи электронов K-оболочки превышает изменение энергии связи других электронных состояний.

Описанная выше особенность поведения сдвигов энергий рентгеновских лучей является важным эффектом, который необходимо иметь ввиду при анализе характеристического рентгеновского излучения с целью определения ионизационного состояния атома.

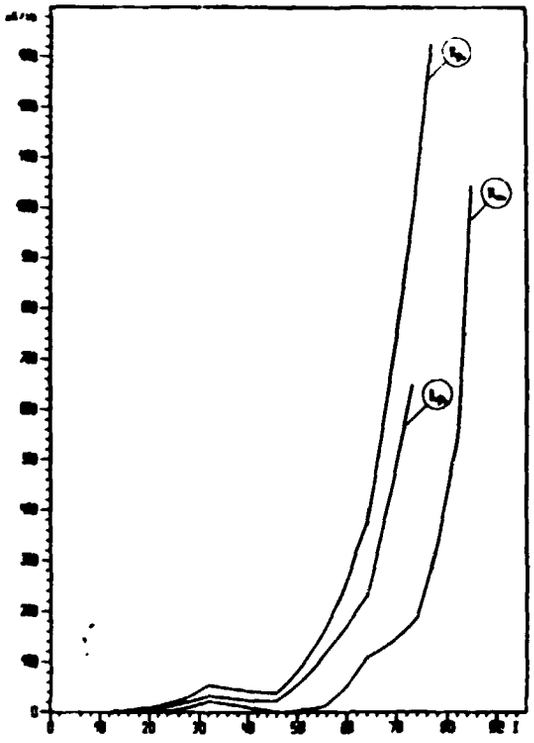

Чтобы проверить этот эффект, проводились также расчеты с помощью программ типов Хартри-Фока-Слетера [6] и Дирака-Фока [7]. При этом получены те же самые качественные результаты, что еще раз подтверждает существование найденного эффекта.

Рис. 2 Энергетические сдвиги выбранных рентгеновских переходов атома урана как функции ионизационного состояния I атома

Литература

[1] Х.-У. Зиберт и др. ОИЯИ, Р9-9366, Дубна 1975

[2] D.A. Liberman et al., Comp. Phys. Commun. 2 (1971) 1o7

[3] J.C. Slater, Phys. Rev. 81 (1951) 385

[4] R. Latter, Phys. Rev. 99 (1955) 51o

[5] Г. Шорнак и др. ОИЯИ, Р7-11876, Дубна 1978

[6] F. Hermann and S. Skillman, Atomic Structure Calculations, Prentice-Hall, Inc. Englewood Cliffs, New Jersey 1963

[7] J.P. Deslaux, Comp. Phys. Commun. 9 (1975) 31